

JYU DISSERTATIONS 496

Essi Taipale

**Synthetic and Structural Studies
on the Effect of Non-Covalent
Interactions on $N(sp^2)$ -Heterocyclic
Molecules**



UNIVERSITY OF JYVÄSKYLÄ
FACULTY OF MATHEMATICS
AND SCIENCE

JYU DISSERTATIONS 496

Essi Taipale

**Synthetic and Structural Studies on the
Effect of Non-Covalent Interactions on
 $N(sp^2)$ -Heterocyclic Molecules**

Esitetään Jyväskylän yliopiston matemaattis-luonnontieteellisen tiedekunnan suostumuksella
julkisesti tarkastettavaksi helmikuun 25. päivänä 2022 kello 12.

Academic dissertation to be publicly discussed, by permission of
the Faculty of Mathematics and Science of the University of Jyväskylä,
on February 25, 2022, at 12 o'clock.



JYVÄSKYLÄN YLIOPISTO
UNIVERSITY OF JYVÄSKYLÄ

JYVÄSKYLÄ 2022

Editors

Kari Rissanen

Department of Chemistry, University of Jyväskylä

Timo Hautala

Open Science Centre, University of Jyväskylä

Copyright © 2022, by University of Jyväskylä

ISBN 978-951-39-9039-8 (PDF)

URN:ISBN:978-951-39-9039-8

ISSN 2489-9003

Permanent link to this publication: <http://urn.fi/URN:ISBN:978-951-39-9039-8>

ABSTRACT

Taipale, Essi

Synthetic and Structural Studies on the Effect of Non-Covalent Interactions on $N(sp^2)$ -Heterocyclic Molecules

Jyväskylä: University of Jyväskylä, 2022, 67 p.

(JYU Dissertations

ISSN 2489-9003; 496)

ISBN 978-951-39-9039-8

The thesis herein describes the synthesis and characterization of compounds designed to be utilized as acceptor molecules in non-covalent interactions. The non-covalent interactions are applied in fluorescence modulation and construction of novel halogen-bonded complexes. In the literature part, an introduction to supramolecular chemistry and non-covalent interactions is given. It presents the concepts of light absorption and emission and discusses host-guest chemistry of larger supramolecular structures. At the end of the literature part, some common $N(sp^2)$ -heterocyclic molecules as hydrogen and halogen bond acceptor molecules are reviewed, highlighting the target compounds most relevant to the thesis work.

The results and discussion part of the thesis describes the synthesis and characterization of imidazole- and carbazole-derived small-molecules as fluorescence emitters and hydrogen and halogen bond acceptors. The acceptor molecules were further utilized in the synthesis of larger tripodal N -donor ligands which were employed in the construction of halogen-bonded iodine(I) capsular assemblies manifesting three $[N-I-N]^+$ three-center four-electron bonds through the intermediate silver(I) metallocage formation.

The publication **I** focuses on the fundamentals of protonation and its potential in fluorescence modulation for simple, commercially available $N(sp^2)$ -heterocyclic molecules, *viz.* quinoline derivatives. This work was broadened in the publication **II** to carbazole derivatives. The publications **III** and **IV** focused on the development of small symmetric halogen-bonded iodine(I) carbazole complexes (publication **III**) and tris-imidazole based cage complexes (publication **IV**).

Keywords: hydrogen bond, halogen bond, halogen(I) ions, halonium, iodonium, metallocage, supramolecular chemistry, non-covalent interactions, self-assembly, fluorescence, X-ray crystallography

TIIVISTELMÄ

Taipale, Essi

$N(sp^2)$ -Heterosyklisten molekyylien vety- ja halogeenisitoutuneiden kompleksien synteettiset ja rakenteelliset tutkimukset

Jyväskylä: Jyväskylän yliopisto, 2022, 67 p.

(JYU Dissertations

ISSN 2489-9003; 496)

ISBN 978-951-39-9039-8

Tässä väitöskirjassa käsitellään heikkojen vuorovaikutusten vastaanottajamolekyylien synteesiä ja karakterisointia. Heikkoja vuorovaikutuksia sovelletaan fluoresenssin modulaatiossa ja uusien halogeenisitoutuneiden kompleksien muodostamisessa. Kirjallisuuskatsauksessa esitellään lyhyesti supramolekylikemia tieteenalana ja johdanto heikkoihin vuorovaikutuksiin. Johdanto käsittelee valokemian konsepteja, kuten valon absorptiota ja emissiota, sekä esittelee suurten supramolekyylien isäntä-vieras kemiaa. Kirjallisuuskatsauksen lopussa esitellään muutamia yleisiä $N(sp^2)$ -heterosyklisiä molekyyliä, jotka voivat toimia sekä vety- että halogeenisidoksen vastaanottajamolekyyleinä. Näistä valittiin tarkempaan käsittelyyn muutamia tälle työlle merkityksellisimpiä aromaattisia amiineja.

Tulokset-osiossa kuvataan fluoresenssiemittereinä sekä vety- ja halogeenisidoksen vastaanottajamolekyyleinä käytettävien imidatsoli- ja karbatsoli-johdannaisten synteetit ja rakennekarakterisoinnit. Näitä yhdisteitä hyödynnetään myös suurempien tripodaalisten vastaanottaja-ligandien synteetissä, joita käytetään halogeenisitoutuneiden jodi(I) kapseli-rakenteiden muodostamisessa. Häkit muodostuvat reaktiota edeltävistä hopea(I) häkeistä kolmen symmetrisen $[N-I-N]^+ 3c-4e$ sidoksen avulla.

Ensimmäinen julkaisu (I) keskittyy amiinien protonaation perusteisiin ja potentiaaliin fluoresenssin modulaatiossa tutkimalla yksinkertaisia $N(sp^2)$ -heterosyklisiä molekyyliä, erityisesti kinoliini-yhdisteitä. Työtä laajennettiin toisessa julkaisussa (II) karbatsoli-yhdisteisiin. Julkaisut III ja IV keskittyivät pienten symmetristen halogeenisitoutuneiden jodi(I) imidatsoli- ja karbatsoli-kompleksien kehittämiseen (III) ja tris-imidatsoli rakenteisten häkki-kompleksien synteettiin (IV).

Avainsanat: vetysidos, halogeenisidos, halogeeni(I) ionit, halonium, jodonium, metallöhäkki, supramolekylikemia, heikot vuorovaikutukset, itsejärjestäytyminen, fluoresenssi, röntgenkristallografia

Author

Essi Taipale
Department of Chemistry
Nanoscience Center
P.O. Box 35
FI-40014 University of Jyväskylä
Finland
ORCID 0000-0001-9638-3525

Supervisor

Professor Kari Rissanen
Department of Chemistry
Nanoscience Center
University of Jyväskylä
Finland

Reviewers

Professor Michael Hardie
School of Chemistry
University of Leeds
United Kingdom

Professor Christer Aakeröy
Department of Chemistry
Kansas State University
United States

Opponent

Professor Risto Laitinen
Environmental and Chemical Engineering
Inorganic Chemistry
University of Oulu
Finland

PREFACE

This thesis work was carried out at the Department of Chemistry, University of Jyväskylä, Finland, between 2019 and 2022. At times it was stressful, yet mostly rewarding and many times I found myself full of excitement. I consider myself lucky, as it has been less than three years (and feels even shorter), yet it is already time to conclude this chapter of my life. I guess it is true, time flies when you are having fun! With these words, I would like to express my gratitude to everyone supporting this journey.

The work herein was founded by the Academy of Finland as a part of the *Halonium supramolecular Chemistry: New Molecular Machines and Nanoreactors* -project. The Academy of Finland is gratefully acknowledged for my making the work financially possible.

Professor Kari Rissanen is thanked for the opportunity to work in his group, and for the ever-so-inspiring guidance and supervision – I have learned so much from you, and the work herein would not have been possible without you. Thank you for being the best supervisor anyone could ask for, and for the endless flexibility and support, making the whole process significantly easier even amongst some major changes in my personal life all throughout this project.

Professors Michael Hardie and Christer Aakeröy are sincerely thanked for the pre-examination of this thesis. I feel honored that my work has been evaluated by such distinguished scientists. In addition, Jas Ward is thanked for the language revision.

The staff of the Department of Chemistry is thanked for making the University a wonderful place to work in, and all the help during this project. A special thanks to the Rissanen Group for welcoming me into to the group and for the nice working atmosphere within it. Special thanks to Jas, to my friend and mentor, for the guidance, encouragement and the endless research ideas, as well as for being the best puppy-sitter in my time of need. Both Jas and Khai are thanked for their patience and the endless hours spent teaching me crystallography.

And to my dear collaborators at Tampere University, especially Arri and Tero-Petri, introducing me to the world of supramolecular chemistry and providing me help and support all the way from my master's thesis to the end of my PhD. The insightful discussions on my thesis work and all the support during the publications is greatly appreciated.

And lastly, a big thank you to my friends and family, especially to my husband Jussi, for all the love and encouragement in the past ten years that has led to this day. Without your support, this journey would have been considerably harder.

Kuopio 09.01.2022
Essi Taipale

LIST OF ORIGINAL PUBLICATIONS

This thesis is based on the following original publications, which are referred to in the text by their Roman numerals.

- I** E. Tervola, K.-N. Truong, J. S. Ward, A. Priimagi, K. Rissanen, Fluorescence enhancement of quinolines by protonation, *RSC Adv.*, **2020**, *10*, 29385 – 29393.
- II** E. Taipale, N. A. Durandin, J. Salunke, N. R. Candeias, T.-P. Ruoko, J. S. Ward, A. Priimagi, K. Rissanen, Protonation-Induced Fluorescence Modulation of Carbazole-Based Emitters, *Mat. Adv.*, **2022**, *3*, 1703 – 1712.
- III** E. Taipale, M. Siepmann, K.-N. Truong, K. Rissanen, Iodine(I) and Silver(I) Complexes of Benzoimidazole and Pyridylcarbazole Derivatives, *Chem. Eur. J.* **2021**, *27*, 17412 – 17419.
- IV** E. Taipale, J. S. Ward, G. Fiorini, D. L. Stares, C. A. Schalley, K. Rissanen, Dimeric Iodine(I) and Silver(I) Capsules Cages from Tripodal N-donor Ligands, *Inorg. Chem. Front.* **2022**, submitted.

Author's contribution

The author has synthesized all the compounds used in the experimental work of publications **I - IV** excluding Scheme 3 and compound **50**. All NMR measurements, as well as the solution state absorption and fluorescence spectroscopy, were performed by the author. In publication **I**, the author (*nee* Tervola) carried out the crystallization experiments, yet the single crystal X-ray diffraction was performed by other experts. In publications **II - IV**, the author carried out most of the crystallographic work including crystallizations, data collection, and structure modelling. In publication **IV**, in addition to the SCXRD work, the author also analyzed the structures using Hirshfeld surface analysis. The author has written the first drafts of the publications and has been actively involved in the editorial process of all publications listed above.

CONTENTS

ABSTRACT

PREFACE

LIST OF ORIGINAL PUBLICATIONS

CONTENTS

ABBREVIATIONS

1	INTRODUCTION	11
1.1	Non-covalent interactions in supramolecular chemistry.....	11
1.1.1	Hydrogen bonding.....	11
1.1.2	Halogen bonding.....	14
1.1.3	Halogen(I) ions	18
1.2	Fluorescence and non-covalent interactions.....	19
1.2.1	Non-covalent interactions and fluorescence in heterocyclic compounds.....	21
1.2.2	Solid-state fluorescence	22
1.3	Host-guest chemistry	22
1.3.1	Hydrogen-bonded capsular assemblies.....	24
1.3.2	Halogen-bonded capsular assemblies.....	25
1.4	HB and XB acceptors	28
1.4.1	Quinolines	28
1.4.2	Imidazoles	29
1.4.3	Carbazoles	31
2	RESULTS AND DISCUSSION	33
2.1	Aim of the work	33
2.2	Materials and design	34
2.2.1	Syntheses of ligands.....	34
2.2.1.1	Syntheses of imidazole-based ligands ^{III,IV}	34
2.2.1.2	Synthesis of carbazole-based ligands ^{II,III}	36
2.2.2	Synthesis of iodine(I) complexes ^{III,IV}	38
2.3	Protonation-induced fluorescence modulation ^{I,II}	39
2.3.1	The effect of protonation on quinoline derivatives.....	39
2.3.2	The effect of protonation on carbazole derivatives.....	42
2.4	Self-assembly of silver(I) [N-Ag-N] ⁺ and iodine(I) [N-I-N] ⁺ complexes ^{III,IV}	49
2.4.1	Iodine(I) and silver(I) complexes of benzoimidazole and pyridylcarbazole derivatives.....	49
2.4.2	Dimeric iodine(I) and silver(I) cages from tripodal N-donor ligands.....	53
	REFERENCES.....	61

ORIGINAL PAPERS

ABBREVIATIONS

CSD	Cambridge Structural Database
DCM	dichloromethane
DMAP	4-dimethylaminopyridine
DMF	dimethylformamide
DMSO	dimethylsulfoxide
ESI-MS	electrospray ionization mass spectrometry
Et	ethyl
HB	hydrogen bond
HBeXB	hydrogen-bond enhanced halogen bond
HMBC	heteronuclear multiple bond correlation
ic	internal conversion
ICT	intramolecular charge transfer
IM-MS	ion mobility mass spectrometry
isc	intersystem crossing
IUPAC	International Union of Pure and Applied Chemistry
L	ligand
LUMO	lowest-lying molecular orbital
Me	methyl
MeCN	acetonitrile
NMR	nuclear magnetic resonance spectroscopy
OAc	acetyloxy
OLED	organic light-emitting diode
PhOLED	phosphorescent organic light-emitting diode
R	atom or a molecule
risc	reverse intersystem crossing
TADF	thermally activated delayed fluorescence
TD-DFT	time-dependent density functional theory
THF	tetrahydrofuran
TOF	time-of-flight
UV	ultraviolet
UV-Vis	ultraviolet-visible
vr	vibrational relaxation
X	halogen atom
XB	halogen bond
Y	hydrogen- or halogen-bond acceptor
3c-4e	three-center four-electron

1 INTRODUCTION

1.1 Non-covalent interactions in supramolecular chemistry

Supermolecules are to molecules and the intermolecular bond what molecules are to atoms and the covalent bond.¹

Supramolecular Chemistry consists of supermolecules in spontaneous association with multiple components.² It has been defined as ‘chemistry of molecular assemblies and of the intermolecular bond’ or more succinctly, ‘the chemistry beyond the molecule’.¹ The careful design of supermolecules with the understanding of intermolecular interactions can lead to larger assemblies with distinct properties that set them apart from the aggregate properties of constituent molecules, which is the essence of supramolecular chemistry. The field of *Supramolecular Chemistry* is still considered a non-matured discipline of chemistry, even with its first examples dating back to the 1960s in the form of macrocyclic compounds.³ In 1987 Jean-Marie Lehn, Donald Cram, and Charles Pedersen received the Nobel Prize in Chemistry ‘for their development and use of molecules with structure-specific interactions of high selectivity’ and major developments have been made ever since.⁴ The interdisciplinary nature of *Supramolecular Chemistry* has made it one of the most vigorously growing fields of chemistry having a multitude of applications such as molecular devices and machines,⁵ molecular recognition,⁶ self-assembly and self-organization,^{7,8} and host-guest systems⁹⁻¹¹ all benefitting from the reversible nature of the non-covalent bond, prime examples being hydrogen and halogen bonding, as well as metallosupramolecular chemistry.

1.1.1 Hydrogen bonding

The hydrogen bond (HB) has been one of the most studied non-covalent interactions for 100 years, yet a generally accepted definition was stated only recently:

The hydrogen bond is an attractive interaction between a hydrogen atom from a molecule or a molecular fragment X-H in which X is more electronegative than H, and an atom or a group of atoms in the same or a different molecule, in which there is evidence of bond formation.¹²

In the hydrogen bond (R-H \cdots Y), R-H donates the hydrogen and is referred to as the hydrogen bond *donor*, whereas Y is denoted as the hydrogen bond *acceptor*.¹² In the donor moiety (R-H), R does not necessarily need to be strongly electronegative, as long as the R-H bond is polarized leaving the hydrogen with a positive partial charge. In the hydrogen bond, the acceptor is an atom or a group of atoms carrying a negative partial charge, commonly nitrogen, oxygen, sulfur, halide, *etc.* atom with an available pair of electrons.¹³ However, the acceptor does not need to possess a (separate) lone pair, but HBs are also observed for π -systems of alkenes and aromatic systems (CH $\cdots\pi$ interactions).¹⁴ Recent reviews by Herschlag¹⁵ and Scheiner¹⁴ highlight the importance of the hydrogen bond.

Perhaps the ambiguous nature of the hydrogen bond has made it difficult to define. It is an intricate interaction consisting of contributions from electrostatics, polarization, charge-transfer, dispersion, and exchange repulsion.¹³ However, it is further complicated by the sheer lack of boundaries separating it from the covalent bond, ionic interactions, van der Waals interactions, and even from the cation- π interaction.¹³ The strength of the hydrogen bond greatly affects the distance between the donor and the acceptor moiety.¹⁶ Especially at longer donor-acceptor distances, electrostatics is a dominant contributor to the bond strength, even if the charge-transfer has a significant role at shorter distances with optimal geometry.¹³

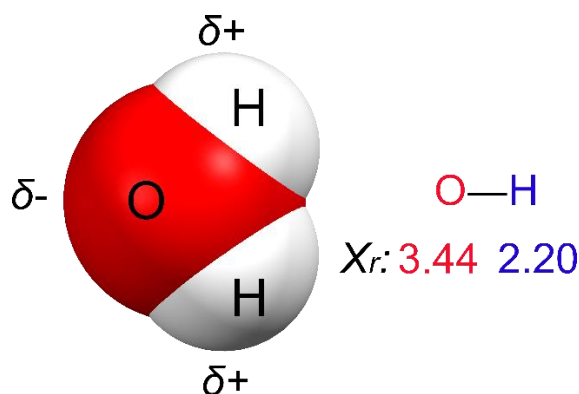


Figure 1 The anisotropic distribution of the electrostatic potential reflected by the Pauling electronegativity scale (X_r).¹⁷

Hydrogen bond strengths vary widely between 0.2 to 40 kcal/mol, occurring also at distances longer than the sum of the H \cdots Y van der Waals radii.¹³ It has been suggested, that this type of interaction with H \cdots Y distances up to 3.2 Å should be considered as hydrogen bonding.¹⁸ Yet typical values of H \cdots Y distances for N-H \cdots O bonds are between 1.7 to 2.0 Å.¹⁹ They can appear intermolecularly (between different molecular entities) or intramolecularly (within the same molecular entity). A hydrogen bond is fairly directional, occurring as

an extension along the R-H covalent bond, yet hydrogen bonds with R-H...Y angles between 110 - 180° have been observed.¹³ In addition to the most common type of hydrogen bond (R-H...Y), hydrogens are also capable of forming more complex structures, such as bifurcated HBs, in which the hydrogen is simultaneously bonded to two HB acceptors.¹³ The ability of hydrogen to form such intricate interactions makes it capable of constructing stable extended networks. An example of bifurcated HBs in the crystal lattice of 1,3-dibromo-2,4,6-trinitrobenzene (**1**) is depicted in Figure 2.

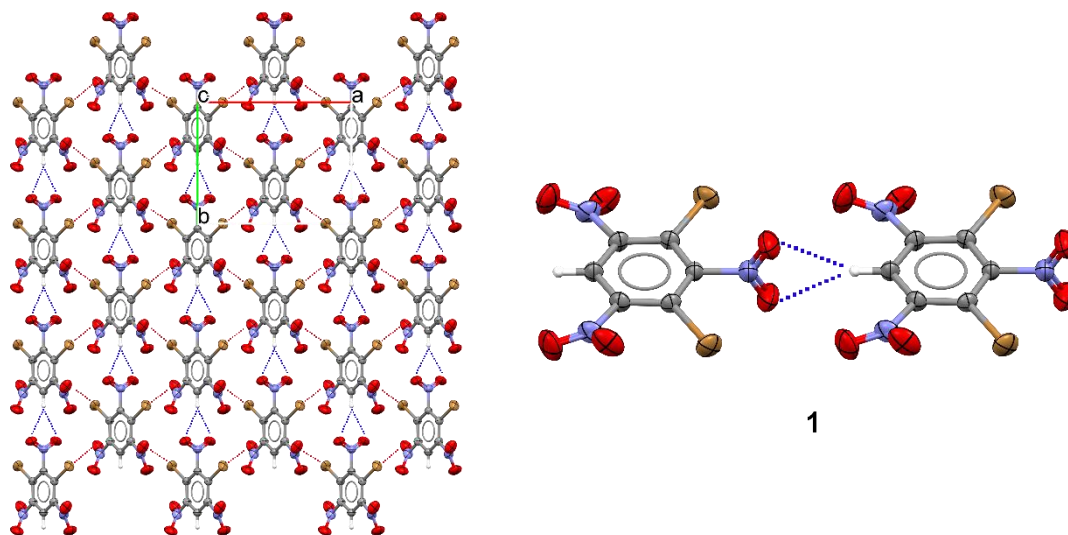


Figure 2 The packing in the crystal structure of 1,3-dibromo-2,4,6-trinitrobenzene (**1**) viewed along the crystallographic *c*-axis. The structure displays a network of intermolecular interactions in the form of bifurcated (C-H...O) hydrogen bonds (blue-dotted lines) along with Br...O interactions (red-dotted lines). CSD ref. code: XOBRIIP.²⁰ Thermal displacement ellipsoids are drawn at the 50% probability level.

In certain situations, a hydrogen bond may be understood as an incipient proton-transfer reaction. In these cases, a moderate hydrogen bond would represent an early stage of proton-transfer, whereas a strong hydrogen bond would represent an advanced stage of proton-transfer without fully being an ionic interaction. Therefore, the H...Y bond is already formed, and the R-H bond is weakened, yet still exists.²¹ Protonation occurs when the proton is fully transferred from the hydrogen bond donor to the hydrogen bond acceptor (typically a Lewis base) making the HB donor negatively charged (R⁻) and the HB acceptor positively charged (HY⁺). The formed ion pair is connected through strong ionic interactions between the two oppositely charged species through the H-atom. Anions that are Lewis bases are considered good hydrogen and halogen bond acceptors and are commonly utilized in non-covalent interactions.²² Much like HB, ionic interactions cannot be strictly defined; they are mainly electrostatic interactions yet possess some covalent character. Ionic interactions are often associated with extremely tight packing in the solid state.²³

Hydrogen bonds can be studied in solution with nuclear magnetic resonance spectroscopy (NMR), wherein they appear as a downfield shift in the chemical shift of the studied compound. Upon protonation, the hydrogen atom is increasingly deshielded with the increasing strength of the hydrogen bond.¹³ Hydrogen bonding in dynamic chromophores can restrict the molecular motion, lower the energy of excited states and reduce aggregation, all resulting in significant effects on the luminescence properties of the compound.³ In an electromagnetic spectrum, hydrogen bonding is generally observed as a red-shift, a wavelength changing to a higher value (towards red in the visible region).²⁴⁻²⁶

In the solid state, hydrogen bonds are highly affected by their surroundings and are rarely observed with optimal geometry.¹³ When it comes to hydrogen bonds, it is all about quantity over quality, and especially in the solid state, they often form extended networks. These weak “*non-bonded*” interactions work up to stabilize intricate intra- and intermolecular configurations and the strongest hydrogen bonds are known to be even stronger than the weakest of covalent bonds.²⁷ This, accompanied by the reversible nature of the hydrogen bond, makes it undeniably the most important interaction in *Supramolecular Chemistry*.

1.1.2 Halogen bonding

In organic chemistry, halogen atoms (X) are typically considered electrophilic leaving groups due to their ability to react with nucleophiles in halogenation reactions.^{28,29} However, when covalently bound to other atoms and polarized, they can form attractive non-covalent interactions with nucleophiles without undergoing chemical reactions. When covalently bound to an atom or a molecule (R), the electron density around the halogen atom is anisotropically distributed forming a negative electrostatic potential surface perpendicular to the R-X bond, while a region of positive electrostatic potential surface, a so-called σ -hole, is formed along the covalent R-X bond.^{30,31} The non-reactive interaction of a halogen atom with a nucleophilic site seemed counter-intuitive at first, yet since the definition of the σ -hole by Politzer and Murray,^{32,33} halogen bonding (XB) has rapidly gained increased attention within the *Supramolecular Chemistry* community.

However, halogen bonding is still considered a non-matured interaction, and until the last decade perhaps the least utilized non-covalent interaction. This interaction was only just defined by IUPAC in 2013:

A halogen bond occurs when there is evidence of a net attractive interaction between an electrophilic region associated with a halogen atom in a molecular entity and a nucleophilic region in another, or the same, molecular entity.²⁸

Halogen bonding (R-X \cdots Y) is typically denoted by three dots between the halogen bond donor (R-X, denoted as the XB donor) and the halogen bond acceptor (Y, denoted as the XB acceptor). The halogen bond is formed from a polarized halogen atom (X), existing in a formal oxidation state of -1,³⁴ covalently bound to an atom or a molecule (R) to a XB acceptor (Y), which is an atom or a molecule with a nucleophilic region.²⁸ Most commonly, XB donor is a alkyl or aryl halide,

R-X, with R having a strong electron-withdrawing character, a dihalogen molecule (*e.g.*, I₂, Br₂), or as an extreme case, a halogen(I) cation (*e.g.*, I⁺, Br⁺). The XB acceptor is often an atom possessing a lone pair of electrons (*e.g.*, N, O, S) or an anion (*e.g.*, Cl⁻, Br⁻, I⁻, NO₃⁻, *etc.*). However, the particular nature of the halogen bond is still somewhat disputed.³⁵ It is agreed upon that the transfer of electron density occurs from the Lewis basic site (the XB acceptor) to the Lewis acidic site (the halogen atom), yet, the true nature (*e.g.*, consisting of electrostatic, charge-transfer, polarization, dispersion, *etc.* forces) depends on the species involved in the halogen bond.³⁵ Additionally, halogen bonds with organic XB donors are generally considered to have more electrostatic character, whereas inorganic XB donors are considered to have a more charge-transfer nature.²²

Often, XB is compared to the more well-known hydrogen bonding. These two interactions are comparable in strength (10 - 150 kJ/mol from weak XBs to very strong),^{29,35} yet XB possesses many features which makes it different from HB. Both XB and HB possess the positive electrostatic potential surface, *viz.* a region capable of the respective interaction. However, due to the anisotropy of the XB electrostatic potential surface of the halogen atom, it is considered amphoteric in nature, also capable of interacting from its nucleophilic region (to an electrophile).²⁹ Yet, this amphoteric behavior of covalently bound halogen is not an exception only limited to halogen atoms, but analogous behavior is also observed for polarized chalcogens (S, Se, Te), pnictogens (N, P), and tetrels (C).²⁹

The anisotropic electron density distribution and the presence of a σ -hole makes XB unique, separating it from the HB and other non-covalent interactions. The strength of the XB is tunable by affecting the magnitude of the σ -hole. The σ -hole is “deeper” (more positive) for more polarizable and less electronegative halogen atoms, so that the XB donor strength increases F \ll Cl < Br < I, with iodine manifesting the strongest XB interactions. Additionally, the σ -hole can be affected by the atom or the molecule covalently bound to the halogen, such that electron-withdrawing substituents increase the σ -hole and thus enhance the XB strength.^{29,35} Furthermore, the charge-transfer from the Lewis basic site is generally increased when the basicity of the XB acceptor (Lewis base) increases, resulting in a formation of a stronger XB bond.^{36,37} To visualize the tunability of the XB, Figure 3 depicts the molecular electrostatic potential surface of CF₃X (where X = F, Cl, Br, or I) showing the anisotropic electron density distribution of the covalently bound halogen atoms.^{35,38} The blue color indicates the negative and the red color the positive electrostatic potential. Figure 3 depicts the negative electrostatic potential belt perpendicular to the covalent bond and the positive σ -hole of the halogen atom along of the covalent bond. The increasing polarizability upon the increasing size of the halogen is most visible with CH₃I having the larger (deeper) σ -hole.

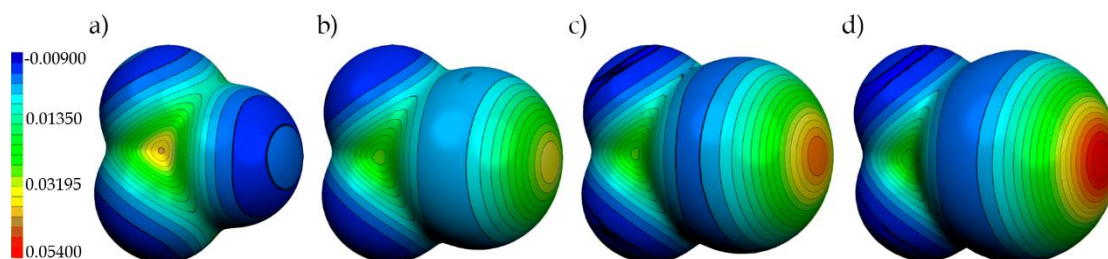


Figure 3 The Molecular electrostatic potential, in Hartrees, at the $0.001 \text{ e}/\text{Bohr}^3$ isodensity surface of a) CF_4 , b) CF_3Cl , c) CF_3Br , and d) CF_3I . Adapted from ref.³⁸

In addition to the tunable strength, XB is considered extremely linear, which is a consequence of the localization of the σ -hole as an extension directly along the covalent bond.²⁹ Therefore, bond angles in XB are usually much closer to 180° than in HB.^{29,35} However, deviations from this may occur due to secondary interactions or crystal packing effects.³⁵ Another characteristic of XB is its hydrophobicity, which evidently makes it suitable for applications in which the HB is incapable of. The hydrophobic nature of the XB has been utilized in biologically active molecules to improve their membrane permeability to tackle the ever-lasting challenge of blood-brain barrier permeation.³⁹ Moreover, the inherent size of the halogen atoms participating in XB renders it dissimilar to HB, since the larger size of the atom results in XB being more susceptible to steric hindrance compared to HB.²⁹

Only very recently, the prevalence of HB has led to the appreciation of its influence on the nucleophilic region of the XB in halogen-bonded systems with adjacent HBs enhancing the interaction (HBeXB).^{17,40} In a recent study by Berryman and co-workers, the authors reported, for the first time, experimental quantification of HBeXB complexes where intramolecular hydrogen bonding to the nucleophilic region of the halogen atom results in both less directional, but shorter XB bonds, inducing stronger halogen bonds in the solid state.⁴⁰ In their report, they also stated that stronger HBs donors will have a greater effect on the XB in HBeXBs.⁴⁰ Figure 4 depicts the bonding geometries in a hydrogen bond (A), a halogen bond (B), and a hydrogen bond enhanced halogen bond (C).

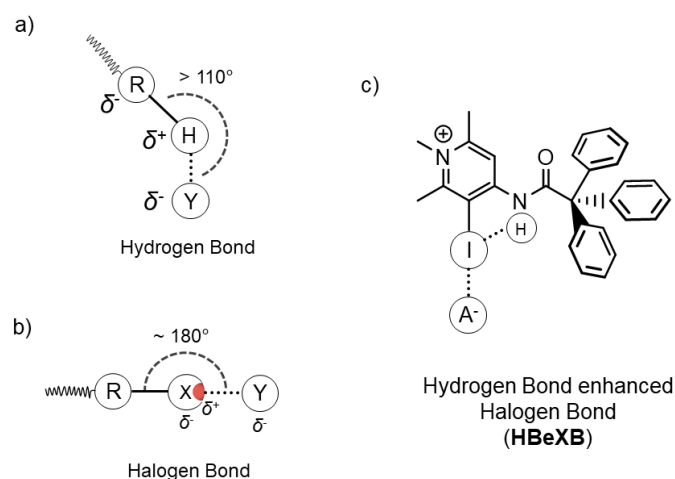


Figure 4 a) Hydrogen bond, b) halogen bond, and c) hydrogen bond enhanced halogen bond (HBeXB), where R = HB/XB donor, H = hydrogen, Y = HB/XB acceptor, X = halogen atom, I = iodine, and A⁻ = anion. Adapted from ref.⁴⁰

Since the 1990s, XB has also developed into an important supramolecular synthon in crystal engineering (Figure 5).^{41,42} Due to the predictable nature of the XB, mainly with respect to the strength and directionality, the ability to control and direct the formation of larger assemblies has led to the design of halogen-bonded organic frameworks,⁴³ molecular receptors,⁴⁴ and supramolecular polymers.⁴⁵ Figure 5 depicts a network of interactions in the crystal lattice of 4-iodophthalonitrile, where the nitrile groups form both HBs and XBs to the neighboring molecules.⁴⁶

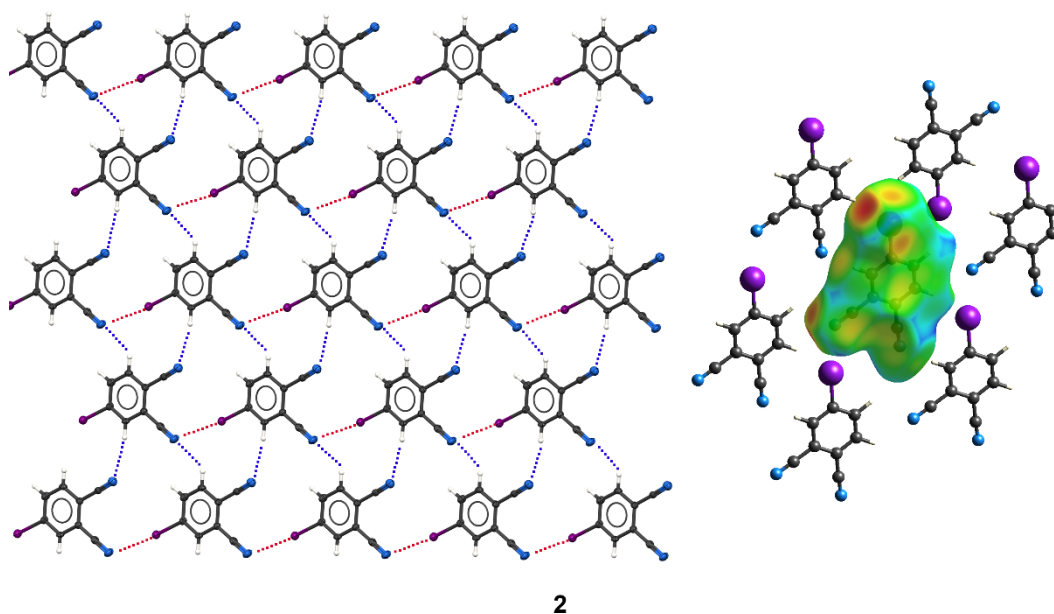


Figure 5 The C≡N...I halogen bonds (red-dotted lines) and C≡N...H hydrogen bonds (blue-dotted lines) in the crystal structure of 4-iodophthalonitrile (**2**) and the Hirshfeld surface analysis of the closest external contacts in one **2** molecule.

CSD ref. code: HEZCEX.⁴⁶ Thermal displacement ellipsoids are drawn at the 50% probability level.

1.1.3 Halogen(I) ions

Halogen-bonded complexes with halogen(I) ions (X^+) can be considered as a subclass of halogen-bonded complexes. In contrast to conventional halogen bonding ($R-X \cdots Y$), removing an electron from the halogen results in a positively charged cation (X^+ , also named as a *halonium* cation). This cation is capable of forming a so-called three-center four-electron (3c-4e) bond, in which the X^+ simultaneously interacts with two XB donors (Lewis bases, L) $[L \cdots X \cdots L]^+$, most commonly identical ones forming a symmetric bond.³⁴ Both Lewis bases contribute a pair of electrons into the bond between the three atoms, hence the 3c-4e bond. First reports of halogen(I) complexes emerged in the 1960s⁴⁷⁻⁴⁹, and since the 1990s they have been widely applied in synthetic chemistry in the form of Barluenga's reagent,⁵⁰⁻⁵³ and in the 2010s were found to be useful as a *bis*-functional XB donor both in solution and in solid-state studies.

The relative strength of halogen bonds can be qualitatively estimated by their R_{XB} values ($R_{XB} = d_{XB}/(X_{vdW} + B_{vdW})$)²⁹, where d_{XB} is the distance (in Å) between the XB donor and the XB acceptors atoms, X_{vdW} is the van der Waals radii⁵⁴ of the halogen atom, and B_{vdW} is the van der Waals radii of the XB acceptor atom. R_{XB} values of less than 0.70 are considered to be indicative of very strong, 0.70 - 0.85 moderate, and 0.85 - 0.99 weak halogen bonds.⁵⁵ The $[L \cdots X \cdots L]^+$ 3c-4e ($R-X$) bonds are of the strongest halogen bonds with remarkably short bond lengths ($R_{XB} = 0.64 - 0.69$) and strengths up to 180 kJ/mol.^{34,56}

In the 1960s, Creighton and coworkers characterized *bis*(pyridine)iodine(I) tetrafluoroborate^{47,49}, however, only after 30 years it became known as Barluenga's reagent when Jose Barluenga and his colleagues published a variety of applications for the *bis*(pyridine)iodine(I) complex as an oxidating agent and as an iodinating agent for aromatic electrophilic substitutions.⁵⁰⁻⁵³ Their inherent reactivity, which makes them excellent iodinating agents, has also made the structural studies of these complexes difficult, especially in solution. However, under suitable conditions, the halogen(I) complexes are very stable and the exceptional strength of the 3c-4e bond has intrigued scientists ever since their discovery, with recent developments in halogen(I) complexes having been made by Erdélyi *et al.*^{34,56-64}, and Rissanen *et al.*⁶⁵⁻⁷³

The halogen bonds of halogen(I) (aka *halonium*) ions have recently been reviewed by Erdélyi and Turunen.³⁴ These complexes are most commonly reported with symmetric $[N \cdots X \cdots N]^+$ bonds and nitrogen acting as the lone pair donor. However, recently, also asymmetric $[N1 \cdots X \cdots N2]^+$ complexes have been reported.^{61,69} Figure 6 depicts crystal structures of Barluenga's reagent (**3**), reported in the solid-state,⁷⁴ and the first-ever unrestrained asymmetric halogen(I) complex (**4**) between pyridine and dimethylaminopyridine (DMAP) in the solid-state by Ward and Rissanen *et al.*⁶⁹

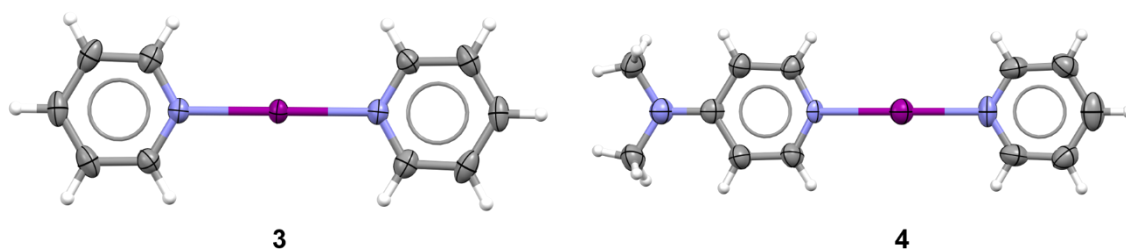


Figure 6 The crystal structure of Barluenga's reagent *bis*(pyridine)iodine(I) tetrafluoroborate (**3**), CSD ref. code: HUMMAD⁷⁴ and the first-ever reported unrestrained asymmetric iodine(I) structure between dimethylaminopyridine (DMAP) and pyridine (**4**). CSD ref. code: SURTIL.⁶⁹ Thermal displacement ellipsoids are drawn at the 50% probability level. Counter anions omitted for clarity.

When aromatic Lewis bases are involved in the interaction, a charge-transfer from the halogen(I) cation to the nucleophilic sites further enhances the interaction.^{34,57,58} However, despite their increased reactivity, tertiary amines have also been shown to form $[N \cdots I \cdots N]^+$ 3c-4e bonds with iodine(I).⁶⁷

Compared to their analogous silver(I) complexes, which are used as precursors in halogen(I) synthesis, the halogen(I) complexes have a distinct preference for a symmetric bond, both in solution^{56,60} and in the solid state.⁶⁷ However, in solution, halogen(I) complexes have been observed to undergo rapid ligand exchange, which is dependent on the Lewis basicity of the XB acceptor.⁶¹ This exchange, occurring for weak Lewis bases, is observed as line broadening in the NMR spectrum.⁶¹ Nevertheless, the symmetric nature of the halogen(I) bond has been perceived to be unaffected by its environment regardless of the solvent polarity⁶³ or counter anion interactions.⁶⁴ The robust nature of the halogen(I) complexes, and the tunability of their strength, together with the possibility of the alteration of the electron density in the three-centered system, has made them a reliable tool both in the construction of large supramolecular structures⁷¹⁻⁷³ and in synthetic chemistry.³⁴

1.2 Fluorescence and non-covalent interactions

Photophysical and photochemical processes are initiated by the absorption of light (a photon) resulting in the formation of electronically excited states. If the energy of a photon interacting with a chromophore (a light-absorbing molecule) corresponds to an energy of the quantized electronic energy levels of the molecule, light is absorbed.⁷⁵ The excited states of a molecule can undergo a variety of relaxation processes described by the Jablonski diagram (Figure 7) where the absorbed energy is dissipated.

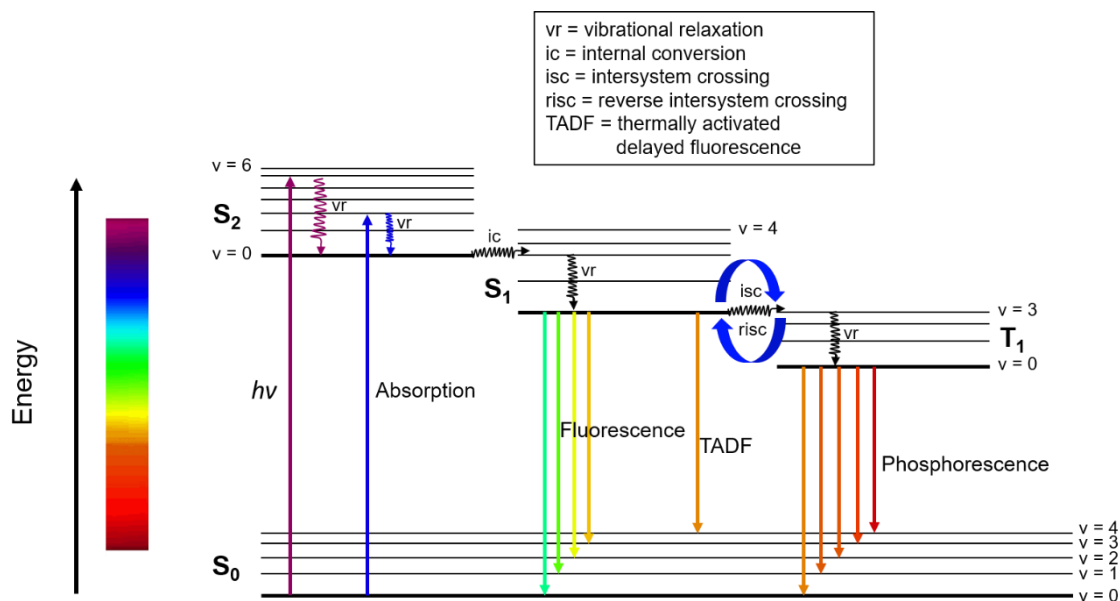


Figure 7 Illustration of a Jablonski diagram depicting excited state (S_1 , S_2 , T_1) photo-physical processes in organic molecules.

The absorption of light occurs from the ground state (S_0) to an excited state (S_n , where $n = 1, 2, \dots$). Each electronically excited state (S_n , T_n) is further divided into vibrational energy states (v) of different energies. The energy of the excited states can be dissipated through non-radiative (non-emissive) transitions *i.e.*, vibrational relaxation (vr), internal conversion (ic), and intersystem crossing (isc).⁷⁵ Vibrational energy levels of $v \neq 0$ lose their energy through a non-radiative process called vibrational relaxation. This process occurs within $10^{-13} - 10^{-9}$ s due to excess vibrational energy leading to collisions with one another or solvent molecules and resulting in relaxation to the lowest vibrational energy of the same electronic energy level. According to Kasha's rule, radiative transitions occur from the lowest-lying electronic state (S_1).⁷⁵ Therefore, in absorption to a higher electronic state, *e.g.* S_2 , the energy is first relinquished through a series of vibrational relaxations and internal conversions from a higher energy electronic state eventually to the lowest vibrational energy level of the lowest-lying electronic state (S_1). Kasha's rule stems from the fact that internal conversion is a rapid process ($10^{-14} - 10^{-11}$ s) ultimately preceding any radiative process.⁷⁵

From the lowest-lying electronic singlet-excited state, the energy can undergo two processes: fluorescence or intersystem crossing.⁷⁵ Fluorescence is a radiative process originating from the S_1 excited state. The rate of fluorescence is typically $10^{-12} - 10^{-6}$ s and it can be seen at a longer wavelength (lower energy) in comparison to an absorption spectrum.⁷⁵ The ratio of the number of photons emitted to the number of photons absorbed gives out fluorescence quantum yield (Φ), which is independent of the excitation wavelength (wavelength of the absorbed light) and can be determined for a molecule with using a reference compound of a known fluorescence quantum yield.⁷⁶ Equation 1⁷⁶ is used in the experimental determination of quantum yield.

$$\Phi = \Phi_{ref} \frac{\eta^2}{\eta_{ref}^2} \frac{I}{I_{ref}} \frac{A_{ref}}{A} \quad (1)$$

In which, Φ is the quantum yield, η is the solvent refractive index, I is the integrated fluorescence intensity, and A is the absorbance of the compound at the excitation wavelength.

The molecular structure determines whether the system undergoes fluorescence or intersystem crossing (ISC). Molecules with lone pairs induce the formation of an n,π^* S_1 excited state, which is longer-lived and susceptible to intersystem crossing due to a smaller energy gap between the S_1 and T_1 states increasing the rate (10^{-11} – 10^{-8} s) of ISC, whereas π,π^* states have shorter lifetimes and are more prone to result in fluorescence.⁷⁵ Additionally, the presence of heavy atoms, such as Br or I, in a molecule results in enhanced spin-orbit coupling and increased ISC.^{75,76}

Phosphorescence can occur after ISC and VR to the lowest-lying triplet state. It is a radiative transition to the ground state with a lifetime of 10^{-3} – 10^{-2} s and is generally observed at higher wavelengths than fluorescence. The longer lifetime of the triplet state renders it susceptible to quenching (non-radiative energy loss) by other molecules (like oxygen) and is therefore not readily observed in room temperature solutions.⁷⁵

Another possible route for the dissipation of triplet state energy is thermally activated delayed fluorescence (TADF).⁷⁵ The characteristics of TADF are very similar to fluorescence, yet it occurs with lifetimes similar to phosphorescence. In this process, intersystem crossing occurs from S_1 to T_1 , yet instead of phosphorescence, the process is thermally activated to result in reverse intersystem crossing (RISC) from T_1 to S_1 where the fluorescence originates.^{75,77} Emission of TADF molecules can be determined with variable temperature measurements by the decreasing fluorescence intensity with lower temperature indicating an energy barrier involved in the process.

1.2.1 Non-covalent interactions and fluorescence in heterocyclic compounds

Generally, most fluorescent molecules are aromatic or highly unsaturated.⁷⁶ The structure of the compound affects the nature of its lowest-lying electronic states and, therefore, its luminescent properties. When heteroatoms are involved in aromatic systems, the lowest-lying electronic state is often n,π^* in nature.⁷⁶ Therefore, heterocyclic aromatics often possess low quantum yields. Furthermore, electron-donating substituents increase the fluorescence of the compound. For example, the lone pairs of a hydroxy group are involved in the aromatic system and do not change the nature of the lowest-lying electronic state.⁷⁶ In contrast, electron-withdrawing substituents reduce the fluorescence quantum yield.⁷⁵

In addition to smart molecular design, non-covalent interactions can be used in fluorescence modulation. Nitrogen heterocyclics commonly possess the non-emissive n,π^* lowest-lying electronic state stemming from the nitrogen lone pair, which is not delocalized in the aromatic system.⁷⁶ However, protonation or even hydrogen and halogen bonding can reverse the order of the lowest-lying

electronic state from n,π^* to π,π^* making the compound fluorescent.⁷⁶ Chen *et al.*, reported an acid-induced tunable multicolor fluorescence of pyridazine derivative with good reversibility and high sensitivity.²⁶ Additionally, protonation has been reported to lower the singlet-triplet energy gap resulting in greater ISC through a new intramolecular charge-transfer state.⁷⁸ Moreover, a carbazole-based emitter was reported with tunable emission through halogen bond assisted intramolecular charge-transfer.⁷⁹

1.2.2 Solid-state fluorescence

The fluorescence of a system is heavily affected by its surroundings. In general, molecular rotation decreases the fluorescence intensity. This can be affected by the molecular design; rigid molecules are generally observed with higher luminescence,⁷⁵ or by rigidifying the surrounding medium by either solid-state crystallization or a polymer matrix in a thin film.

Highly fluorescent molecules often consist of multiple aromatic rings making the system planar. Whereas these molecules exhibit strong fluorescence in solution, the aggregation induced by the planarity of the system might result in aggregation-induced quenching.⁸⁰ However, many applications require the molecules to perform in the solid-state. Molecules with aggregation-induced emission due to the reduction of intramolecular rotation have been observed.⁸⁰ Molecules possessing molecular rotors may dissipate all the excited state energy through intramolecular rotation, which leads to fluorescence quenching. However, the aggregation in the solid state restricts this motion and the energy is forced to dissipate through a radiative pathway.⁸⁰

Molecular packing modes and the intermolecular interactions strongly affect solid-state luminescence.⁸¹ In general, strong intermolecular π - π interactions have been determined as the primary reason for fluorescence quenching in the solid-state.⁸² Furthermore, integration of steric groups in the molecular structure limits tight packing in the solid-state and can improve emission properties by limiting the intermolecular vibrational relaxations.⁸¹ In addition, J-type⁸³ zigzag packing in a solid crystalline state has been associated with a bathochromic shift (to longer wavelengths), which minimizes self-absorption and leads to enhanced luminescence.⁸⁴ Therefore, molecular stacking in a zigzag manner and greater intermolecular distances in the solid state may facilitate stronger fluorescence by reducing the effects of aggregation-induced quenching.⁸¹

1.3 Host-guest chemistry

Non-covalent intermolecular interactions lay the foundation of *Supramolecular Chemistry*. Often called “weak” interactions, they not only come together forming very strong assemblies, but are also reduce the synthesis workload thanks to self-assembly. Self-assembly is a spontaneous process where smaller components organize into larger assemblies or structures using non-covalent interactions.⁷ In

self-assembly, the often preorganized ligands in a spontaneous reaction with other components result in a free energy minimum of the system, therefore forming a new larger and more stable structure.⁸ This phenomenon is widely exploited in crystal engineering, in which molecular recognition occurs in solution and the components pack together as closely as possible, directed by their inherent steric and electronic properties.³ In the solid state, the resulting structure is largely governed by the crystallization conditions, whereas in solution, it is an equilibrium reaction resulting in the most stable structure.³

Clathrates or *cages* as supramolecular host-guest assemblies involve the imprisonment of a *guest* molecule within a lattice or a *host* molecule. The term *clathrate* was first defined by H. M. Powell in 1948 as an inclusion compound:

...in which two or more components are associated without an ordinary chemical union, but through the complete enclosure of one set of molecules in a suitable structure formed by another.³

Generally, *clathrates* are considered as solid-state inclusion compounds, where a guest molecule is trapped into a host matrix, commonly a crystal lattice, whereas host-guest systems include structures such as *capsules* and *cages*, which comprise of one or two molecular components, that along with a guest molecule can spontaneously self-assemble to form capsular assemblies in which the guest is trapped inside the host entity (Figure 8).³

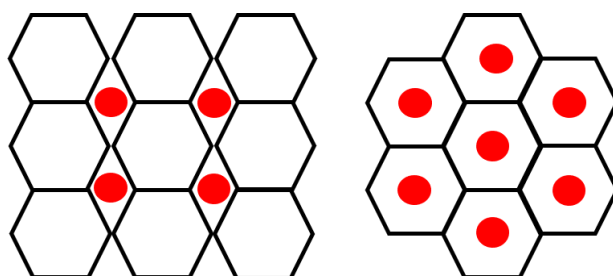


Figure 8 A description of a clathrate (left) and a traditional host-guest assembly (right) in which the hexagonal shapes depict the host molecules and the red circles depict the guest molecules.

A host molecule is generally a larger molecule of suitable conformation and converging binding sites for a guest molecule, whereas a guest molecule is usually a smaller molecule with diverging binding sites.³ A host that does not undergo a significant conformational change upon complexation (formation of a host-guest *complex*) is preorganized. Preorganization plays a major role in host-guest complexation since it lowers the activation energy needed for the complex formation. The possibility of encapsulating various guests inside the hosts has resulted in an array of applications for such complexes including biomedical applications,¹⁰ selective encapsulation,¹¹ and stabilization of reactive compounds.⁹ In 1993, Rebek's hydrogen-bonded capsule proved that the ability to predict and control,⁸⁵ with careful design, allows spontaneous formation of multi-component aggregates and led to major advancements in encapsulation chemistry. Paralleling this

rapid development, the term supramolecular synthon was specified to be a structural motif (*e.g.* hydrogen or halogen bond) and it is nowadays widely exploited in host-guest chemistry and crystal engineering.¹⁹

1.3.1 Hydrogen-bonded capsular assemblies

The prevalent nature of hydrogen bonds has extensively been utilized in the design of supramolecular capsules. Hydrogen bonding between two or more pre-organized calixarene molecules,⁸⁶⁻⁸⁸ including resorcinarenes⁸⁹⁻⁹¹ and pyridinarenes,^{92,93} render them capable of forming dimeric or multimeric capsules encapsulating both neutral and positively charged guests with $\text{CH} \cdots \pi$ and cation- π interactions.⁹⁴ Their three-dimensional bowl-shaped cavity stabilized by intramolecular $\text{O}-\text{H} \cdots \text{O}$ HBs on the upper rim of the molecule and the aromatic rings offering an electron-rich interior as a binding site make these an interesting class of phenolic macrocyclic receptors.⁹⁵ The self-assembly, easy availability, and versatile nature of resorcinarenes has inspired the work on HB capsules since the 1990s,⁹⁶ possibly making them the most studied HB capsular components. What has made resorcinarenes particularly interesting is that the capsule is often formed with bridging solvent molecules. In 2000, Rissanen *et al.* crystallized a dimeric resorcinarene bridged by water molecules and encapsulating a tertiary amine.⁹⁷ In solution, the formation of the capsule was found to be solvent dependent, with competing solvents, such as DMSO and methanol, disrupting the capsule formation.⁹⁷ So far, resorcinarenes have found applications in mimicking biological phenomena (such as enzyme binding), drug release, and microreactors in catalysis.^{90,98}

Figure 9 depicts two dimeric resorcin[4]arene capsules from ethyl resorcinarene and the corresponding 2-methyl derivative.^{91,99} Capsule **8** was formed with a co-crystallization of resorcinarene with a diquat dibromide in aqueous methanol. The resulted crystal structure is composed of a dimeric capsule encapsulating the diquat cation in the electron-rich interior of the capsule and simultaneously binding the bromide anions at the lower rim ethyl groups of the resorcinarene molecules *via* weak $\text{CH} \cdots \text{Br}$ interactions. This interesting structure forms a perfect cone shape in the resorcinarene molecules which is further stabilized by the intramolecular HBs on the upper rim of the molecule. The two halves of the capsule interact through four methanol and eight water molecules, the whole capsular assembly consisting of 20 intermolecular HBs binding the two halves together. A similar 2-methylresorcinarene dimeric capsule was reported more recently,⁹⁹ also bridged through two methanol and two water molecules. Capsule **9** involves an encapsulation of 1,4-diammoniumcyclohexane carrying a positive charge at both ends of the guest molecule. The larger size of the guest and the positively charged nitrogen atoms interacting with the water molecules through $\text{NH} \cdots \text{O}$ interactions, in addition to guest-host $\text{NH} \cdots \pi$ interactions, resulted in a more slanted conformation and an extremely high packing coefficient (the ratio of the molecular volume of the guest divided by the host cavity volume) of 84.2%. However, resorcinarenes are not limited to these dimeric structures, gigantic

structures of a hexameric nature have been observed as well,¹⁰⁰ opening even more potential for guest binding opportunities.

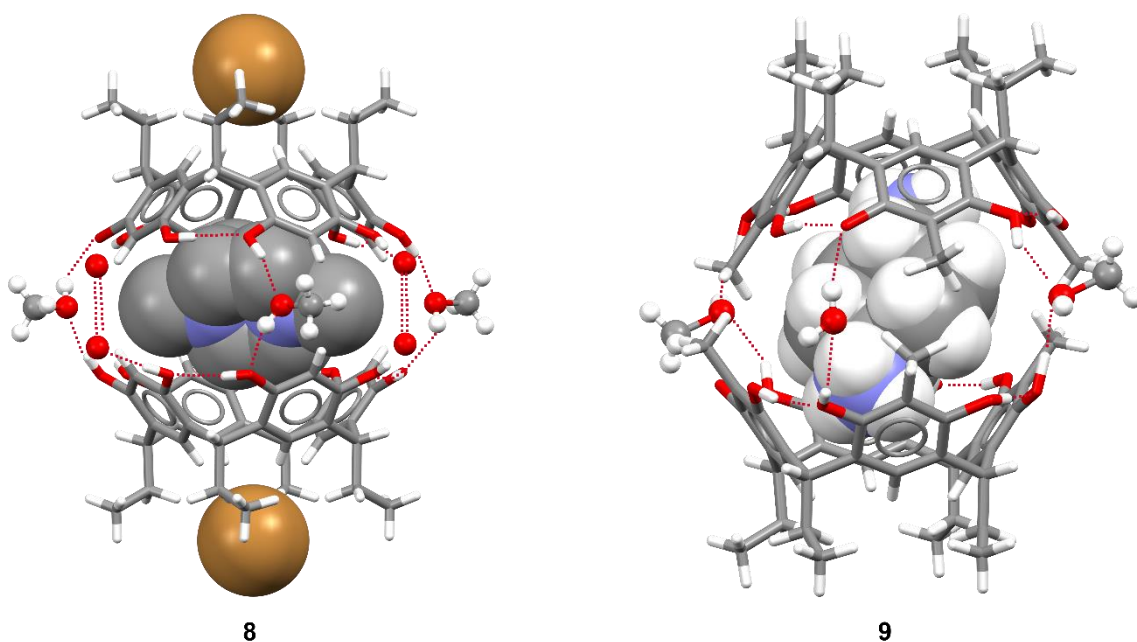


Figure 9 Hydrogen-bonded (red-dotted lines) solvent-bridged resorcinarene capsule encapsulating diquat cation (**8**) CSD ref. code: XOTKOG¹⁰¹ and 2-methylresorcinarene encapsulating *trans*-1,4-diammoniumcyclohexane in solvent-bridged capsule (**9**). CSD ref. code: SEQMUZ.⁹⁹

1.3.2 Halogen-bonded capsular assemblies

Similar to hydrogen bonding, though much more recently, halogen bonds have also been utilized in the formation of supramolecular capsular assemblies. In contrast to the HB capsular assemblies, the XB capsules take advantage of the unique directionality of the XB bond as well as their hydrophobic nature.

Resorcinarenes have found multiple uses also due to their ease of functionalization.⁸⁹ The first reports of XB bonded capsules also involved the resorcinarene backbone now functionalized with known XB acceptor moieties (pyridyl). Aakeröy *et al.* synthesized a tetra-functionalized halogen bond donor by attaching iodotetrafluorobenzene to a flexible ethylenedioxy glycol chain in a calix[4]arene derivative (Figure 10).¹⁰² A slow evaporation of the flexible tetra(4-iodotetrafluorophenyl)calix[4]arene in a self-assembly process with a rigid tetra(3-pyridyl)cavitand resulted in a first structurally characterized halogen-bonded capsular assembly. The congestion caused by the iodotetrafluorobenzene molecules resulted in 40% of the capsule being partially opened by sacrificing one of the bonding $N \cdots I$ interactions. However, the results of this publication¹⁰² shed light to new XB capsules in the solid-state.

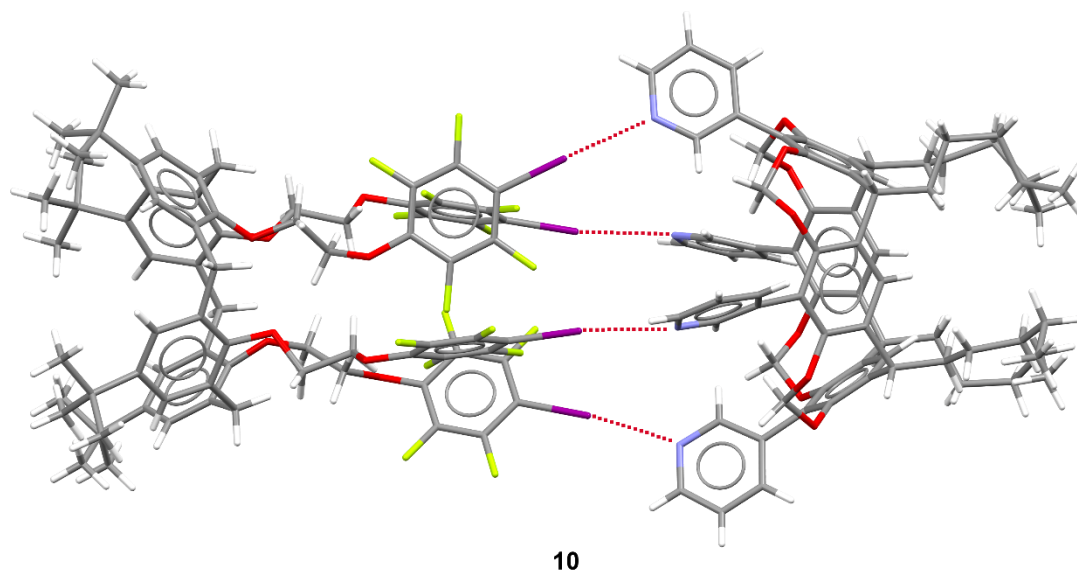


Figure 10 First reported crystal structure of a halogen-bonded (red-dotted lines) capsular assembly (**10**) by Aakeröy *et al.* CSD ref. code: DEGWET.¹⁰²

Three years later and inspired by the Aakeröy *et al.* work,¹⁰² Rissanen *et al.* reported a dimeric resorcinarene capsule (Figure 11) solely based on halogen bonding.²² Iodine acts as a bifunctional XB donor connecting the two resorcinarene cavities by interacting with the chloride anions in the *N*-cyclohexyl ammonium resorcinarene chloride. The $\text{Cl}^- \cdots \text{NH}_2^+$ ionic interaction along with the HBs on the upper rim, which resorcinarenes are known for, help stabilize the concave shape of the capsule molecules. The formation of the capsule through halogen bonding results in encapsulation of three 1,4-dioxane molecules with a packing coefficient of 55% and R_{XB} values ranging from 0.77 to 0.94.²² The small size of the I_2 used as the XB donor has its advantages of not being sterically hindered and having wider opportunities in the capsule formation, though the weaker halogen bonds were postulated to only persist in the solid state.

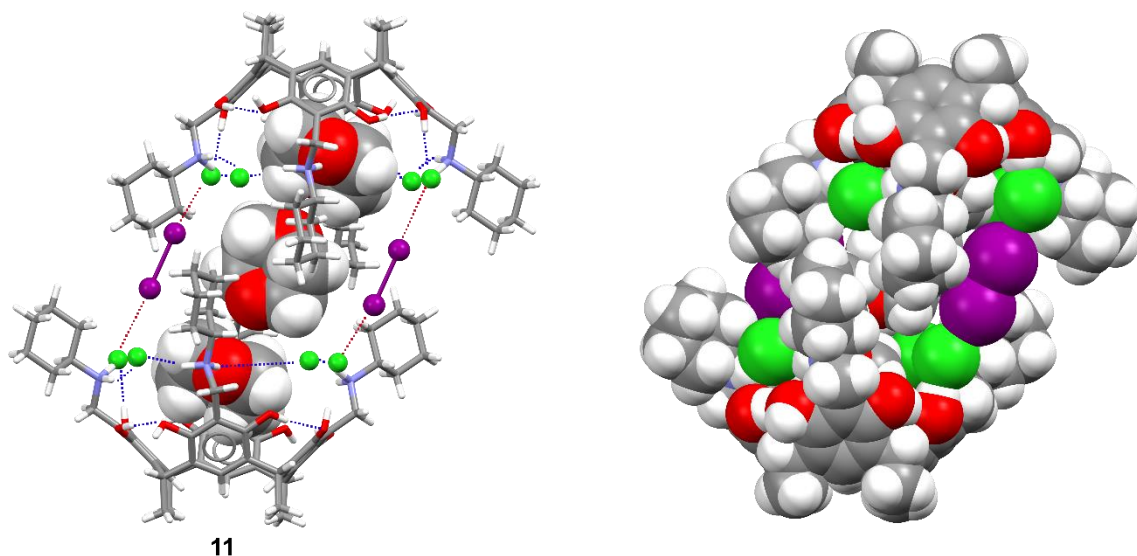


Figure 11 First host-guest capsular assembly (**11**) based solely on XBs. CSD ref. code: CALJUX.²²

Despite classical XB being used in capsular assemblies, very few reports on capsular assemblies based on halogen(I) ions have emerged.^{71–73,103} The extreme strength and robust nature of the $[N-X-N]^+$ halogen bond have made the detection of halogen(I) capsular entities possible both in the solution and gas phase.^{71,72,103} However, perhaps the “anionophobic” nature of the iodine(I) cation has made the observation of the solid-state structures of these capsules more difficult and so far only one dimeric iodine(I) capsule X-ray structure has been obtained (Figure 12).⁷³

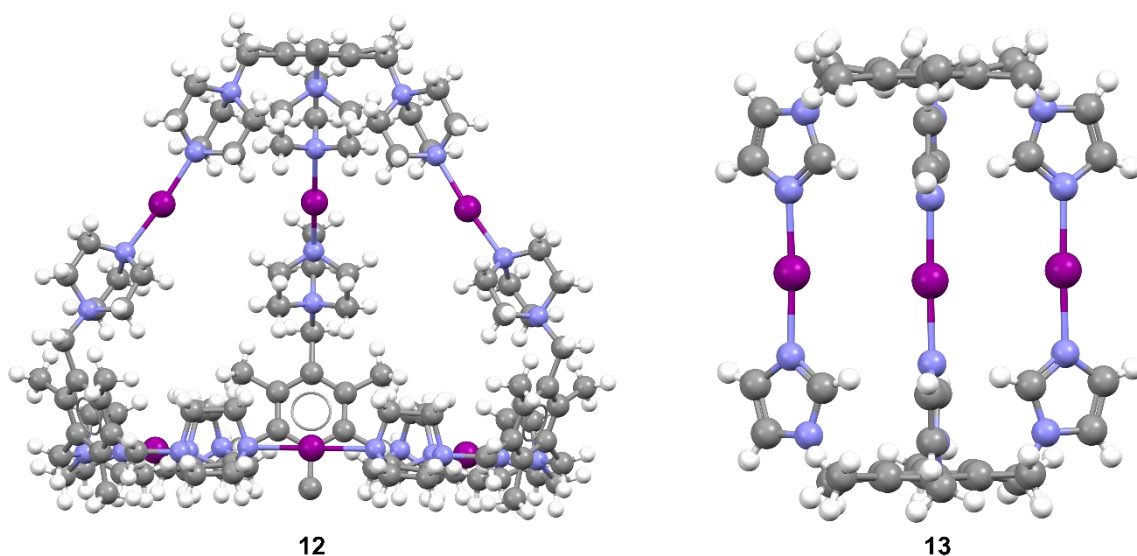


Figure 12 First examples of tetrameric (**12**) and dimeric (**13**) $[N-I-N]^+$ halogen-bonded capsular assemblies.⁷³

Rissanen *et al.* reported the synthesis and characterization of halogen(I) cages of rigid cationic ligand (**12**) and a flexible tripodal ligand (**13**) through the silver(I)

precursor metallocage formation.⁷³ The crystallization of **12** from slow evaporation of acetonitrile resulted in a tetrameric I₆L₄ cage with N–I distances of 2.26 – 2.35 Å. The bond lengths were deemed less symmetric than generally observed for symmetric [N–I–N]⁺ complexes^{67,70,104} however, the bond angles remained close to the linear geometry (>175°) preferred by the iodine(I) cation.⁷³ Significant differences were observed for the more flexible and neutral cage formed by the self-assembly of two 1,1',1''-((2,4,6-trimethylbenzene-1,3,5-triyl)tris(methylene))tris(1*H*-imidazole) molecules. The corresponding cage (**13**) crystallized from slow evaporation of acetonitrile with hexagonal symmetry, and therefore, all bond lengths and angles were symmetrical and close to linear (2.233(6) Å, 177.0(4)°). The results of these studies are what partly inspired the work within this thesis.

1.4 HB and XB acceptors

Anions and neutral nucleophilic molecules can act as HB and XB acceptors.²⁸ The most widely exploited HB and XB acceptor atom is nitrogen possessing a lone pair of electrons capable of these interactions. Figure 13 displays a set of commonly utilized HB and XB acceptors, all derivatives of pyridine (**14**). Other aromatic compounds (such as *N*-alkyls and π -systems) are also suitable as acceptor molecules. However, and especially in the case of halogen(I) complexes, the aromaticity of the acceptors is a stabilizing factor through the enhanced charge-transfer interactions between the halogen(I) cation and the nucleophilic nitrogen atoms.^{34,57,58}

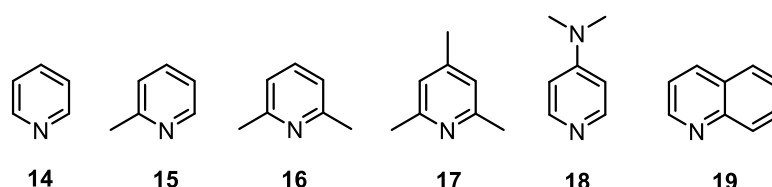


Figure 13 Examples of the commonly used pyridine derivatives as HB and XB acceptors.

As mentioned, stronger Lewis bases, as better HB and XB acceptors, are known to form stronger HB and XB interactions.^{36,37} The ease of functionalization, and therefore tunability, of pyridine as an acceptor moiety has made it widely popular in simple halogen-bonded complexes, yet pyridine and its derivatives are also commonly exploited in the construction of more complex acceptor molecules. In the following sections, aromatic amines relevant to this thesis work are described.

1.4.1 Quinolines

Quinoline (benzo[*b*]pyridine) has been known since the early 1800s.¹⁰⁵ Quinoline and isoquinoline were historically extracted from coal tar,¹⁰⁵ however, various

quinolines are now commercially available. Quinolines are prime examples of pyridine functionalization and molecular structures with multiple aromatic rings have been designed. The enhanced aromaticity in the molecular structure generally produces photoactive compounds with interesting features. Quinoline (**19**) and its benzo derivatives are weak bases and form salts with strong acids.¹⁰⁶ They are abundant in nature and possess a large variety of biological activities.^{106,107} Quinoline and its derivatives have been shown to have antimalarial, antifungal, and anticancer activities, amongst others, and are commonly used in medicinal chemistry.^{106,107} Figure 14 displays chemical structures of isoquinoline (**20**), acridine (benzo[*b*]quinoline) (**21**) and benzo[*h*]quinoline (**22**).

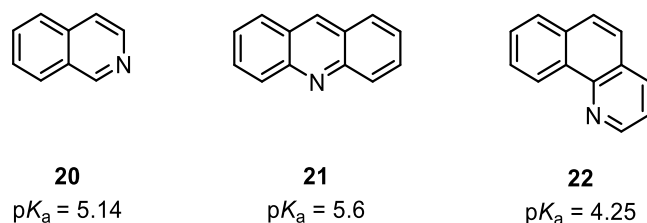


Figure 14 Structures of isoquinoline (**20**), acridine (**21**), and benzo[*h*]quinoline (**22**) with their corresponding pK_a values.

The delocalized electron rings on quinoline derivatives, especially on **21** and **22** as the aromaticity increases, make them suitable as luminescent materials. Moreover, acridine and its derivatives are used as dyes, fluorescent sensors and in laser technology.¹⁰⁸ However, *N*-heterocyclic compounds are known to be weakly fluorescent in comparison to their isoelectric hydrocarbons, as the nitrogen lone pair gives rise to $n-\pi^*$ excited states resulting in spin-orbit coupling and, therefore, loss in fluorescence quantum yield.¹⁰⁹⁻¹¹¹

Compounds **20**, **21**, and **22**, are all suitable HB and XB acceptors possessing nucleophilic regions in the form of the nitrogen lone pairs. However, the steric hindrance of the nearby hydrogens in **21** and **22** might interfere with XB formation due to the larger size of a halogen in comparison to a hydrogen atom.

1.4.2 Imidazoles

Imidazole is a molecule with an aromatic five-membered ring and two annular nitrogen atoms at the 1,3-positions. Figure 15 presents imidazole (**23**), a few of its common derivatives (2,2-dimethyl-2*H*-imidazole **24** and 1*H*-benzo[*d*]imidazole **25**), and the chemical structure of histamine (**26**), an example of imidazole's abundance in biological compounds. Moreover, imidazoles are amphoteric in nature and can act both as an acid or a base.¹¹² With a pK_a value of 7, imidazole is slightly more basic than pyridine. Much like quinolines, imidazole also plays an important role in biological systems and is known to have diverse biological activity as, *e.g.*, antibacterial, anticancer, and antifungal agents.¹¹² It is a key structure in biological compounds such as histidine, vitamin B12, and biotin.¹¹²

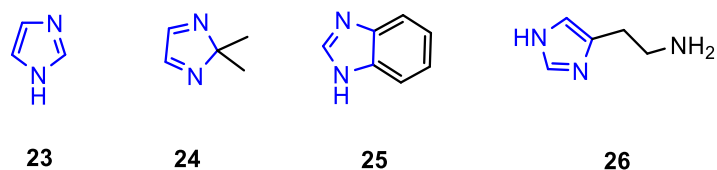


Figure 15 Chemical structures of imidazole (**23**) and its common derivatives 2,2-dimethyl-2H-imidazole (**24**), 1H-benzo[d]imidazole (**25**), and histamine (**26**).

Besides their biological importance, imidazoles have been utilized in crystal engineering. Park *et al.*⁸¹ synthesized a novel class of hydroxy-substituted tetraphenyl imidazole compounds (**27**, Figure 16), which in the solid state, form intermolecular interaction mediated packing, reducing the non-radiative relaxation processes and producing strongly fluorescent crystals associated with excited-state intramolecular proton transfer. The incorporation of the tetraphenyl group with an extended π -framework on the imidazole increases the photoactive nature of the compound, however, the planar aromatic rings often lead to tight packing in the solid state, which then results in intermolecular vibronic relaxations leading to fluorescence quenching. By adding steric groups (OAc) to the molecule, Park *et al.* successfully synthesized strongly fluorescent imidazole-based single crystals by suppressing the concentration quenching of fluorescence by maintaining proper intermolecular distances.⁸¹

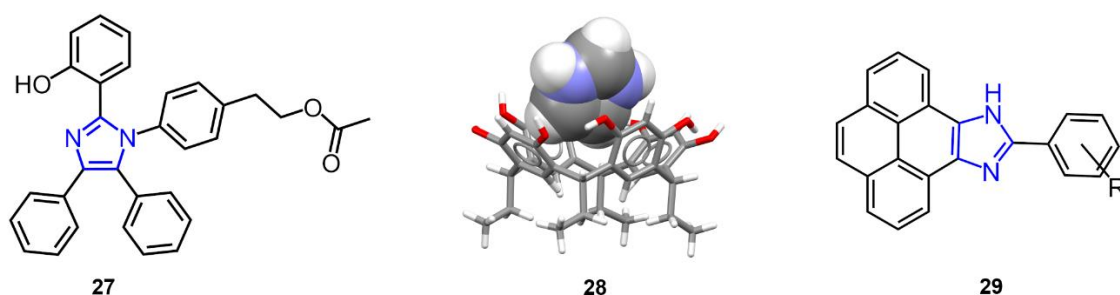


Figure 16 Imidazole-containing compounds **27**,⁸¹ **28**,¹¹³ (CSD ref. Code: EMOZOV¹¹³) and **29**¹¹⁴ were studied for their intermolecular interactions and the effect on crystal packing, fluorescence properties, and inclusion compounds.

Furthermore, Rissanen *et al.* investigated the solid-state complexation and deprotonation of resorcinarene with aromatic *N*-heterocycles.¹¹³ Imidazole was found to spontaneously form inclusion compounds with resorcinarene (**28**, Figure 16) by forming intermolecular interactions (π - π and $\text{CH} \cdots \pi$) inside the resorcinarene cavity. The Lewis basic nature of imidazole leads to deprotonation of the resorcinarene, and the imidazole is therefore tightly bound inside the cavity as an imidazolium cation, ensuring stronger interactions with the resorcinarene host. Moreover, deprotonation of the resorcinarene host was not observed with the other *N*-heterocycles under investigation.¹¹³

Zhao *et al.* synthesized a series of phenyl-substituted π -conjugated pyrene-imidazole systems (**29**, Figure 16) and thoroughly examined their photophysical properties and crystal packing.¹¹⁴ In the solid state, the π - π interactions and

hydrogen bonding were determined as directing interactions in the crystal packing. In addition, they investigated the influence of various substituents on the fluorescence of these aromatic systems. Weak-to-moderate electron-withdrawing and donating substituents had no significant effect on the UV-Vis, however, strongly electron-withdrawing groups led to the deprotonation of the imidazolyl N-H giving rise to substantial changes in the photophysical properties of the studied compounds.¹¹⁴

The results highlighted here come to show the versatile nature of the imidazole moiety, the abundance in biological systems, and the utility of the amphoteric nature it possesses. The practicality of imidazole stems from its ability to form intermolecular interactions in such versatile systems, and will most definitely, be utilized in many more future studies.

1.4.3 Carbazoles

Carbazoles are *N*-heterocyclic compounds consisting of two benzene rings fused onto a five-membered pyrrole ring. Like quinolines and imidazole, carbazole is widespread in nature and possesses biological activities including anticancer, antibacterial, anti-histaminic, antioxidant, and is used in commercial drugs.^{115,116} Moreover, carbazole has strong absorption in the UV region and blue-light emission, which has been applied in photovoltaic devices,¹¹⁷ organic light-emitting diodes (OLEDs),¹¹⁸⁻¹²⁰ and molecular rotors.¹²¹ The low cost, ease of functionalization, high thermal and chemical stability make carbazoles enticing components in synthetic design.^{120,122,123} Moreover, carbazole has a high triplet energy ensuring efficient energy transfer and easy charge injection for optimal device performance, which has made it extensively utilized in the design and construction of blue-light emitting diodes.¹²⁴

The ease of functionalization has produced countless carbazole derivatives since its first discovery in 1872.¹²⁵ Examples of carbazole functionalization for different applications is depicted in Figure 17. Structures **30** and **31** are compounds utilized as bipolar materials (having separated electron donors and acceptors) in OLEDs for carbazoles' good hole-transporting properties.¹¹⁹ Unsurprisingly, carbazole is widely used in OLEDs demonstrated by an ever-increasing number of significant results being published. Li *et al.* studied the importance of molecular engineering on the performance of host materials with a series of carbazole hosts (**30**) and reported devices with high efficiencies (23.1%) and great thermal stabilities.¹²⁴ Compound **31** uses carbazole's electron-rich core as the electron-donating moiety and a quinoline as the electron-accepting group. Utilizing **31** as a host material in phosphorescent OLED (PhOLED) devices, an external quantum efficiency of 25.6% was achieved, which for orange PhOLEDs with a single host material is rare.¹¹⁹

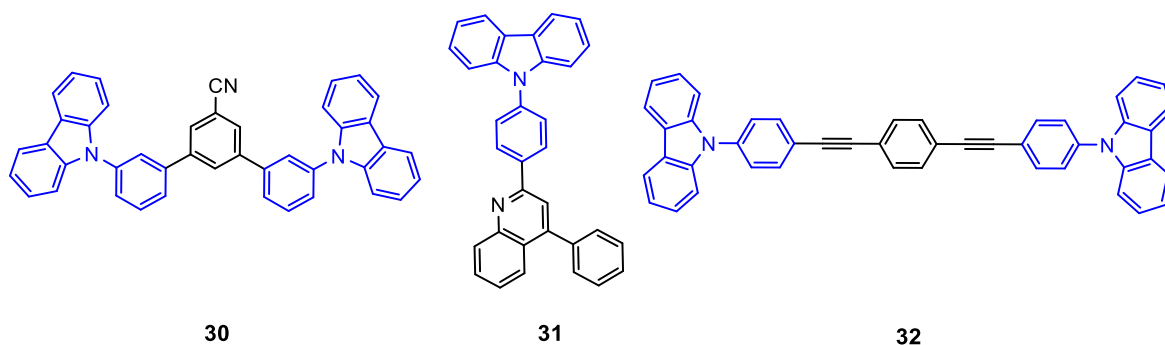


Figure 17 Carbazole derivatives utilized as bipolar host materials in OLEDs (**30**¹²⁴, **31**¹¹⁹) and luminescent molecular rotors (**32**).¹²¹

Slightly different usage for the carbazole moiety was devised in the form of a molecular rotor.¹²¹ In compound **32**, 1,4-diethynylbenzene is used as a rigid spacer between two carbazole units with a great ability to form edge-to-face interactions with other carbazoles. The crystallization of **32** resulted in simultaneous solid-state internal rotation and enhanced fluorescence with $\Phi = 0.28$ when compared to its THF solution ($\Phi = 0.06$). In addition to carbazole's other various possibilities, the high demand for efficient blue-light emitting diodes with long lifetimes remains an issue, which is why carbazole derivatives will continue to be an intriguing subject of study.

2 RESULTS AND DISCUSSION

2.1 Aim of the work

The aim of this work was to probe supramolecular interactions in a novel context. The study involved the synthesis of new hydrogen and halogen bond acceptors, which served as multipurpose targets toward fluorescent emitters, and ligands in discrete silver(I) and iodine(I) complexes, as well as tripodal ligands for halogen-bonded supramolecular cages. The chapter 1.4 above introduced quinolines, imidazoles, and carbazoles, and reasoned the interest for their synthesis and utilization within this work.

The thesis work is based on four individual publications starting from small commercial XB acceptors and developing into larger iodine(I) based cage complexes. Non-covalent bonds commonly benefit from the cooperative effect in their bulk material, however, the effect of a single bond was studied in the first publication^I in the form of fluorescence modulation in quinoline derivatives. Furthermore, in addition to the effect of the charge-assisted hydrogen bond in the fluorescence modulation, the second publication^{II} investigated the accumulative effect of the intermolecular interactions in single crystals. Both hydrogen and halogen bonds were found intriguing, and the third publication^{III} focused on the synthesis and characterization of iodine(I) complexes with the extremely strong 3c-4e halogen bond. Inspired by this work, and previous publications,⁷³ the fourth publication^{IV} set out to synthesize and characterize iodine(I) capsular assemblies based on the tripodal ligands, which in turn are prepared from the smaller ligands used in publications I - III.

Techniques of steady-state absorption and fluorescence spectroscopy,^{I,II} in addition to nuclear magnetic resonance spectroscopy (NMR)^{I-IV} were utilized in solution, single crystal X-ray diffraction^{I-IV} in the solid state, mass spectroscopy^{IV} in the gas phase together with some theoretical methods, such as time-dependent density functional theory (TD-DFT)^{III} and Hirshfeld surface analysis.^{IV}

2.2 Materials and design

Acid interaction with a nucleophilic region results in proton transfer and the formation of an ion pair. A hydrogen atom is transferred from an acidic site to a Lewis basic site resulting in a negatively charged anion from the acid and a positively charged cation from the base. The opposite charges attract each other and connect through charge-assisted hydrogen bonding. The strength of the interaction can be affected by altering the substituents on the acids, and therefore, affecting the stability of the counter anion resulting from the protonation. Generally, a larger size of the substituent atom and greater electronegativity decrease pK_a indicating a stronger acid.¹²⁶ This is depicted in Figure 18, in which a range of acetic acids (along with one aromatic sulfonic acid) are shown along with their corresponding pK_a values.

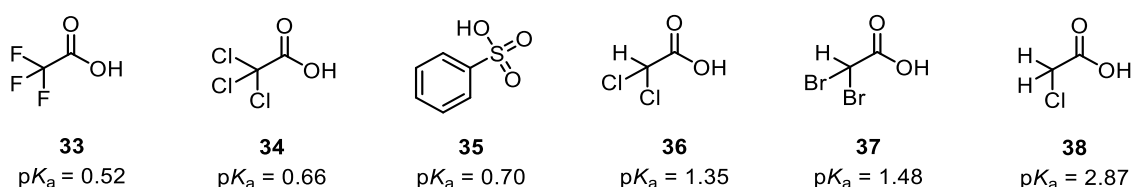


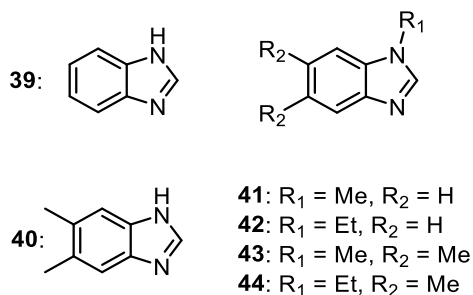
Figure 18 Hydrogen bond acceptors (Lewis acids) of varying pK_a values in ionic pairs after proton transfer.^{I,II}

The acids depicted in Figure 18 were used in original papers **I** and **II** in the evaluation of the effect of protonation on fluorescence modulation of quinoline and carbazole derivatives. A range of acetic acids was chosen to limit the effect of the counter anion stability, yet one aromatic acid was also included to probe this very subject.

2.2.1 Syntheses of ligands

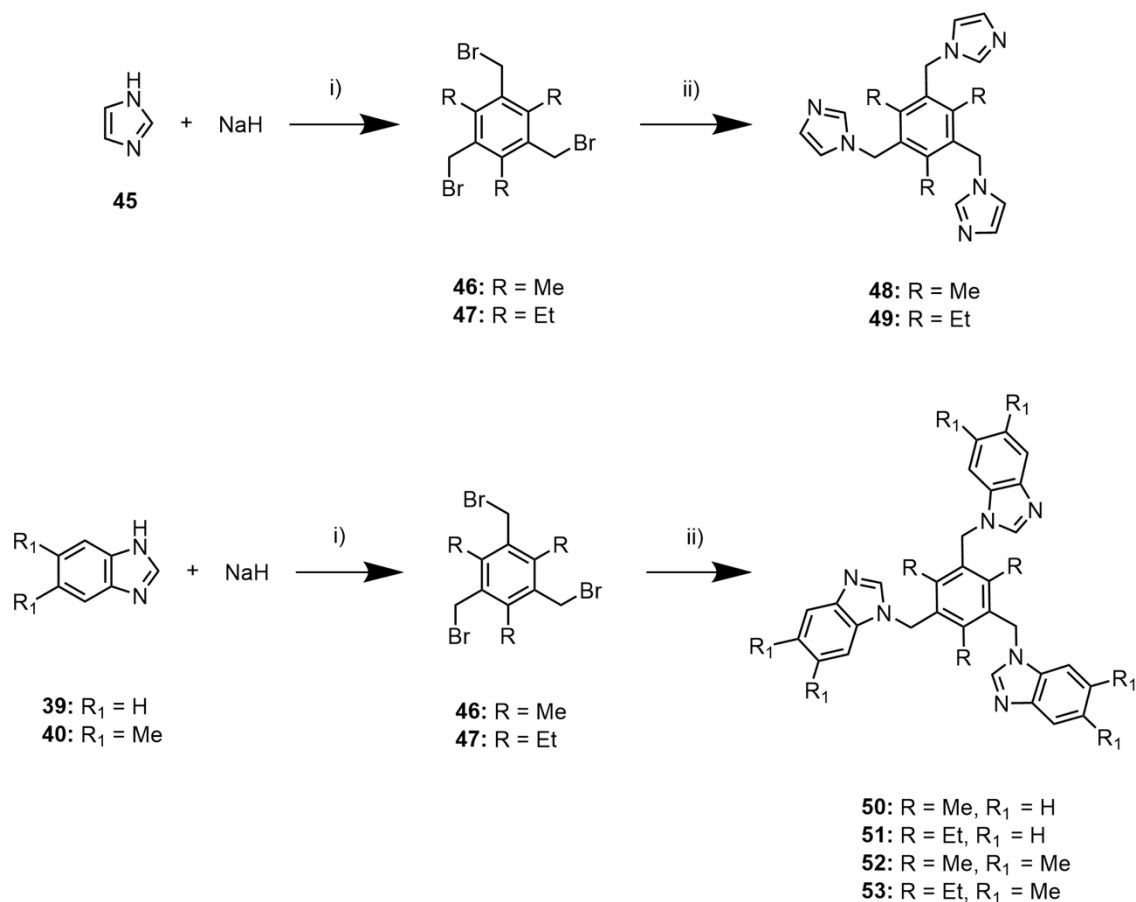
2.2.1.1 Syntheses of imidazole-based ligands^{III,IV}

Small imidazole-based ligands **41-44** (Scheme 1) were synthesized using either **39** or **40** and a previously reported method for compound **39**.^{127,III} The starting material is first deprotonated with 25% aqueous NaOH in acetonitrile followed by the addition of either iodomethane or bromoethane for the corresponding methylation and ethylation reactions, respectively. The reactions resulted in the corresponding ligands **41-44** with yields of 52-91%.



Scheme 1 Chemical structures of the synthesized small imidazole-based ligands **41-44**.^{III, IV}

The resulting small ligands were further utilized in the syntheses of tripodal ligands **48-53** (Scheme 2).^{128, IV} A controlled reaction of imidazole with **46** under basic conditions resulted in the formation of ligand **48**.¹²⁸ Similar reaction conditions with an alteration of the solvent for increased solubility were used in the synthesis of the remaining tripodal ligands **49-53**.

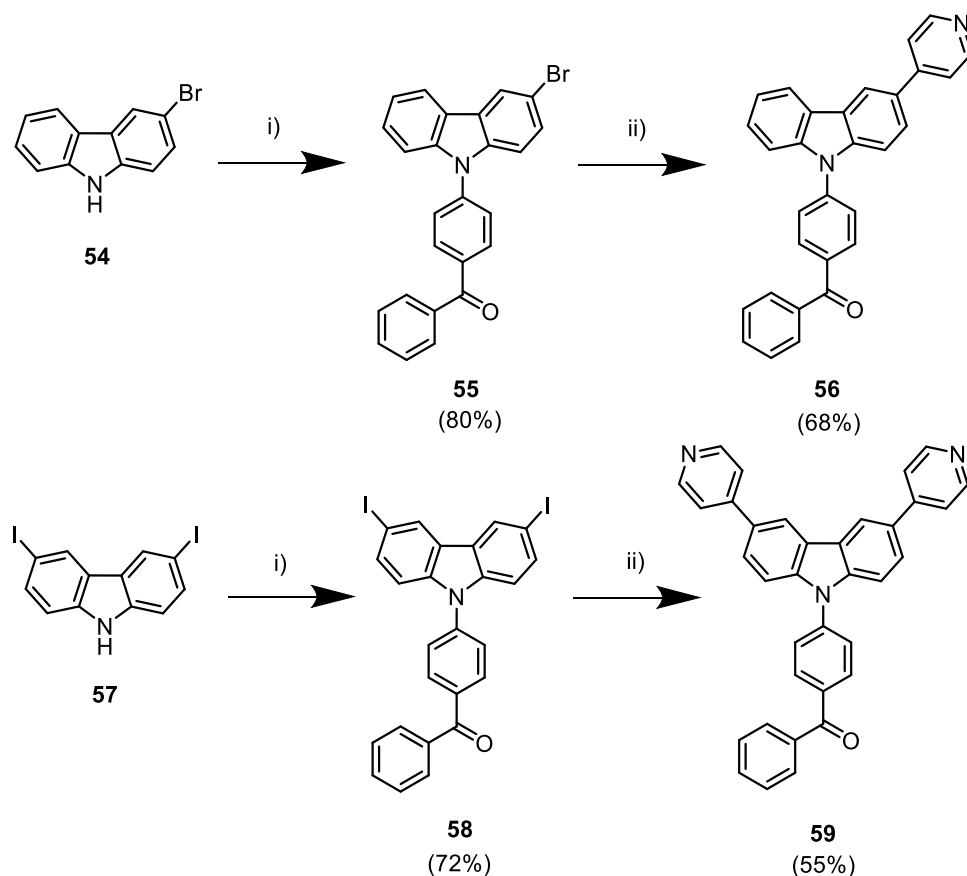


Scheme 2 Syntheses routes for imidazole-based tripodal ligands **48-53**.^{128, IV} Reagents: i) DMF, mixed for 30 min under argon ii) **46**: DMF; **47**: 50:50 DMF:THF, dropwise over 2 hours under argon.

2.2.1.2 Synthesis of carbazole-based ligands^{II,III}

Ligand **56** was synthesized in a two-step synthesis (Scheme 3) *via* compound **55**, which was formed in a reaction of 3-bromo-9*H*-carbazole **54** with 4-fluorobenzophenone under basic conditions in dry DMF. After keeping the reaction at 100 °C for 24 hours, the product was filtrated, washed with methanol, and further purified by column chromatography affording a white solid in an 80% yield. Ligand **56** was synthesized in a reaction of **55** with 4-pyridineboronic acid pinacol ester under basic conditions in dry 1,4-dioxane. After purging for 20 minutes under argon, a palladium catalyst (Pd(PPh₃)₄) was added to the reaction mixture. The reaction was heated to reflux for 24 hours and after solvent evaporation, the crude product was purified using flash column chromatography with a DCM/methanol solvent system affording a white solid in a 68% yield.

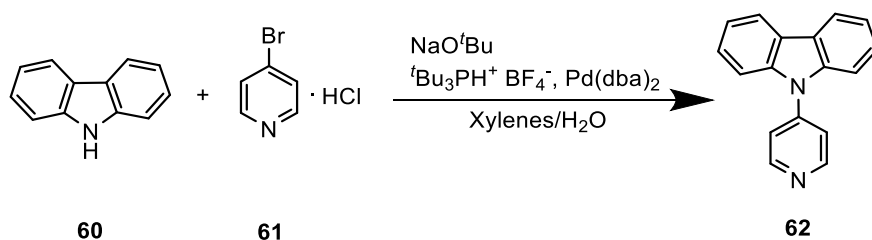
A similar synthesis route was used for ligand **59** (Scheme 3). In the first step, 3,6-diiodo-9*H*-carbazole **57** was reacted with 4-fluorobenzophenone under basic conditions in DMF. The reaction was kept at 100 °C for 24 hours and cooled to room temperature. The residue was filtered and washed with methanol. The crude product was further purified by column chromatography affording a white solid in a 72% yield. The resulting product **58** was reacted with 4-



Scheme 3 Synthesis route for ligands **56** and **59**.^{II} Reagents: i) 4-fluorobenzophenone, potassium *t*-butoxide, DMF, 100 °C, 24 hrs. ii) 4-pyridineboronic acid pinacol ester, 2M K₂CO₃, Pd(PPh₃)₄, 1,4-dioxane, reflux, 24 hrs.

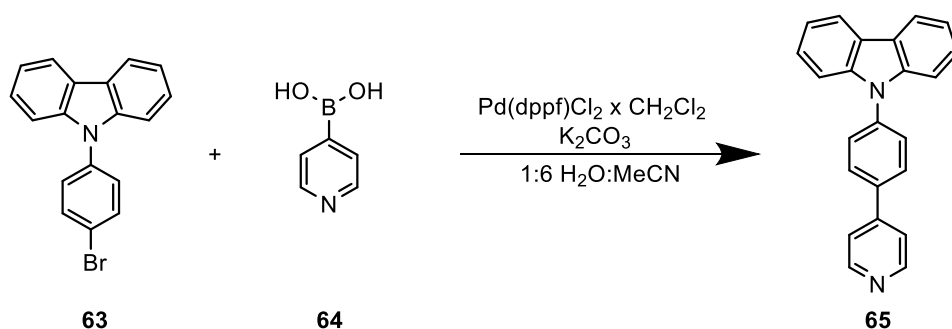
pyridineboronic acid pinacol ester under basic conditions in dry 1,4-dioxane. The reaction was purged for 20 minutes under argon, after which a catalyst was added ($\text{Pd}(\text{PPh}_3)_4$). After refluxing for 24 hours, the reaction was cooled down to room temperature and purified using flash column chromatography (DCM/methanol) affording a white solid in a 55% yield.

Ligand **62** was synthesized according to a previously reported method (Scheme 4).¹²⁹ A reaction of **60** and **61** under basic conditions and with a presence of a catalyst in a mixture of water and xylenes results in the formation of **62**. The product was purified by column chromatography affording a pale-yellow solid with a yield of 81%.



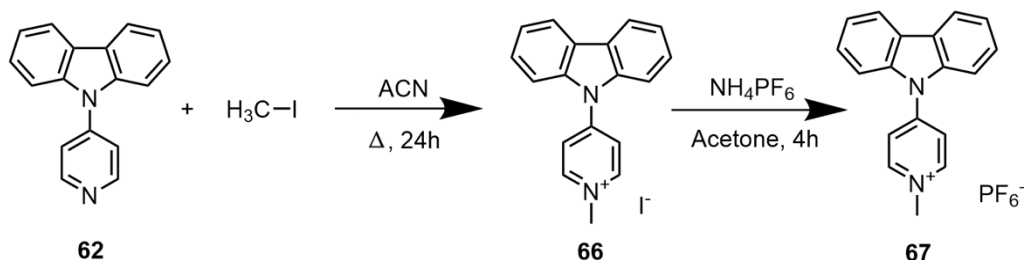
Scheme 4 Synthesis route for ligand **62**.^{129,II,III}

Furthermore, ligand **65** was prepared following a previously reported method (Scheme 5).¹³⁰ A reaction of **63** with **64** under basic conditions and in the presence of a catalyst, using a water-acetonitrile mixture as the solvent, resulted in the formation of **65**. The product was purified by column chromatography with a yield of 78%.



Scheme 5 Synthesis route for ligand **65**.^{130,II,III}

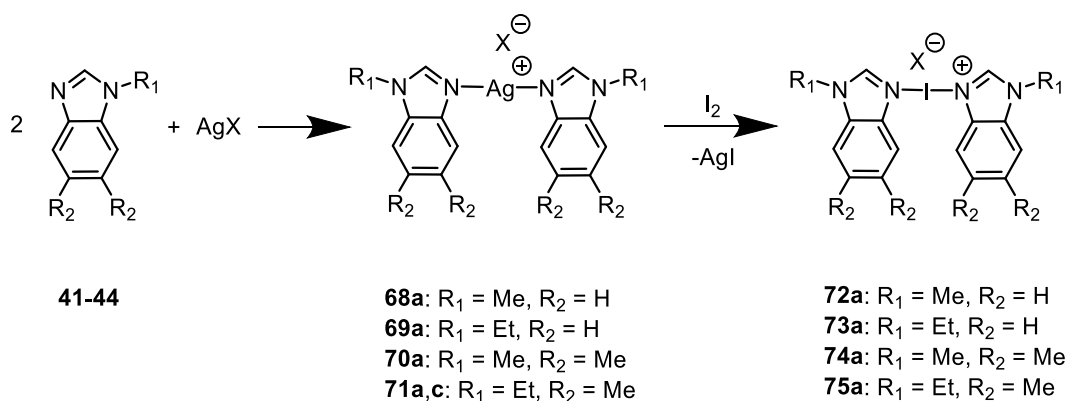
Complex **67** was synthesized for reference purposes (Scheme 6). In the first step, a reaction of **62** (Scheme 4) after a dropwise addition of iodomethane in acetonitrile was heated to reflux for 24 hours. After solvent removal, the residue was washed with diethyl ether. The remaining salt was dispersed in acetone and an anion exchange to a weakly coordinating hexafluorophosphate was performed using a saturated aqueous solution of NH_4PF_6 over 4 hours. The remaining solid was washed with water and filtrated affording the pure product in a 70% yield.



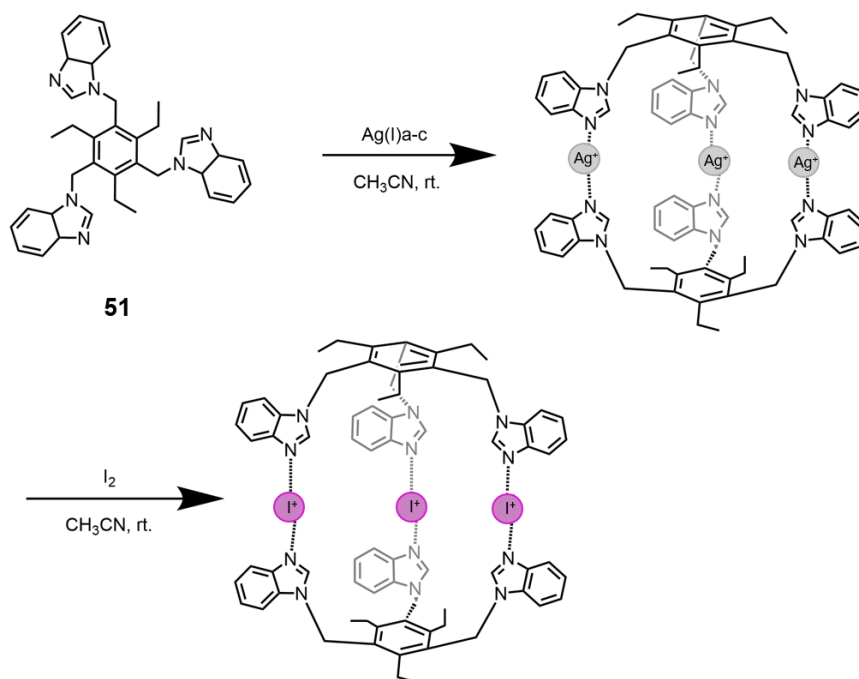
Scheme 6 Synthesis route for complex **67**.^{II}

2.2.2 Synthesis of iodine(I) complexes^{III,IV}

Several of the previously synthesized ligands were used in the synthesis of iodine(I) complexes. The synthesis followed a previously reported method⁵⁶ through an analogous silver(I) complex formation. The general synthesis using the small monotopic ligands is presented in Scheme 7. In addition to ligands in Scheme 7, isoquinoline (**20**, Figure 14), ligand **62**, and **65** were used in the complexation reactions. The silver(I) complexes **68-71** were obtained through a reaction of **41-44** with a silver(I) salt in a 2:1 ratio. Various silver(I) salts (**a** = PF₆⁻, **b** = BF₄⁻, **c** = SbF₆⁻, **d** = OTf⁻) were used to aid solubility. The silver(I) complexes were further reacted with elemental iodine to obtain the analogous iodine(I) complexes **72-75** through a cation exchange reaction after 10 minutes of stirring. The reaction results in the precipitation of silver iodide upon cation exchange, which can be separated by filtration. A similar process was carried out using ligands **20**, **62**, and **65**. The capsular assemblies were obtained through the same synthetic route, only reacting with a 2:3 ratio (ligand:silver(I)/iodine), due to their tripodal nature, and stirring for 1 hour to ensure reaction completion.



Scheme 7 Synthesis route for small silver(I) **68a-71c** complexes and iodine(I) **72a-75a** complexes.^{56,III} Notations **a** and **c** correspond to different counter anions (**a** = hexafluorophosphate, **c** = hexafluoroantimonate).



Scheme 8 Synthesis route for silver(I) and iodine(I) cage formation using ligand **51**.^{56,73,IV} In the second step, CH₃CN was replaced with DMSO for the reactions of **49**, **50**, and **53**.

2.3 Protonation-induced fluorescence modulation^{I,II}

2.3.1 The effect of protonation on quinoline derivatives

The importance of luminescence control is apparent in applications varying from organic light-emitting diodes to fluorescent imaging, and molecular switches. Isoquinoline, acridine, and benzo[*h*]quinoline have been thoroughly studied during the century since their discovery. Moreover, being *N*-heterocycles, they tend to be weakly luminescent. However, systematic studies utilizing a range of acids to estimate the extent of protonation and the effects of the counter anion on these systems have been scarce. In addition, the effect of protonation on the structural properties of these *N*-heterocycles using single crystal X-ray diffraction has not been investigated.

To gain further information on the acid-base interactions, a fundamental study on the effect of protonation on the fluorescence of isoquinoline (**20**, Figure 14), acridine (**21**), and benzo[*h*]quinoline (**22**) was carried out in solution, and in the solid state. The protonation of **20-22** with six different organic acids **33-38** (Figure 18) was evaluated using UV-Vis spectroscopy, NMR spectroscopy, and single crystal X-ray diffraction. The protonation was found to be an effective tool in fluorescence enhancement. The naturally very weakly fluorescent **20** ($\Phi < 1\%$) was observed with a 50-fold increase in the integrated relative fluorescence intensity without the need for a huge excess of acid (1.5:1 acid-to-base ratio used).

Upon protonation, the n,π^* electronic state stemming from the nitrogen lone pair is converted to a π,π^* state. In the absorption spectra (Figure 19), this is observed as an arising broad-band absorption at longer wavelengths due to the π,π^* transition. For compounds **21** and **22**, the protonation-induced changes in the absorption spectra were minor and the protonation was determined to occur predominantly in the excited state, whereas using **35** for protonation, the absorption of the aromatic acid can be seen at 250 – 270 nm when excess acid is added (> 1.0 equivalents). However, this is well below the used excitation wavelength, and bears no change in the fluorescence spectra. The π,π^* state is more likely to undergo fluorescence, and therefore, the protonation was observed as a fluorescence increase (Figure 19). Additionally, for **22**, a significant 50 nm bathochromic shift in the fluorescence maxima was observed. The fluorescence quantum yield upon protonation was determined using Equation 1 and 9,10-diphenylanthracene as a reference. An increase from less than 1% to 27% was obtained for **20** using **35** as the acid.

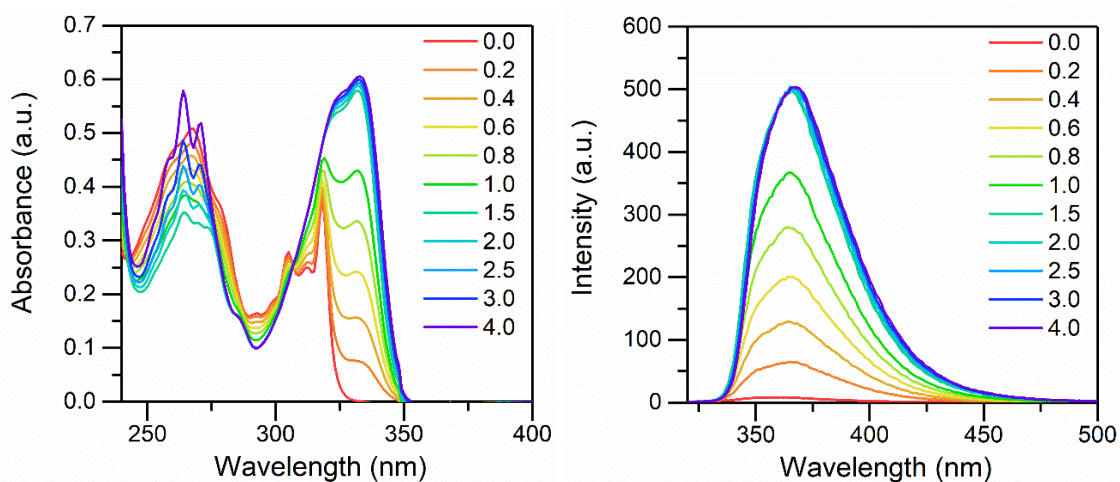


Figure 19 The absorption (left) and fluorescence (right) of isoquinoline (**20**) upon titration with benzenesulfonic acid (**35**) from 0.0 to 4.0 equivalents of acid (10^{-4} M in DCM, $\lambda_{\text{ex}} = 310$ nm).

The strength of the acid ($\text{p}K_{\text{a}}$) was determined to play a directing role in the extent of the effect on the fluorescence of the compounds. The effect grew stronger as the donating powers of the acid increased. A discrepancy was observed with **35**, despite it being a weaker acid than **33** and **34** according to their determined $\text{p}K_{\text{a}}$ values, stronger interactions were observed with each base due to the better stability of the counter anion of the aromatic **35** compared to the acetic acids. Once the $\text{p}K_{\text{a}}$ of the acid was raised above 1, virtually no changes were observed in the absorption and fluorescence spectra due to incomplete protonation. However, in the solid state, protonation was observed regardless of the acid used due to the extremely high concentrations induced by the crystallization process. The strength of the interactions with the acids was further corroborated by binding constants determined in solution from the absorption spectra. The strongest

interaction induced by **35** was supported by the three-fold binding constant in comparison to the stronger acids **33** and **34**.

The crystal structures of the corresponding salts upon protonation were obtained through 1:1 acid-base reactions in CH₃Cl and the single crystals were attained either by slow evaporation of the CH₃Cl solution or by diffusion of hexane into a CH₃Cl solution, or diisopropyl ether into a CH₂Cl₂ solution. The combinations utilizing the weaker acids ($pK_a > 1$) were more difficult to crystallize and some of them remained elusive. The X-ray diffraction studies of the acid-base pairs yielded information on the charge-assisted hydrogen bonds. The O \cdots N distances were determined to have a narrow range from 2.560(2) Å to 2.714(3) Å with the exception of the salt formed from a reaction of **20** with **35**. This salt with the benzenesulfonate counter anion was determined to have O \cdots N distance of 2.862(7) Å, assisted by additional intermolecular interactions in the solid state.

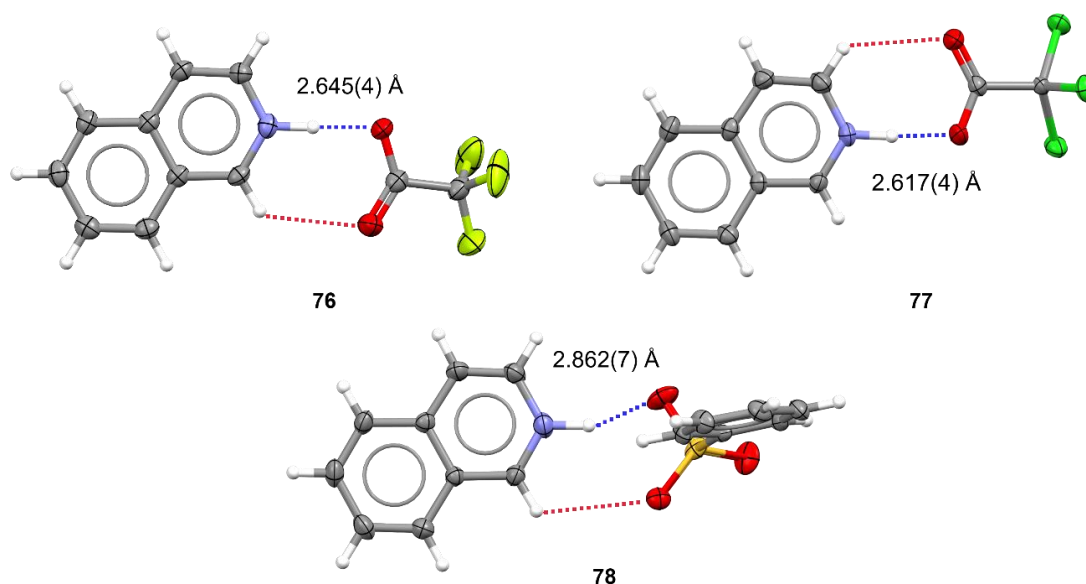


Figure 20 The ORTEP representations of the crystal structures of **76**, **77**, and **78** resulting from the protonation of **20** with various acids.

To further investigate the solid-state interactions, a Hirshfeld analysis was performed on the obtained crystal structures. The Hirshfeld analysis¹³¹ supported the explanation of the longer O \cdots N distance for the **20**:**35** salt, where a multitude of H \cdots O interactions to adjacent benzenesulfonate anions were observed only in the case of **20**. However, the solid-state interaction was determined to be mainly induced by the lattice interactions and not necessarily reflecting the true nature of the interaction in solution.

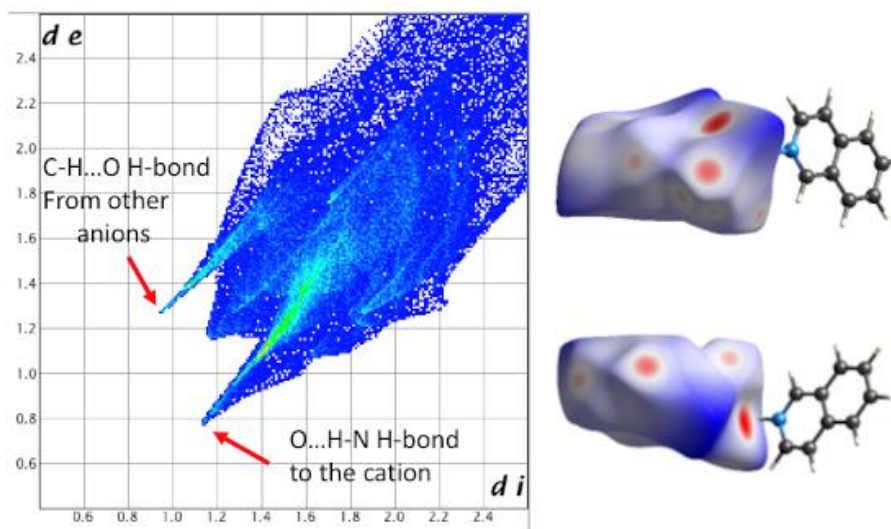


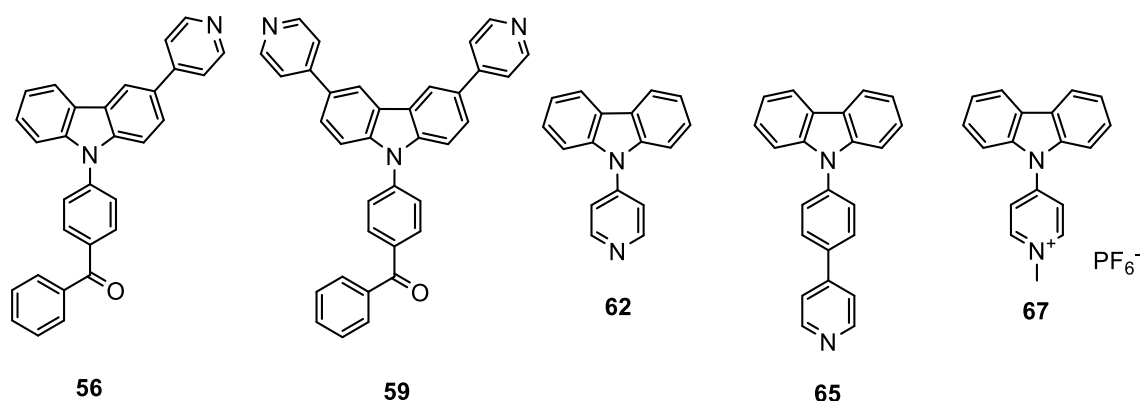
Figure 21 Full fingerprint regions of the benzenesulfonate anion (**35**) in the salt formed upon protonation of **20** and two views of the intermolecular contacts to the Hirshfeld surface of the anion. In the fingerprint plot, d_i represents the closest internal distance from a given point on the Hirshfeld surface, and d_e is the closest external contact (in Å).

2.3.2 The effect of protonation on carbazole derivatives

The results of the above study enabled us to gain further information on the use of acid-base interactions for supramolecular emission control and inspired us to broaden the scope to carbazole derivatives with more prominent application potential. The fluorescence of the quinoline derivatives was studied only in solution, however, many applications require good luminescence properties also in the solid state. Commonly, fluorescent molecules are studied in conventional thin films, though single crystals are free of boundary defects making them important research goals for applications such as in organic diode lasers.⁸¹

The development of purely organic emitters is imperative for their non-toxicity, low cost, and high performance. Carbazole has high triplet energy making it an enticing material for the development of blue-light emitting diodes.^{118,124,132} However, concurrently achieving high efficiency, long lifetime, and low cost with purely organic blue emitters is still considered a challenge.¹³² Bipolar host materials are a newly developed method for smarter molecular design, which holds spatially separated electron-withdrawing and electron-donating units within the same molecule promoting balanced charge flux and broadened exciton recombination.¹³³⁻¹³⁵ However, this design might lead to the formation of an intramolecular charge-transfer state (ICT), which, if twisted, could lead to the excited state energy being quenched by the rotary motion of the molecule.^{80,136,137}

Compounds in Scheme 9 were studied in solution and the solid state upon protonation with acids (Figure 18). Other than **67**, a pyridyl-moiety was used as a protonation site. Compounds **56** and **59** utilized the benzophenyl moiety as the electron-withdrawing unit, whereas **62** and **65** have pyridyl and phenylpyridyl



Scheme 9 The synthesized carbazole-based emitters used to study the effect of protonation on the fluorescence properties.

moieties as the corresponding units localized differently on the electron-rich carbazole core. Compound **67** was used as a reference for a constant positive charge localized on the pyridyl nitrogen with a weakly coordinating PF_6^- anion.

Compounds **56** and **59** behaved as expected based on the quinoline studies.¹ From the two possible HB acceptor sites on **56**, the pyridyl moiety is predominantly protonated due to greater basicity. The protonation of **56** (Figure 22) resulted in a total fluorescence enhancement factor of 2.8, and all the original absorption bands diminishing while two new bands were observed at 319 and 382 nm, the latter being characteristic of the cationic species.¹ Moreover, the two nucleophilic sites led to the saturation at 2.0 equivalents upon protonation. Similarly, this was observed for **59** at the 3.0 equivalents point due to the two pyridyl-acceptor units and the benzophenyl moiety. Additionally, a noteworthy increase in the Φ from 16% to 80% was observed for **56**. Upon reaching the saturation point, the fluorescence intensity of **56** and **59** began to decrease possibly due to the increased polarity of the solution, which is supported by the loss of isosbestic points in the absorption spectra.²⁵

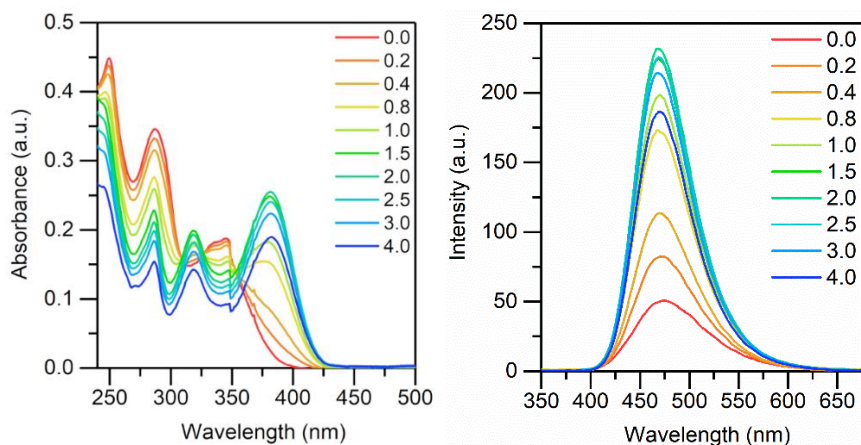


Figure 22 The absorption (left) and fluorescence (right) spectra of **56** upon titration with benzenesulfonic acid (**35**) from 0.0 to 4.0 equivalence of acid (10^{-5} M in DCM, $\lambda_{\text{ex}} = 340$ nm).

The observed changes in the absorption and fluorescence spectra of **56** and **59** were explained by a time-dependent density functional theory (TD-DFT/CAM-B3LYP/6-31G(d,p)) study, which showed significant changes in the LUMO orbitals of **56** upon protonation (Figure 23). The relocalization of the LUMO orbital along with the easier planarization of the protonated pyridyl and carbazole moieties were determined as the principal grounds for fluorescence enhancement in **56** and **59**.

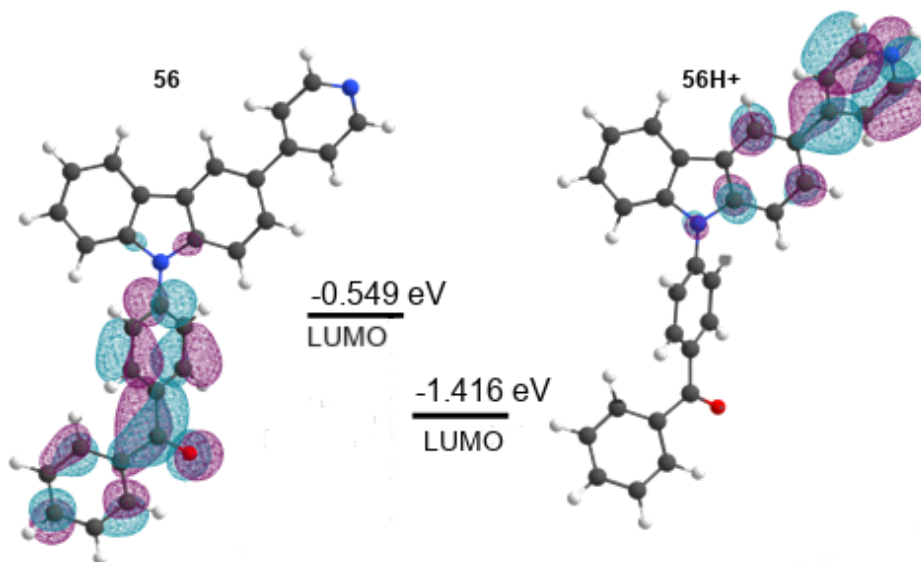


Figure 23 Different localization of the LUMO orbital on **56** and its protonated form (**56H⁺**) (TD-DFT/CAM-B3LYP/6-31G(d,p)).

The different localization of the electron-withdrawing moiety on **62** and **65** induced changes dissimilar to **56** and **59** upon protonation (Figure 24). Unexpectedly, the fluorescence of **62** and **65** was quenched upon protonation to the point where **62** was observed with a Φ of 0.97% and **65** with a Φ of 0.14% with 2.0 and

4.0 equivalents of acid **35**, respectively. Natural population analysis at the same DFT level of theory as above and a Wiberg-index analysis on **62** bond lengths and strengths indicated changes in the lengths of the pyridyl endocyclic bonds due to reorganization of the electron density to accommodate the extra positive charge on the pyridyl-moiety. An easier rotation about the carbazole-pyridyl N-C was determined as the principal reason for the fluorescence quenching in **62**.

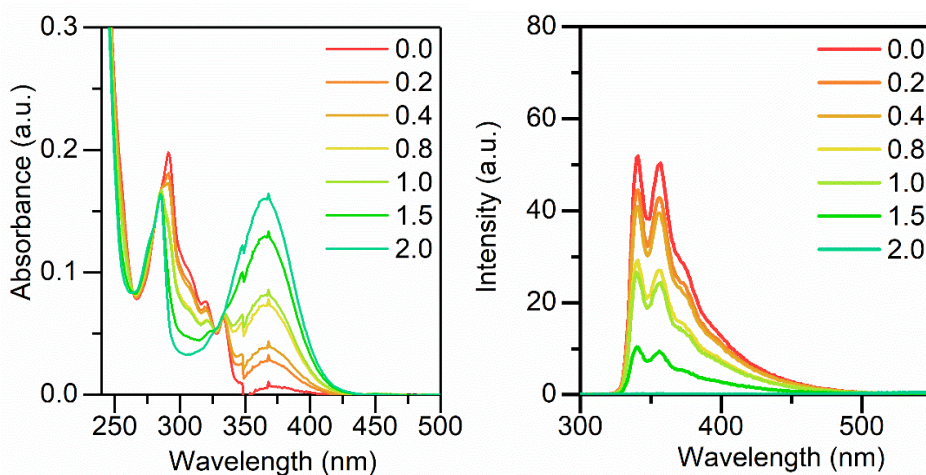


Figure 24 The absorption (left) and fluorescence (right) of **62** upon upon titration with benzenesulfonic acid (**35**) from 0.0 to 2.0 equivalents of acid (10^{-5} M in DCM, $\lambda_{\text{ex}} = 290$ nm).

For potential application purposes, the fluorescence of these systems was evaluated in the solid state (except for **59** due to extremely poor solubility preventing valid crystallization efforts). For all the solid-state samples, protonation resulted in a significant bathochromic shift in the fluorescence maxima suggesting a J-type packing for these compounds. J-type packing with a large Stokes shift limits self-absorption and enhances fluorescence in the solid-state.⁸⁴ A comparison of the solid-state fluorescence of the pure compound and the protonated form for all suitable samples is presented in Figure 25. Without the charge-assisted hydrogen bonding, the samples resulted in low fluorescence quantum yields (1-3%). A comparison of the fluorescence data obtained in the solution and the solid state is presented in Table 1.

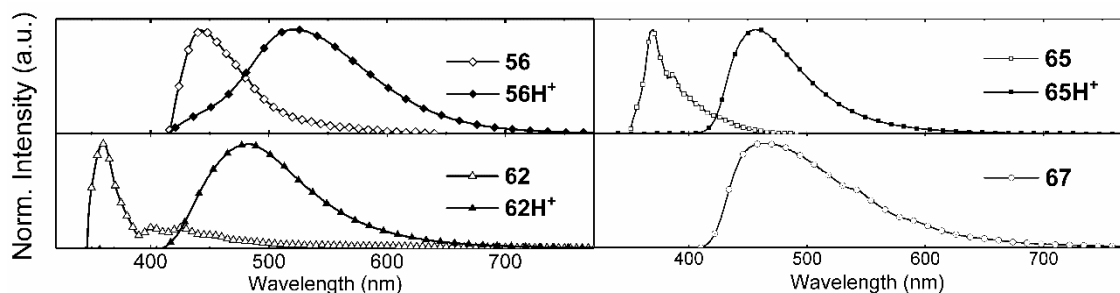


Figure 25 The fluorescence spectra of the solid-state samples of **56**, **62**, **65**, and **67**, and the protonated forms of **56**, **62**, and **65** denoted with H^+ . (Excitation wavelengths of 330 nm, 333 nm, 331 nm, 303 nm, 326 nm, 310 nm, and 320 nm were used, respectively).

Table 1 The fluorescence data of **56**, **59**, **62**, and **65** (and their corresponding benzenesulfonate salts), and **67** with absolute quantum yield values both in solution and in the solid state.

Compound	In dichloro- methane ^a			Solid-state		
	λ_{ex} (nm)	F_{max} (nm) ^b	Φ_f (sol) ^c	λ_{ex} (nm)	F_{max} (nm)	Φ_f (ss, %)
56	340	458	16.14	330	442	1.51
56H⁺	340	472	79.45	326	521	15.81
59	340	473	18.06	-	-	-
59H⁺	340	451	79.18	-	-	-
62	290	341, 356	10.52	333	360	2.46
62H⁺	290	341, 356	0.97	310	483	25.09
65	340	415	32.03	331	369	1.21
65H⁺	340	420	0.14	320	457	49.02
67^d	-	-	-	303	469	21.65

^a Measured at the concentration of 1.0×10^{-5} M at 25 °C.

^b Reported at 1.0 or 2.0 equivalents of benzenesulfonic acid according to the number of protonation sites.

^c Reported at 4.0 equivalents of benzenesulfonic acid for the protonated ligands, except for **62H⁺** at 2.0 equivalents.

^d Not soluble in dichloromethane, hence no solution studies were performed.

To further analyze the contradicting solid-state fluorescence results, the acid-base pairs were crystallized and analyzed with single crystal X-ray diffraction. The hydrogen bond distances $\text{O} \cdots \text{N}$ were observed between 2.588(2) – 2.784(3) Å for all acid-base pairs. The interaction of **56** with **35** is presented in Figure 26. The differences in the bond lengths were determined to occur as a result of crystal packing effects.

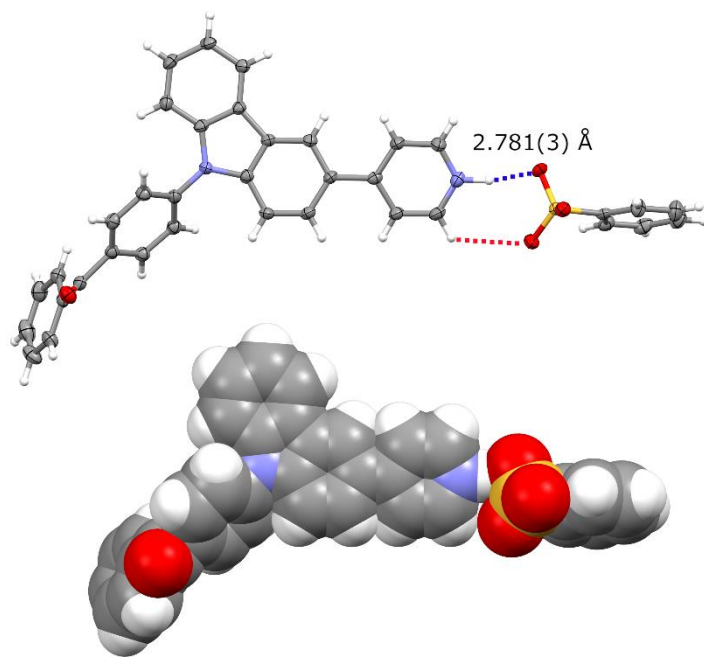


Figure 26 The ORTEP (top) and spacefill (bottom) representations of the crystal structure of **56** protonated with **35** with an N \cdots O distance of 2.781(3) Å. Thermal displacement ellipsoids drawn at the 50% probability level.

Compound **62** crystallizes in the chiral $P2_12_12_1$ orthorhombic space group in a dimer-type packing stabilized by off-center π - π interactions as well as C-H $\cdots\pi$ edge-to-face and C-H \cdots N interactions from the pyridyl nitrogen. Compounds **62** and **65** are structurally separated only by a phenyl group, and as expected, have very similar packing in the solid state. Compound **65** also crystallizes in an orthorhombic space group, though now in the centrosymmetric $Pbca$ space group, and is stabilized by similar off-center π - π , C-H $\cdots\pi$ edge-to-face and C-H \cdots N interactions. These intricate 3D networks of intermolecular interactions resulted in most of the fluorescence being quenched with **62** and **65** having significantly lower Φ values (2.46% and 1.21%, respectively) than in solution. Unfortunately, the unprotonated **56** single crystals remained elusive.

The reference compound **67** was found in a centrosymmetric monoclinic $C2/c$ space group in a brick pattern familiar for the J-type packing. Along with the stabilizing intermolecular interactions (π - π , C-H \cdots F) and the anionic interactions reducing the rotation of the pyridinium moiety, this type of packing resulted in a moderate solid-state Φ (21.65%).

In addition to a large bathochromic shift, the protonation of all the solid-state samples **56**, **62**, and **65**, resulted in an increase in the Φ value reaching a significant improvement for **65** from 1% to 49%. Complex **56H⁺** was found crystallizing in a triclinic $P\bar{1}$ space group in a dimer-type head-to-tail packing of the pyridyl-carbazole motif. A staircase pattern was stabilized by weak off-center π - π interactions (3.8 Å interplanar distance of the aromatic rings) as well as C-H $\cdots\pi$ edge-to-face interactions, and N-H \cdots O (2.781(3) Å) charge-assisted hydrogen bonding. Similarly, complex **65H⁺** was found in a monoclinic $P2_1/c$ space group

with weak off-center π - π interactions (3.7 Å interplanar distance of the aromatic rings) and intermolecular interactions between the ionic pairs (N-H \cdots O, 2.706(2) Å) in a staircase pattern. Unfortunately, good-quality single crystals for **62H**⁺ were not obtained.

The difference between the two protonated structures is in the packing of the carbazole moieties, which for **56H**⁺ are coplanar, yet for **65H**⁺ was found packing at a 45.9° angle making the off-center π - π interactions less effective. The crystal packing in **65H**⁺ forces the molecule into a twisted conformation with an angle of 165.7° between the centroid of the five-membered carbazole ring, the carbazole nitrogen, and the carbon of the adjacent phenyl ring (Figure 27). However, for other structures, this angle lies very close to 180°, explaining the significantly larger increase in the Φ value for the protonated solid-state sample of **65H**⁺ due to the less densely packed, yet highly restricted, crystal lattice compared to the other protonated samples.

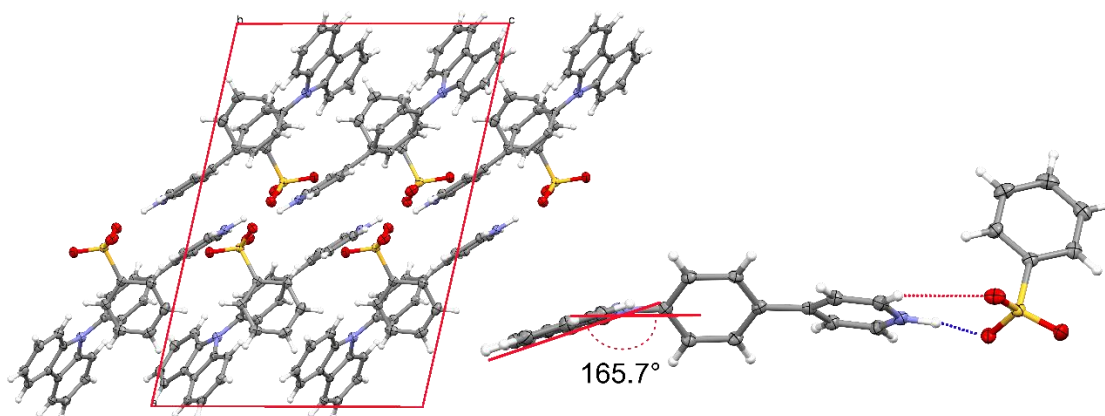


Figure 27 The packing in the crystal structure of **65H**⁺ resulting from the protonation with **35** viewed along the crystallographic *b*-axis and the steric hindrance induced by the bent conformation of the carbazole moiety.

The protonation-induced easier planarization and the relocation of the LUMO orbital on the protonated species with **56** and **59** led to the enhanced fluorescence in the solution state. In the solid state, the rotation about the N-C bond was restricted upon protonation in each complex. The bent conformation and the resulting loose packing of **65H**⁺ led to weaker intermolecular interactions in the crystalline form and a significant increase in the fluorescence quantum yield. The pronounced bathochromic spectral shift observed for the protonated species indicated a noticeable decrease in the energy gap between the emissive state and the first triplet state of the molecules, which could facilitate a more efficient TADF process. Therefore, implementing this strategy could further boost the development of future bipolar emitters.

2.4 Self-assembly of silver(I) [N–Ag–N]⁺ and iodine(I) [N–I–N]⁺ complexes^{III,IV}

2.4.1 Iodine(I) and silver(I) complexes of benzoimidazole and pyridylcarbazole derivatives

The exceptional strength of the halogen(I) complexes has made them an interesting subclass of halogen bonding. However, as per their reactivity, not many unique complexes have been reported in the solid state.^{59,62,64,69,138–143} Within this study, we set out to synthesize and characterize, in solution and in the solid state, new iodine(I) complexes and their parent silver(I) complexes based on bicyclic benzoimidazole and pyridylcarbazole. Ligands **20**, **41–44**, **62**, and **65** were used in the complexation reactions. The crystallization process from ligand **41** to the silver(I) complex (**68a**) and the analogous iodine(I) complex (**72a**) is presented in Figure 28. The solvent choice was dictated by the solubility of the

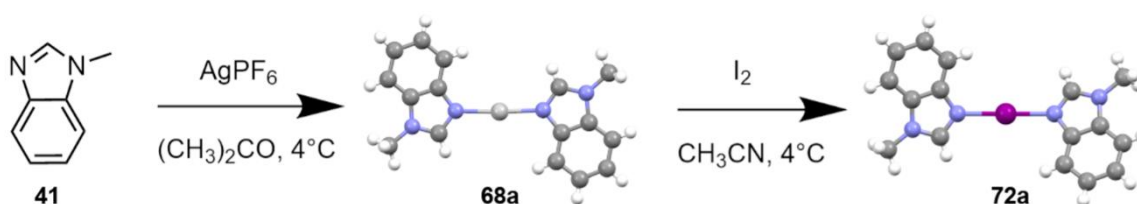


Figure 28 The crystallization of the silver(I) complex **68a** and the iodine(I) complex **72a** using ligand **41** through steps of evaporation of acetone and acetonitrile in the fridge, respectively.

complexes, which for some, was relatively poor. When using DMSO, the silver iodide remained dispersed in solution and required centrifugation for optimal separation.

The formation of the silver(I) and iodine(I) complexes was monitored using ¹H and ¹H-¹⁵N NMR spectroscopy. For all reactions, a full conversion from the ligand to the silver(I) complexes was supported by the complexation-induced downfield shifts between 0.02 – 0.47 ppm in the ¹H NMR spectra (see Figure 29 for ligand **44**). Similarly, full conversion from the silver(I) complex to the analogous iodine(I) complex was evident from the ¹H NMR spectra with further downfield shifts of 0.13 – 0.59 ppm upon complexation. However, the complexes resulting from a reaction with **65** were fairly insoluble and were therefore not characterized in solution. Additionally, less than ideal solubility was observed for **74a** resulting in a broadened ¹H NMR spectrum.

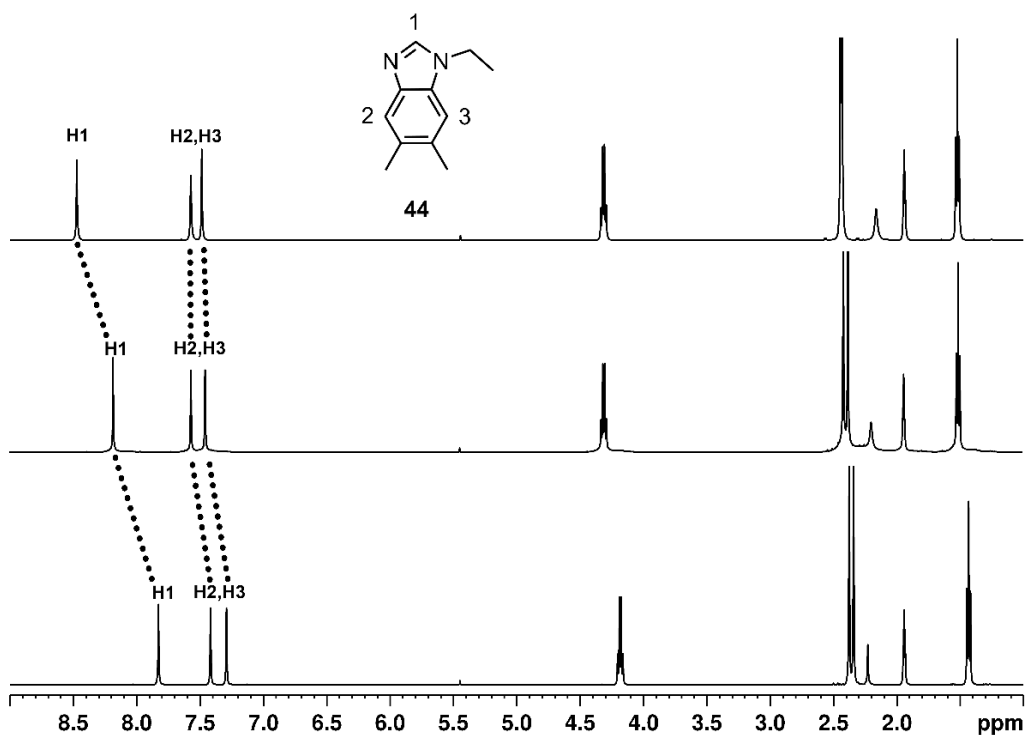


Figure 29 The comparison of the ^1H NMR spectra of ligand **44**, the corresponding silver(I) complex $[\text{L-Ag-L}]\text{PF}_6$ (**71a**), and the iodine(I) complex $[\text{L-I-L}]\text{PF}_6$ (**75a**) (from bottom to top). All values are in ppm and referenced to residual CH_3CN (^1H) (500 MHz, 298 K).

The wide chemical shift range and the direct involvement of the nitrogen in the complexation resulting in large chemical shift changes renders ^1H - ^{15}N HMBC measurements convenient for monitoring the $[\text{N-I-N}]^+$ halogen bond formation.¹⁴⁴ However, the longer measurement time required for the ^{15}N measurements, due to the less abundant nature of ^{15}N in comparison to ^1H , in some cases inherently led to the precipitation of the iodine(I) complex in the time required for the measurement completion. Thus, not all the HMBC spectra for the iodine(I) complexes were obtained. Nevertheless, most of the spectra were obtained, and the comparison of the ^1H - ^{15}N HMBC spectra of **44**, **71a**, and **75a** is presented in Figure 30. Additionally, the chemical shifts observed for all measured ligands and their complexes are presented in Table 2. In addition to the low solubility, the previously observed line broadening might occur due to the ongoing dissociation-association reaction commonly observed for weakly nucleophilic ligands.⁶¹ Close to a 50 ppm change in the chemical shift of the sp^2 -acceptor N -atom (N1) was observed upon silver(I) complexation and another 50 ppm upon iodine(I) complexation, the largest complete change from ligand to iodine(I) being 111 ppm. Additionally, the chemical shifts of the non-coordinating nitrogen (N2) were found to change in the opposite direction by 5 ppm upon each complexation.

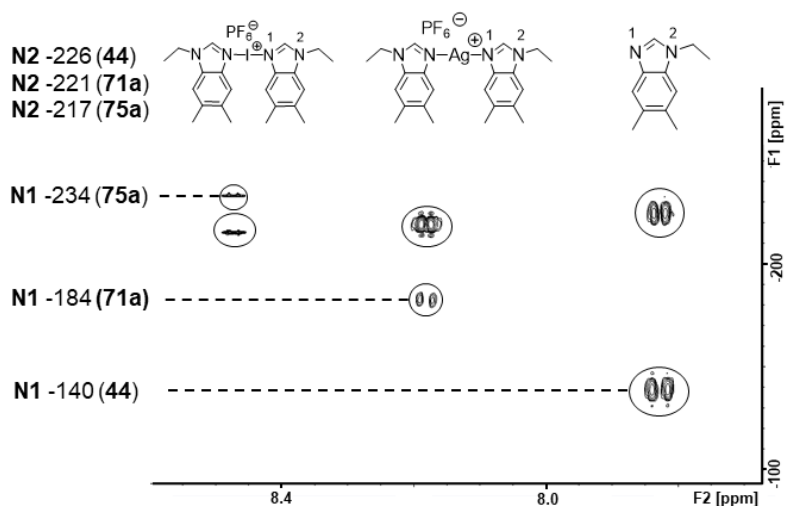


Figure 30 The comparison of the ^1H - ^{15}N HMBC correlation spectra of the ligand **44**, the silver(I) complex (**71a**), and the iodine(I) complex (**75a**). All values are in ppm and referenced to residual CH_3CN (^1H) or CD_3NO_2 (^{15}N) (500 MHz, 298 K).

Further confirmation of the complex formation was sought out by crystallization reactions. From the previous solution state studies, the solubility of the iodine(I) complexes containing **43**, **62**, and **65** was found problematic, and this, eventually made crystallization attempts of these complexes redundant. However, 12 new silver(I) structures and 8 iodine(I) structures, 4 of which are unique (involving ligands with no reported $[\text{N}-\text{I}-\text{N}]^+$ structures), were obtained. The silver(I) complexes were found with $\text{Ag}-\text{N}$ bond lengths 2.086(3) –

Table 2 The ^1H NMR of the proton most affected upon complexation and ^1H - ^{15}N HMBC chemical shifts of the N1 (top) and N2 (bottom) nuclei upon silver(I) and iodine(I) complexation for ligands **41–44**, **20**, and **62** (where N1 is an acceptor for the silver(I) and iodine(I), and N2 is the non-coordinating nitrogen). All values reported in ppm. For experimental information, see the original publication.ⁱⁱⁱ

Complex ^[a]	^1H			^1H - ^{15}N HMBC		
	Ligand	$[\text{N}-\text{Ag}-\text{N}]^+$	$[\text{N}-\text{I}-\text{N}]^+$	Ligand	$[\text{N}-\text{Ag}-\text{N}]^+$	$[\text{N}-\text{I}-\text{N}]^+$
[41–X–41]⁺	7.912	8.247	8.575	-138.9	-178.5	-232.0
				-238.3	-233.1	-228.5
[42–X–42]^{+[b]}	7.976	8.306	8.649	-138.4	-180.7	-232.2
				-223.1	-218.2	-214.1
[43–X–43]^{+[b]}	8.000	8.468	9.062	-138.0	-180.2	-
				-239.1	-235.0	-229.7
[44–X–44]⁺	7.828	8.181	8.473	-140.3	-184.2	-234.4
				-225.9	-220.6	-216.6
[20–X–20]^{+[c]}	9.256	9.277	9.629	-70.1	-106.1	-181.9
[62–X–62]^{+[b]}	8.868	9.097	9.230	-67.7	-124.8	-
				-251.9	-251.0	-

[a] With PF_6^- counter-anion. [b] Poor solubility of the iodine(I) complex. [c] Only N1.

2.177(2) Å and angles of 149.11(8) – 180°. The silver(I) structures demonstrated well the ability of silver to coordinate to a wide range of molecules. Several

silver(I) complexes were found with argentophilic $\text{Ag}^+ \cdots \text{Ag}^+$ interactions leading to dimer-type packing in the solid-state. The $\text{Ag}^+ \cdots \text{Ag}^+$ bond lengths were found between 3.018(8) – 3.3438(9) Å, though longer separations were observed as well. The crystal structure of the silver(I) complex of ligand **65** with 4-coordinating silver(I) atoms is presented in Figure 31. In addition to the argentophilic interactions, silver(I) structures were commonly observed with coordinating solvent molecules, especially when CH_3CN was used as the crystallization solvent. The ability of carbazole to form the $\text{C-H} \cdots \pi$ edge-to-face interactions previously observed in the protonation studies¹¹ became evident also in these silver(I) structures.

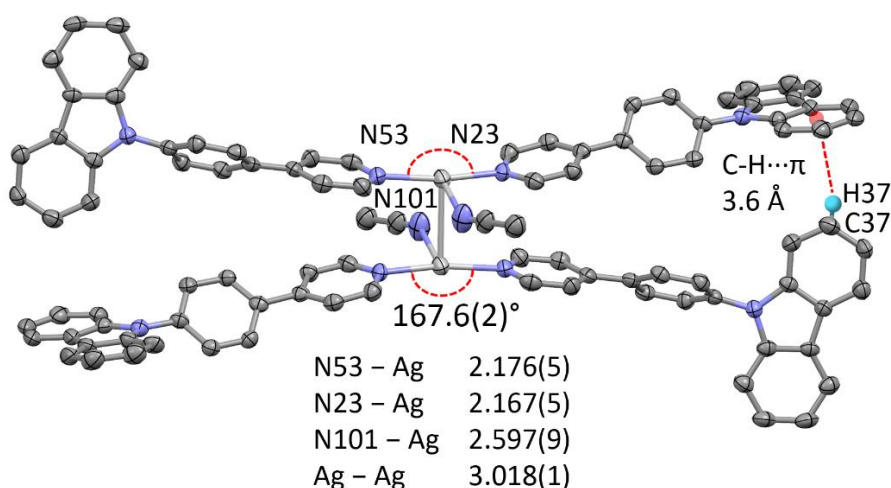


Figure 31 The strongest argentophilic interaction found in the crystallization of the silver(I) complexes using ligand **65**. All lengths are in Å.

For the seven ligands investigated, the iodine(I) structures were obtained for four of them (Figure 32). In contrast to the silver(I) structures with multiple coordinating molecules and a wide variety of coordination angles, the iodine(I) $[\text{N-I-N}]^+$ halogen bonds have demonstrated a strict preference for linearity due to the electronic origin of this interaction.^{56,57,59,60,63} Furthermore, the I^+ cation in the 3c-4e halogen bond does not possess the required empty orbitals for the interaction with more than two molecules. The N–I bond lengths were found between 2.238(2) – 2.261(5) Å and bond angles of 176.9(2) – 180°, which further validated the linear nature of the I^+ cation. The 3c-4e halogen bonds of these complexes experienced bond lengths shorter than usual corresponding to R_{XB} values of 0.63 – 0.64 and indicating even stronger interactions than usually reported for the $[\text{N-I-N}]^+$ complexes ($R_{\text{XB}} = 0.65 - 0.69$, $d(\text{N-I}) = 2.23 - 2.31$).^{34,142}

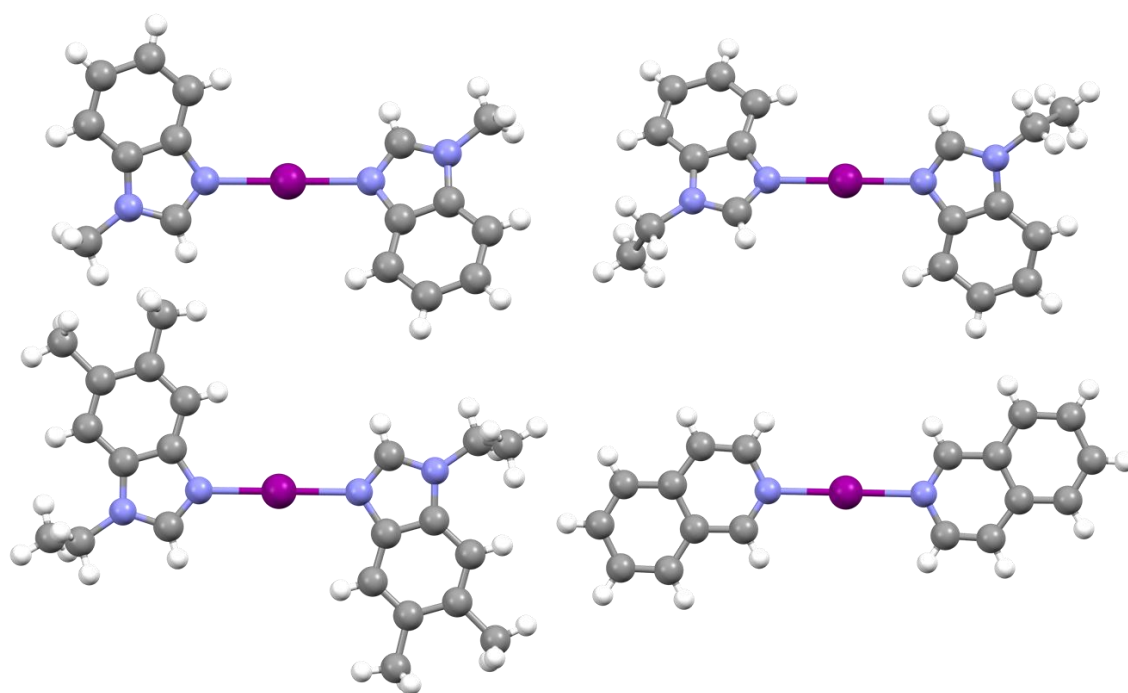


Figure 32 The four unique crystal structures of the $[\text{N-I-N}]^+$ complexes using ligands **20**, **41**, **42**, and **44**. The symmetric N-I bond lengths were between 2.238(2) – 2.261(5) Å and bond angles 176.9(2) – 180°. Thermal displacement ellipsoids drawn at the 50% probability level and counter anions omitted for clarity.

In addition to the expected silver(I) and iodine(I) structures, a few unexpected ones were also obtained including an interesting asymmetric two-coordinate silver(I) structure of ligand **65** and a molecule of CH_3CN , with the only similar two-coordinate acetonitrile structure being reported more than 20 years ago.¹⁴⁵ The asymmetric structure was observed with a slightly shorter **65**- Ag^+ bond length than the corresponding symmetric structure, and a symmetry enforced linear 180° angle. Herein, we demonstrated the reliable nature of the I^+ cation as a supramolecular synthon. Despite the limited solubility of some of the ligands, all of them were capable of the interaction. Furthermore, it was envisioned that the results presented herein could lead to enhanced development of future XB-based materials.

2.4.2 Dimeric iodine(I) and silver(I) cages from tripodal N-donor ligands

The third publication^{III} demonstrated the well-known linear and symmetric nature of the iodine(I) cation.^{56,57,59,60,63} Furthermore, a rare example of a solid-state structure of iodine(I) capsular assembly has been reported using ligand **48**.⁷³ These results, in addition to several analogous metallocages,¹⁴⁶⁻¹⁵¹ led us to believe similar 3c-4e capsular assemblies for ligands **49-53** could be prominent. Herein, six tripodal N-donor ligands were synthesized and used in the construction of silver(I) and iodine(I) capsular assemblies.

The addition of elemental iodine to the parent silver(I) cages formed by a reaction of the ligand and a silver(I) salt in a 2:3 ratio resulted in the formation of the analogous iodine(I) cage through the $[N-Ag-N]^+$ to $[N-I-N]^+$ cation exchange reaction.^{34,56} All complexation reactions were performed in either CH_3CN or DMSO due to the poor solubility of the complexes. The formation of the capsular assemblies in solution was studied by 1H and $^1H-^{15}N$ NMR spectroscopy (Figure 33). Rissanen *et al.* have previously performed similar studies on the cage formed using **48a**,⁷³ which was, therefore, excluded from the NMR spectroscopy. Similar to previous reports,^{67,69,73,III} the formation of a silver(I) complex resulted in down-field shifts in the ligand chemical shift affecting most prominently the proton (H1) closest to the coordinating nitrogen (N1). Chemical shift changes from the uncomplexed ligand to the silver(I) cage were observed between 0.16 ppm and 0.48 ppm for the different ligands. Upon the Ag^+ to I^+ cation exchange reaction, an additional 0.16 ppm to 1.21 ppm change was observed. In a previous publication,^{III} the solubility of the complexes was observed to decrease upon silver(I) and iodine(I) complexation, especially as the size of the ligand grew larger. Moreover, similar obstacles were observed within this study as well. For a few of the iodine(I) cages, a clean spectrum indicating full conversion from a silver(I) to iodine(I) cage was obtained, however, some showed a mixture of species, possibly due to the low solubility and therefore incomplete cation exchange. The $^1H-^{15}N$ correlation measurements provided further indication of the cage formation. However, in most cases, the time required for the ^{15}N measurements resulted in precipitation of the iodine(I) cage, and for some cages, only the parent silver(I) cage measurements were successful. A full set of ^{15}N resonances was obtained for only one species (**49**), and even then, indicated a mixture already present in the 1H NMR spectrum. A chemical shift change of 50 ppm was observed for N1 upon silver(I) complexation, whereas the non-coordinating nitrogen (N2) experienced a change of 5 ppm.

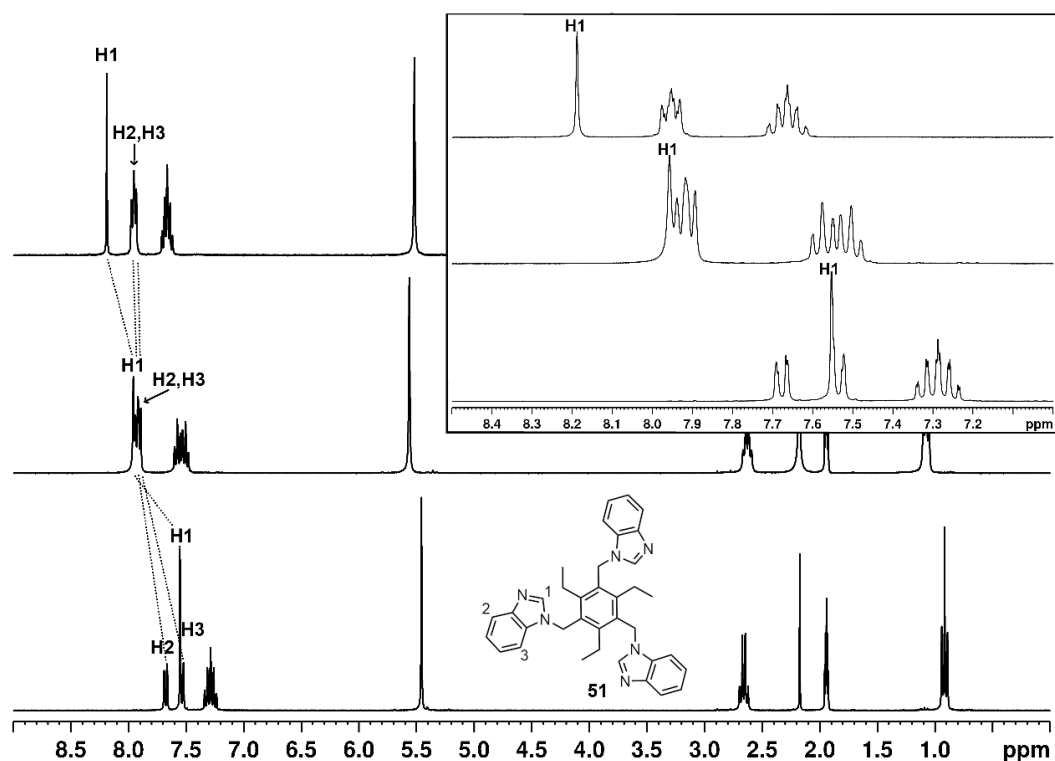


Figure 33 The comparison of the ^1H NMR spectra of ligand **51**, the corresponding silver(I) complex $[\text{L-Ag-L}]\text{PF}_6$, and the iodine(I) complex $[\text{L-I-L}]\text{PF}_6$ (from bottom to top). All values are in ppm and referenced to residual CH_3CN (^1H) (500 MHz, 303 K).

The dimeric cage composition for all ligands was confirmed in the gas phase with electrospray ionization mass spectrometry (ESI-MS) and ion mobility-mass spectrometry (IM-MS).^{103,152} Cage formed using ligand **51** (L) was observed with ions $[\text{L}_2\text{Ag}_3+\text{PF}_6]^{2+}$ and $[\text{L}_2\text{I}_3+\text{PF}_6]^{2+}$ at m/z values of 787 and 815, respectively (Figure 34 and Figure 35). Moreover, cages were observed with other anions, such as I^- and PF_2O_2^- . All the silver(I) and iodine(I) cages showed good agreement between the theoretical and experimental isotopic patterns. The IM-MS analysis depicted similar arrival-time distributions with narrow peak widths for both Ag^+ and I^+ cages, indicating discrete, well-defined structures. A slight increase in the size was observed for the I^+ cage, compared to the Ag^+ cage, which is consistent with the previously reported structures of similar cages.⁷³ A comparison of the determined single crystal structure of the Ag(I) cage of **53** with hexafluorophosphate and the analogous iodine(I) structure determined computationally is depicted in Figure 36.

Despite extensive efforts, crystal structures of the iodine(I) cages remained elusive. However, 11 silver(I) cage structures, 9 of which unique, were obtained. The previous publication^{III} was merely an example of the significance of the surrounding environment in silver coordination. Once more, the silver(I) structures were observed with a wide range of bond lengths (2.068(12) - 2.170(7) Å) and angles (163.1(2) - 180.0(5)°), however, the cage formation seemed to

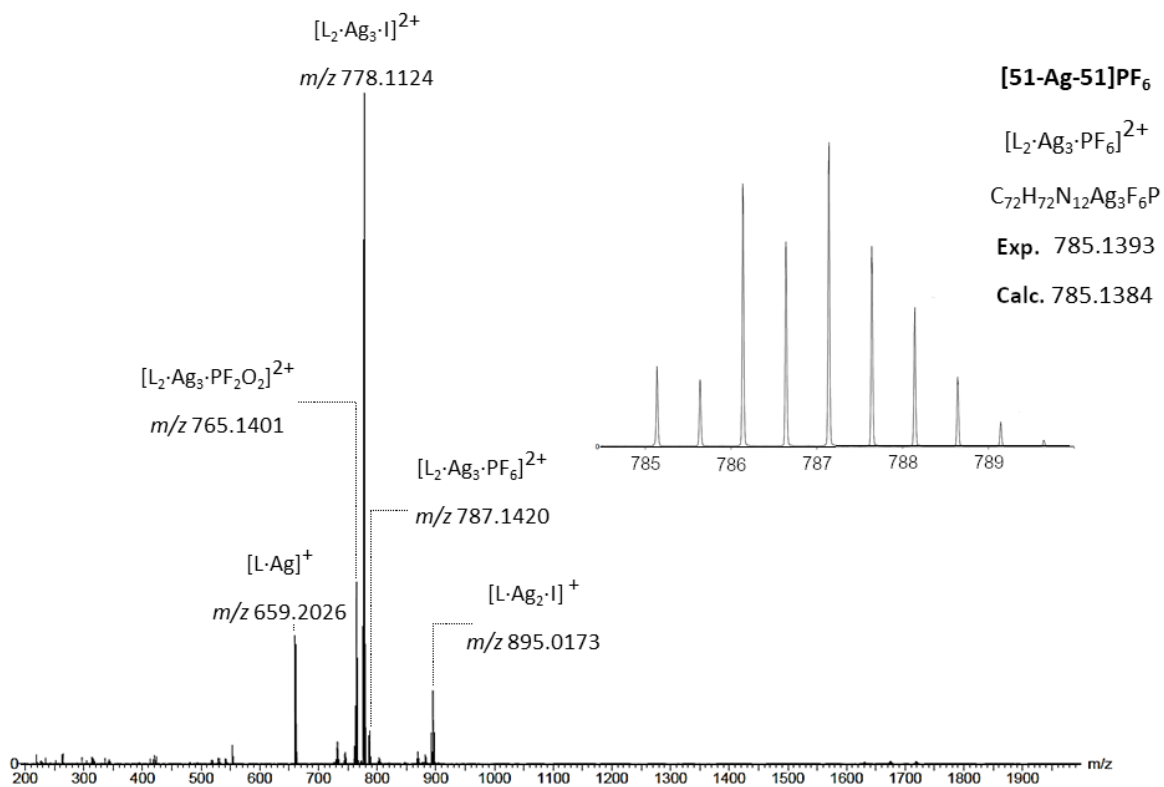


Figure 34 The ESI-TOF mass spectrum of Ag(I) cage of **51**. Insets show the zoomed views for the peak at m/z 785.

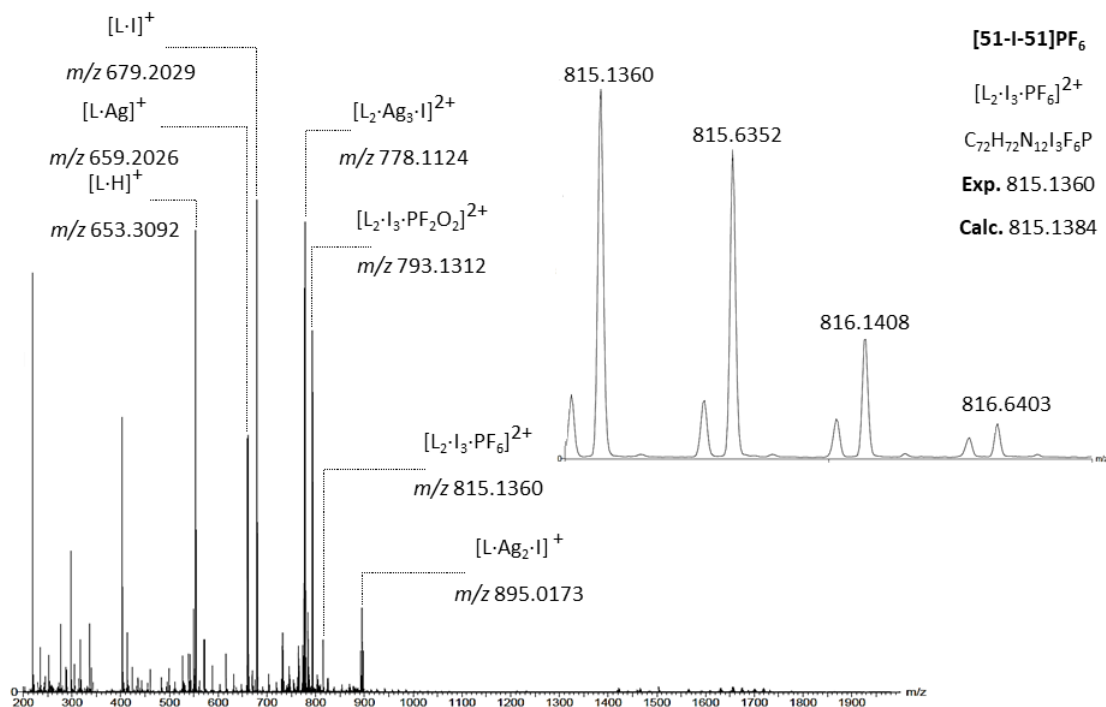


Figure 35 The ESI-TOF mass spectrum of iodine(I) cage of **51**. Insets show the zoomed views for the peak at m/z 815.

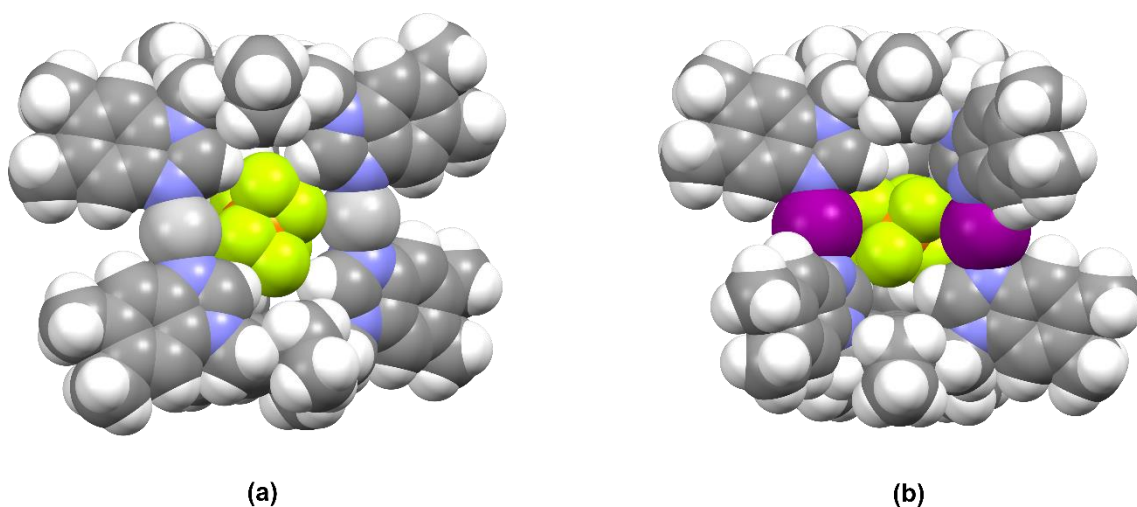


Figure 36 (a) The crystal structure of silver(I) cage with **53** encapsulating a hexafluorophosphate anion and (b) the computational model of the analogous iodine(I) cage.

slightly restrict these values and the angles were in general closer to linear than observed for the monodentate ligands.^{III} The main objective in the cage design was anion encapsulation, which was successful in 9 of the structures. However, as is common in supramolecular host-guest chemistry,¹⁵³ in two cases the anion was found heavily disordered inside the cage and therefore required an untenable number of restraints and constraints to, at best, poorly model their disorder, which was further complicated by their high symmetry, resulting in the best possible solution of accounting for the corresponding electron density from these structures computationally. However, some anions were tightly encapsulated and nicely ordered in their cages (Figure 37). To further investigate the interactions between the ionic counterparts, the shortest distances between the anionic and cationic species were evaluated. The shortest silver(I) distances to the anionic fluorenes were found between 2.66(1) and 2.802(9) Å. In addition, hydrogen bonds between the fluorine atoms and the aromatic imidazole C–H moieties were estimated to be between 2.33 Å and 2.66 Å, which along with the ionic interactions remain shorter than the sum of the van der Waals radii⁵⁴ of the corresponding atoms (Ag–F = 3.19 Å, F···H = 2.67 Å). However, the distances rely on the orientation of the anion, and therefore, an additional Hirshfeld analysis¹³¹ using CrystalExplorer¹⁵⁴ was performed. The Ag(I) cage of **53** encapsulating a hexafluoroantimonate is presented in Figure 37 and the Hirshfeld analysis performed on the same structure is presented in Figure 38. Both the Ag–F and F···H interactions can be seen on the Hirshfeld surface as bright red dots indicating contacts closer than the van der Waals radii. From the surface analysis, the cation-anion interactions seem to be governing the anion encapsulation, however, a significant contribution comes from the hydrogen bonding which is depicted by the 2D fingerprint plot (Figure 38), where the Ag–F and F···H interactions are displayed as spikes at the bottom-left part of the plot. In general, the Ag–F interaction was determined to contribute 9.2 – 17.0% of the interactions in all cage

structures and the F...H interactions contributed 81.8 – 90.8% with minor contributions from other interactions.

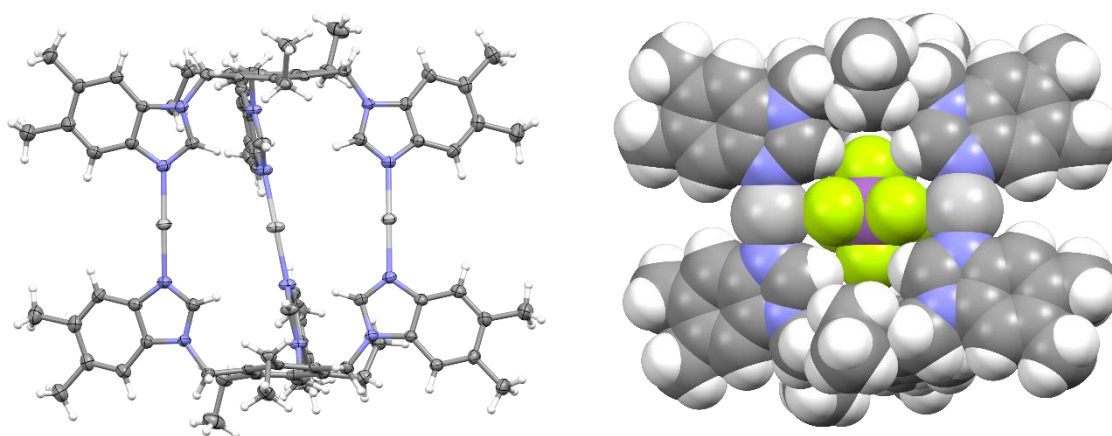


Figure 37 The ORTEP (guest omitted) and spacefill (guest present) representations of the silver(I) cage crystal structure of **53** with a hexafluorophosphate anion. Anions outside the cage omitted for clarity. Thermal displacement ellipsoids drawn at the 50% probability level.

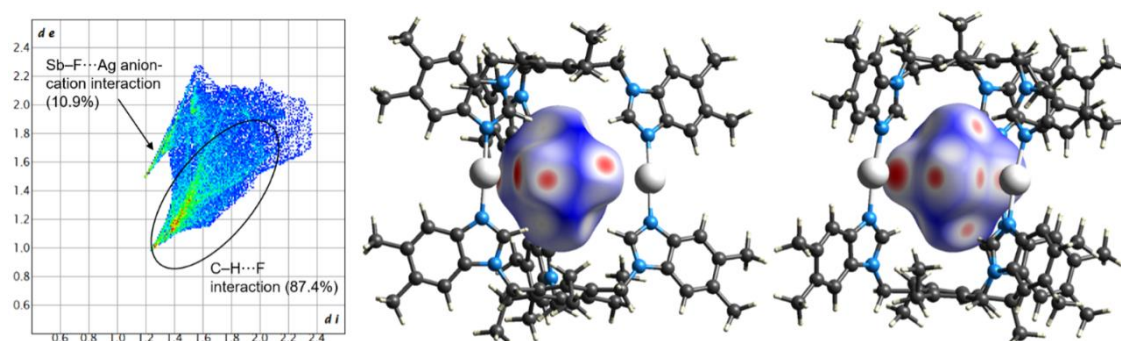


Figure 38 Full fingerprint regions of the hexafluoroantimonate anion in the silver(I) cage of **53** and two views of the intermolecular contacts to the Hirshfeld surface of the anion. Other interactions contributing to the anion binding: Sb-F...C (1.7%). In the fingerprint plot, d_i represents the closest internal distance from a given point on the Hirshfeld surface, and d_e is the closest external contact (in Å).

In summary, the formation of the dimeric iodine(I) cages based on imidazole-derived tripodal ligands was confirmed in solution with NMR spectroscopy as well as in the gas phase with ESI-MS and IM-MS. In addition, the parent silver(I) cages were crystallized and analyzed with single crystal X-ray diffraction. Structural similarities were observed between the analogous silver(I) and iodine(I) cages by comparing the Ag⁺ crystal structures to the theoretical I⁺ cages, in addition to the comparable IM-MS spectra of the two species. Unfortunately, the crystal structures of the iodine(I) cages remained elusive. For all the cages, [L₂X₃]²⁺ ions were observed in the mass spectra, indicating stronger interactions between the cage and one of the anions. These results would suggest that the anion

encapsulation occurs also in the gas phase, and therefore, would also support the postulation that anion encapsulation could occur in solution as well. However, during crystallization, in the iodine(I) cages, the anisotropic nature of the I^+ cation might result in repulsive interactions with the fluorinated anions preventing the encapsulation of the anion. This would lead to problems in terms of packing in the solid state with excess voids in the structure, which would inevitably result in a powder form. However, the work herein serves as further proof of the practicality of the iodine(I) synthon in the design of more complex supramolecular structures.

CONCLUSIONS

The work within this thesis focused on the synthetic and structural studies on hydrogen- and halogen-bonded complexes of selected aromatic amines. The self-assembly and reversibility of non-covalent interactions render them imperative tools in smarter molecular design and functionalization. The effect of charge-assisted hydrogen bonding on simple *N*-heterocycles was used as a preliminary study to gain further information on acid-base interactions for supramolecular emission control. Protonation was found to be an effective tool in fluorescence enhancement of both quinolines as well as the synthesized novel carbazole emitters. An over 50-fold increase in the naturally very weakly fluorescent isoquinoline was observed upon protonation with benzenesulfonic acid. In addition, 50 nm bathochromic shift was observed in the fluorescence maximum of benzo[*h*]quinoline, which demonstrated the tunability of the fluorescence of *N*-heterocycles using intermolecular interactions.

Moreover, the density functional theory provided information on the inner-workings of the carbazole molecules upon protonation. The intramolecular rotation was determined to direct the excited state relaxation processes resulting in either fluorescence enhancement or quenching upon protonation. The studies on the carbazole emitters yielded further insight into the effects of protonation on the solid-state luminescence properties. The control over the charge-assisted hydrogen bonding provides tools for directing the excited state relaxation pathways, and therefore, emission control. Furthermore, the results of the second publication suggested protonation to lower the energy gap between the first excited singlet and the triplet state, which could enhance reverse intersystem crossing and result in a more efficient thermally activated delayed fluorescence process. The protonation-induced restriction of intramolecular rotation was proposed as a way for future development of emitter materials.

The novelty of 3c-4e halogen bonds of halonium ions was discussed in the publications **III** and **IV** when new [N–I–N]⁺ halogen-bonded complexes based on imidazole and carbazole moieties were designed and synthesized. Both publications yielded information on the [N–I–N]⁺ halogen bond as well as on the parent silver(I) complexes. It was postulated, that the inherent anisotropic nature of the I⁺ cation prevented the anion encapsulation in the dimeric [N–I–N]⁺ cages in the solid state, which could explain the elusiveness of the X-ray crystal structures of the [N–I–N]⁺ capsular assemblies. However, the systematic study of the [N–I–N]⁺ cages provided indisputable evidence of the importance of the 3c-4e halogen bond as a supramolecular synthon to be used in future materials based on halogen bonding.

REFERENCES

- 1 J.-M. Lehn, *Angewandte Chemie International Edition in English*, 1988, **27**, 89–112.
- 2 V. I. Minkin, *Pure and Applied Chemistry*, 1999, **71**, 1919–1981.
- 3 J. W. Steed and J. L. Atwood, *Supramolecular chemistry*, Wiley, Chichester, UK, 2nd ed., 2009.
- 4 The Nobel Prize in Chemistry 1987. NobelPrize.org. Nobel Prize Outreach AB 2021. Wed. 8 Sep 2021.
- 5 S. Erbas-Cakmak, D. A. Leigh, C. T. McTernan and A. L. Nussbaumer, *Chemical Reviews*, 2015, **115**, 10081–10206.
- 6 A. K. Gatiatulin, M. A. Ziganshin and V. v. Gorbachuk, *Frontiers in Chemistry*, 2020, **7**, 1–8.
- 7 G. M. Whitesides and B. Grzybowski, *Science*, 2002, **295**, 2418–2421.
- 8 A. S. Iyer and K. Paul, *IET Nanobiotechnology*, 2015, **9**, 122–135.
- 9 A. Galan and P. Ballester, *Chemical Society Reviews*, 2016, **45**, 1720–1737.
- 10 T. R. Cook, V. Vajpayee, M. H. Lee, P. J. Stang and K. W. Chi, *Accounts of Chemical Research*, 2013, **46**, 2464–2474.
- 11 K. Harris, D. Fujita and M. Fujita, *Chemical Communications*, 2013, **49**, 6703–6712.
- 12 E. Arunan, G. R. Desiraju, R. A. Klein, J. Sadlej, S. Scheiner, I. Alkorta, D. C. Clary, R. H. Crabtree, J. J. Dannenber, P. Hobza, H. G. Kjaergaard, A. C. Legon, B. Mennucci and D. J. Nesbitt, *Pure and Applied Chemistry*, 2011, **83**, 1637–1641.
- 13 S. Thomas, *Angewandte Chemie International Edition*, 2002, **41**, 48–76.
- 14 S. Scheiner, *Journal of the Indian Institute of Science*, 2020, **100**, 61–76.
- 15 D. Herschlag and M. M. Pinney, *Biochemistry*, 2018, **57**, 3338–3352.
- 16 V. May and O. Kühn, *Charge and Energy Transfer Dynamics in Molecular Systems*, Wiley, Weinheim, Germany, 3rd ed., 2011.
- 17 A. M. S. Riel, R. K. Rowe, E. N. Ho, A. C. C. Carlsson, A. K. Rappé, O. B. Berryman and P. S. Ho, *Accounts of Chemical Research*, 2019, **52**, 2870–2880.
- 18 G. A. Jeffrey, *An Introduction to Hydrogen Bonding*, Oxford University Press, Oxford, UK, 1997.
- 19 G. R. Desiraju, *Angewandte Chemie International Edition in English*, 1995, **34**, 2311–2327.
- 20 P. K. Thallapally, G. R. Desiraju, M. Bagieu-beucher and R. Masse, *Optical Materials*, 2002, 1052–1053.
- 21 H. B. Bürgi and J. D. Dunitz, *Accounts of Chemical Research*, 1983, **16**, 153–161.
- 22 N. K. Beyeh, F. Pan and K. Rissanen, *Angewandte Chemie - International Edition*, 2015, **54**, 7303–7307.
- 23 S. S. Zumdahl, *Chemical Principles*, Houghton Mifflin Company, USA, 2009.
- 24 N. Mataga and S. Tsuno, *Bulletin of the Chemical Society of Japan*, 1957, **30**, 368–374.

- 25 S. Achelle, J. Rodríguez-Lopez, C. Katan and F. Robin-Le Guen, *Journal of Physical Chemistry C*, 2016, **120**, 26986–26995.
- 26 M. Li, Y. Yuan and Y. Chen, *ACS Applied Materials and Interfaces*, 2018, **10**, 1237–1243.
- 27 C. B. Aakeröy and K. R. Seddon, *Chemical Society Reviews*, 1993, **22**, 397–407.
- 28 G. R. Desiraju, P. Shing Ho, L. Kloo, A. C. Legon, R. Marquardt, P. Metrangolo, P. Politzer, G. Resnati and K. Rissanen, *Pure and Applied Chemistry*, 2013, **85**, 1711–1713.
- 29 G. Cavallo, P. Metrangolo, R. Milani, T. Pilati, A. Priimagi, G. Resnati and G. Terraneo, *Chemical Reviews*, 2016, **116**, 2478–2601.
- 30 J. S. Murray, P. Lane and P. Politzer, *Journal of Molecular Modeling*, 2009, **15**, 723–729.
- 31 P. Politzer, J. S. Murray and T. Clark, *Physical Chemistry Chemical Physics*, 2013, **15**, 11178–11189.
- 32 R. S. Miller, J. S. Murray, K. Paulsen and P. Politzer, *Proc. Indian Acad. Sci.*, 1994, **106**, 267–275.
- 33 T. Brinck, J. S. Murray and P. Politzer, *International Journal of Quantum Chemistry*, 1993, **48**, 73–88.
- 34 L. Turunen and M. Erdélyi, *Chemical Society Reviews*, 2020, **49**, 2688–2700.
- 35 L. C. Gilday, S. W. Robinson, T. A. Barendt, M. J. Langton, B. R. Mullaney and P. D. Beer, *Chemical Reviews*, 2015, **115**, 7118–7195.
- 36 J. Liefbrig, O. Jeannin, A. Frąckowiak, I. Olejniczak, R. Świetlik, S. Dahaoui, E. Aubert, E. Espinosa, P. Auban-Senzier and M. Fourmigué, *Chemistry - A European Journal*, 2013, **19**, 14804–14813.
- 37 F. F. Awwadi, R. D. Willett and B. Twamley, *Journal of Molecular Structure*, 2009, **918**, 116–122.
- 38 T. Clark, M. Hennemann, J. S. Murray and P. Politzer, *Journal of Molecular Modeling*, 2007, **13**, 291–296.
- 39 R. Kurczab, K. Kucwaj-Brysz and P. Śliwa, *Molecules*, , DOI:10.3390/molecules25010091.
- 40 D. A. Decato, A. M. S. Riel, J. H. May, V. S. Bryantsev and O. B. Berryman, *Angewandte Chemie - International Edition*, 2021, **60**, 3685–3692.
- 41 P. Metrangolo, F. Meyer, T. Pilati, G. Resnati and G. Terraneo, *Angewandte Chemie - International Edition*, 2008, **47**, 6114–6127.
- 42 C. B. Aakeröy, N. R. Champness and C. Janiak, *CrystEngComm*, 2010, **12**, 22–43.
- 43 N. Chongboriboon, K. Samakun, T. Inprasit, F. Kielar, W. Dungkaew, L. W. Y. Wong, H. H. Y. Sung, D. B. Ninković, S. D. Zarić and K. Chainok, *CrystEngComm*, 2019, **22**, 24–34.
- 44 L. Kovbasyuk and R. Krämer, *Chemical Reviews*, 2004, **104**, 3161–3187.
- 45 G. Berger, J. Soubhye and F. Meyer, *Polymer Chemistry*, 2015, **6**, 3559–3580.
- 46 Ö. D. Ateş, Y. Zorlu, S. D. Kanmazalp, Y. Chumakov, A. G. Gürek and M. M. Ayhan, *CrystEngComm*, 2018, **20**, 3858–3867.
- 47 J. A. Creighton, I. Haque and J. L. Wood, *Chemical Communications (London)*, 1966, 892.

- 48 I. Haque and J. L. Wood, *Journal of Molecular Structure*, 1968, **2**, 217–238.
- 49 J. A. Creighton, I. Haque and J. L. Wood, *Chemical Communications (London)*, 1966, 892.
- 50 G. Espuña, G. Arsequell, G. Valencia, J. Barluenga, M. Pérez and J. M. González, *Chemical Communications*, 2000, 1307–1308.
- 51 J. Barluenga, J. M. González, M. A. Garcia-Martin, P. J. Campos and G. Asensio, *Journal of the Chemical Society, Chemical Communications*, 1992, **4**, 1016–1017.
- 52 J. Barluenga, F. González-Bobes, M. C. Murguía, S. R. Ananthoju and J. M. González, *Chemistry - A European Journal*, 2004, **10**, 4206–4213.
- 53 J. Ezquerra, C. Pedregal, C. Lamas, J. Barluenga, M. Pérez, M. A. García-Martín and J. M. González, *Journal of Organic Chemistry*, 1996, **61**, 5804–5812.
- 54 A. Bondi, *J. Phys. Chem.*, 1964, **68**, 441–451.
- 55 R. Puttreddy, J. M. Rautiainen, T. Mäkelä and K. Rissanen, *Angewandte Chemie - International Edition*, 2019, **58**, 18610–18618.
- 56 A. C. C. Carlsson, J. Gräfenstein, J. L. Laurila, J. Bergquist and M. Erdélyi, *Chemical Communications*, 2012, **48**, 1458–1460.
- 57 S. B. Hakkert and M. Erdélyi, *Journal of Physical Organic Chemistry*, 2015, **28**, 226–233.
- 58 A. Karim, M. Reitti, A. C. C. Carlsson, J. Gräfenstein and M. Erdélyi, *Chemical Science*, 2014, **5**, 3226–3233.
- 59 A. C. Reiersølmoen, S. Battaglia, S. Øien-Ødegaard, A. K. Gupta, A. Fiksdahl, R. Lindh and M. Erdélyi, *Chemical Science*, 2020, **11**, 7979–7990.
- 60 A. C. C. Carlsson, J. Gräfenstein, A. Budnjo, J. L. Laurila, J. Bergquist, A. Karim, R. Kleinmaier, U. Brath and M. Erdélyi, *Journal of the American Chemical Society*, 2012, **134**, 5706–5715.
- 61 D. von der Heiden, K. Rissanen and M. Erdélyi, *Chemical Communications*, 2020, **56**, 14431–14434.
- 62 A. C. C. Carlsson, K. Mehmeti, M. Uhrbom, A. Karim, M. Bedin, R. Puttreddy, R. Kleinmaier, A. A. Neverov, B. Nekoueishahraki, J. Gräfenstein, K. Rissanen and M. Erdélyi, *Journal of the American Chemical Society*, 2016, **138**, 9853–9863.
- 63 A. C. C. Carlsson, M. Uhrbom, A. Karim, U. Brath, J. Gräfenstein and M. Erdélyi, *CrystEngComm*, 2013, **15**, 3087–3092.
- 64 M. Bedin, A. Karim, M. Reitti, A. C. C. Carlsson, F. Topić, M. Cetina, F. Pan, V. Havel, F. Al-Ameri, V. Sindelar, K. Rissanen, J. Gräfenstein and M. Erdélyi, *Chemical Science*, 2015, **6**, 3746–3756.
- 65 J. S. Ward, A. Frontera and K. Rissanen, *Chemical Communications*, 2021, **57**, 5094–5097.
- 66 J. S. Ward, A. Frontera and K. Rissanen, *Inorganic Chemistry*, 2021, **60**, 5383–5390.
- 67 J. S. Ward, A. Frontera and K. Rissanen, *Dalton Transactions*, 2021, **50**, 8297–8301.
- 68 S. Yu, J. S. Ward, K. Truong and K. Rissanen, *Angewandte Chemie International Edition*, 2021, **60**, 20739–20743.

- 69 J. S. Ward, G. Fiorini, A. Frontera and K. Rissanen, *Chemical Communications*, 2020, **56**, 8428–8431.
- 70 S. Yu, P. Kumar, J. S. Ward, A. Frontera and K. Rissanen, *Chem*, 2021, **7**, 948–958.
- 71 L. Turunen, U. Warzok, R. Puttreddy, N. K. Beyeh, C. A. Schalley and K. Rissanen, *Angewandte Chemie - International Edition*, 2016, **55**, 14033–14036.
- 72 L. Turunen, U. Warzok, C. A. Schalley and K. Rissanen, *Chem*, 2017, **3**, 861–869.
- 73 L. Turunen, A. Peuronen, S. Forsblom, E. Kalenius, M. Lahtinen and K. Rissanen, *Chemistry - A European Journal*, 2017, **23**, 11714–11718.
- 74 C. Álvarez-Rúa, S. García-Granda, A. Ballesteros, F. González-Bobes and J. M. González, *Acta Crystallographica Section E Structure Reports Online*, 2002, **58**, o1381–o1383.
- 75 B. Wardle, *Principles and Applications of Photochemistry*, John Wiley & Sons, Ltd., Chichester, UK, 2009.
- 76 B. Valeur, *Molecular Fluorescence: Principles and Applications*, Wiley, Weinheim, Germany, 2002.
- 77 Z. Yang, Z. Mao, Z. Xie, Y. Zhang, S. Liu, J. Zhao, J. Xu, Z. Chi and M. P. Aldred, *Chemical Society Reviews*, 2017, **46**, 915–1016.
- 78 W. Sun, Z. Wang, T. Wang, L. Yang, J. Jiang, X. Zhang, Y. Luo and G. Zhang, *Journal of Physical Chemistry A*, 2017, **121**, 4225–4232.
- 79 J. K. Salunke, N. A. Durandin, T. P. Ruoko, N. R. Candeias, P. Vivo, E. Vuorimaa-Laukkanen, T. Laaksonen and A. Priimagi, *Scientific Reports*, 2018, **8**, 1–8.
- 80 N. L. C. Leung, N. Xie, W. Yuan, Y. Liu, Q. Wu, Q. Peng, Q. Miao, J. W. Y. Lam and B. Z. Tang, *Chemistry - A European Journal*, 2014, **20**, 15349–15353.
- 81 S. Park, O. H. Kwon, S. Kim, S. Park, M. G. Choi, M. Cha, S. Y. Park and D. J. Jang, *Journal of the American Chemical Society*, 2005, **127**, 10070–10074.
- 82 B. Kupcewicz and M. Małecka, *Crystal Growth and Design*, 2015, **15**, 3893–3904.
- 83 F. Würthner, T. E. Kaiser and C. R. Saha-Möller, *Angewandte Chemie - International Edition*, 2011, **50**, 3376–3410.
- 84 C. Maeda, T. Todaka, T. Ueda and T. Ema, *Chemistry - A European Journal*, 2016, **22**, 7508–7513.
- 85 R. Wyler, J. de Mendoza and J. Rebek, *Angewandte Chemie International Edition in English*, 1993, **32**, 1699–1701.
- 86 I. Thondorf, F. Broda, K. Rissanen, M. Vysotsky and V. Böhmer, *Journal of the Chemical Society. Perkin Transactions 2*, 2002, **2**, 1796–1800.
- 87 M. Chas, G. Gil-Ramírez and P. Ballester, *Organic Letters*, 2011, **13**, 3402–3405.
- 88 D. Ken and J. Rebek, 1995, **92**, 12403–12407.
- 89 K. Twum, K. Rissanen and N. K. Beyeh, *Chemical Record*, 2021, **21**, 386–395.
- 90 N. K. Beyeh and K. Rissanen, *Israel Journal of Chemistry*, 2011, **51**, 769–780.
- 91 H. Mansikkamäki, M. Nissinen and K. Rissanen, *CrystEngComm*, 2005, **7**, 519–526.

- 92 A. Kiesilä, L. Kivijärvi, N. K. Beyeh, J. O. Moilanen, M. Groessel, T. Rothe, S. Götz, F. Topić, K. Rissanen, A. Lützen and E. Kalenius, *Angewandte Chemie - International Edition*, 2017, **56**, 10942–10946.
- 93 A. Kiesilä, N. K. Beyeh, J. O. Moilanen, R. Puttreddy, S. Götz, K. Rissanen, P. Barran, A. Lützen and E. Kalenius, *Organic and Biomolecular Chemistry*, 2019, **17**, 6980–6984.
- 94 D. P. Weimann and C. A. Schalley, *Supramolecular Chemistry*, 2008, **20**, 117–128.
- 95 N. K. Beyeh, F. Pan, A. Valkonen and K. Rissanen, *CrystEngComm*, 2015, **17**, 1182–1188.
- 96 L. R. MacGillivray and J. L. Atwood, *Nature*, 1997, **389**, 469–472.
- 97 A. Shivanyuk, K. Rissanen and E. Kolehmainen, *Chemical Communications*, 2000, 1107–1108.
- 98 C. M. A. Gangemi, A. Pappalardo and G. Trusso Sfrassetto, *RSC Advances*, 2015, **5**, 51919–51933.
- 99 R. Puttreddy, N. K. Beyeh, E. Kalenius, R. H. A. Ras and K. Rissanen, *Chemical Communications*, 2016, **52**, 8115–8118.
- 100 L. Avram, Y. Cohen and J. Rebek, *Chemical Communications*, 2011, **47**, 5368–5375.
- 101 H. Mansikkam, M. Nissinen and K. Rissanen, *ChemComm*, 2002, 1902–1903.
- 102 C. B. Aakeröy, A. Rajbanshi, P. Metrangolo, G. Resnati, M. F. Parisi, J. Desper and T. Pilati, *CrystEngComm*, 2012, **14**, 6366–6368.
- 103 U. Warzok, M. Marianski, W. Hoffmann, L. Turunen, K. Rissanen, K. Pagel and C. A. Schalley, *Chemical Science*, 2018, **9**, 8343–8351.
- 104 E. Taipale, M. Siepmann, K.-N. Truong and K. Rissanen, *Chem Eur J*.
- 105 B. S. Matada, R. Pattanashettar and N. G. Yernale, *Bioorganic and Medicinal Chemistry*, 2021, **32**, 115973.
- 106 Y. B.R.D. Rajesh, *Heterocycles - Synthesis and Biological Activities*, , DOI:10.5772/intechopen.81239.
- 107 V. Antoci, L. Oniciuc, D. Amariuca-mantu, C. Moldoveanu, V. Mangalagiu and G. Zbancioc, .
- 108 M. Gensicka-Kowalewska, G. Cholewiński and K. Dzierzbicka, *RSC Advances*, 2017, **7**, 15776–15804.
- 109 N. K. Joshi, H. C. Joshi, R. Gahlaut, N. Tewari, R. Rautela and S. Pant, *Journal of Physical Chemistry A*, 2012, **116**, 7272–7278.
- 110 N. Mataga, *Bulletin of the Chemical Society of Japan*, 1958, **31**, 459–462.
- 111 M. F. Anton and W. R. Moomaw, *The Journal of Chemical Physics*, 1976, **66**, 1808–1818.
- 112 A. Verma, S. Joshi and D. Singh, *Journal of Chemistry*, , DOI:10.1155/2013/329412.
- 113 M. Nissinen and K. Rissanen, *Supramolecular Chemistry*, 2003, **15**, 581–590.
- 114 Z. A. Tabasi, J. C. Walsh, G. J. Bodwell, D. W. Thompson and Y. Zhao, *Crystall Growth and Design*, 2020, **20**, 1681–1693.
- 115 T. Aggarwal, Sushmita and A. K. Verma, *Organic and Biomolecular Chemistry*, 2019, **17**, 8330–8342.

- 116 R. H. P, B. D. Emmanuel, J. Beevi and S. S. Dharan, 2020, **12**, 1271–1277.
- 117 T. W. Chen, V. K. Karapala, J. T. Chen and C. S. Hsu, *Journal of the Chinese Chemical Society*, 2021, **68**, 1186–1196.
- 118 W. Li, J. Li, D. Liu and Q. Jin, *ACS Applied Materials and Interfaces*, 2016, **8**, 22382–22391.
- 119 C. H. Chen, L. C. Hsu, P. Rajamalli, Y. W. Chang, F. I. Wu, C. Y. Liao, M. J. Chiu, P. Y. Chou, M. J. Huang, L. K. Chu and C. H. Cheng, *Journal of Materials Chemistry C*, 2014, **2**, 6183–6191.
- 120 B. Wex and B. R. Kaafarani, *Journal of Materials Chemistry C*, 2017, **5**, 8622–8653.
- 121 A. Aguilar-Granda, S. Pérez-Estrada, A. E. Roa, J. Rodríguez-Hernández, S. Hernández-Ortega, M. Rodriguez and B. Rodríguez-Molina, *Crystal Growth and Design*, 2016, **16**, 3435–3442.
- 122 D. Zhang, M. Cai, Y. Zhang, D. Zhang and L. Duan, *ACS Applied Materials and Interfaces*, 2015, **7**, 28693–28700.
- 123 W. Liu, C. J. Zheng, K. Wang, M. Zhang, D. Y. Chen, S. L. Tao, F. Li, Y. P. Dong, C. S. Lee, X. M. Ou and X. H. Zhang, *ACS Applied Materials and Interfaces*, 2016, **8**, 32984–32991.
- 124 W. Li, J. Li, D. Liu, F. Wang and S. Zhang, *Journal of Materials Chemistry C*, 2015, **3**, 12529–12538.
- 125 H. J. Knölker and K. R. Reddy, *Chemical Reviews*, 2002, **102**, 4303–4427.
- 126 J. Clayden, N. Greeves and S. Warren, *Organic Chemistry 2nd ed.*, Oxford University Press, New York, USA, 2012.
- 127 R. C. Nishad and A. Rit, *Chemistry - A European Journal*, 2021, **27**, 594–599.
- 128 Y. Yuan, Z. L. Jiang, J. M. Yan, G. Gao, A. S. C. Chan and R. G. Xie, *Synthetic Communications*, 2000, **30**, 4555–4561.
- 129 W. J. Yoo, T. Tsukamoto and S. Kobayashi, *Organic Letters*, 2015, **17**, 3640–3642.
- 130 K. Leduskrasts, A. Kinens and E. Suna, *Chemical Communications*, 2019, **55**, 12663–12666.
- 131 M. A. Spackman and D. Jayatilaka, *CrystEngComm*, 2009, **11**, 19–32.
- 132 P. Rajamalli, D. Rota Martir and E. Zysman-Colman, *Journal of Photonics for Energy*, 2018, **8**, 1.
- 133 Y. Shirota, M. Kinoshita, T. Noda, K. Okumoto and T. Ohara, *Journal of the American Chemical Society*, 2000, **122**, 11021–11022.
- 134 A. Chaskar, H. F. Chen and K. T. Wong, *Advanced Materials*, 2011, **23**, 3876–3895.
- 135 M. Sarma and K. T. Wong, *Chemical Record*, 2019, **19**, 1667–1692.
- 136 Z. Shi, D. Zhang, J. Huo, H. Wang, J. Yu, H. Shi and B. Z. Tang, *Journal of Materials Research*, 2019, **34**, 3000–3010.
- 137 A. Endo, K. Sato, K. Yoshimura, T. Kai, A. Kawada, H. Miyazaki and C. Adachi, *Applied Physics Letters*, 2011, **98**, 2011–2014.
- 138 T. Okitsu, S. Yumitate, K. Sato, Y. In and A. Wada, *Chemistry - A European Journal*, 2013, **19**, 4992–4996.

- 139 Y. Kim, E. J. McKinley, K. E. Christensen, N. H. Rees and A. L. Thompson, *Crystal Growth and Design*, 2014, **14**, 6294–6301.
- 140 L. C. F. Morgan, Y. Kim, J. N. Blandy, C. A. Murray, K. E. Christensen and A. L. Thompson, *Chemical Communications*, 2018, **54**, 9849–9852.
- 141 E. Kukkonen, H. Malinen, M. Haukka and J. Konu, *Crystal Growth and Design*, 2019, **19**, 2434–2445.
- 142 A. Vanderkooy, A. K. Gupta, T. Földes, S. Lindblad, A. Orthaber, I. Pápai and M. Erdélyi, *Angewandte Chemie - International Edition*, 2019, **58**, 9012–9016.
- 143 O. Hassel and H. Hope, *Acta Chem Scand*, 1961, **15**, 407–416.
- 144 S. B. Hakkert, J. Gräfenstein and M. Erdelyi, *Faraday Discussions*, 2017, **203**, 333–346.
- 145 H. Stephan, T. Krüger-Rambusch, R. Gloe, W. Hasse, B. Ahlers, K. Cammann, K. Rissanen, G. Brodesser and F. Vögtle, *Chemistry - A European Journal*, 1998, **4**, 434–440.
- 146 C. Y. Su, Y. P. Cai, C. L. Chen, F. Lissner, B. S. Kang and W. Kaim, *Angewandte Chemie - International Edition*, 2002, **41**, 3371–3375.
- 147 W. Y. Sun, J. Fan, T. A. Okamura, J. Xie, K. B. Yu and N. Ueyama, *Chemistry - A European Journal*, 2001, **7**, 2557–2562.
- 148 S. Bhattacharya and B. K. Saha, *Journal of Chemical Sciences*, 2016, **128**, 207–216.
- 149 H. K. Liu, X. Huang, T. Lu, X. Wang, W. Y. Sun and B. S. Kang, *Dalton Transactions*, 2008, **3**, 3178–3188.
- 150 J. Fan, W. Y. Sun, T. aki Okamura, J. Xie, W. X. Tang and N. Ueyama, *New Journal of Chemistry*, 2002, **26**, 199–201.
- 151 J. Fan, H. F. Zhu, T. A. Okamura, W. Y. Sun, W. X. Tang and N. Ueyama, *Chemistry - A European Journal*, 2003, **9**, 4724–4731.
- 152 E. Kalenius, M. Groessl and K. Rissanen, *Nature Reviews Chemistry*, 2019, **3**, 4–14.
- 153 K. Rissanen, *Chemical Society Reviews*, 2017, **46**, 2638–2648.
- 154 P. R. Spackman, M. J. Turner, J. J. McKinnon, S. K. Wolff, D. J. Grimwood, D. Jayatilaka and M. A. Spackman, *Journal of Applied Crystallography*, 2021, **54**, 1006–1011.



ORIGINAL PAPERS

I

FLUORESCENCE ENHANCEMENT OF QUINOLINES BY PROTONATION

by

E. Tervola, K.-N. Truong, J. S. Ward, A. Priimagi & K. Rissanen 2020

RSC Adv., 2020, 10, 29385–29393

<https://doi.org/10.1039/D0RA04691D>

Article is licensed under a Creative Commons
Attribution-NonCommercial 3.0 Unported (CC BY-NC 3.0) licence.


 Cite this: *RSC Adv.*, 2020, 10, 29385

Fluorescence enhancement of quinolines by protonation†

 Essi Tervola,^a Khai-Nghi Truong,^a Jas S. Ward,^a Arri Priimagi^b and Kari Rissanen^{*,a}

A study of the fluorescence enhancement of isoquinoline, acridine (benzo[*b*]quinoline) and benzo[*h*]quinoline is reported with six organic acids of different pK_a values. Protonation was found to be an effective tool in the fluorescence enhancement of quinolines. A significant increase in the fluorescence intensity is observed only when strong acids are used, resulting in an over 50-fold increase in fluorescence with trifluoroacetic or benzenesulfonic acid and isoquinoline in a 1.5 : 1 ratio. The benzenesulfonic acid was found to be the most effective in the protonation of the bases despite its higher pK_a value compared to trifluoro- and trichloroacetic acid. The X-ray crystal structures of 14 salts reveal the charge-assisted hydrogen bond O...N distances to vary very little, from 2.560(2)–2.714(3) Å, with the exception of the isoquinolinium benzenesulfonate where the O...N distance of 2.862(7) Å is caused by additional intermolecular interactions in the solid-state.

Received 27th May 2020

Accepted 23rd July 2020

DOI: 10.1039/d0ra04691d

rsc.li/rsc-advances

Introduction

Supramolecular chemistry has been defined as “the chemistry of the intermolecular bond, covering the structures and functions of the entities formed by association of two or more chemical species”.¹ The field of supramolecular chemistry has gained notable interest in the past decades due to its great potential in many subfields of molecular self-assembly, molecular recognition, and molecular machinery, all gaining advantage from non-covalent bonds.² Non-covalent interactions cover electrostatic, hydrogen-bonding, halogen-bonding, aromatic donor–acceptor, cation– and anion– π interactions, and solvophobic effects. Understanding the chemistry and intermolecular interactions of molecular entities and their associations provides significant advantages in the synthetic design of new systems, and are essential for understanding the world around us.

The importance of luminescence control is apparent not only in biological applications, *e.g.*, as a biosensing tool,³ but also as an emission control in optical applications, such as lighting or organic light-emitting diodes.⁴ A pH-dependent fluorescence has been reported in various occasions: de Silva *et al.* reported pH-dependent fluorescence of naphthalenic derivatives for molecular sensing and switching,^{5,6} Ma *et al.*

have reported pH-dependent fluorescent probes for cancer cell imaging,⁷ and already decades ago Mataga *et al.* studied the hydrogen bonding effect on the fluorescence of some N-heterocycles.⁸

N-Heterocycles, such as quinolines, are known to be weakly fluorescent in comparison to their isoelectronic hydrocarbons. These heterocycles possess non-bonding electrons which give rise to ($n-\pi^*$) excited states resulting in an increased spin–orbit coupling.^{9–11} This coupling leads to an enhanced intersystem crossing, effectively decreasing the fluorescence quantum yield. It is also commonly observed that the protonation of the “aromatic” nitrogen results in a loss of emission fine structure and a notable red-shift in the emission wavelength.¹² Thus, studies of structurally simple N-heterocycles are vital for understanding further the effects of protonation on the emission of molecules.

The first report on the fluorescence of isoquinoline was recorded in frozen ethanol by Zimmermann and Joop nearly 50 years ago,¹³ and later Ziegler and El-Sayed reported the phosphorescence of isoquinoline.¹⁴ Additionally, the luminescence properties of nitrogen-containing heterocycles have been known to be strongly affected by the choice of solvent.¹⁵ The excited-state proton transfer in N-heterocycles, including isoquinoline and benzo[*h*]quinoline, has been previously studied in acidic media.^{9,16–18} Benzo[*h*]quinoline and acridine (benzo[*b*]quinoline), belonging to a group of polycyclic aromatic N-heterocycles, have been discovered to be particularly interesting since they possess different pK_a values in the ground and excited state.^{19–22} However, there has been no studies that are based on comparing different acids and the effects of the resulting counter-anion. The previous research in this area has

^aDepartment of Chemistry, University of Jyväskylä, P.O. Box 35, Surfontie 9B, 40014 Jyväskylä, Finland. E-mail: kari.t.rissanen@jyu.fi

^bSmart Photonic Materials, Faculty of Engineering and Natural Sciences, Tampere University, P.O. Box 541, FI-33101 Tampere, Finland

† Electronic supplementary information (ESI) available. CCDC 2000976–2000989. For ESI and crystallographic data in CIF or other electronic format see DOI: 10.1039/d0ra04691d



been scarce and focused on studying the emission of these compounds with a single base and, to the best of our knowledge, there are no reports of studies using single crystal X-ray diffraction to study the structural effects of protonation on these N-heterocycles.

Herein, we have compiled a comprehensive study on the effects of protonation on the fluorescence of three different quinolines using six different organic acids in solution and the structures of the resulting salts in the solid-state using single crystal X-ray diffraction.

Results and discussion

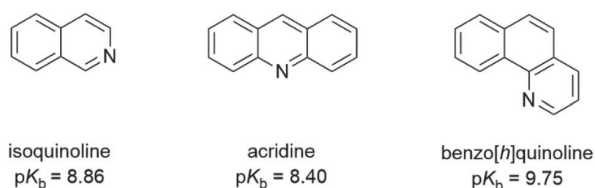
The protonation of isoquinoline, acridine, and benzo[*h*]quinoline (see Scheme 1) was studied using absorption and fluorescence spectroscopy in dichloromethane (DCM, $0.5\text{--}1.0 \times 10^{-4}$ M). The compounds were chosen due to their aromatic nature, commercial availability and the single site for protonation. The protonation was studied using six organic acids with different pK_a values (see Scheme 2). Dichloromethane as an aprotic solvent was chosen to reduce the effects of solvation.

The full protonation of the base leads to an ion pair (a salt). An example of the protonation is depicted in Scheme 3 and investigated further in the following sections.

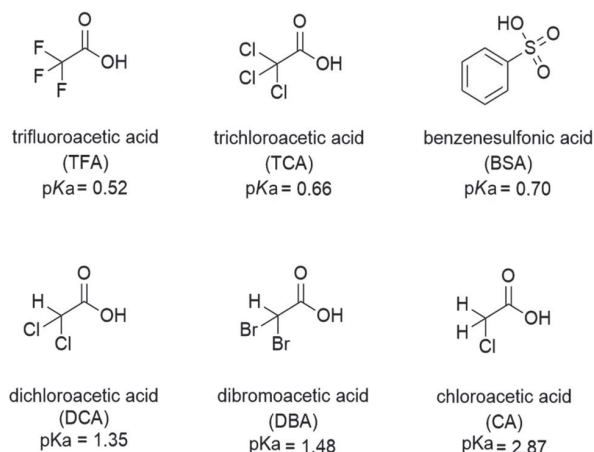
Spectroscopic studies in solution

Fluorescence studies. The absorption and fluorescence spectra of isoquinoline titrated with trifluoroacetic acid (TFA) up to a 4 : 1 acid–base ratio are presented in Fig. 1 (for other acids, see ESI†). Based on the pK_a value of 0.52,²⁴ TFA is the strongest acid used in the experiments. The natural absorbance of isoquinoline in DCM is shown in red. Isoquinoline has three slightly overlapping absorption bands at 268 nm, 305 nm, and 318 nm. As the protonation of the isoquinoline increases, the band at 268 nm decreases and experiences a bathochromic shift of 5 nm. During the protonation process, the band at 305 nm remains roughly the same and a new band arises at 328 nm. At 2.0 equivalents of the acid the spectrum shows saturation indicating a complete protonation of the base, as higher amounts of the acid do not induce any more spectral changes. Interestingly enough, based on the fluorescence spectra isoquinoline seems to be only 68% protonated with 1.0 equivalent of TFA.

The protonation of isoquinoline occurs in the ground state as deduced from the characteristics observed in the absorption spectrum. From the observed changes during the titration, the



Scheme 1 The structures of isoquinoline, acridine, and benzo[*h*]quinoline used as bases and their pK_b values in water.²³

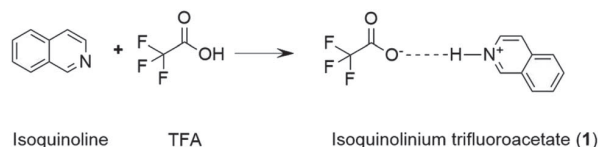


Scheme 2 The structures and pK_a values of the acids used for the protonation of the bases.

absorption at 268 nm can be assigned to the neutral species, whereas the band arising at 328 nm is assigned to the protonated species due to the (π, π^*) transitions at longer wavelengths. Joshi *et al.* observed similar structureless broadband absorption in acidic medium at 330 nm for isoquinoline.⁹ The absorption spectra of acridine and benzo[*h*]quinoline (see ESI†) show similar spectral changes at longer wavelengths due to protonation, but from these spectra, the absorption bands of the neutral and protonated species are difficult to distinguish. The smaller changes in the spectra could indicate that in those compounds, protonation occurs more easily in the excited state than in the ground state.²⁰

The fluorescence intensity of isoquinoline increases significantly upon titration with acid. Similar to the absorption spectra, protonation induces an increase in the fluorescence intensity until the base is fully protonated. Isoquinoline and acridine (Fig. S4†) show only an increase in the intensity while the structure of the spectra remains the same. However, for benzo[*h*]quinoline a bathochromic shift of 50 nm of the fluorescence maxima of the neutral and the cationic species is observed. The absorption and fluorescence spectra of all the bases with different acids are presented in the ESI (see Fig. S1–S6).†

The absorption and fluorescence properties of aromatic N-heterocyclic compounds are strongly dependent on the properties of the solvent environment showing stronger fluorescence in polar solvents and weaker fluorescence in nonpolar solvents.^{25a} In dichloromethane, isoquinoline itself is only weakly fluorescent due to its non-bonded electrons giving rise to an



Scheme 3 The protonation of isoquinoline with trifluoroacetic acid resulting in the isoquinolinium trifluoroacetate salt.



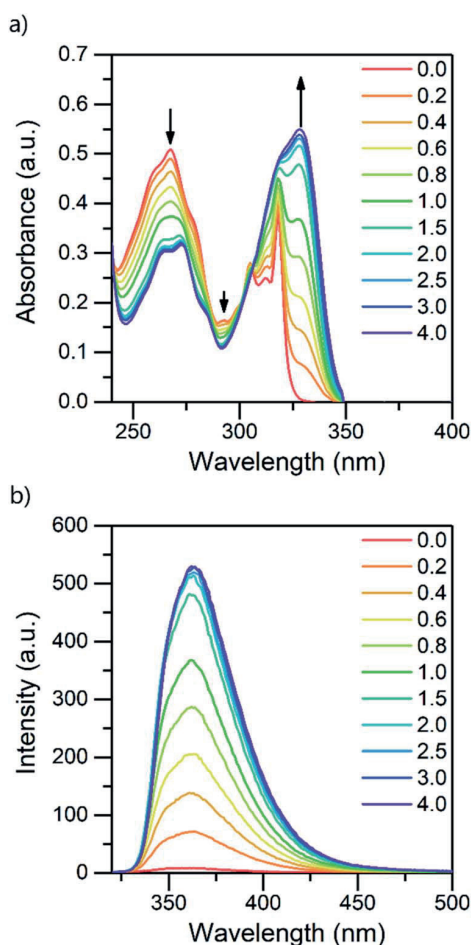


Fig. 1 Absorption (a) and fluorescence (b) spectra of isoquinoline while titrating with TFA from 0.0 to 4.0 equivalents of acid in DCM (10^{-4} M, $\lambda_{\text{ex}} = 310$ nm).

(n, π^*) excited state.²⁶ The lone-pair of the nitrogen atom in the heterocyclic system interacts with the π -electrons restricting the freedom of the π -electrons and making the system π -deficient, and therefore restricting the fluorescence of the whole system.²⁷ Once the nitrogen gets protonated, the lone pair is shared with the hydrogen atom and the S_1 excited state is converted to a (π, π^*) excited state resulting in a state more likely to undergo fluorescence which is observed as an increase in the fluorescence intensity. The fluorescence intensity increases until full protonation after which the intensity remains unchanged. Titration with TFA causes an over 50-fold increase in the fluorescence intensity of isoquinoline. Similar titrations were performed with all the acids shown in Scheme 2. Once the $\text{p}K_{\text{a}}$ value of the acid is higher than 1, the changes in fluorescence decrease significantly to an extent where chloroacetic acid ($\text{p}K_{\text{a}} = 2.87$) induces virtually no changes to the fluorescence properties of isoquinoline due to insufficient donating power of the acid for protonation to occur. The fluorescence spectra of all studied quinolines treated with 1.0 equivalent of acid are presented in Fig. 2.

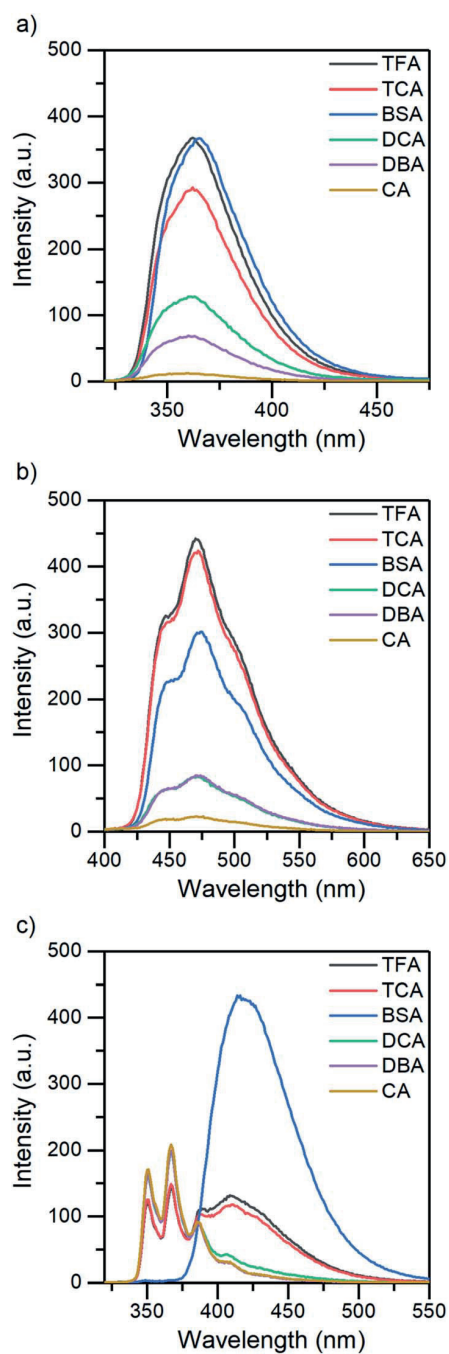


Fig. 2 The fluorescence spectra of (a) isoquinoline, (b) acridine, and (c) benzo[*h*]quinoline treated with 1.0 equivalent of acid in DCM (5×10^{-5} M, $\lambda_{\text{ex}} = 355$ nm for acridine; and 10^{-4} M, $\lambda_{\text{ex}} = 310$ nm for isoquinoline and benzo[*h*]quinoline).

Determination of relative fluorescence intensity change and the fluorescence quantum yield. Joshi *et al.* have previously reported excitation-dependent emission of isoquinoline in an aqueous medium where they distinguished structured fluorescence ($\lambda_{\text{ex}} = 310$ nm) originating from a neutral species and broad emission at longer wavelengths ($\lambda_{\text{ex}} = 330$ nm) due to



(π, π^*) transitions in a cationic species.⁹ The changes in the spectra are dependent on the pK_a value of the acid. The relative fluorescence intensities of the N-heterocycles become larger as the donating power of the acids increase resulting in more effective protonation. The relative intensity change can also be described as the fluorescence enhancement factor proportional to the acid addition. The change in the fluorescence intensity of the compounds was determined in relation to the native fluorescence of the compound. The changes in the fluorescence intensity of isoquinoline with all the acids are shown in Fig. 3a. The relative intensity change follows primarily the same trend with pK_a , excluding benzenesulfonic acid (BSA), the conjugate anion of which has much greater stability than the acetate anions. Due to the more stable anion, even though the pK_a of BSA is higher, it is as effective in protonating the isoquinoline as TFA and similarly manifests an over 50-fold enhancement of the fluorescence intensity from the unprotonated isoquinoline. Similar results were obtained for acridine as well, with a maximum fluorescence enhancement factor of 25. For benzo[h]quinoline, the enhancement is not as significant for the fluorescence intensity since the neutral and cationic species

emit in a very different wavelength and the fluorescence intensity experiences only a 5-fold increase with BSA (see ESI, Fig. S7†).

The fluorescence quantum yield (QY) was studied using eqn (1)^{25b} and 9,10-diphenylanthracene as reference ($\Phi_{FL} = 0.90$, cyclohexane²⁸).

$$\Phi = \Phi_{ref} \frac{\eta^2}{\eta_{ref}^2} \frac{I}{A} \frac{A_{ref}}{I_{ref}} \quad (1)$$

where Φ is the quantum yield, η is the solvent refractive index, I is the integrated fluorescence intensity and A is the absorbance of the compound at the excitation wavelength.

Quantum yields for the quinolines in their native state were determined to be less than 1% for isoquinoline and acridine and 15% for benzo[h]quinoline. Again, by excluding BSA from the analysis, the QY evolution follows the trend of the pK_a values. The greatest increase in QY can be observed for isoquinoline, changing from virtually zero to up to 27% (see Fig. 3b). The maximum fluorescence quantum yields obtained for all the compounds with each acid are listed in Table 1.

The change from the (n, π^*) to (π, π^*) excited state increases the fluorescence quantum yield. This is due to the (n, π^*) states having longer radiative lifetimes than the (π, π^*) states, and shorter lifetimes are more likely to undergo fluorescence before intersystem crossing.²⁶ However, the fluorescence quantum yield is defined as $\Phi_{FL} = 1 - \Phi_{ISC} - \Phi_{IC}$, where Φ_{ISC} is the phosphorescence quantum yield and Φ_{IC} is the quantum yield of internal conversion.

Isoquinoline experiences significant changes in its absorption spectra upon protonation. Distinctive absorption bands can be assigned to the neutral and cationic species differentiating isoquinoline from the other two N-heterocycles. Similar changes can be observed for acridine as well, merely to a smaller extent. Acridine has a different electronic structure leading to very narrow absorption bands and rendering the observation of the change and isosbestic points more challenging. As found for isoquinoline and acridine, the absorption of the cationic species can also be observed for benzo[h]quinoline at higher wavelengths, but contrary to isoquinoline and acridine, the absorption increases throughout the spectrum and no isosbestic points are observed.

In addition to that, benzo[h]quinoline also differs in terms of fluorescence: isoquinoline and acridine only experience an increase in their fluorescence intensity until eventually reaching

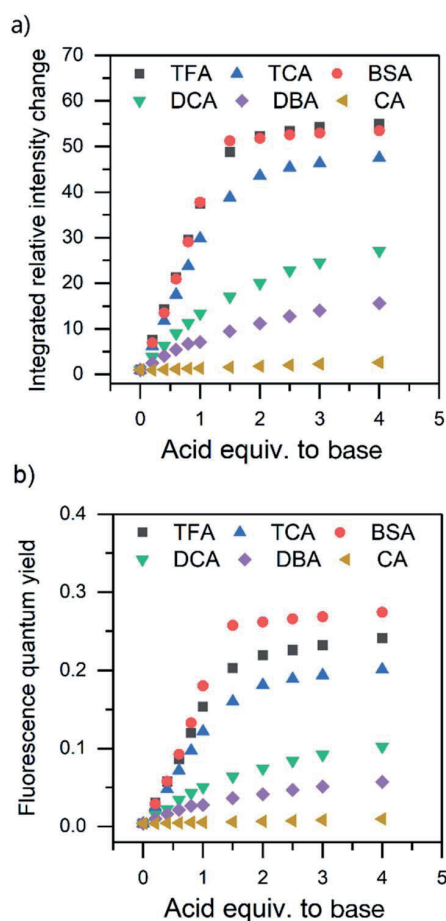


Fig. 3 (a) The integrated relative intensity change, and (b) the changes in the fluorescence quantum yield of isoquinoline while titrating with various acids (DCM, 10^{-4} M, $\lambda_{ex} = 310$ nm, 0.0 to 4.0 acid equivalents).

Table 1 Maximum fluorescence quantum yield (Φ_{FL}) achieved for each base with different acids

	Isoquinoline	Acridine	Benzo[h]quinoline
TFA	0.241	0.089	0.157
TCA	0.201	0.082	0.156
BSA	0.274	0.101	0.148
DCA	0.102	0.035	0.157
DBA	0.057	0.031	0.156
CA	0.010	0.007	0.158
Free base	0.004	0.008	0.147



Paper

a saturation point, whereas the spectra of benzo[*h*]quinoline changes significantly. Neutral benzo[*h*]quinoline has a fluorescence maximum at 367 nm, whereas after protonation, the cationic species arises at 416 nm, shifting the fluorescence maximum 50 nm and changing the spectra from three distinctive bands to one broadband fluorescence. These drastic changes affect the overall fluorescence intensity change making it minuscule in comparison to the isoquinoline and acridine 50-fold and 25-fold increases, respectively.

All three compounds also share similarities in their fluorescence intensity. The intensity changes vary between the compounds, but in each case, BSA has the largest effects, while the acetic acids follow the trend of their respective pK_a values. Considering the chemical structure of benzo[*h*]quinoline, it is apparent that it is more prone to steric hindrance than isoquinoline and acridine due to the hydrogen at C10 (see ESI, Fig. S35†) which causes a severe clash with the hydrogen at the nitrogen atom during the protonation.

Determination of the binding constants. Isoquinoline, acridine, and benzo[*h*]quinoline have been classified as having pK_b values of 8.86, 8.40, and 9.75, respectively.²³ For isoquinoline, the protonation saturation is observed with all the stronger acids (TFA, TCA, and BSA), but in variable ratios (2.0, 2.5 and 1.5, respectively). Using BSA, the saturation is observed in the fluorescence spectra for isoquinoline at 1.5 equivalents, whereas for acridine this occurs at 2.5, and for benzo[*h*]quinoline at 1.0, the latter indicating easier protonation than for isoquinoline and acridine. The above-presented differences in the protonation efficiency can be explained by the difference of the pK_b values in the ground state and the excited state of the base. From the absorption and fluorescence spectra, it can be concluded that benzo[*h*]quinoline, like its isomer benzo[*f*]quinoline,²⁰ is more readily protonated in the excited state.

Due to the unsuitability of the NMR spectroscopy (see ESI, Fig. S11–S14†) for binding constant determination, the absorption and fluorescence spectra of the bases were used instead. Due to the difficulty in determining pH values in DCM, the binding constants were determined only for isoquinoline, for which the absorbance of the neutral and cationic species could be easily determined from the absorption spectrum. For isoquinoline, the absorption band at 268 nm signifies the absorbance of the neutral species, which decreases upon addition of the acids, whereas the band at 328 nm is contributed by the cationic species (see Fig. 4). These changes can be used to determine the ratio of $c(\text{bound})$ and $c(\text{unbound})$. Binding constants for the ground state are determined using eqn (2)²⁹

$$\frac{c(\text{bound})}{c(\text{unbound})} = K_a[\text{Q}] \quad (2)$$

where K_a is the binding constant for the protonation of the base and $[\text{Q}]$ is the concentration of the added acid. The intensity changes at 268 and 328 nm and their ratio during titration with TFA are presented in Fig. 4. Binding constants can be determined from the linear fit of the two bands designated to the two different species. It should be noted that for all the compounds, the titration points exceeding the saturation limit were excluded from the fit. For some of the spectra, the changes were insignificant, and the binding constants could not be determined

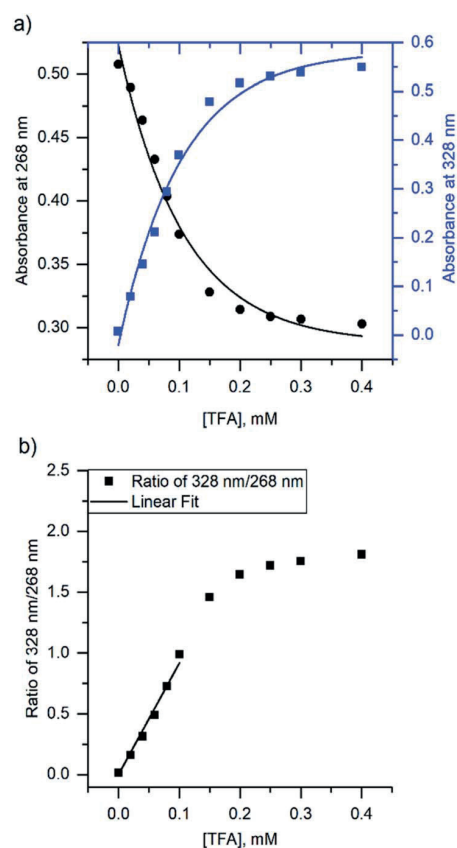


Fig. 4 (a) The change in absorbance of isoquinoline at 268 nm and 328 nm upon addition of TFA, and (b) ratio of the intensities at 268 nm and 328 nm with linear fit.

using this method. The determined binding constants are listed in Table 2.

The binding constant for the protonation of isoquinoline with CA was not determined simply because the changes in the spectra are too small and within experimental error. The determined binding constants (see ESI, S9 and S10†) obey the trend of the pK_a values of the acids yet again excluding BSA, which has a significantly higher binding constant for isoquinoline than the other acids. Although the binding constants for acridine and benzo[*h*]quinoline were not determined, similar results are expected based on the fluorescence spectra.

Table 2 Binding constants (K_a) for the protonation of isoquinoline in the ground state determined from the absorption spectra according to eqn (2).²⁹

	K_a (M^{-1})
TFA	9200 ± 330
TCA	8300 ± 190
BSA	32 700 ± 1590
DCA	4000 ± 100
DBA	3100 ± 120
CA	N/A



Table 3 Nomenclature of the obtained single crystals

	TFA	TCA	BSA	DCA	DBA	CA
Isoquinoline	1	2	3	—	—	—
Acridine	4	5	6	7	8	9
Benzo[<i>h</i>]quinoline	10	11	12	13	14	—

Single crystal X-ray crystallography

The crystallizations of the acid–base pairs were carried out with 1 : 1 acid–base ratio in chloroform and the single crystals of the corresponding salts were obtained either by slow evaporation of the chloroform solution or by vapor diffusion using chloroform/hexane or dichloromethane/diisopropyl ether as the solvent/antisolvent system. Unfortunately, not all of the crystallizations were successful and some of the salts from weaker acids were obtained as a gel or amorphous powder. The suitable single crystals were subjected to single crystal X-ray study. To simplify the crystallographic nomenclature, the salts are referred to as numbers, *e.g.* isoquinolinium trifluoroacetate is denoted as **1**. The numbering of all the salts is shown in Table 3.

The salt formation, *viz.* full protonation of isoquinoline, acridine, and benzo[*h*]quinoline, was observed in the solid-state in all cases, regardless of the pK_a values of the used acid. All solid-state structures, except **7**, **8**, **13** and **14**, have the expected

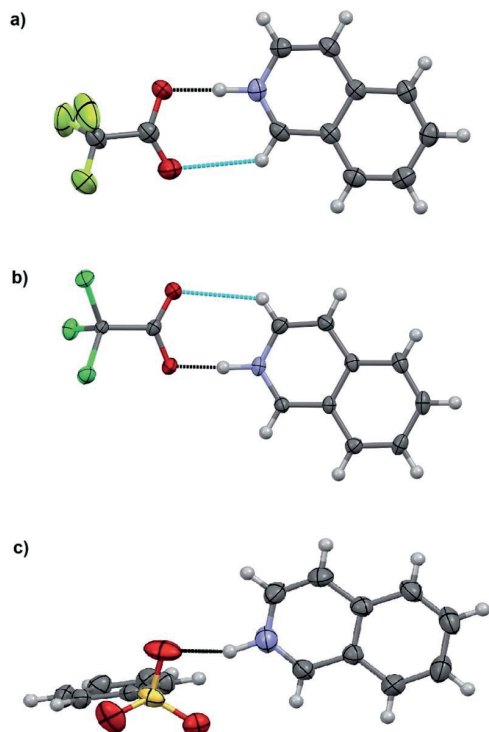


Fig. 5 X-ray structures of (a) **1**, (b) **2**, and (c) **3**. Displacement ellipsoids are drawn at the 50% probability level. The black-dotted lines are the N–H...O hydrogen bonds and the blue-dotted lines represent weak C–H...O interactions.

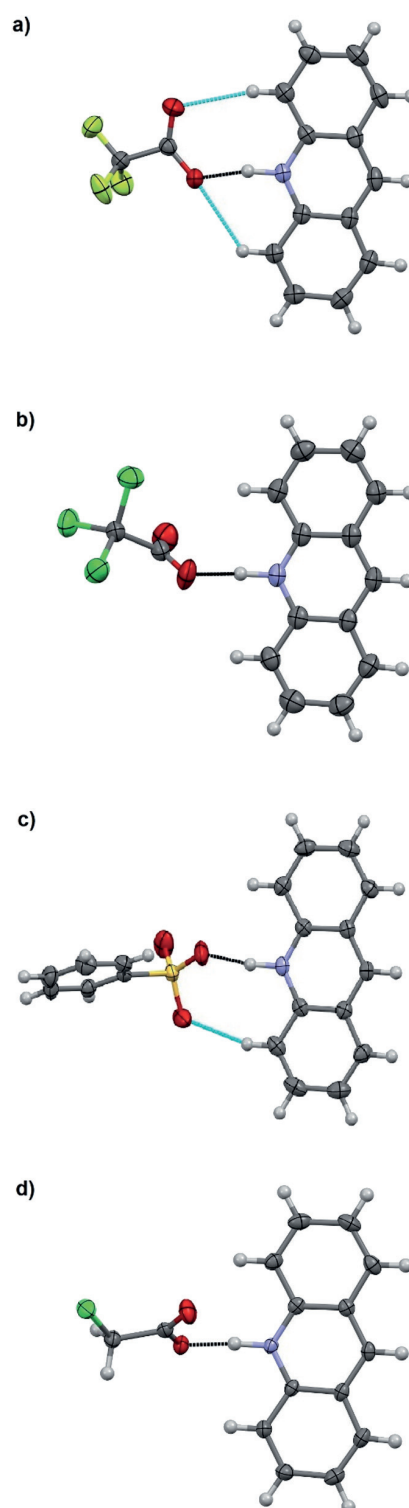


Fig. 6 X-ray structures of (a) **4**, (b) **5**, (c) **6**, and (d) **9**. Displacement ellipsoids are drawn at the 50% probability level. The black-dotted lines are the N–H...O hydrogen bonds and the blue-dotted lines represent C–H...O interactions.

1 : 1 stoichiometry (see Fig. 5 and 6). The deprotonated acid dimer (R–COOH...OOC–R) found in **7**, **8**, **13** and **14** is H-bonded to the H–N⁺ moiety from the deprotonated acid, unlike in the



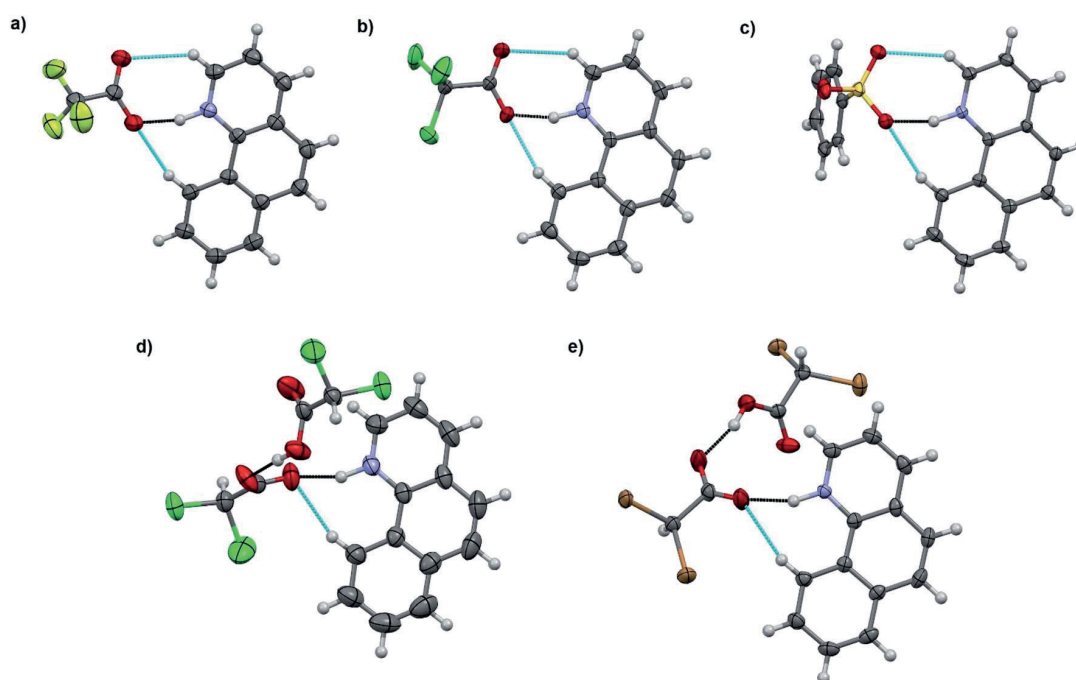


Fig. 7 X-ray structures of (a) **10**, (b) **11**, (c) **12**, (d) **13**, and (e) **14**. Displacement ellipsoids are drawn at the 50% probability level. The black-dotted lines are the N–H···O hydrogen bonds and the blue-dotted lines represent weak C–H···O interactions.

other studied structures, and has formally a 2 : 1 stoichiometry (see Fig. 7).

The charge-assisted hydrogen bond distances between the corresponding acetate or sulfonate oxygen and the nitrogen of the protonated base (O···N) are listed in Table 4. Due to the unreliable positioning of the hydrogen atom from X-ray data, only the distances between the heavier atoms (O and N) are discussed. However during the refinements, a realistic H–N bond distance of 1.04 Å, based on an average of neutron diffraction values,³⁰ was used.

The charge-assisted H-bond distances for TFA and TCA (**1**, **2**, **4**, **5**, **10**, and **11**) salts are very close to each other ($\Delta\delta = 0.02$ – 0.05 Å). From the solution studies (see above), it was concluded that the protonation of isoquinoline by BSA was the most effective as it had the greatest effect on the fluorescence intensity and induced the largest chemical shift change in the ¹H NMR spectra (see ESI,† NMR studies). Yet in the solid-state, the O···N distance for **3** is found to be the longest, 2.862(7) Å, being 0.245–0.148 Å longer than for **1**, **2**, **6** or **12**. The plausible explanation for the longer O···N distance in the BSA–isoquinoline salt are the slightly acidic H-atoms of the phenyl ring of the benzenesulfonate anion, resulting in a multitude of additional H-bonds to the adjacent anions, and thus elongating the charge-assisted N–H···O–S hydrogen bond. The same phenomenon does not occur in the corresponding acridine (**6**) and benzo[*h*]quinoline (**12**). This is evidenced by the Hirshfeld surface analysis of **3**, **6** and **12** (see ESI, Fig. S45†) which clearly indicates a multitude of H···O interactions to adjacent benzenesulfonate anions only in the case of **3**. The DFT-level (SPARTAN18,³¹ M062X, def2-TZVP, nonpolar solvent model) calculations for **3**, **6** and **12** also

support this reasoning, as all optimized structures give the nonpolar solvent phase O···N distances between 2.6–2.7 Å (see ESI, Fig. S46†).

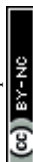
The acridinium cation in the DCA and DBA salts (**7** and **8**, see Fig. S27–S32,† respectively) reside on a symmetry element resulting in disorder of the ⁺N–H and C–H parts of the acridine skeleton. This is manifested by the abnormally long O···N distances, as they actually represent the average of the 2.7 Å (⁺N–H···O[−]) and 3.5 Å (C(arm)–H···O) distances, thus these XRD based distances for **7** and **8** are excluded from the discussion. The same DFT-level (SPARTAN18,³¹ M062X, def2-TZVP, nonpolar solvent model) calculations for **7** and **8** confirm the normal solution phase O···N distances to be 2.6 Å (see ESI, Fig. S47†). In contrast to the 1 : 1 salts, the structures of **7** and **8** are formed in a 2 : 1 ratio in the solid-state, consisting of one

Table 4 The charge-assisted hydrogen bond O···N distances for the salts [Å]

	Isoquinoline	Acridine	Benzo[<i>h</i>]quinoline
TFA	1 : 2.645(4)	4 : 2.636(2)	10 : 2.644(3)
TCA	2 : 2.617(4)	5 : 2.617(3)	11 : 2.633(4) ^a , 11 : 2.634(4) ^a
BSA	3 : 2.862(7)	6 : 2.666(3)	12 : 2.714(3)
DCA	Gel	7 : 3.031(4) ^b	13 : 2.657(3)
DBA	Gel	8 : 3.102(6) ^b	14 : 2.709(6)
CA	Gel	9 : 2.560(2)	Powder

^a Two independent 1 : 1 acid–base pairs in the asymmetric unit.

^b Acridine moiety is disordered over a symmetry element resulting in unreliable O···N distances.



(disordered) acridinium cation and a H-bonded DCA or DBA dimer (see ESI, Fig. S27 and S28†). Similar acid dimers in a 2 : 1 acid–base ratio were observed for benzo[*h*]quinoline with DCA (13) and DBA (14), respectively. Yet, due to the non-disordered structures of 13 and 14, the O⋯N distances are very similar to the 1 : 1 salts (see Table 4). Surprisingly, the shortest O⋯N interaction distance is observed in 9 with 2.560(2) Å which is even 0.03 Å shorter than in the reported quinolinium trifluoroacetate structure,³² and very close to the DFT-level (SPARTAN18,³¹ M062X, def2-TZVP, nonpolar solvent model) calculated O⋯N distance of 2.61 Å for 9 (see ESI, Fig. S47†).

A search in the Cambridge Structural Database (CSD)³³ for protonated isoquinoline, acridine and benzo[*h*]quinoline resulted in 22 hits, respectively. The average charge-assisted hydrogen bond O⋯N distance calculated from the CSD structures^{34–47} is 2.658 Å, precisely matching the average of 2.644 Å calculated from 1, 2, 4, 5, 6, 9, 10, 11, 12, 13 and 14 (excluding the abnormally long O⋯N distances in 3, 7 and 8).

Conclusions

The protonation of simple N-heterocycles was successfully used as a preliminary study to gain further information on the use of acid–base interactions for supramolecular emission control. The protonation was found to significantly boost fluorescence emission, hence being an effective tool to be used in fluorescence enhancement and avoiding time-consuming synthetic procedures. In the solution studies, the protonation was observed to increase the fluorescence intensity with an over 50-fold increase observed for isoquinoline. Surprisingly, the protonation was found to be incomplete in a 1 : 1 acid–base ratio, despite the single protonation site of the bases. No structural changes were observed in the fluorescence spectra of isoquinoline or acridine, but interestingly, benzo[*h*]quinoline experiences a bathochromic shift of 50 nm upon protonation. Benzo[*h*]quinoline and acridine were also observed to be more easily protonated in the excited state than in the ground state, whereas the isoquinoline absorption spectra display effective protonation in the ground state.

The relative fluorescence intensities of the N-heterocycles become larger as the donating powers of the proton donors increase. The increase in the fluorescence intensity followed the same trend with the pK_a values of the acids with the exception of BSA, which was the most effective in protonating all the bases. Acids with pK_a values higher than 1 did not have significant effects on the fluorescence of the compounds due to insufficient donating power of the acid for protonation to occur. Binding constants for isoquinoline in the ground state were determined based on the absorption spectra and similar results were observed in these values as well, with BSA having a three times larger binding constant compared to the other, stronger acids (TFA and TCA).

In the solid-state, the protonation of isoquinoline, acridine and benzo[*h*]quinoline was observed in each case regardless of the pK_a value of the acid. In solution, BSA was determined to be the most effective in the protonation of the bases, yet, in single-crystal X-ray structures, the O⋯N distance was found to be the

longest in the BSA–isoquinoline salt due to additional intermolecular interactions in the solid-state. The solid-state studies suggested that the O⋯N distances were mainly affected by the lattice interactions and do not directly reflect the acid–base or the anion–cation interactions in solution.

Conflicts of interest

There are no conflicts to declare.

Acknowledgements

We gratefully acknowledge financial support from the Academy of Finland (KR: grant no. 317259; AP: grant no. 311142) and the University of Jyväskylä, Finland.

Notes and references

- J. M. Lehn, *Angew. Chem., Int. Ed. Engl.*, 1988, **27**, 89–112.
- J. Steed and J. Atwood, *Supramolecular Chemistry*, John Wiley & Sons Ltd., Chippingham, United Kingdom, 2009.
- S. Vigneshvar, C. C. Sudhakumari, B. Senthilkumaran and H. Prakash, *Front. Bioeng. Biotechnol.*, 2016, **4**, 11.
- J.-H. Lee, C.-H. Chen, P.-H. Lee, H.-Y. Lin, M.-K. Leung, T.-L. Chiu and C.-F. Lin, *J. Mater. Chem. C*, 2019, **7**, 5874–5888.
- A. P. de Silva, A. Goligher, N. Gunaratne and T. E. Rice, *ARKIVOC*, 2003, **7**, 229–243.
- S. Zheng, P. L. M. Lynch, T. E. Rice, T. S. Moody, H. Q. N. Gunaratne and A. P. de Silva, *Photochem. Photobiol. Sci.*, 2012, **11**, 1675–1681.
- J. Ma, W. Li, J. Li, R. Shi, G. Yin and R. Wang, *Talanta*, 2018, **182**, 464–469.
- N. Mataga and S. Tsuno, *Bull. Chem. Soc. Jpn.*, 1957, **30**, 368–374.
- N. K. Joshi, H. C. Joshi, R. Gahlaut, N. Tewari, R. Rautela and S. Pant, *J. Phys. Chem. A*, 2012, **116**, 7272–7278.
- N. Mataga, *Bull. Chem. Soc. Jpn.*, 1958, **31**, 459–462.
- M. F. Anton and W. R. Moomaw, *J. Chem. Phys.*, 1977, **66**, 1808–1818.
- S. A. Tucker, W. E. Acree Jr and C. Upton, *Polycyclic Aromat. Compd.*, 1993, **3**, 221–229.
- H. Zimmermann and N. Joop, *Z. Elektrochem.*, 1961, **65**, 61–66.
- S. M. Ziegler and M. A. El-Sayed, *J. Chem. Phys.*, 1970, **52**, 3257–3268.
- I. Janic and A. Kowski, *Adv. Mol. Relax. Processes*, 1973, **5**, 185–191.
- K. Kumari, N. Tewari, M. S. Mehta, N. Pandey, K. Tiwari, R. K. Ratnesh, H. C. Joshi and S. Pant, *J. Mol. Struct.*, 2019, **1180**, 855–860.
- M. Norek, J. Dresner and J. Prochorow, *Acta Phys. Pol., A*, 2003, **104**, 425–439.
- M. Norek, B. Kozankiewicz and J. Prochorow, *Acta Phys. Pol., A*, 2004, **106**, 77–94.
- E. T. Ryan, T. Xiang, K. P. Johnston and M. A. Fox, *J. Phys. Chem. A*, 1997, **101**, 1827–1835.



Paper

- 20 M. Nakamizo, *Spectrochim. Acta*, 1966, **22**, 2039–2053.
- 21 A. Grabowska, B. Pakula and J. Pancir, *Photochem. Photobiol.*, 1969, **10**, 415–425.
- 22 E. Vander Donckt, R. Dramaix, J. Nasielski and C. Vogels, *Trans. Faraday Soc.*, 1969, **65**, 3258–3262.
- 23 H. C. Brown, *et al.*, in *Determination of Organic Structures by Physical Methods*, ed. E. A. Braude, and F. C. Nachod, Academic Press, New York, 1955.
- 24 Acid Dissociation Constants, *CRC Handbook of Chemistry and Physics*, retrieved on 20.12.2018.
- 25 (a) B. Valeur, *Molecular Fluorescence: Principles and Applications*, Wiley-VCH Verlag GmbH, New York, 2001, p. 59; (b) B. Valeur, *Molecular Fluorescence: Principles and Applications*, Wiley-VCH Verlag GmbH, New York, 2001, p. 161.
- 26 B. Wardle, *Principles and Applications of Photochemistry*, John Wiley & Sons, Ltd., United Kingdom, 2009.
- 27 R. T. Williams and J. W. Bridges, *J. Clin. Pathol.*, 1964, **17**, 371–394.
- 28 D. F. Eaton, *Pure Appl. Chem.*, 1988, **60**, 1107–1114.
- 29 G. Gryniewicz, M. Poenie and R. Tsien, *J. Biol. Chem.*, 1985, **260**, 3440–3450.
- 30 F. H. Allen and I. J. Bruno, *Acta Crystallogr., Sect. B: Struct. Sci.*, 2010, **66**, 380–386.
- 31 SPARTAN18, Wavefunction Inc., Irvine, CA, USA, 2018.
- 32 Effendy, P. C. Junk, C. J. Kepert, L. M. Louis, T. C. Morien, B. W. Skelton and A. H. White, *Z. Anorg. Allg. Chem.*, 2006, **632**, 1312–1325.
- 33 C. R. Groom, I. J. Bruno, M. P. Lightfoot and S. C. Ward, *Acta Crystallogr., Sect. B: Struct. Sci., Cryst. Eng. Mater.*, 2016, **72**, 171–179.
- 34 X.-H. Chang, *Z. Kristallogr. – New Cryst. Struct.*, 2019, **234**(6), 1253–1254.
- 35 N. Kobayashi, T. Naito and T. Inabe, *Bull. Chem. Soc. Jpn.*, 2003, **76**, 1351–1362.
- 36 H. Eshtiagh-Hosseini, A. Hassanpoor, M. Mirzaei and A. R. Salimi, *Acta Crystallogr., Sect. E: Struct. Rep. Online*, 2010, **66**, o2996.
- 37 P. Bora, B. Saikia and B. Sarma, *Cryst. Growth Des.*, 2018, **18**(3), 1448–1458.
- 38 L. Plasseraud and H. Cattey, *C. R. Chim.*, 2013, **16**, 613–620.
- 39 H. Aghabozorg, J. A. Gharamaleki, M. Parvizi and Z. Derikvand, *Acta Crystallogr., Sect. E: Struct. Rep. Online*, 2010, **66**, m83–m84.
- 40 N. Bedekovic, V. Stilinovi and T. Piteša, *Cryst. Growth Des.*, 2017, **17**, 5732–5743.
- 41 X. Mei and C. Wolf, *Eur. J. Org. Chem.*, 2004, 4340–4347.
- 42 Z. Derikvand, M. M. Olmstead and J. A. Gharamaleki, *Acta Crystallogr., Sect. E: Struct. Rep. Online*, 2011, **67**, o416.
- 43 K. Fennig and A. Sikorski, *Z. Kristallogr. – New Cryst. Struct.*, 2018, **233**(4), 675–676.
- 44 P. P. Devi and D. Kalaivani, *Acta Crystallogr., Sect. B: Struct. Sci., Cryst. Eng. Mater.*, 2016, **72**, 570–574.
- 45 D. E. Lynch, A. N. Kirkham, M. Z. J. Chowdhury, E. S. Wane and J. Heptinstall, *Dyes Pigm.*, 2012, **94**, 393–402.
- 46 A. Garai, S. Mukherjee, S. K. Ray and K. Biradha, *Cryst. Growth Des.*, 2018, **18**, 581–586.
- 47 E.-Y. Xia, J. Sun, R. Yao and C.-G. Yan, *Tetrahedron*, 2010, **66**, 3569–3574.





II

PROTONATION-INDUCED FLUORESCENCE MODULATION OF CARBAZOLE-BASED EMITTERS

by

E. Taipale, N. A. Durandin, J. Salunke, N. R. Candeias, T.-P. Ruoko,
J. S. Ward, A. Priimagi & K. Rissanen 2022

Mat. Adv., 2022, 3, 1703–1712

<https://doi.org/10.1039/D1MA00438G>

Article is licensed under a Creative Commons
Attribution-NonCommercial 3.0 Unported (CC BY-NC 3.0) licence.

PAPER



Cite this: *Mater. Adv.*, 2022,
3, 1703

Received 14th May 2021,
Accepted 1st January 2022

DOI: 10.1039/d1ma00438g

rsc.li/materials-advances

Protonation-induced fluorescence modulation of
carbazole-based emitters†

Essi Taipale,^a Nikita A. Durandin,^b Jagadish K. Salunke,^b Nuno R. Candeias,^{b,c}
Tero-Petri Ruoko,^b Jas S. Ward,^a Arri Priimagi^{b,*} and Kari Rissanen^{a,*}

The development of purely organic fluorescence emitters is of great importance for their low cost and high performance. Responding to this demand, carbazole is a promising emitter due to its extensive freedom for functionalisation, high thermal and chemical stability, as well as low cost. Herein, the effect of protonation on the fluorescence of various pyridine-functionalised carbazole-based bipolar host materials was studied both in solution and in the solid-state. The restriction of intramolecular rotation of the molecules upon protonation of the pyridyl-moiety together with easier planarization of the protonated acceptor and the donor moieties and relocalisation of the LUMO orbital on the protonated species was found to increase the fluorescence quantum yield from 16% to 80%. Additionally, in the solid-state, the J-type packing of the molecules further facilitated the increase in the fluorescence quantum yield from 1% to 49%. In both cases, the pronounced bathochromic spectral shift was observed indicating that the gap between the emissive state and the first triplet state of the molecules was diminished upon protonation. Therefore, implementing this strategy could further boost the development of future emitters.

Introduction

Over the last 35 years the field of supramolecular chemistry, studying molecular assemblies held together by weak intermolecular interactions, has become one of the most intriguing fields of chemistry.¹ Supramolecular chemistry offers insight into smart molecular design, taking advantage of the directionality of non-covalent bonds and the self-assembling capabilities of molecules. It encompasses a wide variety of applications: weak interactions have been utilised in emission modulation of organic luminescent materials,² which have widely been applied in fluorescent imaging,^{3,4} drug release,^{5–7} sensors,^{4,8–10} photoelectric devices,¹¹ and organic light-emitting diodes (OLEDs).¹²

The various applications of the purely organic luminescent materials speak for the importance of their development. However, simultaneously achieving high efficiency, long lifetime and low cost with blue organic emitters is still a considerable challenge.¹³ Additionally, carbazole has commonly been

utilised in the design of blue-light emitting diodes for its high triplet energy.^{14,15} Herein, we have selected it as a central unit due to its extensive freedom for functionalisation, high thermal and chemical stability, as well as low cost.^{16–18} A relatively new approach to smarter emitter design is bipolar host materials.^{19–23} They are designed to hold both electron-donating and electron-withdrawing units within the same molecule. The highest occupied molecular orbital (HOMO) and the lowest unoccupied molecular orbital (LUMO) are determined by the electron-donating and electron-withdrawing units, respectively. In comparison to unipolar host materials, bipolar host materials promote balanced charge flux and broaden the exciton recombination.^{20,21,24} However, the construction of bipolar host molecules with spatially separated donor and acceptor moieties allows the formation of an intramolecular charge transfer (ICT) state, which may exhibit a twisted structure resulting in the excited state energy being consumed by the rotary motion of the molecule.^{25–27} This results in quenching of the fluorescence and low emission quantum yield.

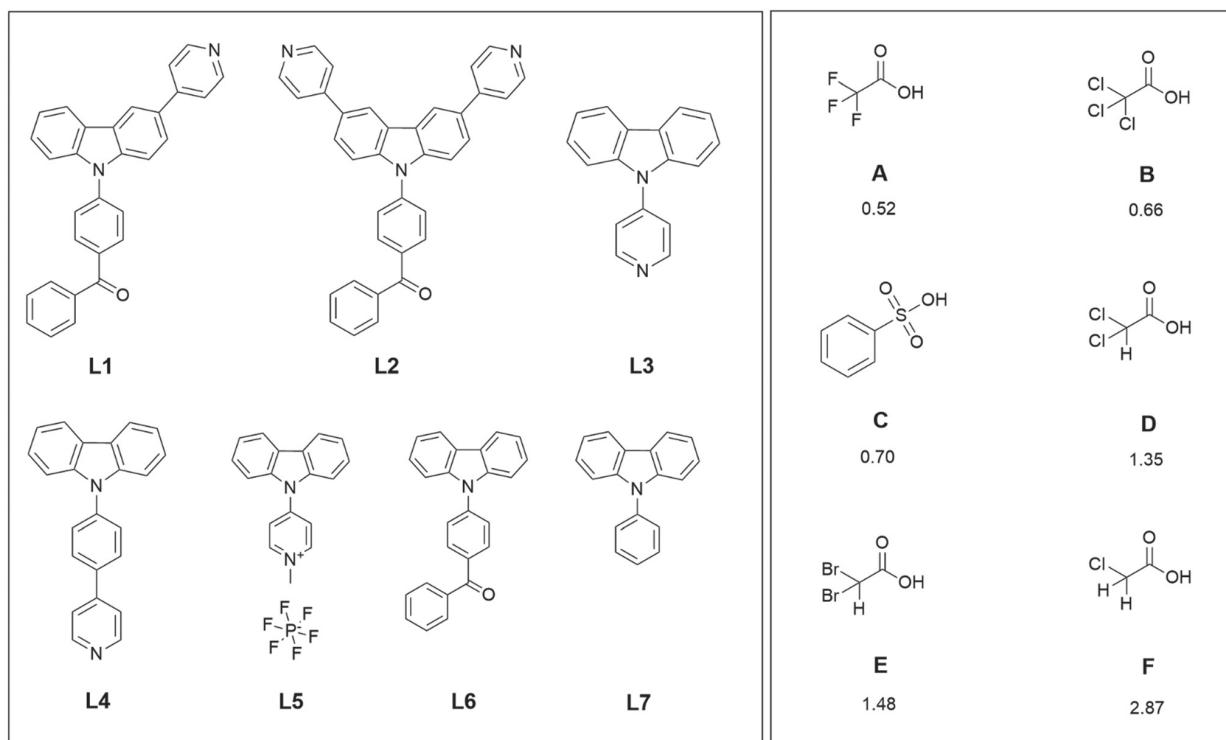
A way of improving the quantum yield without the tedious work of redesigning the molecular structure is the restriction of the intramolecular rotation by weak interactions.^{28,29} Intermolecular interactions, such as strong hydrogen-bonding upon protonation, can be used to affect the fluorescence of a compound.^{30,31} The effect on the fluorescence depends on the strength of the acid, *i.e.*, the stabilising power of the

^a University of Jyväskylä, Department of Chemistry, P.O. Box 35, Surfontie 9B,
40014 Jyväskylä, Finland. E-mail: kari.t.rissanen@jyu.fi

^b Faculty of Engineering and Natural Sciences, Tampere University, P.O. BOX 541,
FI-33101 Tampere, Finland. E-mail: arri.priimagi@tuni.fi

^c LAQV-REQUIMTE, Department of Chemistry, University of Aveiro, 3810-193 Aveiro,
Portugal

† Electronic supplementary information (ESI) available. CCDC 2080281–2080294.
For ESI and crystallographic data in CIF or other electronic format see DOI:
10.1039/d1ma00438g



Scheme 1 The compounds **L1–L4** studied for the protonation-induced fluorescence enhancement, reference compounds **L5–L7**, and the acids used in the protonation with their corresponding pK_a values.⁴³

counter-anion involved in the protonation process.^{32–34} In our previous studies, protonation significantly enhanced the fluorescence intensity of quinoline derivatives over 50-fold increasing the fluorescence quantum yield up to 30%.³² Herein, the effect of the intermolecular interactions on the emission characteristics of the carbazole-based materials upon protonation both in solution and in the solid-state were investigated. Protonation of **L1** and **L2** (Scheme 1) was found to facilitate the planarization of the pyridyl and the carbazole units, while hindering the complete rotation of the pyridyl moiety. This phenomenon together with changes in the electronic profile due to protonation explain the bathochromic shift in the fluorescence spectra and the enhancement of the fluorescence quantum yield. In **L3** and **L4**, the complete rotation of the pyridyl became more accessible upon protonation, thus leading to fluorescence quenching. However, in solid-state, protonation enhanced fluorescence quantum yield of all the compounds increasing the fluorescence quantum yield of **L4** from 1% to a noteworthy 49%.^{35,36} We envision this strategy to further enhance the development of purely organic emitter materials.

Results and discussion

Materials

The rationale behind the molecular design is to improve the emission quantum yield by protonation-induced fluorescence enhancement.

Therefore, aromatic, moderately electron-accepting benzophenyl and pyridyl groups were introduced to the electron-rich carbazole core to achieve donor–acceptor bipolar host materials.^{19,37,38} Here the benzophenyl unit is chosen as the electron-withdrawing moiety for **L1** and **L2**, but several research groups have opted for other solutions, such as quinoline or pyridine groups.^{39,40} For compounds **L3–L5**, pyridyl, phenylpyridyl, and methylpyridinium groups were chosen as the electron-withdrawing moieties. Compound **L5** was studied for the intriguing alternative of the methylated pyridyl group with a constant positive charge on the nitrogen instead of protonation by an acid. In all the other compounds, the pyridyl group acts as a Lewis base for the efficient protonation of the compound. The mono-substituted pyridine-functionalised carbazole-based bipolar host emitter (**L1**) was synthesised by simple two-step synthesis and studied alongside with a similar di-substituted carbazole derivative (**L2**).¹⁹ The *N*-substituted pyridine-containing carbazole derivatives **L3** and **L4** were studied for the different position of the electron-withdrawing moiety on the carbazole core.^{41,42} Compounds **L5–L7** were used as reference compounds that do not have pyridyl groups as effective protonation sites. Six different organic acids (**A–F**) with pK_a values ranging from 0.52 to 2.87 (Scheme 1) were used for the protonation of the carbazole derivatives.⁴³ Several acetic acid derivatives were selected to investigate the effect of acidity (pK_a) on fluorescence enhancement of the parent compounds *via* protonation. Additionally, benzenesulfonic acid (**C**) was selected to study the stability of aromatic *vs.* aliphatic counter-anions.

UV-Vis and fluorescence spectroscopy

The normalised absorption and fluorescence spectra of compounds **L1**–**L4** are shown in Fig. 1 (see Fig. S1 and S2 in the ESI† for absorption and fluorescence spectra of other compounds). Compounds **L1**/**L2** show three distinctive absorption bands at 250/260 nm, 287/300 nm, and 345/323 nm, respectively. The additional pyridyl group of **L2** slightly changes the electronic structure of the molecule and induces minor changes in the spectrum. According to the time-dependent density functional theory (TDDFT) calculations performed by Rajamalli *et al.*, these absorption bands can be assigned to the intramolecular charge transfer bands from the carbazole moiety to the benzophenyl at 345 nm (**L1**) and 323 nm (**L2**), and to the absorption of the pyridylcarbazole donor at 287 nm (**L1**) and 300 nm (**L2**). The spectra of **L3** and **L4** are also structurally similar to each other showing absorption bands at 291 nm (**L3**) and 292 nm (**L4**) of the carbazole moiety and bands at 333 nm (**L3**) and 326–339 nm (**L4**) attributed to the pyridyl and phenylpyridyl groups.

The fluorescence of **L1**, **L2** and **L4** were measured in 10^{-5} M dichloromethane (DCM) solution using 340 nm excitation and they all display broadband fluorescence reaching a maximum at 474 nm, 473 nm, and 415 nm, respectively. An excitation wavelength of 290 nm was used for **L3**, which shows two fluorescence maxima at 341 nm and 356 nm. The fluorescence data were also used to calculate the fluorescence quantum yields for **L1**–**L4**, and values of 16.1%, 18.1%, 10.5%, and 32.0% were obtained at room temperature.

The titration of compounds **L1** and **L3** with benzenesulfonic acid (**C**) from 0 to 2.0 (**L3**) or 4.0 (**L1**) equivalents of acid is presented in Fig. 2. Titrations with other acid–base pairs are shown in the SI (see Fig. S3–S14, ESI†). Protonation of **L1** with benzenesulfonic acid results in a decrease of the intensity of all original absorption bands, while new bands arise at 319 and 382 nm, from which the latter is characteristic of the cationic species.³² From Scheme 1, it can be seen that **L1** has two possible protonation or hydrogen-bond acceptor sites: the

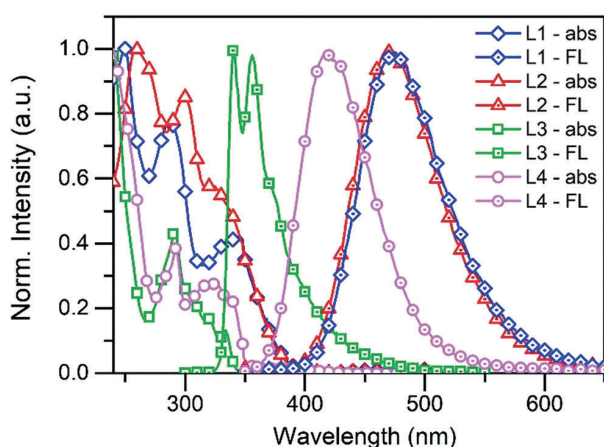


Fig. 1 The normalised absorption and fluorescence spectra of **L1**–**L4** in solution (10^{-5} M in DCM, $\lambda_{\text{ex}} = 340$ nm for **L1**, **L2**, and **L4**, and 290 nm for **L3**).

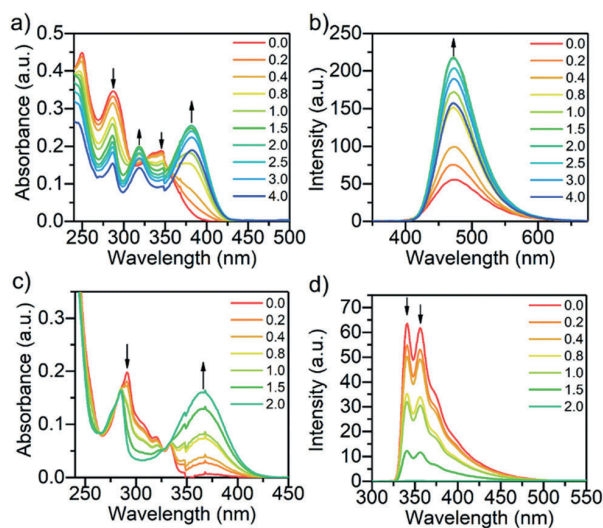


Fig. 2 The absorption (a) and fluorescence (b) of **L1**, and the absorption (c) and fluorescence (d) of **L3** while titrating with benzenesulfonic acid (**C**) from 0.0 to 2.0–4.0 equivalents of acid (10^{-5} M in DCM, $\lambda_{\text{ex}} = 340$ nm (**L1**) and 290 nm (**L3**)). The fluorescence intensities have been corrected for inner filter effects.⁴⁴

pyridyl and the carbonyl group of the benzophenyl. Due to greater basicity of the pyridyl nitrogen compared to the benzoyl oxygen, the protonation occurs predominantly on the pyridyl group. The protonation leads to an observable increase in the fluorescence intensity until the titration reaches 2.0 equivalents of the acid (see Fig. S15a, ESI†). The most significant increase in the fluorescence intensity for **L1** was observed while titrating with trichloroacetic acid, reaching a fluorescence enhancement factor of 2.8 due to the protonation of the pyridine unit at 2.0 equivalents of acid (see Fig. S15a, ESI†). Similar results were obtained for **L2** (see Fig. S15b, ESI†), with the fluorescence increasing up to 3.0 equivalents of acid due to two pyridyl acceptor units in addition to the benzophenyl unit. A hypsochromic shift of 30 nm of the fluorescence maximum was observed for **L2**, possibly due to improper hydrogen bonding shortening the length of the interaction between the proton acceptor and donor causing also a reduction in intensity.⁴⁵ After the saturation point is reached, the fluorescence intensity begins to decrease in the case of **L1** and **L2** possibly due to change in polarity upon excess acid, which is also supported by the loss of isosbestic points in the absorption spectra beyond the saturation limit.³¹

A time-dependent density functional theory (TD-DFT) study was performed to shed light on the different photochemical behaviour of **L1** upon protonation, specifically on the observed fluorescence increase. The CAM-B3LYP level theory was selected as the working method as in previous computational studies for carbazole systems,⁴⁶ which have resulted in similar and acceptable relative deviations between experimental and calculated transition energies (up to 0.6 eV). Analysis of the two less energetic vertical transitions (Table 1) clearly indicates a different absorption profile between the two species. The first

Table 1 The electronic transition, absorption wavelengths λ_{\max} (nm), electronic excitation energies E_{ex} (eV), oscillator strengths (f), and configurations of the 2 low-lying excited states of **L1** and its protonated form (**L1H⁺**) obtained by TDDFT/CAM-B3LYP/6-31G(d,p) based on the optimized ground state geometries in DCM

Compound	Electronic transition	λ_{\max}	E_{ex}	f	Wave functions ^a	CI (%) ^b
L1	$S_0 \rightarrow S_1$	319	3.89	0.02	H-9 \rightarrow L	42
					H-3 \rightarrow L	28
					H-6 \rightarrow L	11
					H \rightarrow L	4
					H-2 \rightarrow L	3
	$S_0 \rightarrow S_2$	294	4.22	0.70	H-9 \rightarrow L+10	3
					H \rightarrow L	69
					H \rightarrow L+2	7
					H-9 \rightarrow L	5
					H \rightarrow L+3	4
L1H⁺	$S_0 \rightarrow S_1$	335	3.70	0.86	H-3 \rightarrow L	2
					H \rightarrow L	84
					H-4 \rightarrow L	5
					H-1 \rightarrow L	3
					H-7 \rightarrow L+1	38
	$S_0 \rightarrow S_2$	319	3.89	0.00	H-2 \rightarrow L+1	28
					H-5 \rightarrow L+1	20
					H-7 \rightarrow L+11	3

^a The wave functions based on the eigenvectors predicted by TD-DFT. H stands for HOMO and L stands for LUMO. ^b Percentage contribution of the wavefunction configuration interaction to the excitation.

vertical transition of **L1** is unlikely to be observed, as indicated by its small oscillator strength. The most energetic absorption band experimentally observed should correspond to the second vertical excitation, being mostly composed by an interaction between the frontier molecular orbitals. The first vertical excitation expected upon protonation is largely bathochromically shifted and is associated with a large oscillator strength. In **L1H⁺**, the interaction between the frontier molecular orbitals becomes predominant in the transition to S1, whilst the second transition is unlikely to be observed. Graphic inspection of the HOMO and LUMO orbitals (Fig. 3) shows a significant difference in LUMO upon protonation, shifting its location from the benzophenyl to the pyridyl moieties. The observed more energetic absorptions in **L1** and its protonated form correspond mostly to intramolecular charge transfer. This occurs in the former case between the carbazole and the benzophenyl moieties and in the latter between the same carbazole and the protonated pyridyl. The enhancement in the fluorescence is likely a result of two factors, the change of the lowest lying electronic transition and the easier planarization of the protonated pyridyl and the carbazole moieties in **L1H⁺** (ca. 1 kcal mol⁻¹, see Fig. S64, ESI[†]).

Compounds **L3** and **L4** were found to behave conversely to **L1** and **L2** as they do not exhibit fluorescence enhancement upon protonation. The case of **L3** is discussed here in detail. The absorption and fluorescence spectra of **L3** upon protonation with benzenesulfonic acid is presented in Fig. 2c and d (For **L4** see Fig. S11c, ESI[†]). Molecules **L3** and **L4** experience similar changes in their absorption upon protonation as **L1** and **L2**, displaying a band arising at 366 nm (for **L3**), characteristic

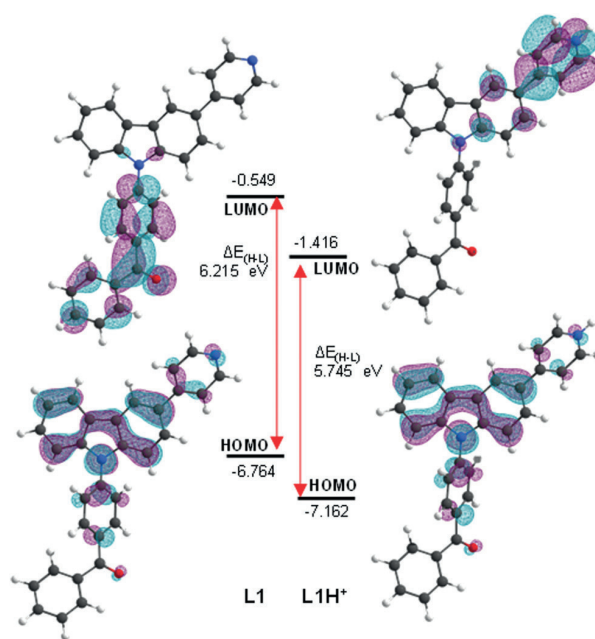


Fig. 3 Graphic representation of frontier molecular orbitals and respective energies (eV) of **L1** and its protonated congener (**L1H⁺**), as determined by TD-DFT at CAM-B3LYP/6-31G(d,p) level.

of the cationic species (Fig. 2c). Two fluorescence bands were observed for **L3** in DCM at 341 and 357 nm. However, due to the greater stability of the aromatic counter anion, benzenesulfonic acid has the greatest effect on the fluorescence of **L3**, and titration points up to 4.0 were not acquired since the fluorescence of **L3** is completely quenched upon addition of 2.0 equivalents of acid. Compound **L4** depicts similar effects as **L3**, only not as prominently due to the extra phenyl spacer separating the pyridyl from the carbazole core. Compound **L4** also displays a new broad low-intensity red-shifted fluorescence band arising at 575 nm likely as a result of a charge transfer state of the protonated species.

Inspection of the vertical transitions of **L3** and **L4**, (TD-DFT/CAM-B3LYP/6-31G(d,p)), reveals that the most energetic transitions correspond to local excitation states ($\pi-\pi^*$), with the orbitals located over the carbazole and its *N*-substituents. Protonation of these species results in stabilization of the frontier molecular orbitals (and a decrease on the HOMO–LUMO gap by 1–1.2 eV) accompanied with moving of the electron acceptor orbital, almost exclusively, to the carbazole *N*-substituent (Tables S5, S6 and Fig. S61, S62, ESI[†]).

The fluorescence quantum yield (Φ_f) of all the compounds were determined during the acid titrations. Titration with benzenesulfonic acid (**C**) shows a saturation point at 2.0 achieving a remarkable increase in the Φ_f of **L1** from 16% to 80% (Table S1 and Fig. S16a, ESI[†]). With the exception of benzenesulfonic acid, the acids follow the expected trend of their respective pK_a values, trifluoro- and trichloroacetic acid each time having very similar effects and chloroacetic acid (**F**) barely having any effect on the Φ_f . Similar results were obtained

also for **L2** (see Fig. S16b, ESI[†]). Compounds **L6** and **L7** were studied for the sole purpose of demonstrating that the observed effects were due to protonation and no other interactions. As expected, neither of the compounds show changes in fluorescence upon protonation (see Fig. S12–S14, ESI[†]), assuring that the observed effects for **L1–L4** are due to protonation of the pyridyl group.

¹H NMR spectroscopy

Protonation of the pyridyl group of **L3** with benzenesulfonic acid was further studied with ¹H NMR spectroscopy (Fig. 4) in order to elaborate the difference leading to quenching of the fluorescence compared to the fluorescence enhancement of **L1** and **L2**. The ¹H NMR of other compounds are shown in the ESI[†] (see Fig. S17–S30). The spectra showed characteristic behaviour of protonation, with chemical shifts moving to a lower field due to the deshielding effect upon protonation. Saturation can be seen at 1.0 equivalents of acid, as expected. Additionally, H_c experiences an unusually large change in its chemical shift of up to 0.61 ppm upon 2.0 equivalents of acid, indicating a strong interaction between **L3** and benzenesulfonic acid compared to the 0.20 ppm shift in **L1** at 1.0 equivalents of the same acid (see Fig. S23, ESI[†]). Natural population analysis of **L3** and its protonated form (Fig. 5a), taken at the same DFT level of theory as above, showed a 0.05 increase in the natural charge of H_a upon protonation. This is accompanied by a more significant change in the natural charge of the H_a-bound carbon due to the proximity to the established N–H bond. The NMR shift change of H_c is also reflected by the 0.03 change in the natural charges. Inspection on the bond lengths and strengths through Wiberg indexes (WI) analysis shows that protonation results in the N–C bond between the carbazole and the pyridyl moiety to shorten (1.41 Å in **L3** vs. 1.38 Å in **L3H⁺**) and to strengthen (WI = 0.99 in **L3** vs. 1.08 in **L3H⁺**). The changes in the length of pyridyl

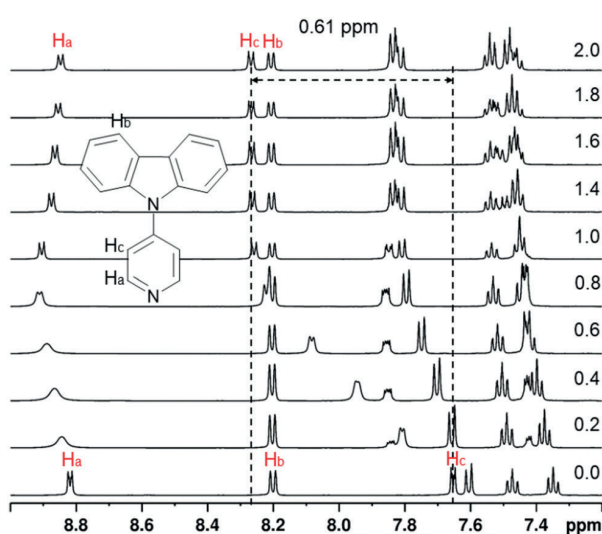


Fig. 4 The ¹H NMR spectra of **L3** while titrating with benzenesulfonic acid from 0.0 to 2.0 equivalents of acid (30 mM in CD₃CN, 500 MHz at 303 K).

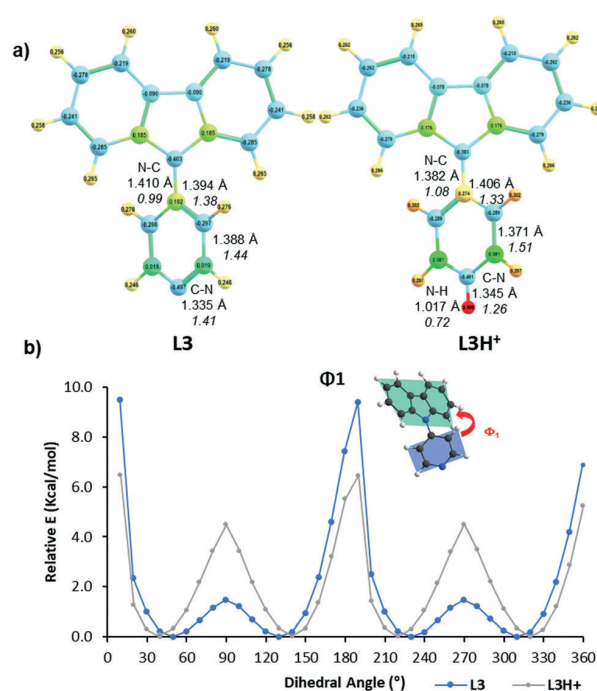


Fig. 5 Selected electronic and conformational parameters of **L3** and its protonated form (**L3H⁺**) as determined by TD-DFT at CAM-B3LYP/6-31G(d,p) level: (a) Natural charges determined from natural population analysis. The lengths (in Å) and Wiberg index (in italics) of selected bonds are indicated; (b) plane figure optimised structures, dihedral angle and energy profiles for rotation of pyridyl.

endocyclic bonds indicate the reorganisation of the electron density in the pyridyl to accommodate the extra positive charge, with only a slight disturbance on the carbazole moiety (Fig. S71, ESI[†]). The significant change in the chemical shift of H_c can also be attributed to the easier rotation about the carbazole-pyridyl N–C bond in solution upon protonation (Fig. 5b). Moreover, the placement of the pyridyl unit out of the carbazole plane decreases 3.0 kcal mol⁻¹ in the protonated species, thus making the complete rotation about the N–C bond even more accessible. The easier pyridyl rotation out of the carbazole plane in **L3** (and in **L4** to some extent) results in lower fluorescence quantum yield in solution (<1%).

Solid-state fluorescence

From the perspective of applications, the compounds were also studied in the solid state. For the purpose of discussing solid-state samples, the salts were named consistent with the ligand numbering (**L1–L7**) with an added H to describe proton transfer and with letters (a–f) representing the anion resulting from the deprotonation of the acid (A–F) and in square brackets to indicate a salt. The solid-state fluorescence spectra of **L1**, **L3**, **L4** (and their corresponding benzenesulfonate salts) and **L5** are shown in Fig. 6 and listed in Table 2. Compound **L2** was not studied in solid state due to the insolubility of the protonated solution due to its solubility only in high polarity solvents

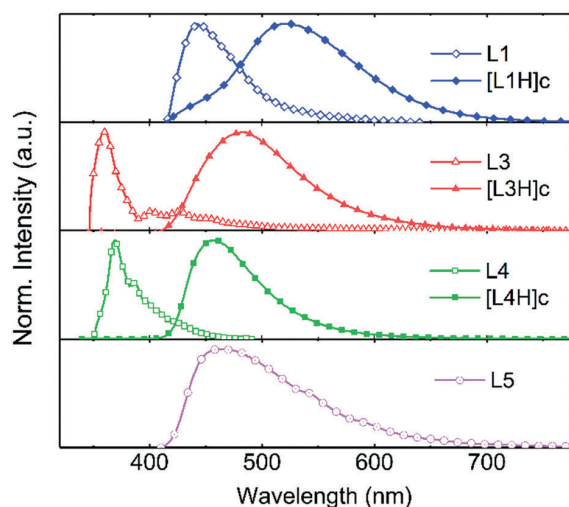


Fig. 6 Fluorescence of the solid-state samples of **L1**, **L3**, **L4**, and **L5**, and the acid complexes of **L1**, **L3**, and **L4**, at an excitation wavelength of 330 nm, 333 nm, 331 nm, 303 nm, 326 nm, 310 nm, and 320 nm, respectively.

Table 2 The fluorescence data of **L1–L4** (and their corresponding benzenesulfonate salts), and **L5** with absolute quantum yield values both in solution and in the solid state

Compound	In dichloromethane ^a			Solid state		
	λ_{ex} (nm)	F_{max}^b (nm)	Φ_f^c (sol)	λ_{ex} (nm)	F_{max} (nm)	Φ_f (SS, %)
L1	340	474	16.14	330	442	1.51
[L1H]c	340	472	79.45	326	521	15.81
L2	340	473	18.06	—	—	—
[L2H]c	340	451	79.18	—	—	—
L3	290	341, 356	10.52	333	360	2.46
[L3H]c	290	341, 356	0.97	310	483	25.09
L4	340	415	32.03	331	369	1.21
[L4H]c	340	420	0.14	320	457	49.02
L5^d	—	—	—	303	469	21.65

^a Measured at the concentration of 1.0×10^{-5} M at 25 °C. ^b Reported at 1.0 or 2.0 equivalent of benzenesulfonic acid according to the number of protonation sites. ^c Reported at 4.0 equivalent of benzenesulfonic acid for the protonated ligands, except for **[L3H]c** at 2.0. ^d Not soluble in dichloromethane, hence no solution studies were performed.

making the comparison to other compounds measured in DCM ineffectual.

The fluorescence maxima (F_{max}) of the ligands and their respective benzenesulfonate salts in solution remain almost identical for all compounds during the titration. When changing to solid state, the F_{max} of the pure ligand experiences a hypsochromic shift, or stays invariable, whereas the protonated ligand in the solid state displays a bathochromic shift compared to the F_{max} in solution. In contrast to solution, the fluorescence quantum yield of **L3** and **L4** increases in solid state and **L4** experiences a remarkable increase from 1% to 49% in the protonated form.^{35,36} The bathochromic shift of the fluorescence maxima observed for all the protonated ligands (Fig. 6) in the solid state suggests J-type packing for these

compounds. This type of packing is described as having a large Stokes shift, which readily limits self-absorption and leads to strong fluorescence in the solid state.⁴⁷ The hypsochromic shift, or no change, of the pure ligands indicates that this type of packing is not dominant for these compounds, and results in weak fluorescence in the solid state due to quenching as a result of aggregation.

Crystallography

Crystallisations of all studied compounds were carried out to further analyse the changes in the solid-state fluorescence. The crystallisation of the acid–base pairs was performed with a 1 : 1 acid–base ratio in various solvent systems (see ESI,† Fig. S34–S58). Unfortunately, not all crystallisations yielded X-ray diffraction quality crystals, and obtaining the weaker acid–base pairs proved to be difficult. The suitable single crystals obtained were subjected to a single-crystal X-ray diffraction analysis. The molecular packing of **L3**, **L4**, **[L1H]c**, and **[L4H]c** is shown in Fig. 7 along with the most common packing patterns described as J-type.⁴⁸ Despite the weaker acids (**D–F**) having little to no effect on the fluorescence of the compound in solution, in the solid-state the protonation seems to occur regardless of the strength of the acid.

All obtained solid-state structures had the expected 1 : 1 stoichiometry. The charge-assisted hydrogen bond distances between the oxygen of the conjugate base and the protonated nitrogen ($\text{O} \cdots \text{N}$) were found to be between 2.588(2)–2.784(3) Å (see ESI,† Table S3). The bond lengths were affected by the crystal packing due to the size of the anion. Due to the non-determinable positions of H atoms from X-ray diffraction analysis, all N–H bonds were refined to 1.04 Å based on the average of neutron diffraction studies of similar compounds.⁴⁹ The structures of **[L1H]a** and **[L4H]b** (see Fig. S39 and S51, ESI†) have two independent acid–base pairs in the asymmetric unit cell, whereas other structures were observed with one acid–base pair in the asymmetric unit cell. Additionally, in the structures of **[L1H]a–b**, **[L3H]a**, and **[L4H]a–b** (see ESI,† Fig. S39–S42, S47 and S49–S52, respectively) the counter anion was found to be disordered over two or three positions. Counter anions that are disordered might show that their location is to simply satisfy charge balance, having no preference as to where they were in the packing, *i.e.*, no strong bonding or interaction results from their presence. This again might create differences between the solid-state and solution studies. In addition to these, **[L1H]c** (see ESI,† Fig. S43) crystallised with a solvent molecule interacting with the carbonyl group of the benzophenyl acceptor [$\text{C74–H74} \cdots \text{O27}$, 3.437(4) Å].

From the solid-state fluorescence samples, X-ray diffraction quality single crystals could be obtained for compounds **[L1H]c**, **L3**, **L4**, **[L4H]c**, and **L5** (in addition to other acid–base pairs not studied for their solid-state fluorescence). Compound **L3** crystallises in the chiral orthorhombic space group $P2_12_12_1$ in a dimer-type zigzag packing stabilised by off-centre π – π interactions between the carbazole cores of two molecules with an interplanar distance of 3.6 Å (Fig. 7a). Compound **L3** also forms intermolecular interactions through $\text{C–H} \cdots \pi$ edge-to-face

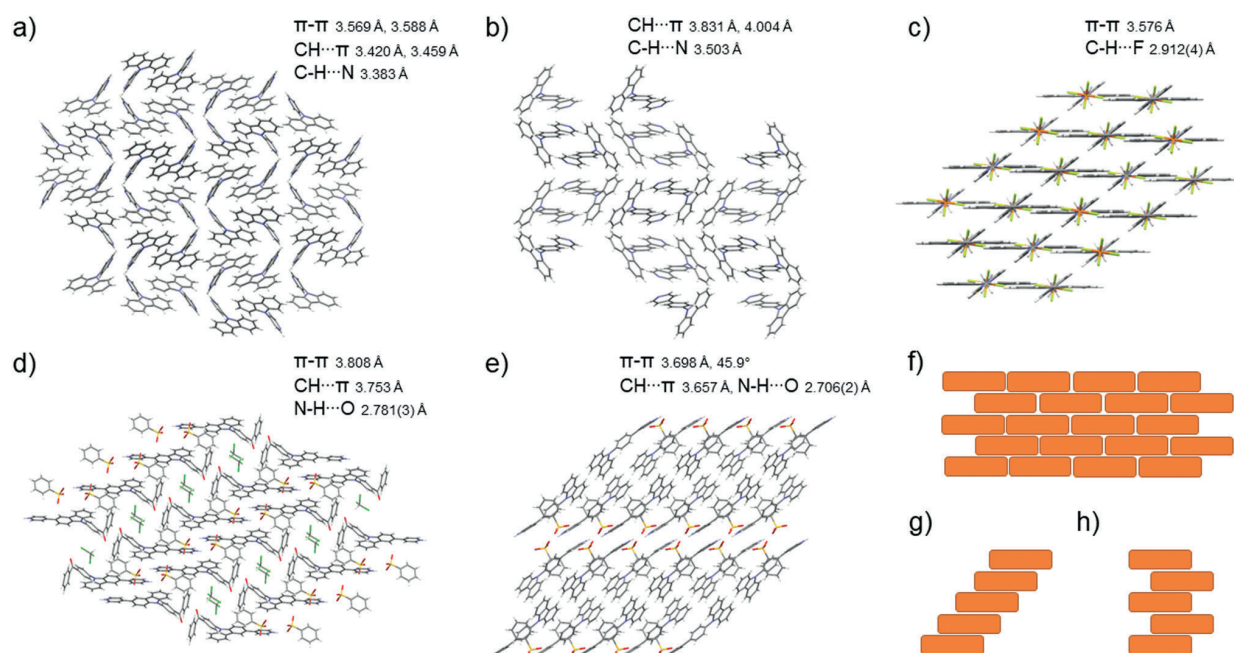


Fig. 7 Molecular packing patterns and most dominant interactions of (a) **L3** (b) **L4** (c) **L5** (d) **[L1H]c**, and (e) **[L4H]c** determined by single-crystal X-ray diffraction and the schematic presentations of different J-type packing patterns, where (f) brick (g) staircase, and (h) ladder pattern.

interactions to the carbazole core (Fig. 7a) and C-H...N interactions of the pyridyl nitrogen to the neighbouring hydrogens all together forming a three-dimensional network of intermolecular interactions. Similar to **L3**, **L4** also crystallises in the orthorhombic space group, yet now in centrosymmetric *Pbca* stabilised by similar off-centre π - π (3.8 Å), C-H... π edge-to-face, and C-H...N interactions (Fig. 7b). Supported by the hypsochromic shift in the solid-state fluorescence results, compounds **L3** and **L4** were determined to have H-type packing, which ultimately leads to quenching of the fluorescence. Compound **L5** crystallises in the centrosymmetric monoclinic *C2/c* space group in a J-type packing in a brick pattern (Fig. 7c and f) stabilised by strong π - π (3.6 Å) and C-H...F interactions from the surrounding anions. This type of packing induced by the ionic interactions gives rise to fairly strong fluorescence due to restricted intramolecular rotation of the pyridine moiety. However, the methylene group was found to be disordered over two positions possibly leading to some fluorescence quenching. Complex **[L1H]c** crystallises in the centrosymmetric triclinic *P* space group in a dimer-type head-to-tail packing of the pyridyl-carbazole motif in a staircase pattern (Fig. 7d and g) stabilised by off-centre π - π interactions of two aromatic rings with an interplanar distance of 3.8 Å. The complex **[L1H]c** is also stabilised by acid-base pair hydrogen bonding (N1-H1...O51, 2.781(3) Å), and C-H... π edge-to-face interactions (H29) to the aromatic ring of the benzenesulfonate. The complex **[L4H]c** crystallises in the centrosymmetric monoclinic *P2₁/c* space group with weak off-centre π - π interactions and intermolecular interactions between the ligand and the anion (N23-H23...O71, 2.706(2) Å) also in a staircase pattern

(Fig. 7e and g) inducing strong fluorescence commonly observed in J-type packing, which was also suggested by the bathochromic shift in the solid-state fluorescence maxima for these compounds. In the crystal structure of **[L1H]c** the packing of the carbazole moiety is coplanar, in contrast to **[L4H]c** where the carbazoles pack at a 45.9° angle making the off-centre π - π interactions observed for **[L4H]c** at an interplanar distance of 3.7 Å less effective. For **[L4H]c**, the π - π interactions are observed between the carbazole core and the phenyl ring attached to the carbazole moiety. The off-centre packing of **[L4H]c** forces the carbazole backbone to a bent conformation with an angle of 165.7° between the centroid of the central carbazole ring (C3 C4 C9 N10 C11), the carbazole nitrogen (N10), and the carbon of the adjacent phenyl ring (C14), whereas for most of the determined structures the carbazole lies close to parallel to the neighbouring phenyl or pyridyl ring with an angle close to 180°. Molecules of **[L4H]c** with twisted conformation have to be less densely packed in the highly restricted crystal lattice resulting in weaker intermolecular interactions.⁵⁰

The protonation of all the compounds shows also an increase in the Φ_f of solid-state samples due to restricted internal rotation of the molecule, as sterically hindered molecules show stronger fluorescence in solid-state.⁵¹ Unfortunately, attempts to crystallise **[L3H]c** did not yield X-ray diffraction quality crystals, and therefore, could not be compared to **[L1H]c** and **[L4H]c**. However, for **L3** and **L4**, the more structural packing induced by the planar conformation of the ligand, strong π - π /C-H... π interactions, and hydrogen bonding effectively quench the fluorescence in the solid-state.⁵⁰

For compounds **L5**, [**L1H**]**c**, and [**L4H**]**c**, there is a compromise between the quenching due to intermolecular interactions and both the J-type packing and steric hindrance inducing stronger fluorescence. Additionally, the network of intermolecular interactions in the crystal structure of [**L1H**]**c** may dissipate the excited-state energy to some degree through internal conversion,⁵⁰ a process that does not occur in the less dense packing of [**L4H**]**c**, resulting in a much higher Φ_f in the solid state compared to [**L1H**]**c**.

Conclusions

The effect of protonation on the fluorescence of small pyridine-functionalised carbazole donors has been studied in both solution and solid state. In these compounds, a carbazole core acts as a donor, whereas benzophenyl, pyridyl, and phenylpyridyl moieties were chosen for acceptors in the design of bipolar host materials. All compounds showed absorption bands in the UV region and a wide variety of emission wavelengths from 300 to 600 nm. All compounds could be protonated using six different organic acids displaying a diversity of interaction strengths related to the pK_a of the acid used in the protonation. The observed bathochromic shift and the increase in the fluorescence intensity of **L1** and **L2** was explained primarily by the different localisation of the LUMO orbital on the protonated species and secondly by the easier planarization of the protonated pyridyl and the carbazole moieties. The fluorescence quantum yield of **L1** increased from 16% to 80% upon protonation in solution. The bathochromic shift upon protonation, in addition to DFT, suggests that the protonation of these compounds effectively lowers the energy of the emissive state lowering the energy gap between the emissive state and the first triplet state, which could facilitate reverse intersystem crossing and result in more efficient TADF. In compound **L3**, the placement of the pyridyl unit out of the carbazole plane decreased in energy upon protonation making the rotation about the N–C bond even more accessible, thus quenching the fluorescence. In the solid state, the rotation around the N–C bond was restricted in all the compounds upon protonation. All protonated compounds also favoured the beneficial J-type packing resulting in a large bathochromic shift in the fluorescence intensity, with the quantum yield changing from 1% to 49% upon protonation in the best case, whereas all the pure ligands acted much like many other organic compounds in solid state and the fluorescence was quenched due to aggregation effects. Hereby, we have proposed an effective way for fluorescence modulation through protonation-induced restriction of the intramolecular rotation, which could enable the development of future bipolar host materials.

Experimental

All reagents and solvents were obtained from commercial suppliers and used without further purification. Absorption spectra were collected using Varian Cary 100, 300 Series II

Series UV-Visible Spectrophotometer, and fluorescence spectra were collected using Varian Cary Eclipse Fluorescence Spectrophotometer. The measurements were taken in a 1 cm quartz cuvette and the excitation and the emission bandpasses were set to 2.5 nm and 2.5 nm, respectively. All the measurements were performed at room temperature. The integrated relative intensities were determined in respect to the natural fluorescence of the compound using that as a zero point and 9,10-diphenylanthracene was used as a reference in determination of the fluorescence quantum yield of the compounds.

For NMR assignments, ¹H and ¹³C NMR spectra were recorded using either Bruker 300 Avance or Bruker Avance III 500 MHz spectrometer at 303 K. Chemical shifts are reported on the δ scale in ppm using the residual solvent signal as internal standard (CDCl₃; δ H 7.26, CD₂Cl₂; δ H 5.32, CD₃CN; δ H 1.94, DMSO-*d*₆; δ H 2.50). For ¹H NMR spectroscopy, each resonance was assigned according to the following conventions: chemical shift (δ) measured in ppm, observed multiplicity, number of hydrogens, observed coupling constant (J Hz), and assignment. Multiplicities are denoted as s (singlet), d (doublet), t (triplet), q (quartet), m (multiplet), and br (broad).

The absorption, fluorescence, excitation spectra, and absolute fluorescence quantum yield values for the solid-state samples were obtained by using an FLS-1000 spectrofluorometer equipped with a calibrated integrating sphere (Edinburgh Instruments, UK). Absorption spectra did not show sharp peaks hence the initial fluorescence spectra measurements were performed by using 340 nm excitation wavelength as it was done during solution studies. Then by using fluorescence wavelength maxima the excitation spectra were measured and excitation wavelength maxima were detected. These wavelengths were chosen then to measure both fluorescence spectra and absolute fluorescence quantum yields.

The experimental and refinement details for all complexes studied with single-crystal X-ray diffraction are given in the ESI.† All structures were measured using a Bruker-Nonius KappaCCD diffractometer with an APEX-II detector with graphite-monochromatized Mo-K α ($\lambda = 0.71073$ Å) radiation or Agilent Super-Nova dual wavelength diffractometer with an Atlas detector using mirror-monochromated Cu-K α ($\lambda = 1.54184$ Å) radiation. The program CrysAlisPro5 was used for the data collection and reduction on the Super-Nova diffractometer. Data collection and reduction the Bruker-Nonius KappaCCD diffractometer were performed using the program COLLECT⁵² and HKL DENZO AND SCALEPACK,⁵³ respectively, and the intensities were corrected for absorption using SADABS.⁵⁴ The structures were solved with intrinsic phasing (SHELXT)⁵⁵ and refined by full-matrix least-squares on F^2 using the OLEX2 software,⁵⁶ which utilises the SHELXL-2015 module.⁵⁷ Non-hydrogen atoms were assigned anisotropic displacement parameters unless stated otherwise. Hydrogen atoms bonded to oxygen were located from Fourier difference maps and refined with an O–H distance restraint of approximately 0.84 Å. Other hydrogen atoms were placed in idealised positions and included as riding, with a value of 1.04 Å used for N–H bonds, which was based on an average of neutron

diffraction values reported for this moiety with similarly hybridised neighbouring atoms.⁴⁹ Isotropic displacement parameters for all H atoms were constrained to multiples of the equivalent displacement parameters of their parent atoms with $U_{\text{iso}}(H) = 1.2U_{\text{eq}}(\text{parent atom})$.

All theoretical calculations were carried out using the Gaussian 16⁵⁸ software package without symmetry constrains. Solvent effects (dichloromethane) were considered in every calculation using the Polarizable Continuum Model (PCM) initially devised by Tomasi and coworkers^{59–61} as implemented on Gaussian 16, with radii and non-electrostatic terms for Truhlar and coworkers' SMD solvation model.⁶² Density Functional Theory (DFT) and Time-Dependent DFT (TD-DFT) were used for the ground and vertical excitations of L1, L3, L4 and their corresponding cationic forms, respectively. All calculations have been performed using the CAM-B3LYP⁶³ functional and 6-31G(d,p)^{64–68} basis set. The ground state geometry of L1, L3, L4 and their corresponding cationic forms has been fully optimised with default cut-offs on forces and step size to determine convergence. The analytical calculation of the vibrational frequencies at the same level of theory verified the optimised structure by checking that they corresponded to true minima of the potential energy surface by the absence of imaginary frequencies. The first six low-lying excited states have been determined within the vertical TD-DFT, with the default linear response non-equilibrium solvation procedure. A Natural Population Analysis (NPA)^{69–76} and the resulting Wiberg indices^{77,78} were calculated as implemented on Gaussian 16 to study the electronic structure and bonding of the optimised species.

Conflicts of interest

There are no conflicts to declare.

Acknowledgements

AP is thankful to the Academy of Finland (SUPREL project, decision numbers 311142 & 326416) for financial support. JSW gratefully acknowledges the Finnish Cultural Foundation Central Fund (Grant number 00201148) for funding. NRC is thankful to Fundação para a Ciência e Tecnologia for the financial support (CEE-CINST/2018), and to CSC-IT Center for Science Ltd, Finland for the allocation of computational resources. NAD acknowledges the financial support from Academy of Finland (Grant number 316893).

Notes and references

- 1 J.-M. Lehn, *Angew. Chem., Int. Ed. Engl.*, 1988, **27**, 89–112.
- 2 J. K. Salunke, N. A. Durandin, T.-P. Ruoko, N. R. Candeias, P. Vivo, E. Vuorimaa-Laukkanen, T. Laaksonen and A. Priimagi, *Sci. Rep.*, 2018, **8**, 14431.
- 3 X. Zhu, J.-X. Wang, L.-Y. Niu and Q.-Z. Yang, *Chem. Mater.*, 2019, **31**, 3573–3581.
- 4 M. Zuo, W. Qian, T. Li, X.-Y. Hu, J. Jiang and L. Wang, *ACS Appl. Mater. Interfaces*, 2018, **10**, 39214–39221.
- 5 T. Senthilkumar, L. Zhou, Q. Gu, L. Liu, F. Lv and S. Wang, *Angew. Chem., Int. Ed.*, 2018, **57**, 13114–13119.
- 6 R. Chang and X. Yan, *Small Struct.*, 2020, **1**, 2000068.
- 7 P. Xing and Y. Zhao, *Adv. Mater.*, 2016, **28**, 7304–7339.
- 8 T. L. Mako, J. M. Racicot and M. Levine, *Chem. Rev.*, 2019, **119**, 322–477.
- 9 X. Chang, Z. Zhou, C. Shang, G. Wang, Z. Wang, Y. Qi, Z.-Y. Li, H. Wang, L. Cao, X. Li, Y. Fang and P. J. Stang, *J. Am. Chem. Soc.*, 2019, **141**, 1757–1765.
- 10 J.-X. Wang, L.-Y. Niu, P.-Z. Chen, Y.-Z. Chen, Q.-Z. Yang and R. Boulatov, *Chem. Commun.*, 2019, **55**, 7017–7020.
- 11 Y. Cai, A. Qin and B. Z. Tang, *J. Mater. Chem. C*, 2017, **5**, 7375–7389.
- 12 C.-H. Lee, M.-H. Tang, W.-L. Cheung, S.-L. Lai, M.-Y. Chan and V. Yam, *Chem. Sci.*, 2018, **9**, 6228–6232.
- 13 Z. Xu, B. Z. Tang, Y. Wang and D. Ma, *J. Mater. Chem. C*, 2020, **8**, 2614–2642.
- 14 W. Li, J. Li, D. Liu, F. Wang and S. Zhang, *J. Mater. Chem. C*, 2015, **3**, 12529–12538.
- 15 W. Li, J. Li, D. Liu and Q. Jin, *ACS Appl. Mater. Interfaces*, 2016, **8**, 22382–22391.
- 16 B. Wex and B. R. Kaafarani, *J. Mater. Chem. C*, 2017, **5**, 8622–8653.
- 17 W. Liu, C.-J. Zheng, K. Wang, M. Zhang, D.-Y. Chen, S.-L. Tao, F. Li, Y.-P. Dong, C.-S. Lee, X.-M. Ou and X.-H. Xiang, *ACS Appl. Mater. Interfaces*, 2016, **8**, 32984–32991.
- 18 D. Zhang, M. Cai, Y. Zhang, D. Zhang and L. Duan, *ACS Appl. Mater. Interfaces*, 2015, **7**, 28693–28700.
- 19 P. Rajamalli, D. R. Martir and E. Zysman-Colman, *J. Photonics Energy*, 2018, **8**(3), 032106.
- 20 Y. Shiota, M. Kinoshita, T. Noda, K. Okumoto and T. Ohara, *J. Am. Chem. Soc.*, 2000, **122**, 11021–11022.
- 21 A. Chaskar, H.-F. Chen and K.-T. Wong, *Adv. Mater.*, 2011, **23**, 3876–3895.
- 22 K. S. Yook and J. Y. Lee, *Chem. Rec.*, 2016, **16**, 159–172.
- 23 S. M. Kim, J. H. Yun, S. H. Han and J. Y. Lee, *J. Mater. Chem. C*, 2017, **5**, 9072–9079.
- 24 M. Sarma and K. T. Wong, *Chem. Rec.*, 2019, **19**, 1667–1692.
- 25 A. Endo, K. Sato, K. Yoshimura, T. Kai, A. Kawada, H. Miyazaki and C. Adachi, *Appl. Phys. Lett.*, 2011, **98**, 083302.
- 26 Z. Shi, D. Zhang, J. Huo, H. Wang, J. Yu, H. Shi and B. Z. Tang, *Mater.*, 2019, **34**(17), 3000–3010.
- 27 N. L. C. Leung, N. Xie, W. Yuan, Y. Liu, Q. Wu, Q. Peng, Q. Miao, J. W. Y. Lam and B. Z. Tang, *Chem. – Eur. J.*, 2014, **20**, 15349–15353.
- 28 W. Sun, Z. Wang, T. Wang, L. Yang, J. Jiang, X. Zhang, Y. Luo and G. Zhang, *J. Phys. Chem. A*, 2017, **121**, 4225–4232.
- 29 L. Xie, G. Han, Y. Chen, H. Wang, X. Kong, X. Wei, J. Liu, Y. Yi, B. Chen, P. Wang and Y. Wang, *J. Mater. Chem. C*, 2016, **4**, 10776–10780.
- 30 M. Li, Y. Yuan and Y. Chen, *ACS Appl. Mater. Interfaces*, 2018, **10**, 1237–1243.
- 31 S. Achelle, J. Rodríguez-López., C. Katan and F. Robin-le Guen, *J. Phys. Chem. C*, 2016, **120**, 26986–26995.
- 32 E. Tervola, K.-N. Truong, J. S. Ward, A. Priimagi and K. Rissanen, *RSC Adv.*, 2020, **10**, 29385–29393.

- 33 N. Mataga and S. Tsuno, *Bull. Chem. Soc. Jpn.*, 1957, **30**, 368–374.
- 34 N. Mataga, *Bull. Chem. Soc. Jpn.*, 1958, **31**, 459–462.
- 35 A. Aguilar-Granda, S. Pérez-Estrada, A. E. Roa, J. Rodríguez-Hernández, S. Hernández-Ortega, M. Rodríguez and B. Rodríguez-Molina, *Cryst. Growth Des.*, 2016, **6**, 3435–3442.
- 36 J. Jiao, J.-X. Kang, Y. Ma, Q. Zhao, H. Li, J. Zhang and X. Chen, *Front. Chem.*, 2019, **7**, 768.
- 37 Q. Wei, N. Fei, A. Islam, T. Lei, L. Hong, R. Peng, X. Fan, L. Chen, P. Gao and Z. Ge, *Adv. Opt. Mater.*, 2018, **6**, 1800512.
- 38 B. Huang, X. Ban, K. Sun, Z. Ma, Y. Mei, W. Jiang, B. Lin and Y. Sun, *Dyes Pigm.*, 2016, **133**, 380–386.
- 39 C.-H. Chen, L.-C. Hsu, P. Rajamalli, Y.-W. Chang, F.-L. Wu, C.-Y. Liao, M.-J. Chiu, P.-Y. Chou, M.-J. Huang, L.-K. Chu and C.-H. Cheng, *J. Mater. Chem. C*, 2014, **2**, 6183–6191.
- 40 X.-H. Zhao, Z.-S. Zhang, Y. Qian, M.-D. Yi, L.-H. Xie, C.-P. Hu, G.-H. Xie, H. Xu, C.-M. Han, Y. Zhao and W. Huang, *J. Mater. Chem. C*, 2013, **1**, 3482–3490.
- 41 S. J. Nemat, H. Jedrzejewska, A. Prescimone, A. Szumna and K. Tiefenbacher, *Org. Lett.*, 2020, **22**, 5506–5510.
- 42 K. Leduskrasts, A. Kinens and E. Suna, *Chem. Commun.*, 2019, **55**, 12663–12666.
- 43 Acid Dissociation Constants, CRC Handbook of Chemistry and Physics, retrieved on 20.12.2018.
- 44 T. Larsson, M. Wedborg and D. Turner, *Anal. Chim. Acta*, 2007, **583**, 357–363.
- 45 B. J. van der Veken, W. A. Herrebout, R. Szostak, D. N. Shchepkin, Z. Havlas and P. Hobza, *J. Am. Chem. Soc.*, 2001, **123**, 12290–12293.
- 46 Z. Zara, J. Iqbal, K. Ayub, M. Irfan, A. Mahmood, R. A. Khera and B. Eliasson, *J. Mol. Struct.*, 2017, **1149**, 282–298.
- 47 C. Maeda, T. Todaka, T. Ueda and T. Ema, *Chem. – Eur. J.*, 2016, **22**, 7508–7513.
- 48 F. Würthner, T. E. Kaiser and C. R. Saha-Möller, *Angew. Chem., Int. Ed.*, 2011, **50**, 3376–3410.
- 49 F. H. Allen and I. J. Bruno, *Acta Crystallogr., Sect. B: Struct. Sci.*, 2010, **66**, 380–386.
- 50 D.-E. Wu and M. Lu, *New J. Chem.*, 2015, **39**, 6465–6473.
- 51 K. Shirai, M. Matsuoka and K. Fukunishi, *Dyes Pigm.*, 1999, **42**, 95–101.
- 52 R. W. W. Hoof, *COLLECT*, Nonius BV, Delft, the Netherlands, 1998.
- 53 Z. Otwinowski and W. Minor, in *Methods in Enzymology, Macromolecular Crystallography, Part A*, ed. C. W. Carter Jr and R. M. Sweet, Academic Press, New York, 1997, vol. 276, pp. 307–326.
- 54 G. M. Sheldrick, *SADABS*, Version 2008/2, University of Göttingen, Germany, 1996.
- 55 G. M. Sheldrick, *Acta Crystallogr., Sect. A: Found. Adv.*, 2015, **71**, 3–8.
- 56 O. V. Dolomanov, L. J. Bourhis, R. J. Gildea, J. A. K. Howard and H. Puschmann, *J. Appl. Crystallogr.*, 2009, **42**, 339–341.
- 57 G. M. Sheldrick, *Acta Crystallogr., Sect. C: Struct. Chem.*, 2015, **71**, 3–8.
- 58 M. J. Frisch, G. W. Trucks, H. B. Schlegel, G. E. Scuseria, M. A. Robb, J. R. Cheeseman, G. Scalmani, V. Barone, G. A. Petersson and H. Nakatsuji *et al.*, *Gaussian 16, Revision C.01*, Gaussian, Inc., Wallingford CT, 2019.
- 59 E. Cancès, B. Mennucci and J. Tomasi, *J. Chem. Phys.*, 1997, **107**(8), 3032.
- 60 B. Mennucci and J. Tomasi, *J. Chem. Phys.*, 1997, **106**(12), 5151.
- 61 M. Cossi, V. Barone, B. Mennucci and J. Tomasi, *Chem. Phys. Lett.*, 1998, **286**(3–4), 253.
- 62 A. V. Marenich, C. J. Cramer and D. G. Truhlar, *J. Phys. Chem. B*, 2009, **113**(18), 6378.
- 63 T. Yanai, D. P. Tew and N. C. Handy, *Chem. Phys. Lett.*, 2004, **393**(1–3), 51.
- 64 R. Ditchfield, W. J. Hehre and J. A. Pople, *J. Chem. Phys.*, 1971, **54**(2), 724.
- 65 W. J. Hehre, R. Ditchfield and J. A. Pople, *J. Chem. Phys.*, 1972, **56**(5), 2257.
- 66 P. C. Hariharan and J. A. Pople, *Mol. Phys.*, 1974, **27**(1), 209.
- 67 M. S. Gordon, *Chem. Phys. Lett.*, 1980, **76**(1), 163.
- 68 P. C. Hariharan and J. A. Pople, *Theor. Chim. Acta*, 1973, **28**(3), 213.
- 69 J. E. Carpenter, PhD thesis, University of Wisconsin, 1987.
- 70 J. E. Carpenter and F. Weinhold, *J. Mol. Struct.*, 1988, **46**, 41.
- 71 J. P. Foster and F. Weinhold, *J. Am. Chem. Soc.*, 1980, **102**(24), 7211.
- 72 A. E. Reed and F. Weinhold, *J. Chem. Phys.*, 1983, **78**(6), 4066.
- 73 A. E. Reed and F. Weinhold, *J. Chem. Phys.*, 1985, **83**(4), 1736.
- 74 A. E. Reed, R. B. Weinstock and F. Weinhold, *J. Chem. Phys.*, 1985, **83**(2), 735.
- 75 A. E. Reed, L. A. Curtiss and F. Weinhold, *Chem. Rev.*, 1988, **88**(6), 899.
- 76 F. Weinhold and J. E. Carpenter, *The Structure of Small Molecules and Ions*, Plenum, 1988.
- 77 K. B. Wiberg, *Tetrahedron*, 1968, **24**(3), 1083.
- 78 K. B. Wiberg and J. R. Snoonian, *J. Org. Chem.*, 1998, **63**(5), 1390.



III

IODINE(I) AND SILVER(I) COMPLEXES OF BENZOIMIDAZOLE AND PYRIDYL-CARBAZOLE DERIVATIVES

by

E. Taipale, M. Siepmann, K.-N. Truong & K. Rissanen 2021

Chem. Eur. J. 2021, 27, 17412–17419

<https://doi.org/10.1002/chem.202103152>

Reproduced with kind permission by John Wiley and Sons.

Iodine(I) and Silver(I) Complexes of Benzoimidazole and Pyridylcarbazole Derivatives

Essi Taipale,^[a] Marcel Siepmann,^[a] Khai-Nghi Truong,^[a] and Kari Rissanen^{*[a]}

Abstract: The synthesis of iodine(I) complexes with either benzoimidazole or carbazole-derived sp^2 N-containing Lewis bases is described, as well as their corresponding silver(I) complexes. The addition of elemental iodine to the linear two-coordinate Ag(I) complexes produces iodine(I) complexes with a three-center four-electron (3c–4e) $[N-I-N]^+$ bond. The 1H and 1H - ^{15}N HMBC NMR studies unambiguously confirm the formation of the complexes in all cases via the $[N-Ag-N]^+ \rightarrow [N-I-N]^+$ cation exchange, with the ^{15}N NMR chemical shift


change between 94 to 111 ppm when compared to the free ligand. The single crystal X-ray crystallographic studies on eight I^+ complexes revealed highly symmetrical $[N-I-N]^+$ bonds with I–N bond distances of 2.21–2.26 Å and N–I–N angles of 177–180°, whilst some of the corresponding Ag^+ complexes showed a clear deviation from linearity with N–Ag–N angles of ca. 150° and Ag–N bond distances of 2.09–2.18 Å.

Introduction

The basis of halogen bonding has been known for more than two centuries, and since then, it has played a major role in important achievements especially by R. S. Mulliken^[1] and O. Hassel,^[2] which earned them the Nobel prize in chemistry in 1966 and 1969, respectively. However, at the time, the results were not collectively understood, and it took roughly 30 years for it to gain its footing as a truly intriguing interaction in the field of supramolecular chemistry.^[3] This relatively novel interaction was defined in 2013 to “occur when there is evidence of a net attractive interaction between an electrophilic region associated with a halogen atom (X) in a molecular entity and a nucleophilic region in another, or the same, molecular entity”, where X = Cl, Br, or I.^[4,5] Although halogens are generally viewed as electronegative, since the 1990s it has been well established that strongly polarized halogen atoms manifest a positively charged electrostatic potential, a so-called σ -hole.^[3,4] Alternatively, this phenomenon can be explained by the charge-transfer theory by Mulliken^[6] or polar flattening.^[7] Therefore, a halogen atom is capable of interacting with a nucleophilic site, i.e. a Lewis base.^[4] Since its discovery, halogen bonding has begun to unearth its potential in the design and preparation of self-assembled systems, as well as in crystal engineering.^[8–11] This all due to its tunability, strength, and high directionality, making it an essential addition to the ‘modern chemist’s toolbox’.^[3,11]

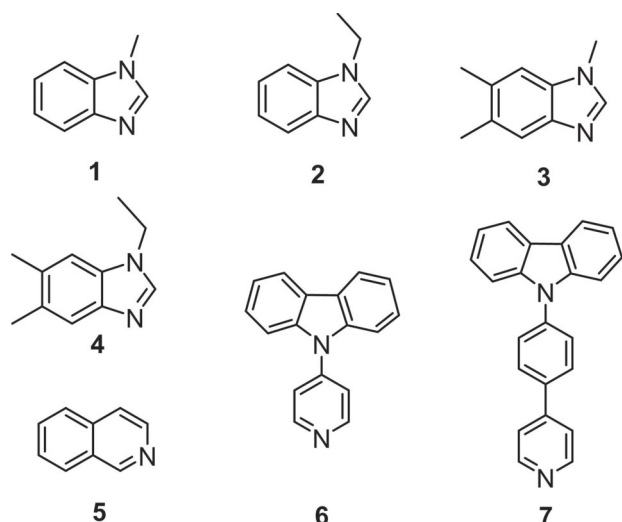
In a classical halogen bond consisting of a covalent bond and a halogen bond (D–X...D), the halogen atom exists in a formal oxidation state of –1 (e.g. in alkyl halides).^[12] When electron is removed from the halogen atom, it becomes a positively charged halogen(I) cation (X^+), which forms three-center four-electron (3c–4e) $[N-X-N]^+$ bonds, in which X^+ simultaneously interacts with two nucleophiles (Lewis bases, D) both contributing a lone pair to stabilize the interaction $[D...X...D]^+$.^[12–16] When aromatic Lewis bases are involved, the interaction is further enhanced by efficient charge transfer from the halogen(I) cation to the nucleophilic sites.^[12,17,18] These halogen(I) cations were first discovered in the 1960s and since then, they have found applications in form of Barluenga’s reagent^[19] in synthetic chemistry as iodinating agents for aromatic electrophilic substitutions and aromatic amines, yet can also be used as oxidizing agents.^[20–25] The exceptional strength of 3c–4e halogen bonds in halogen(I) complexes has made these an interesting sub-class of halogen-bonded complexes, however, due to their inherent reactivity only a few tens of unique iodine(I) complexes have been reported to date in the solid-state.^[13,26–34] There are no reported X-ray structures of iodine(I) complexes with bicyclic aromatic amines such as benzoimidazoles or quinolines. Herein, benzoimidazole and pyridylcarbazole derivatives were chosen to probe halogen bonding with polycyclic and larger XB acceptors leading to eight new $[N-I-N]^+$ halogen(I) (also known as *halonium*) and $[N-Ag-N]^+$ silver(I) complexes in the solid-state, along with compelling evidence of halogen(I) complex formation in solution.

[a] E. Taipale, M. Siepmann, Dr. K.-N. Truong, Prof. K. Rissanen
University of Jyväskylä
Department of Chemistry
P.O. Box 35, Surfontie 9B, 40014 Jyväskylä (Finland)
E-mail: kari.t.rissanen@jyu.fi

 Supporting information for this article is available on the WWW under <https://doi.org/10.1002/chem.202103152>

Results and Discussion

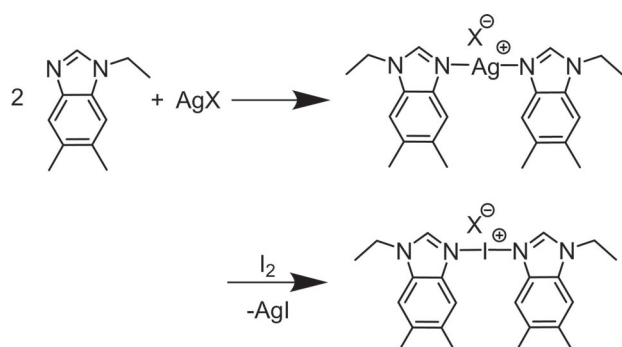
The syntheses of compounds 1–4 and 6–7 (Scheme 1) followed previously reported methods,^[35–37] whilst compound 5 was obtained commercially. The ligands were reacted with silver(I)



Scheme 1. Synthesized ligands 1–7 (compound 5 obtained commercially) used for the formation of the iodine(I) complexes.^[35–37]

salts (AgPF_6 , AgBF_4 , and AgSbF_6) in a 2:1 ratio to obtain the $[\text{N–Ag–N}]^+$ silver(I) complexes. The corresponding $[\text{N–I–N}]^+$ halogen(I) complexes were obtained through the $[\text{N–Ag–N}]^+ \rightarrow [\text{N–I–N}]^+$ cation exchange reaction (Scheme 2) by the addition of elemental iodine (I_2) to a solution of the silver(I) complexes,^[12,15,38] which concomitantly resulted in the immediate precipitation of AgI.

The conversion from the free ligand to the silver(I) and iodine(I) complexes was confirmed with ^1H NMR spectroscopy (Figures S1–S5 and Table S1) and ^1H - ^{15}N HMBC correlation measurements (Figures S6–S10). Ideally, all NMR measurements would have been performed in a non-coordinating solvent such as CD_2Cl_2 , but unfortunately, due to the solubility of either the ligand or the silver salt, all NMR measurements were necessarily^[12,15,38] performed in polar solvents, such as CD_3CN , acetone- d_6 , or $\text{DMSO}-d_6$. The ^1H NMR analyses of the silver complexes $[\text{L–Ag–L}]\text{PF}_6$ (exemplified in Figure 1) indicated a full conversion from the ligands to the silver(I) complexes and



Scheme 2. Synthesis of the $[\text{4–Ag–4}]\text{PF}_6$ silver(I) and $[\text{4–I–4}]\text{PF}_6$ iodine(I) complexes via a cation exchange reaction.^[12,15,38] All other complexes were prepared in an analogous fashion (where $\text{X} = \text{PF}_6^-$, BF_4^- , or SbF_6^-).

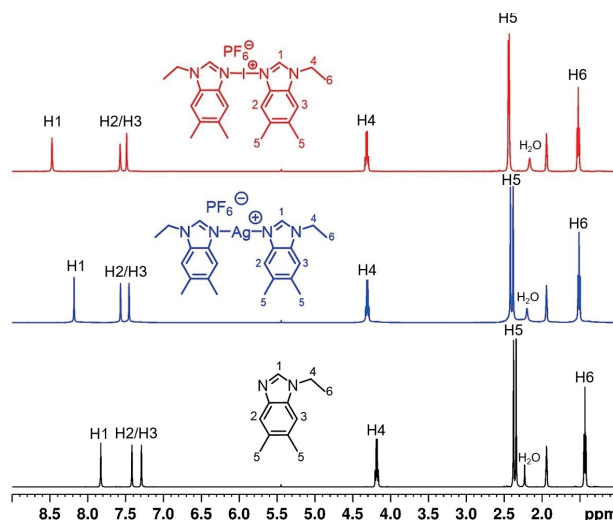


Figure 1. The comparison of the ^1H NMR spectra of ligand 4, the silver(I) complex $[\text{4–Ag–4}]\text{PF}_6$, and the iodine(I) complex $[\text{4–I–4}]\text{PF}_6$ (from bottom to top). All values are in ppm and referenced to CD_3CN (^1H) (500 MHz, 298 K).

demonstrated significant complexation-induced changes in the chemical shifts. Changes in the chemical shifts when going from the free ligand to the silver(I) complex were found in the range of 0.02–0.47 ppm, with the greatest change being observed for $[\text{3–Ag–3}]\text{PF}_6$ (Figure S3).

Measurements of the ligand and silver(I) salts proceeded straightforwardly, but for some of the ligands the solubility of the iodine(I) complex proved problematic. Since the synthesis comprises precipitation of AgI due to the cation exchange reaction, the poor solubility of the iodine(I) complexes could not be readily observed other than by the lower concentration indicated by the ^1H NMR spectra. Nevertheless, the ^1H NMR spectra were recorded for all of the iodine(I) complexes, except for $[\text{7–I–7}]^+$. Complexes from ligand 7 remained elusive, since the Ag^+ and I^+ complexes could not be solubilized, and therefore NMR analysis was not performed for these complexes. The comparison of the ^1H NMR spectra of the ligand 4, the silver(I) complex $[\text{4–Ag–4}]\text{PF}_6$, and the iodine(I) complex $[\text{4–I–4}]\text{PF}_6$ is shown in Figure 1. As expected, the cation exchange from the silver(I) to the iodine(I) results in a further downfield change in the chemical shifts of the bound ligand. Again, none of the silver(I) complex was observed in the spectrum for $[\text{4–I–4}]\text{PF}_6$ (Figure 1), indicating a complete conversion. The changes in the chemical shifts in the ^1H NMR spectrum from the silver(I) complex to the iodine(I) complex are within the range of 0.13–0.59 ppm, making the total chemical shift change from ligand to iodine(I) complex between 0.36–1.06 ppm. The largest change in the chemical shift upon conversion from the ligand to the iodine(I) complex was observed for ligand 3 (Figure S3), however, the poor solubility of $[\text{3–I–3}]\text{PF}_6$ resulted in a broadened and less accurate spectrum.

The use of ^1H - ^{15}N HMBC NMR spectroscopy provides a more powerful tool compared to the relatively small changes in the ^1H NMR spectra. The wide chemical shift range of the ^{15}N NMR

and the direct involvement of the nitrogen nuclei in the complexation event render ^{15}N a convenient technique for monitoring the cation exchange reaction.^[14,18,30,32,38,39] However, due to the fact that the ^{15}N nuclei is much less abundant in comparison to ^1H , not all the ^1H - ^{15}N HMBC spectra could be obtained owing to the low solubility of several of the iodine(I) complexes. This is potentially made worse due to line broadening caused by an ongoing association-dissociation equilibrium, observed more prominently for weaker halogen-bond acceptors.^[40] However, all three spectra of the complexation (ligand, silver(I), and iodine(I)) were obtained for several of the ligands (Figures S6-S10). The comparison of the ^1H - ^{15}N HMBC correlation spectra of the ligand **4**, the silver complex **[4-Ag-4]PF₆**, and the iodine(I) complex **[4-I-4]PF₆** is shown in Figure 2. All ligands, except **5** (as predicted), provided two signals for the two nitrogen atoms in different environments. The sp^2 -acceptor *N*-atom (N1) signal change was 44 ppm going from the ligand to the silver(I) complex **[4-Ag-4]PF₆**. Upon addition of the molecular iodine, an additional change of 50 ppm was observed for **[4-I-4]PF₆**, making it a total difference of 94 ppm (between the uncoordinated ligand and the iodine(I) complex). The largest change in the chemical shift from the

ligand to the iodine(I) complex was observed for **[5-I-5]PF₆** (111 ppm, Figure S9).

Whilst the ^{15}N NMR resonances of the acceptor N1 are deshielded upon complexation, the inert N2 is shielded and experiences only minor changes in the chemical shift (9–10 ppm). Due to the low solubility of **[3-I-3]PF₆**, only the inert N2 resonance was observed, however the same trend was found in these chemical shift changes (Figure S8). The ^1H - ^{15}N HMBC chemical shifts are summarized in Table 1.

The solvent and counter-anion coordination to the silver(I) cation has previously been reported to affect the pyridine ^{15}N NMR coordination shifts.^[12,30,41] Here, only AgPF_6 was used in the NMR analysis, and as a weakly coordinating anion, PF_6^- should not compete to coordinate to the silver(I). However, the CD_3CN is a coordinating solvent and interacts with the silver(I), decreasing its positive charge and, consequently, decreasing the charge transfer from the nitrogen atoms of the ligands to the silver(I) metal centers, resulting in smaller ^{15}N NMR coordination shifts. A significant change (48%) in the ^{15}N NMR resonance has previously been reported for the *bis*(pyridine) silver(I)⁺ triflate complex upon solvent change from CDCl_3 to CD_3CN .^[41] However, this should not be the case with the iodine(I) complexes due to the 3c–4e halogen bond, which forms only linear, two-coordinate $[\text{N}—\text{I}—\text{N}]^+$ species.

To further confirm the formation of the iodine(I) complexes, extensive efforts were made to crystallize and analyze the solid-state structures of these complexes. To date, only a limited number of X-ray structures of iodine(I) complexes have been reported due to their inherent reactivity as halogenating and oxidizing reagents.^[23–25] The X-ray structures of ligands **3–4** and **6–7** (Figures S22, S26, S39, and S48), silver(I) complexes of all seven ligands, and the iodine(I) complexes of **1, 2, 4, and 5** (Figures S13, S15, S20, S28, S34, S35, S36, and S37) were successfully obtained. As seen in the above NMR analysis, the iodine(I) complexes for **3, 6, and 7** were found to be problematic with regards to solubilizing them, even in the most polar solvents, rendering meaningful crystallization attempts moot.

The silver(I) complexes (Figures S11, S17, S18, S23, S27, S30, S32, S33, S40, S42, S44, S49) demonstrated Ag–N bond lengths between 2.086(3) – 2.177(2) Å (listed in Table S2), which is well within the previously reported values for similar structures.^[30,33] Several silver(I) complexes were found to crystallize as dimers bonded through argentophilic closed-shell (d^{10} - d^{10}) interactions. The $\text{Ag}^+ \cdots \text{Ag}^+$ argentophilic interactions were determined to be between 3.02 – 3.34 Å (Table S2) for the argentophilic dimers, yet longer interactions were also observed for two complexes **[5-Ag-5]PF₆** ($d(\text{Ag}^+ \cdots \text{Ag}^+) = 3.81$ Å, Figure S31) and **[6-Ag-6]PF₆** ($d(\text{Ag}^+ \cdots \text{Ag}^+) = 3.61$ Å, Figure S41). Figure 3 depicts the single crystal X-ray structure of **[7-Ag-7]PF₆** with coordinating acetonitrile and the argentophilic interactions between two **[7-Ag-7]⁺** cations. The complex experiences a decisively short $\text{Ag}^+ \cdots \text{Ag}^+$ interaction of 3.018(2) Å, well below the van der Waals radii of two Ag atoms (3.44 Å).^[42] The strong $\text{Ag}^+ \cdots \text{Ag}^+$ interaction causes torsion and applies strain to the ligand, but due to the inherent flexibility of **7**, close ligand-assisted $\text{Ag}^+ \cdots \text{Ag}^+$ contact is possible, such as the perpendicular C–H $\cdots\pi$ (C37 to centroid = 3.6 Å) interactions.

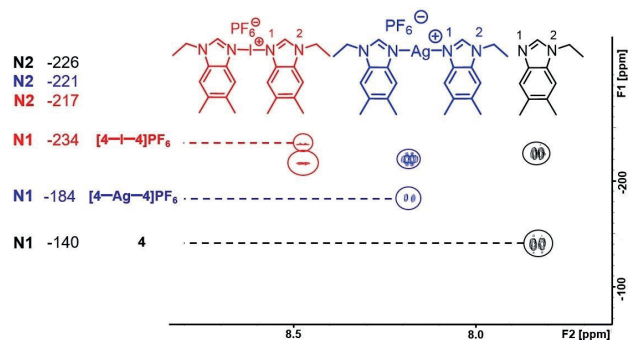


Figure 2. The comparison of the ^1H - ^{15}N HMBC correlation spectra of the ligand **4**, the silver(I) complex **[4-Ag-4]PF₆**, and the iodine(I) complex **[4-I-4]PF₆**. All values are in ppm and referenced to CD_3CN (^1H) or CD_3NO_2 (^{15}N) (500 MHz, 298 K).

Complex ^[a]	Ligand	[N-Ag-N] ⁺	[N-I-N] ⁺
[1-X-1]⁺	–138.9	–178.5	–232.0
	–238.3	–233.1	–228.5
[2-X-2]^[b]	–138.4	–180.7	–232.2
	–223.1	–218.2	–214.1
[3-X-3]^[b]	–138.0	–180.2	–
	–239.1	–235.0	–229.7
[4-X-4]⁺	–140.3	–184.2	–234.4
	–225.9	–220.6	–216.6
[5-X-5]^[c]	–70.1	–106.1	–181.9
[6-X-6]^[b]	–67.7	–124.8	–
	–251.9	–251.0	–

[a] With PF_6^- counter-anion. [b] Poor solubility of the iodine(I) complex. [c] Only N1.

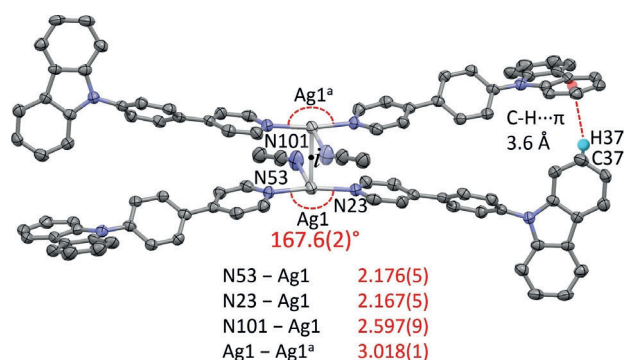


Figure 3. The X-ray structure of [7-Ag-7]PF₆, showing the argentophilic dimer observed in solid-state (counter-anions and hydrogen atoms omitted for clarity. Thermal displacement ellipsoids drawn at the 50% probability level; all lengths in Å). Symmetry operator: a = 1–x, 1–y, 1–z.

Silver(I) has a flexible coordination sphere and is able to accommodate multiple coordination geometries, which is also evident in these structures.^[43] In addition to argentophilic interactions, structures were commonly observed with solvates, especially when acetonitrile was used as the crystallization solvent. In the structure of [6-Ag-6]SbF₆ (Figure S44) and [7-Ag-7]PF₆ (Figure 3), the acetonitrile is bonded to the silver making it three or even four-coordinate (in case of Ag⁺...Ag⁺ interactions as well). Both the argentophilic interactions and the coordinating solvates affect the [N-Ag-N]⁺ bond angle varying it from 149.11(8)° to a symmetry enforced, perfect linear geometry of 180°.

The silver(I) complexes favor two types of packing; either a dimeric packing with argentophilic interactions or an alternating anion-ligand packing with slipped π - π interactions between the ligands. The positively charged silver(I) complex results, in both cases, in the anions closely interacting with the C–H of the five-membered ring (1–4) and the aromatic C–H motifs. These two types of packing are depicted in Figure 4. The interactions in the complex naturally vary depending on the ligand, anion, and solvent.

From the seven ligands investigated, iodine(I) complexes for four ligands were obtained in solid-state and all the [N-I-N]⁺ bond lengths and angles are listed in Table S2 as well as in Figure 5. In contrast to the silver(I) complexes with varying coordination angles, the iodine(I) structures have a strong preference toward linearity due to the highly directional nature of the I⁺ cation, with the largest deviation being observed for [1-I-1]PF₆ with 176.9(2)°, which is still less than the previously reported [N–I–N]⁺ bond angle of 175°.^[3,32] All N–I bond lengths were also found to be within the narrow range of 2.213(3)–2.263(3) Å, corresponding to the R_{XB} values of 0.63–0.64 shown in Table S3 ($R_{XB} = d_{XB}/(X_{vdW} + B_{vdW})$, where d_{XB} is the distance between the halogen atom and the electron donor, X_{vdW} is the van der Waals radii of the halogen atom and B_{vdW} is the van der Waals radii of the electron donor atom^[44]). These values indicate even stronger interactions than usually reported for 3c-4e halogen(I) complexes ($R_{XB} = 0.65$ – 0.69 , $d(N-I) = 2.23$ – 2.31 Å).^[12,31]

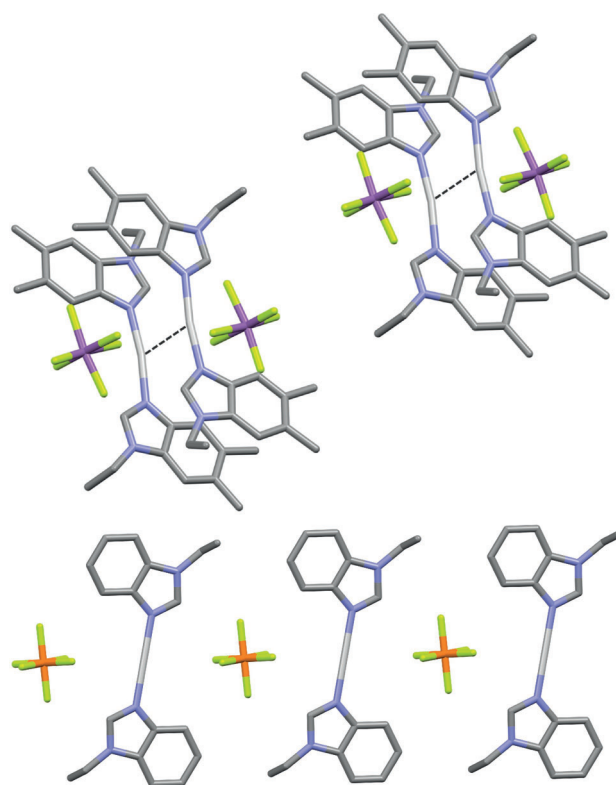


Figure 4. The packing of [4-Ag-4]SbF₆ as argentophilic dimers (top) and [2-Ag-2]PF₆ (bottom) as three monomers.

In contrast to the silver(I) complexes, the packing of the iodine(I) complexes always occurs in the same way (Figure 6) resembling the monomeric packing pattern of the silver(I) structures with slipped π - π interactions between the ligands. Whereas silver(I) complexes prefer anion-coordination and argentophilic interactions, the halogen(I) complexes do not possess the required empty orbitals for such an interaction.^[15] The anions in the iodine(I) complexes do not interact with the halogen(I) ions, and only affect the solubility of the species and the packing in the crystal structure.^[30] Even when packing asymmetrically in solid-state, anions do not induce any effect on the symmetry of the [N–I–N]⁺ bond.^[15] Short I⁺...I⁺ inter-complex distances in solid-state, reminiscent to the Ag⁺...Ag⁺ argentophilic interactions, are very rare.^[31,33] In the case of the iodine(I) complexes studied here, no short I⁺...I⁺ inter-complex distances were observed.

Due to the inherent reactivity of the iodine(I) ion, protonated side products are fairly common in the pursuit of iodine (I) complexes, and in this case, one protonated species [3-H]I of ligand 3 with iodide as a counter-anion was obtained (Figure S25). In addition, repeated attempts were made to crystallize [6-I-6]⁺ and [7-I-7]⁺, though with no success. The larger size of the ligand and low solubility of the Ag⁺ and I⁺ complexes play a critical role in the crystallization of these species. Due to the weak C–H and π - π interactions observed for ligand 7, crystals recovered from the crystallization of [7-I-7]PF₆,

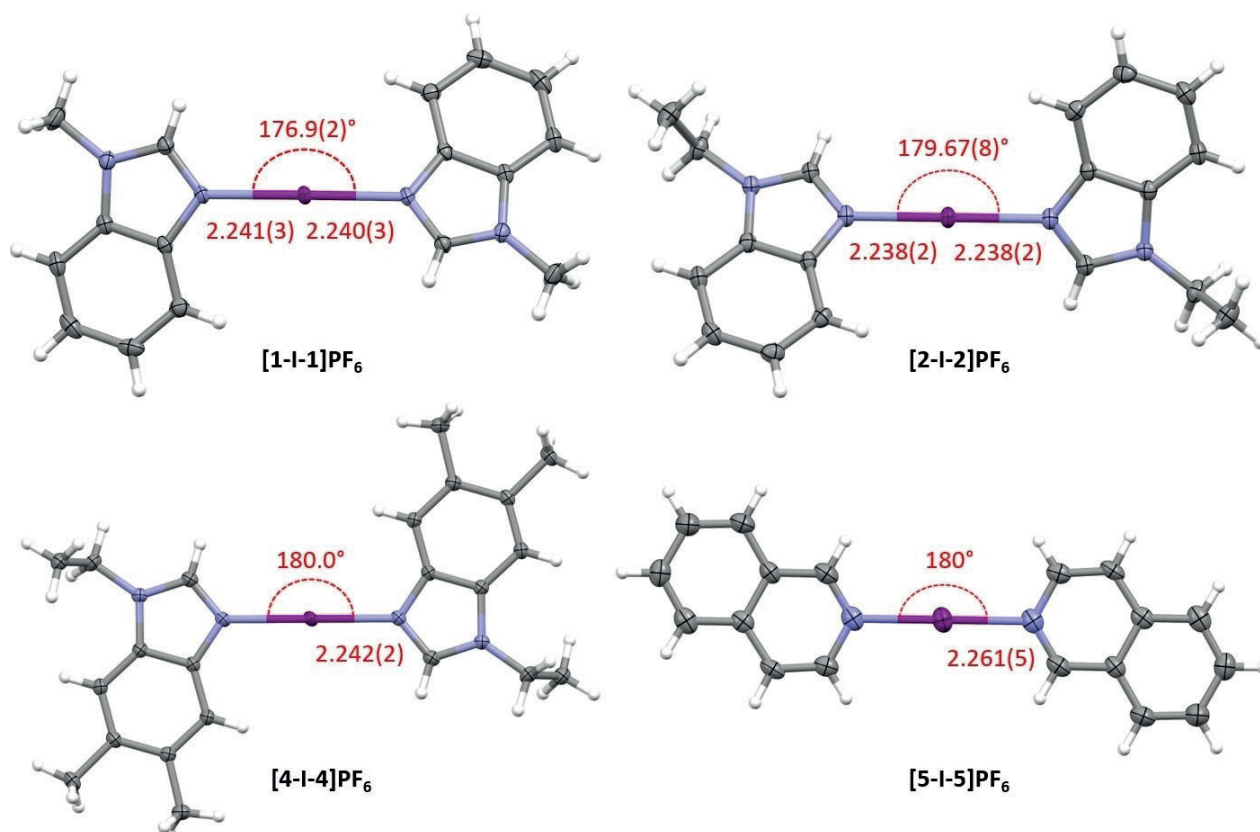


Figure 5. Single crystal X-ray structures of the determined halogen(I) complexes [1-I-1]PF₆, [2-I-2]PF₆, [4-I-4]PF₆, and [5-I-5]PF₆ (counter-anions omitted for clarity. Thermal displacement ellipsoids drawn at the 50% probability level; all lengths in Å).

were revealed to be the parent ligand itself (Figure S43). Additionally, in most cases with ligands **6** and **7**, acetonitrile was also found coordinating to the silver(I), making the N–Ag–N angles deviate from linearity (152.19(9)°).

An unusual case also arose whilst pursuing the solid-state structures, with the observation of an asymmetric [7-Ag-MeCN]PF₆ complex (Figure 7), where acetonitrile coordination to the Ag⁺ is retained despite the 2:1 stoichiometry. This rare asymmetric 2-coordinate silver(I) structure also suggests an enhanced nucleophilicity of the ligand **7**, or the existence of steric hindrance between the ligands in the close argentophilic dimer of the symmetric [7-Ag-7]⁺ (Figure 3) complex, making the asymmetric structure [7-Ag-MeCN]PF₆ isolable as a minor product.

The asymmetric [7-Ag-MeCN]PF₆ shows a slightly shorter bond length between the silver(I) and **7** compared to its symmetric counterpart (cf. 2.167(5) Å). The crystallization conditions could also affect whether asymmetric or symmetric complexes are formed. The symmetric complex was obtained from acetonitrile evaporation, whereas the asymmetric complex was obtained from an acetonitrile/dichloromethane mixture diffused with pentane at 277 K. The only similar linear two-coordinate N–Ag–CH₃CN complex was reported by Vögtle et al. more than 20 years ago.^[45]

Due to the difficulties in obtaining the iodine(I) complex from ligand **6**, an alternative approach was attempted to synthesize it. It has been previously reported that the addition of elemental iodine in excess, could lead to an I₂ adduct formation, which eventually undergoes heterolytic cleavage of the I₂ to form an iodine(I) complex with a I₃[−] counter-anion (due to a second molecule of I₂).^[34] This was also supported by the X-ray structure of [5-I-5]I₃ (Figures S37–38). Due to the consistency with other complexes' names, the I⁺ complex of ligand **5** is named as [5-I-5]I₃ (despite there being three elemental iodine solvates in the crystal lattice, viz. [5-I-5]I₃ · 3 I₂). For the [5-I-5]I₃ complex, though the normal synthesis route was used, the resulting iodine(I) complex crystallized more readily with I₃[−] as the counter-anion, rather than with PF₆[−]. However, whilst attempting to crystallize [6-I-6]I₃ in the presence of excess I₂, a neutral halogen-bonded complex **6**·I₂ was observed, where the I₂ is directly bonded to the ligand's nitrogen atom (Figure 8). For this complex, the N–I bond length was found to be similar (2.397(9)^[46] Å, R_{XB} = 0.68, Table S3) to other aromatic amine–I₂ complexes.^[46] Similarly the iodine I–I bond length was found to be 2.810(1) Å, which is much longer than that of free iodine (2.715 Å) in solid-state, and in-line to those previously reported for the analogous pyridine–I₂ halogen-bonded complexes.^[46]

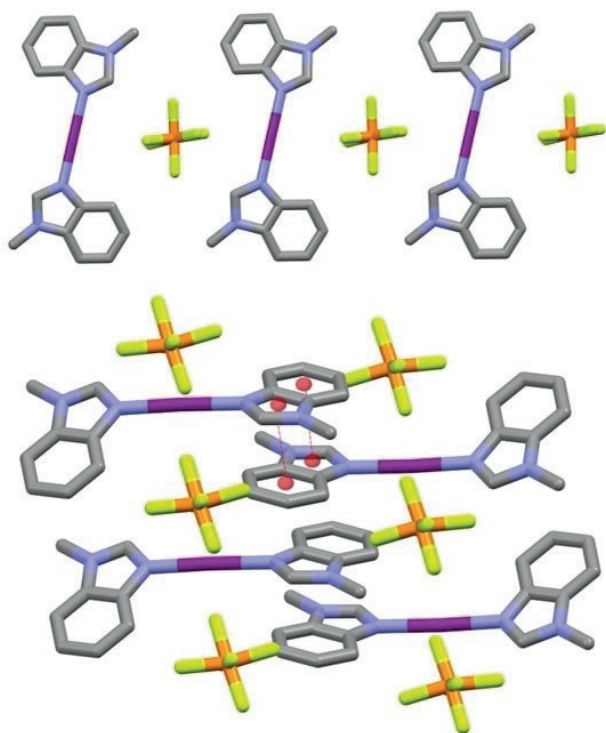


Figure 6. The packing of [1-I-1]PF₆ in solid-state. Intermolecular π - π (centroid-centroid) interactions highlighted in red.

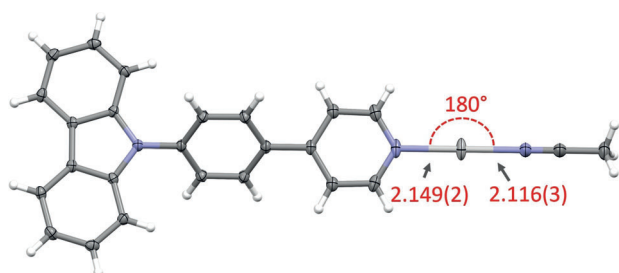


Figure 7. The asymmetric silver(I) structure of [7-Ag-MeCN]PF₆ (counter-anion omitted for clarity. Thermal displacement ellipsoids drawn at the 50% probability level; all lengths in Å).

In addition to structural studies the halogen-bonded complex **6-I**₂ was further studied with UV-Vis and fluorescence spectroscopy due to the fascinating photophysical properties ligand **6** has previously revealed upon protonation.^[47] In the protonation experiments of **6**,^[47] the protonation was found to decrease the energy of the placement of the pyridyl unit out of the plane making the molecular rotation more accessible, as well as change the lowest lying electronic transition, which resulted in quenching of the fluorescence. However, similar behavior with the halogen-bonded species was not observed. In contrast to the protonated species, an 8% increase in the integrated fluorescence intensity was observed (Figure S47),

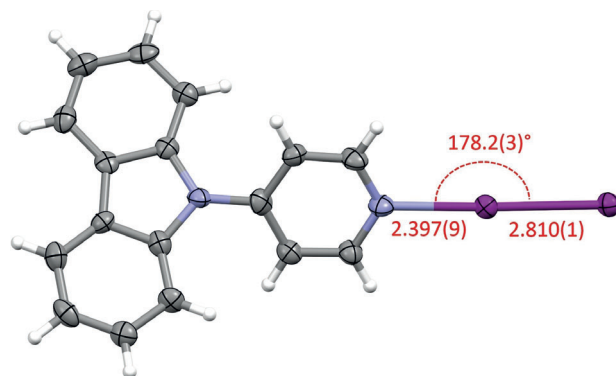


Figure 8. X-ray structure of the halogen-bonded complex **6-I**₂ (thermal displacement ellipsoids drawn at the 50% probability level; all lengths in Å).

which is most likely a result of halogen-bond assisted intramolecular charge-transfer.^[48]

Conclusion

Herein, we have prepared symmetric 2-coordinate silver(I) complexes for ligands 1–7, along with an asymmetric [7-Ag-MeCN]PF₆ acetonitrile-adduct complex. Some of the ligands manifested short argentophilic interactions and were observed as dimeric complexes in the solid-state. The silver(I) complexes served as precursors to the target iodine(I) complexes. The formation of the complexes was confirmed via ¹H and ¹H-¹⁵N HMBC NMR analyses, which showed 0.36–1.06 ppm changes in the ¹H NMR chemical shifts, and 94–111 ppm changes in the ¹⁵N NMR chemical shifts from the free ligand to an iodine(I) complex. The conversion from the ligand to the silver (I) and iodine(I) complexes lowers the solubility of the species, even in the most polar solvents such as DMSO. The crystallization process, being highly dependent on the crystallization conditions such as solvent and solubility, was unsuccessful for the few low-solubility complexes, and therefore the identity of some of the iodine(I) complexes was only confirmed in solution. However, further confirmation of the identity of the iodine(I) complexes was provided by single crystal X-ray structures for four of the ligands. The iodine(I) complexes experienced extremely strong halogen bonds with *R*_{XB} values of 0.63–0.64, even surpassing most of the previously reported 3c–4e bonded [N–I–N]⁺ complexes. The work herein has extensively studied iodine(I) complexes of benzoimidazole and pyridylcarbazole derivatives, and despite limited solubility, demonstrated each of the ligands being capable of this interaction. The results reported here, within this fast-growing field of research, provide valuable information for the development of XB-based materials for future applications.

Experimental Section

All reagents and solvents obtained from commercial suppliers were used without further purification. Synthesis of all prepared compounds is described in the Supporting Information. For NMR assignments, ^1H and ^1H - ^{15}N HMBC NMR spectra were recorded using either Bruker 300 Avance or Bruker Avance III 500 MHz spectrometer at 303 K. Chemical shifts are reported on the δ scale in ppm using the residual solvent signal as internal standard (CDCl_3 , δH 7.26; CD_2Cl_2 , δH 5.32; CD_3CN , δH 1.94; $(\text{CD}_3)_2\text{CO}$, δH 2.05; $\text{DMSO-}d_6$, δH 2.50). For ^{15}N NMR, CD_3NO_2 is used as an external reference. For ^1H NMR spectroscopy, each resonance was assigned according to the following conventions: chemical shift (δ) measured in ppm, observed multiplicity, number of hydrogens, observed coupling constant (J Hz), and assignment. Multiplicities are denoted as s (singlet), d (doublet), t (triplet), q (quartet), m (multiplet), and br (broad).

The UV-Vis and fluorescence studies of 6-I_2 were performed at room temperature. Absorption spectra were collected using a Varian Cary 100, 300 Series II Series UV-Visible Spectrophotometer, and fluorescence spectra were collected using a Varian Cary Eclipse Fluorescence Spectrophotometer. The measurements were taken in a 1 cm quartz cuvette and the excitation and the emission band passes were set to 2.5 nm and 2.5 nm, respectively.

The single crystal X-ray crystallographic experimental and refinement details for all complexes are given in the Supporting Information. Deposition Numbers 2106003 (for [1-Ag-1]PF₆), 2106004 (for [1-I-1]PF₆), 2106005 (for [1-I-1]PF₆ \cdot >2), 2106006 (for [2-Ag-2]PF₆), 2106007 (for [2-Ag-2]PF₆ \cdot >2), 2106008 (for [2-I-2]PF₆), 2106009 (for 3), 2106010 (for [3-Ag-3]PF₆), 2106011 (for [3-H]I), 2106012 (for 4), 2106013 (for [4-Ag-4]SbF₆), 2106014 (for [4-I-4]PF₆), 2106015 (for [5-Ag-5]PF₆), 2106358 (for [5-Ag-5]BF₄), 2106359 (for [5-Ag-5]OTf), 2106360 (for [5-I-5]PF₆), 2106361 (for [5-I-5]BF₄), 2106362 (for [5-I-5]OTf), 2106016 (for [5-I-5]I₃), 2080281 (for 6), 2106017 (for [6-Ag-6]PF₆), 2106018 (for [6-Ag-6]BF₄), 2106019 (for [6-Ag-6]SbF₆), 2106020 (for 6-I_2), 2080282 (for 7), 2106021 (for [7-Ag-7]PF₆), and 2106022 (for [7-Ag-MeCN]PF₆) contain the supplementary crystallographic data. These data can be obtained free of charge by The Cambridge Crystallographic Data Centre and Fachinformationszentrum Karlsruhe Access Structures service.

Acknowledgements

The authors gratefully acknowledge the Academy of Finland (K.R. grant no. 317259) and the University of Jyväskylä, Finland for financial support. Dr. Jas S. Ward (University of Jyväskylä) is thanked for fruitful discussions.

Conflict of Interest

The authors declare no conflict of interest.

Keywords: halogen(I) · halogen bonds · NMR spectroscopy · supramolecular chemistry · X-ray crystallography

[1] R. S. Mulliken, Spectroscopy, Molecular Orbitals, and Chemical Bonding. The Nobel Prize in Chemistry 1966. NobelPrize.org. Nobel Prize Outreach AB 2021. Thu. 16 Sep 2021. <https://www.nobelprize.org/prizes/chemistry/1966/summary/>.

- [2] The Nobel Prize in Chemistry 1969. NobelPrize.org. Nobel Prize Outreach AB 2021. Wed. 15 Sep 2021. <https://www.nobelprize.org/prizes/chemistry/1969/summary/>.
- [3] G. Cavallo, P. Metrangolo, R. Milani, T. Pilati, A. Priimagi, G. Resnati, G. Terraneo, *Chem. Rev.* **2016**, *116*, 2478–2601.
- [4] P. Politzer, P. Lane, M. C. Concha, Y. Ma, J. S. Murray, *J. Mol. Model.* **2007**, *13*, 305–311.
- [5] G. R. Desiraju, P. Shing Ho, L. Kloo, A. C. Legon, R. Marquardt, P. Metrangolo, P. Politzer, G. Resnati, K. Rissanen, *Pure Appl. Chem.* **2013**, *85*, 1711–1713.
- [6] R. S. Mulliken, *J. Am. Chem. Soc.* **1950**, *72*, 600–608.
- [7] R. Sedlak, M. H. Kolář, P. Hobza, *J. Chem. Theory Comput.* **2015**, *11*, 4727–4732.
- [8] L. C. Gilday, S. W. Robinson, T. A. Barendt, M. J. Langton, B. R. Mullaney, P. D. Beer, *Chem. Rev.* **2015**, *115*, 7118–7195.
- [9] H. Wang, W. Wang, W. J. Jin, *Chem. Rev.* **2016**, *116*, 5072–5104.
- [10] M. H. Kolář, P. Hobza, *Chem. Rev.* **2016**, *116*, 5155–5187.
- [11] K. Rissanen, *CrystEngComm* **2008**, *10*, 1107–1113.
- [12] L. Turunen, M. Erdélyi, *Chem. Soc. Rev.* **2020**, *49*, 2688–2700.
- [13] A. C. Reiersølmoen, S. Battaglia, S. Øien-Ødegaard, A. K. Gupta, A. Fiksdahl, R. Lindh, M. Erdélyi, *Chem. Sci.* **2020**, *11*, 7979–7990.
- [14] A. C. C. Carlsson, M. Uhrbom, A. Karim, U. Brath, J. Gräfenstein, M. Erdélyi, *CrystEngComm* **2013**, *15*, 3087–3092.
- [15] S. Yu, P. Kumar, J. S. Ward, A. Frontera, K. Rissanen, *Chem.* **2021**, *7*, 948–958.
- [16] J. S. Ward, A. Frontera, K. Rissanen, *Dalton Trans.* **2021**, *50*, 8297–8301.
- [17] S. B. Hakkert, M. Erdélyi, *J. Phys. Org. Chem.* **2015**, *28*, 226–233.
- [18] A. Karim, M. Reitti, A. C. C. Carlsson, J. Gräfenstein, M. Erdélyi, *Chem. Sci.* **2014**, *5*, 3226–3233.
- [19] J. Barluenga, F. González-Bobes, M. C. Murguía, S. R. Ananthoju, J. M. González, *Chem. Eur. J.* **2004**, *10*, 4206–4213.
- [20] J. A. Creighton, I. Haque, J. L. Wood, *Chem. Commun.* **1966**, No. 8, 229.
- [21] J. A. Creighton, I. Haque, J. L. Wood, *Chem. Commun.* **1966**, No. 23, 892.
- [22] I. Haque, J. L. Wood, *J. Mol. Struct.* **1968**, *2*, 217–238.
- [23] J. Barluenga, J. M. González, M. A. Garcia-Martin, P. J. Campos, G. Asensio, *J. Chem. Soc. Chem. Commun.* **1992**, *4*, 1016–1017.
- [24] J. Ezquerro, C. Pedregal, C. Lamas, J. Barluenga, M. Pérez, M. A. Garcia-Martin, J. M. González, *J. Org. Chem.* **1996**, *61*, 5804–5812.
- [25] G. Espuña, G. Arsequell, G. Valencia, J. Barluenga, M. Pérez, J. M. González, *Chem. Commun.* **2000**, 1307–1308.
- [26] T. Okitsu, S. Yumitate, K. Sato, Y. In, A. Wada, *Chem. Eur. J.* **2013**, *19*, 4992–4996.
- [27] Y. Kim, E. J. McKinley, K. E. Christensen, N. H. Rees, A. L. Thompson, *Cryst. Growth Des.* **2014**, *14*, 6294–6301.
- [28] L. C. F. Morgan, Y. Kim, J. N. Blandy, C. A. Murray, K. E. Christensen, A. L. Thompson, *Chem. Commun.* **2018**, *54*, 9849–9852.
- [29] E. Kukkonen, H. Malinen, M. Haukka, J. Konu, *Cryst. Growth Des.* **2019**, *19*, 2434–2445.
- [30] M. Bedin, A. Karim, M. Reitti, A. C. C. Carlsson, F. Topić, M. Cetina, F. Pan, V. Havel, F. Al-Ameri, V. Sindelar, K. Rissanen, J. Gräfenstein, M. Erdélyi, *Chem. Sci.* **2015**, *6*, 3746–3756.
- [31] A. Vanderkooy, A. K. Gupta, T. Földes, S. Lindblad, A. Orthaber, I. Pápai, M. Erdélyi, *Angew. Chem. Int. Ed.* **2019**, *58*, 9012–9016; *Angew. Chem.* **2019**, *131*, 9110–9114.
- [32] A. C. C. Carlsson, K. Mehmeti, M. Uhrbom, A. Karim, M. Bedin, R. Puttreddy, R. Kleinmaier, A. A. Neverov, B. Nekouishahraki, J. Gräfenstein, K. Rissanen, M. Erdélyi, *J. Am. Chem. Soc.* **2016**, *138*, 9853–9863.
- [33] J. S. Ward, G. Fiorini, A. Frontera, K. Rissanen, *Chem. Commun.* **2020**, *56*, 8428–8431.
- [34] O. Hassel, H. Hope, *Acta Chem. Scand.* **1961**, *15*, 407–416.
- [35] R. C. Nishad, A. Rit, *Chem. Eur. J.* **2021**, *27*, 594–599.
- [36] W. J. Yoo, T. Tsukamoto, S. Kobayashi, *Org. Lett.* **2015**, *17*, 3640–3642.
- [37] K. Leduskrasts, A. Kinens, E. Suna, *Chem. Commun.* **2019**, *55*, 12663–12666.
- [38] A. C. C. Carlsson, J. Gräfenstein, J. L. Laurila, J. Bergquist, M. Erdélyi, *Chem. Commun.* **2012**, *48*, 1458–1460.
- [39] S. B. Hakkert, J. Gräfenstein, M. Erdélyi, *Faraday Discuss.* **2017**, *203*, 333–346.
- [40] D. von der Heiden, K. Rissanen, M. Erdélyi, *Chem. Commun.* **2020**, *56*, 14431–14434.
- [41] R. Kleinmaier, S. Arenz, A. Karim, A. C. C. Carlsson, M. Erdélyi, *Magn. Reson. Chem.* **2013**, *51*, 46–53.
- [42] H. Schmidbaur, A. Schier, *Angew. Chem. Int. Ed.* **2015**, *54*, 746–784; *Angew. Chem.* **2015**, *127*, 756–797.

- [43] E. M. Njogu, B. Omondi, V. O. Nyamori, *J. Coord. Chem.* **2015**, *68*, 3389–3431.
- [44] A. Bondi, *J. Phys. Chem.* **1964**, *68*, 441–451.
- [45] H. Stephan, T. Krüger-Rambusch, R. Gloe, W. Hasse, B. Ahlers, K. Cammann, K. Rissanen, G. Brodesser, F. Vögtle, *Chem. Eur. J.* **1998**, *4*, 434–440.
- [46] M. Tuikka, M. Haukka, *Acta Crystallogr.* **2015**, *71*, o463.
- [47] E. Taipale, N. A. Durandin, J. Salunke, N. R. Candeias, T.-P. Ruoko, J. S. Ward, A. Priimagi, K. Rissanen, *Mater. Adv.* **2021**, Submitted.
- [48] J. K. Salunke, N. A. Durandin, T. P. Ruoko, N. R. Candeias, P. Vivo, E. Vuorimaa-Laukkanen, T. Laaksonen, A. Priimagi, *Sci. Rep.* **2018**, *8*, 1–8.

Manuscript received: August 30, 2021
Accepted manuscript online: October 4, 2021
Version of record online: October 15, 2021



IV

DIMERIC IODINE(I) AND SILVER(I) CAPSULES CAGES FROM TRIPODAL N-DONOR LIGANDS

by

E. Taipale, J. S. Ward, G. Fiorini, D. L. Stares, C. A. Schalley
& K. Rissanen 2022

Inorg. Chem. Front. 2022

Submitted manuscript

Dimeric Iodine(I) and Silver(I) Cages from Tripodal *N*-donor Ligands

Essi Taipale,^a Jas S. Ward,^{a*} Giorgia Fiorini,^a Daniel L. Stares,^b Christoph A. Schalley,^b and Kari Rissanen^{a*}

Received 00th January 20xx,
Accepted 00th January 20xx

DOI: 10.1039/x0xx00000x

The directionality of the [N–I–N]⁺ halogen bond makes iodine(I) ions impeccable tools in the design and construction of [N–I–N]⁺ halogen-bonded assemblies. The synthesis of dimeric iodine(I) cages with imidazole-derived *N*-donor tripodal ligands is described, as well as their corresponding silver(I) precursors. The addition of elemental iodine to the parent two-coordinate Ag(I) complexes produces iodine(I) complexes with three-center four-electron (3c-4e) [N–I–N]⁺ bonds. Complex formation *via* this cation exchange was confirmed by ¹H and ¹H-¹⁵N HMBC NMR studies in solution, and additionally by electrospray ionisation and ion mobility mass spectrometry analysis (MS) in the gas phase. The structural analysis of the single crystal X-ray structures of 11 silver(I) cages and the computationally modelled iodine(I) cages, along with MS analysis, revealed structural similarities between the two different capsular assemblies. In addition to strong electrostatic interactions, C–H⋯F hydrogen bonds were determined to have a directing effect on the silver(I) cage formation and binding of suitably sized anions into the cavities in the solid state.

Introduction

The term *clathrate* was first devised by H. M. Powell in 1948 when the first definition of a solid-state cage-like supramolecular structure came to life. According to Powell, a clathrate was a kind of a solid-state inclusion compound “*in which two or more components are associated without an ordinary chemical union, but through the complete enclosure of one set of molecules in a suitable structure formed by another*”.¹ These structures are generally further divided into two categories: the first are clathrates, viz lattice inclusion compounds, in which guests are trapped into a host matrix, generally speaking, a crystal lattice; the second are molecular host-guest inclusion compounds, in which the guest is trapped inside a larger, often macro- or multimacrocyclic, host molecule or a self-assembled concave entity comprising multiple components, *e.g.*, molecular capsules and cages.¹

Molecular hosts and capsular assemblies have attracted much interest since Rebek's first hydrogen-bonded supramolecular capsule in 1993.² The possibility of encapsulating various guests in these cages has yielded a plethora of applications,³ ranging from biomedical applications and selective encapsulation,^{4,5} to stabilisation of reactive compounds using supramolecular capsular entities and catalysis in confined spaces.^{6,7} To date, various host-guest capsular

assemblies have been reported using molecules such as resorcin[4]arenes,^{8–11} calix[4]-arenes,^{12–14} and pyridine[4]arenes.^{15,16} The self-assembled capsular assemblies comprise two or more suitable preorganised molecules spontaneously forming capsular entities with either metal coordination,^{17–21} or hydrogen bonding.^{22,23}

Ever since the 1990s, halogen bonding has developed into a true competitor for hydrogen bonding and other non-covalent interactions to the point that, to date, it is one of the most studied interactions in supramolecular chemistry.^{24–27} Halogen bonding was only recently defined by IUPAC as a net attractive interaction between the positive regions of the electrostatic potential associated with a halogen atom and a Lewis base.²⁸ Perhaps the controversial nature of the halogen bond led to its late definition, however, halogen bonding has been deftly utilised in the formation of supramolecular assemblies, amongst other non-covalent interactions, for its strength, tunability, and directionality, which provides the necessary tools for sufficient control of the self-assembly processes. Despite its utility, the use of halogen bonding in the formation of discrete molecular capsules is rare, with only a few examples previously reported using the classical halogen bond.^{29–31}

More recently, halogen bonding has also received interest in the form of halogen(I), especially iodine(I), cations.^{32–34} The halogen(I) cations, also known as halonium ions (X⁺), can be considered as extremely polarised halogen atoms which are capable of forming symmetric three-center four-electron (3c-4e) [L–X–L]⁺ bonds and constructing a halogen(I) complex by simultaneously interacting with two Lewis bases (L; commonly aromatic amines).^{35–38} The [N–X–N]⁺ 3e-4e bonds are found to be among the strongest halogen bonds, which in addition to their high directionality and robust nature, has made them an

^a University of Jyväskylä, Department of Chemistry, P.O. Box 35, Surfontie 9B, 40014 Jyväskylä (Finland)

^b Institut für Chemie und Biochemie, Organische Chemie, Freie Universität Berlin, Arnimallee 20, 14195 Berlin, Germany

Electronic Supplementary Information (ESI) available: [details of any supplementary information available should be included here]. See DOI: 10.1039/x0xx00000x

interesting supramolecular synthon in modern-day crystal engineering.

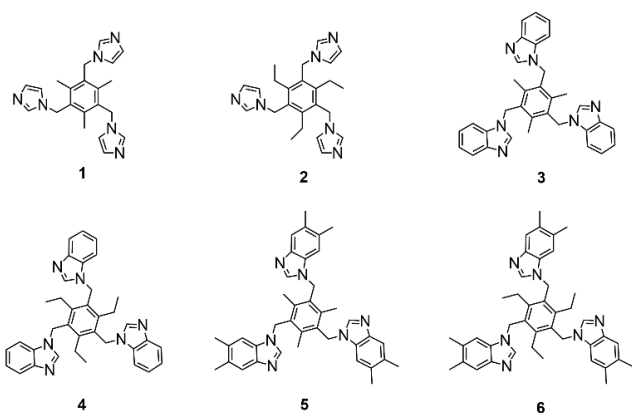
Iodine(I) ions are commonly used in organic chemistry as halogenating agents^{39–42} and their inherent reactivity makes them harder to isolate and structurally characterise. Recently, a number of heteroleptic or unconventional iodine(I) complexes have been prepared and characterised, mainly in the solid state.^{37,38,43–48} So far, only a few supramolecular capsular or macrocyclic⁴⁹ assemblies incorporating $[N-I-N]^+$ halogen bonds have been reported,^{50–53} which are obtained using the analogous silver(I) metallocages as the starting point for the iodine(I) cages, obtained via the $[N-Ag-N]^+$ to $[N-I-N]^+$ cation exchange reaction.⁵⁴

Herein, we report the solid-state structures of 11 parent silver(I) tripodal metallocages, and a comprehensive theoretical, gas, and solution-state study confirming the formation of iodine(I) $[N-I-N]^+$ cages. This report serves as further proof of the indisputable importance of halogen(I) ions as supramolecular synthons, and not just in simple monodentate ligand-complexes, but also in more sophisticated capsular assemblies.

Results and Discussion

Synthesis of the silver(I) and iodine(I) cages

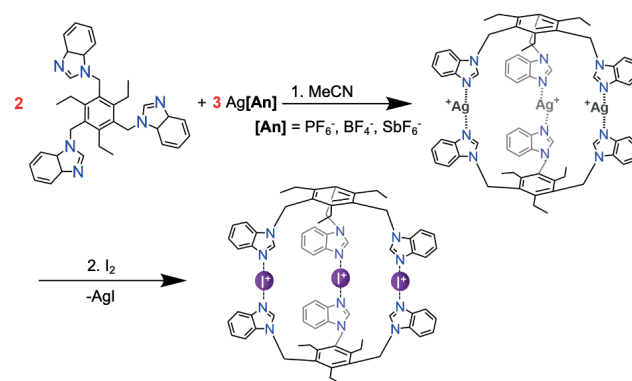
The imidazole- and benzoimidazole-based *N*-donor tripodal ligands **1** - **6** with a trialkylbenzene backbone were chosen for the capsular assembly (Scheme 1).



Scheme 1 The structures of *N*-donor tripodal ligands **1** - **6** used in the formation of the iodine(I) cages.

Ligands **1** - **6** were straightforwardly synthesised, with only **6** not being previously described in the literature. Imidazole, benzoimidazole, or dimethyl-benzoimidazole moieties are attached to the core benzene ring *via* methylene-linkers, making the ligands flexible and large enough to accommodate guests inside. The ligands must be able to first bind silver(I), and then iodine(I), cations leading to two distinct complexes, which in many cases prefer slightly different conformations with dissimilar bond lengths and angles. The syntheses of the ligands are straightforward and mostly follow literature procedures, with a few adaptations stated in the Supporting Information.⁵⁵

The most common route for iodine(I) complex formation is through the $[N-Ag-N]^+ \rightarrow [N-I-N]^+$ cation exchange reaction.⁵⁴ All cage reactions were performed in either acetonitrile or DMSO dictated by the lower solubility of some of the complexes. In the first step, presented in Scheme 2, two equivalents of ligand are mixed with three equivalents of a silver(I) salt (here $AgPF_6$, $AgBF_4$, or $AgSbF_6$). Many different weakly coordinating anions can be used, as it has been shown that the counteranions do not influence the linear centrosymmetric geometry of the $[N-I-N]^+$ halogen bond neither in solution nor in solid state.⁵⁶ In the second step, elemental iodine (I_2) is added to the parent silver(I) cage solution and stirred for an hour. Due to the more complex structure of the cages the reaction requires more time for completion than for the previously reported small-ligand iodine(I) complexes.⁴⁵ Upon completion of the reaction, the silver iodide (AgI) precipitates from the solution leaving the cationic tris-iodine(I) cage with the three anions in the solution.



Scheme 2 The synthesis of the iodine(I) cage of tripodal ligand **4** through its analogous silver(I) metallocage.

Crystallography of the silver(I) cages

The X-ray structures of ligands **1** - **5** have been previously reported,^{21,57–60} as well as the $[1-Ag-1]X$ cages with various counter-anions.^{17,20,61,62} In addition, cages $[3-Ag-3]BF_4$ ¹⁸ and $[4-Ag-4]BF_4$ ²¹ have been X-ray structurally characterised. In total, 11 single crystal X-ray structures of the analogous silver(I) cages were determined (Figures S1-S11), two of them polymorphs to previously reported structures.^{17,20} Unlike the halogen(I) 3c-4e bonds, the $[N-Ag-N]^+$ environment is easily distorted by the solvent or anion coordination to the silver(I) cations and angles of as small as 149° have previously been reported.⁴⁴ Further demonstrating this, the silver(I) cages were determined to have varying N-Ag bond lengths from 2.068(12) Å to 2.170(7) Å and N-Ag-N angles ranging from $163.1(2)^\circ$ to $180.0(5)^\circ$. These bond lengths are similar to previously observed ones with smaller monodentate versions of these ligands.⁴⁵ However, in the silver (I) cage formation the N-Ag-N angles are more linear when compared to the simple mononuclear complexes where the anion to silver(I) cation interactions can cause distortion from linearity.⁴⁵

The cages were designed to encapsulate small guests inside the cavities of the cages. In nine out of 11 cases, the electron

density map of the X-ray crystallographic analysis indicated that one of the counterions was positioned inside the cages. However in the case of **[1-Ag-1]SbF₆** and **[3-Ag-3]SbF₆** the electron density inside the cavity was diffuse, indicating a heavily disordered SbF₆ anion, and due to this they could not be modelled adequately, and were accounted for using SQUEEZE in the final model.⁶³ Figure 1 depicts, as an example, the encapsulation of a hexafluoroantimonate(V) anion in **[6-Ag-6]SbF₆** as a result of the C–H⋯anion and cation⋯anion interactions between the ligand, the Ag(I) cations and the SbF₆ anion. Moreover, the complexes observed in the solid state generally encapsulate one anion leaving the two remaining anions outside the cage.

The anion interactions inside the cage were estimated by determining the shortest distances between the anionic and cationic species for structures **[3-Ag-3]BF₄** and **[3-Ag-3]PF₆**, **[5-Ag-5]BF₄** and **[5-Ag-5]PF₆**, and also for **[6-Ag-6]PF₆** and **[6-Ag-6]SbF₆**, in which the anion resides inside the cage cavity.

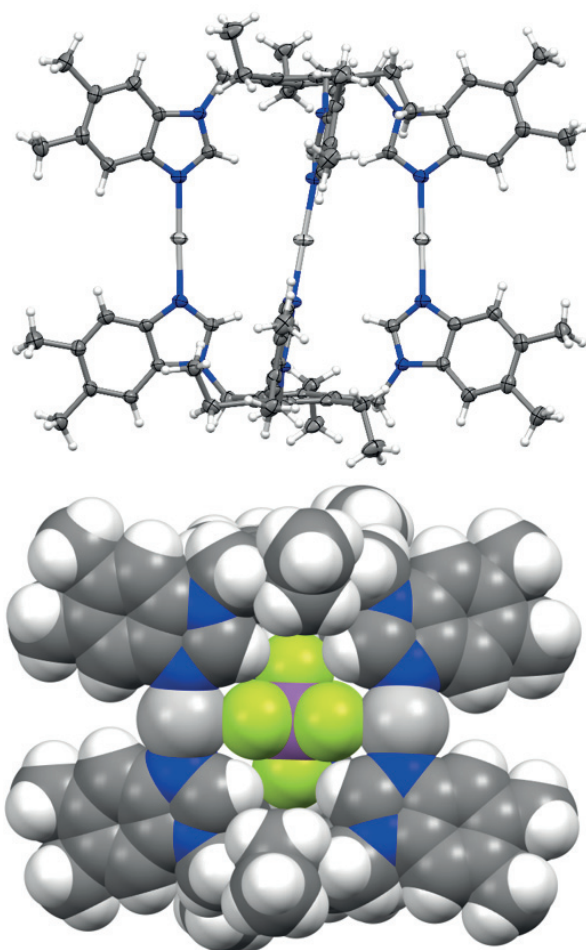


Figure 1 The thermal ellipsoid (top) and spacefill (bottom) representations of the X-ray crystal structure of **[6-Ag-6]SbF₆**. Solvents and anions omitted for clarity except for the encapsulated SbPF₆ anion in the bottom image. Thermal displacement ellipsoids are drawn at the 50% probability level. The N–Ag–N bond lengths and angles were determined to be between 2.091(4) – 2.095(4) Å and 172.3(2) – 173.0(2)°.

The shortest silver(I) to fluorine (Ag⋯F) contact distances were found to be between 2.66(1) Å – 2.802(9) Å, whereas the C–H⋯F hydrogen bonds were found to vary between 2.33 Å – 2.66 Å. All these C–H⋯F(anion) hydrogen-bond distances are shorter than the sum of the van der Waals radii of Ag, F and H atoms (Ag⋯F = 3.19 Å, F⋯H = 2.67 Å). However, for cages with the shortest Ag⋯F contacts, the hydrogen-bond distances (C–H⋯F) were found to be the longest, indicating that these distances rely heavily on the orientation of the anion inside the cage cavity.

The anion-to-cage interactions were further studied with Hirshfeld surface analysis (Figures S12–S17) using CrystalExplorer.^{64,65} In each case, large bright red spots can be observed on the Hirshfeld surface of the anions in the regions where the fluorines are in close contact with the silver(I) cations confirming the interactions to be shorter than the van der Waals radii. Slightly smaller, though still fairly bright red spots can also be seen for the C–H⋯F interactions. The 2D fingerprint plots of the Hirshfeld surface analysis provide information on the unique crystal packing in each case, at the same time easily revealing similarities between the structures. The fingerprint plot depicts the relationship of the distance to the nearest atom center interior to the surface (d_i) and to the exterior to the surface (d_e).⁶⁴ The fingerprint plots (Figures S12–S17) display the Ag⋯F and C–H⋯F interactions as a pair of spikes at the bottom-left part of the plot. The percentage contributions to the close intermolecular contacts can also be determined from the 2D plots. For all cages, the contribution of the Ag⋯F contacts was determined to be between 9 – 17 % (largest for **[5-Ag-5]BF₄**), whereas the C–H⋯F hydrogen bonds contributed 82 – 91% to the overall interactions. The electrostatic interactions are generally stronger than hydrogen bonding, and in here, they act in unison. Therefore, even though the Hirshfeld surface depicts Ag⋯F contacts to be the closest, the hydrogen bonds most certainly play a role in the stabilisation of the anion. In some cases, a small percentage (< 4%) of other interactions (F⋯N and F⋯C) were observed to contribute to the anion binding. The results from the Hirshfeld surface analysis indicate a multitude of stabilising interactions directed toward the anion. For example, Figure 2 depicts the X-ray crystal structure of **[6-Ag-6]SbF₆** with the calculated Hirshfeld surface for the SbF₆ anion inside the cage, where the punctures in the surface display strong cation-anion (Ag⁺⋯F₆Sb⁻) interactions. Additionally, the strong interactions are supported by the non-disordered nature of the SbF₆ anion with well-defined thermal movement inside the cage due to the supramolecular interactions.^{66,67}

Characterisation of the iodine(I) cages

Despite numerous silver(I) cages, to date, only the solid-state structure of dimeric [N–I–N]⁺ halogen-bonded cage made from **1** has been reported.⁵³ The nucleophilic nature of the iodine(I)³⁸ cation renders the interactions with anions very weak, and the inability to get diffraction quality single crystals of the iodine(I) cages in this study highlights the challenge in obtaining solid-state crystal structures of larger [N–I–N]⁺ halogen(I) assemblies with multiple 3c–4e bonds.^{50,51} Unfortunately, also in this study,

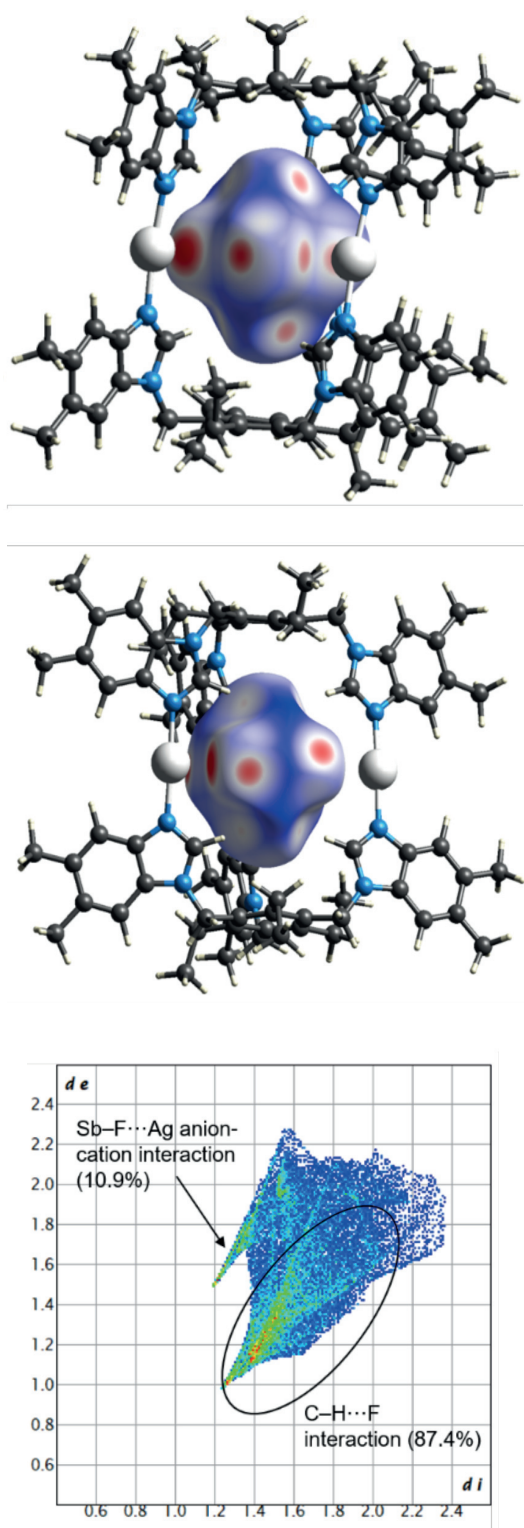


Figure 2 Full fingerprint regions of the hexafluoroantimonate anion in the complex $[6\text{-Ag-6}]\text{SbF}_6$ and two views of the intermolecular contacts to the Hirshfeld surface of the anion. Other interactions contributing to the anion binding: $\text{Sb-F}\cdots\text{C}$ (1.7%). In the fingerprint plot, d_i represents the closest internal distance from a given point on the Hirshfeld surface, and d_e is the closest external contact (in Å).

the crystallisation of the $[\text{N-I-N}]^+$ cages proved to be unsuccessful. Therefore, the iodine(I) cages were modelled with fixed N-I bond lengths of 2.25 Å and 180° angles for the most accurate description based on the known coordination geometry of the $[\text{N-I-N}]^+$ halogen bond (Figure 3 and Figures S18-S23).^{56,68,69} The resulting calculated iodine(I) cage structures are very similar to the analogous silver(I) crystal structures (see below discussion and Figure S10), apart from the slight distortion of the silver(I) cages in the solid state due to packing effects.

The cage composition was further confirmed in the gas phase with electrospray ionisation mass spectrometry (ESI-MS) and ion mobility mass spectrometry (IM-MS) analysis^{51,70} (Figures S24-S41). For ligand **4**, the formation of the cages was verified by the detection of the ions $[\text{4}_2\text{Ag}_3+\text{PF}_6]^{2+}$ and $[\text{4}_2\text{I}_3+\text{PF}_6]^{2+}$ at m/z values of 787 and 815, respectively. Additionally, the cages were observed with other anions in the gas phase, such as I^- and PF_2O_2^- . In ion mobility mass spectrometric experiments, the silver(I) and iodine(I) cages appear with very similar, narrow-width arrival time distributions confirming that the overall cage structures have not changed during the Ag(I)-to-I(I) ion exchange reactions. The IM-MS provided evidence of the cages being close in their sizes, though the iodine(I) cages are slightly bigger than the corresponding silver(I) cages. All silver(I) and iodine(I) cages depicted a narrow peak width in the arrival time distribution indicating a discrete, well-defined structure. Also, the iodine(I) and silver(I) cages show closely related fragmentation patterns in collision-induced dissociation (CID) experiments (Figures S42-S43). The dissociation of the mass-selected doubly charged $[\text{L}_2\text{Ag}_3\text{PF}_6]^{2+}$ and $[\text{L}_2\text{I}_3\text{PF}_6]^{2+}$ ions leads to a singly charged $[\text{LAG}]^+$ and $[\text{LI}]^+$ ions, respectively. The corresponding singly charged $[\text{LAG}_2\text{PF}_6]^+$ and $[\text{LI}_2\text{PF}_6]^+$ fragments are, however, not observed, which indicates a subsequent, rapid loss of AgPF_6 or IPF_6 ion pairs leading again to a second $[\text{LAG}]^+$ and $[\text{LI}]^+$ fragment, respectively. The fact that these ion pair losses do not occur similarly from the parent ions directly is in agreement with an

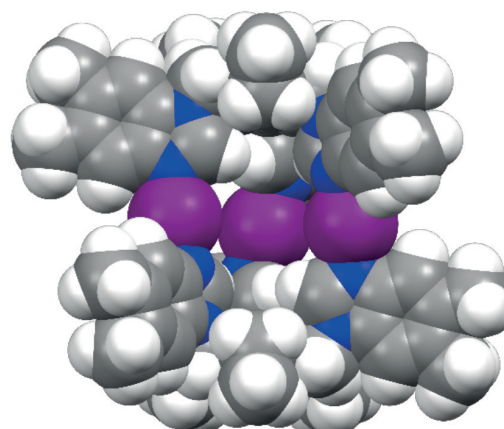


Figure 3 The spacefill representation of the calculated structure of $[\text{6-I-6}]\text{PF}_6$ iodine(I) cage.

encapsulated PF₆ counterion, which can only escape in the form of the ion pairs when the cage has already fragmented. This assumption is also in line with the observation of 2+, but no 1+ or 3+ charge states for the intact cages. The fragmentation was studied at different collision voltages to obtain a survivor yield curve for both the silver(I) and the iodine(I) cages (Figure S44). The 50% survivor yields are obtained at collision energies of 17 V for [L₂I₃PF₆]²⁺ and of 26 V for [L₂Ag₃PF₆]²⁺. Thus, the iodine(I) cage is somewhat less stable in the gas phase than its silver(I) analogue. In conclusion, not only the sizes of the two cages are in the same range, but also the ionisation behavior (only +2 charge states) and the fragmentation patterns. This is straightforward evidence that both cages have analogous capsular structures.

The formation of the silver(I) and iodine(I) cages in solution was studied with ¹H NMR and ¹H-¹⁵N HMBC measurements (Figure 4 and Figures S45-S54). Ligand **1** was not included in the NMR study since similar experiments have been previously reported.⁵³ Earlier studies have shown that the formation of the silver(I) cage results in a downfield change in the ¹H NMR chemical shifts of the ligand,^{43-45,53} most prominently observed for the imidazole C(2) proton (H_a, singlet, Figure 1, top). Changes in the ¹H NMR chemical shift range were between Δδ 0.16 and Δδ 0.48 ppm when going from the uncomplexed ligands to the silver(I) complexes. The cation exchange reaction from Ag⁺ to I⁺ results in a further downfield shift, which for these ligands, ranges from Δδ 0.16 to Δδ 1.21 ppm, resulting in notable shift differences between the free ligands and the iodine(I) cages of up to almost 1.7 ppm. It has been previously observed that the solubility of the complex is often lower for the I⁺ complex than for the Ag⁺ complex, and greatly reduced compared to the respective free ligand.⁴⁵ A complete set of measurements in CD₃CN could be performed only for two ligands (**4** and **5**) out of the five systems, as the solubility of some of the silver(I) and iodine(I) cages required the use of DMSO-*d*₆, and the poor solubility of the silver(I) complexes results in an incomplete conversion of the silver(I) cage to the iodine(I) cage, as confirmed by ¹H NMR spectroscopy. This is most clearly observed for ligand **2**, while being much less pronounced for **3** and **6**. However, the majority of the silver(I) cages fully convert to the iodine(I) cages. The conversion from the ligands to the silver(I) complexes were further studied with ¹H-¹⁵N HMBC measurements (Figures S46, S48, S50, S52, and S54). Even though the ¹H NMR spectra could be obtained for all the silver(I) and iodine(I) cages, in most cases the decreased solubility of the iodine(I) cages would cause them to precipitate out of solution during the time required for satisfactory quality HMBC acquisitions to be collected, and therefore, a full set of ¹⁵N NMR resonances were obtained for only one iodine(I) cage, [2-I-2]PF₆ (Figure S2). However, as demonstrated before,⁴⁵ upon coordination to silver(I), or iodine(I), the resonance of the coordinating nitrogen (N1) is found to change markedly downfield due to the deshielding effect upon complexation. In contrast, the non-coordinating nitrogen (N2) is shielded and experiences only minor changes in the opposite direction. Due to low solubility, the signal of the coordinating nitrogen (N1) is

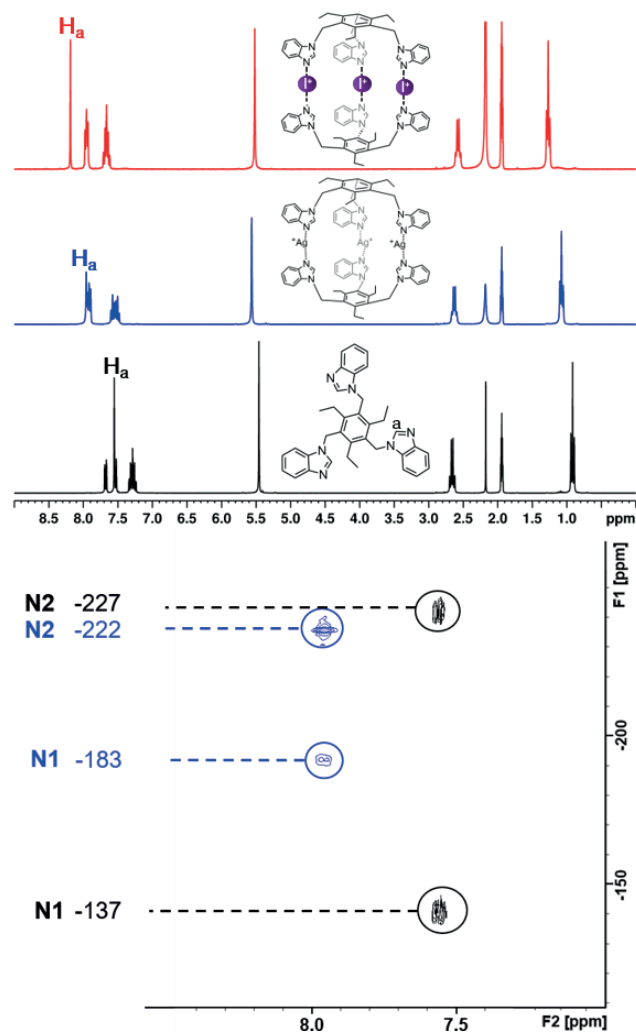


Figure 4 The ¹H (top) and ¹H-¹⁵N HMBC* (bottom) NMR spectra of the uncomplexed ligand **4** (black), the [4-Ag-4]PF₆ silver(I) complex (blue), and the [4-I-4]PF₆ iodine(I) complex (red), where H_a is the proton between the coordinating (N1) and non-coordinating (N2) nitrogens. All values are in ppm and referenced to CD₃CN (¹H) and CD₃NO₂ (¹⁵N) (500 MHz, 303 K). *Due to poor solubility, the ¹H-¹⁵N HMBC NMR spectra of the iodine(I) complex could not be obtained.

in some cases undetectable, making the N2 value ever more important, and giving valuable information about the complexation. The silver(I) complexation induces a coordination shift around -50 ppm in the ¹⁵N NMR resonance of N1 for all ligands, whereas the resonance of N2 only changes by around +5 ppm.

Conclusions

In summary, we have presented comprehensive evidence of dimeric imidazole-based iodine(I) cage formation in the solution and gas phase. The formation of the iodine(I) cages occurs *via* the Ag⁺ to I⁺ cation exchange reaction from the analogous silver(I) cages. In addition to NMR and MS experiments, the silver(I) cages were also crystallised and further studied in the

solid state using X-ray crystallography. The resulting endohedral cavity of the self-assembled dimeric cages yields an anion encapsulation with strong supramolecular interactions. The silver(I) crystal structure of [6–Ag–6]PF₆ and the calculated structure of [6–I–6]PF₆ along with the ion mobility-MS analysis, clearly display structural similarities amongst the two well-defined structures with the silver(I) cage having slightly shorter Ag–N bond lengths (2.068(12) - 2.170(7) Å) and less linear N–Ag–N angles (163.1(2)° - 180.0(5)°) than expected for the iodine(I) cage. This is strongly reflected in the almost identical arrival time distributions determined in ion mobility mass spectrometric experiments, which reveal only a very slight size increase when the silver ions are replaced by iodine(I). The flexibility of the cages enabled them to host anions of varying sizes, forming complexes with strong supramolecular interactions in each case. In addition to anion-cation interactions, a surprisingly large contribution to the anion stabilisation was made by the C–H...F hydrogen bonds.

For all the complexes, [L₂Ag₃]²⁺ ions were observed in the mass spectra, which indicates a stronger interaction of one anion compared to the remaining two. This would suggest that the anion encapsulation occurs for each complex in the gas phase. Furthermore, this would also support the occurrence of the anion encapsulation in solution. However, during the crystallisation, conceivably the inherent anisotropic nature of the 3c-4e [N–I–N]⁺ bond results in conflicting anion interactions, with the repulsive nature of the I⁺...F interactions and the attractive endohedral cavity,⁵³ making the anion encapsulation and the crystallisation process of the iodine(I) cages more problematic. However, the directionality of the [N–I–N]⁺ halogen bond makes iodine(I) ions excellent tools in supramolecular cage design and crystal engineering. The work presented here serves as further proof of the indisputable importance of halogen(I) ions as supramolecular synthons, aiding the design of more complex supramolecular capsular assemblies.

Conflicts of interest

There are no conflicts to declare.

Acknowledgements

We gratefully acknowledge the Academy of Finland (K.R. grant no. 317259), Finnish Cultural Foundation Central Fund (J.S.W. grant number 00201148), the Magnus Ehrnrooth Foundation (J.S.W.), European Union NOAH project (D.L.S. H2020-MSCA-ITN project Ref. 765297) and the University of Jyväskylä, Finland for financial support.

Notes and references

- 1 J. W. Steed and J. L. Atwood, *Supramolecular Chemistry*, 2009, 2nd ed., John Wiley & Sons, Ltd., Chichester, United Kingdom.
- 2 R. Wyler, J. de Mendoza and J. Rebek Jr., *Angew. Chem. Int. Ed. Engl.*, 1993, **32**, 1699.
- 3 C. M. A. Gangemi, A. Pappalardo and G. T. Sfrazzetto, *RSC Adv.*, 2015, **5**, 51919.
- 4 T. R. Cook, V. Vajpayee, M.H. Lee, P. J. Stang and K.-W. Chi, *Acc. Chem. Res.*, 2013, **46**, 2464.
- 5 K. Harris, D. Fujita and M. Fujita, *Chem. Commun.*, 2013, **49**, 6703.
- 6 A. Galan and P. Ballester, *Chem. Soc. Rev.*, 2016, **45**, 1720.
- 7 M. Yoshizawa, M. Tamura and M. Fujita, *Science*, 2006, **312**, 251.
- 8 K. Twum, K. Rissanen and N. K. Beyeh, *Chem. Rec.*, 2021, **21**, 386.
- 9 N. K. Beyeh and K. Rissanen, *Isr. J. Chem.*, 2011, **51**, 769.
- 10 H. Mansikkamäki, M. Nissinen and K. Rissanen, *CrystEngComm*, 2005, **7**, 519.
- 11 R. Puttreddy, N. K. Beyeh, E. Kalenius, R. H. A. Ras and K. Rissanen, *Chem. Commun.*, 2016, **52**, 8115.
- 12 I. Thondorf, F. Broda, K. Rissanen, M. Vysotsky and V. Böhmer, *J. Chem. Soc.*, 2002, **2**, 1796.
- 13 M. Chas, G. Gil-Ramírez and P. Ballester, *Org. Lett.*, 2011, **13**, 3402.
- 14 D. Ken and J. Rebek, *Proc. Natl. Acad. Sci. USA*, 1995, **92**, 12403.
- 15 A. Kiesilä, N. K. Beyeh, J. O. Moilanen, R. Puttreddy, S. Götz, K. Rissanen, P. Barran, A. Lützen and E. Kalenius, *Org. Biomol. Chem.*, 2019, **17**, 6980.
- 16 A. Kiesilä, L. Kivijärvi, N. K. Beyeh, J. O. Moilanen, M. Groessel, T. Rothe, S. Götz, F. Topić, K. Rissanen, A. Lützen and E. Kalenius, *Angew. Chem. Int. Ed.*, 2017, **56**, 10942.
- 17 W.-Y. Sun, J. Fan, T.-A. Okamura, J. Xie, K.-B. Yu and N. Ueyama, *Chem. Eur. J.*, 2001, **7**, 2557.
- 18 C.-Y. Su, Y.-P. Cai, C.-L. Chen, F. Lissner, B.-S. Kang and W. Kaim, *Angew. Chem. Int. Ed.*, 2002, **41**, 3371.
- 19 V. Amendola, M. Boiocchi, B. Colasson, L. Fabbrizzi, M.-J. Rodriguez Douton and F. Ugozzoli, *Angew. Chem. Int. Ed.*, 2006, **45**, 6920.
- 20 H.-K. Liu, X. Huang, T. Lu, X. Wang, W.-Y. Sun and B.-S. Kang, *Dalton Trans.*, 2008, 3178.
- 21 S. Bhattacharya and B. K. Saha, *J. Chem. Sci.*, 2016, **128**, 207.
- 22 H. Mansikkamäki, M. Nissinen and K. Rissanen, *Chem. Commun.*, 2002, 1902.
- 23 H. Mansikkamäki, M. Nissinen, C. A. Schalley and K. Rissanen, *New J. Chem.*, 2003, **27**, 88.
- 24 G. Cavallo, P. Metrangolo, R. Milani, T. Pilati, A. Priimagi, G. Resnati and G. Terraneo, *Chem. Rev.*, 2016, **116**, 2478.
- 25 L. C. Gilday, S. W. Robinson, T. A. Barendt, M. J. Langton, B. R. Mullaney and P. D. Beer, *Chem. Rev.*, 2015, **115**, 7118.
- 26 M. H. Kolář and P. Hobza, *Chem. Rev.*, 2016, **116**, 5155.
- 27 H. Wang, W. Wang and W. J. Jin, *Chem. Rev.*, 2016, **116**, 5072.
- 28 G. R. Desiraju, P. Shing Ho, L. Klöo, A. C. Legon, R. Marquardt, P. Metrangolo, P. Politzer, G. Resnati and K. Rissanen, *Pure Appl. Chem.*, 2013, **85**, 1711.
- 29 C. B. Aakeröy, A. Rajbanshi, P. Metrangolo, G. Resnati, M. F. Parisi, J. Desper and T. Pilati, *CrystEngComm*, 2012, **14**, 6366.
- 30 Y.-J. Zhu, Y. Gao, M.-M. Tang, J. Rebek Jr. and Y. Yu, *Chem. Commun.*, 2021, **57**, 1543.
- 31 N. K. Beyeh, F. Pan and K. Rissanen, *Angew. Chem. Int. Ed.*, 2015, **54**, 7303.
- 32 J. A. Creighton, I. Haque and J. L. Wood, *Chem. Commun.*, 1966, 229.
- 33 J. A. Creighton, I. Haque and J. L. Wood, *Chem. Commun.*, 1966, 892.
- 34 I. Haque and J. L. Wood, *J. Mol. Struct.*, 1968, **2**, 217.
- 35 A.-C. C. Carlsson, M. Uhrbom, A. Karim, U. Brath, J. Gräfenstein and M. Erdélyi, *CrystEngComm*, 2013, **15**, 3087.
- 36 L. Turunen and M. Erdélyi, *Chem. Soc. Rev.*, 2020, **49**, 2688.

- 37 A. C. Reiersølmoen, S. Battaglia, S. Oien-Odegaard, A. K. Gupta, A. Fiksdahl, R. Lindh and M. Erdélyi, *Chem. Sci.*, 2020, **11**, 7979.
- 38 S. Yu, P. Kumar, J. S. Ward, A. Frontera and K. Rissanen, *Chem*, 2021, **7**, 948.
- 39 J. Barluenga, J. M. González, M. A. García-Martín, P. J. Campos and G. Asensio, *J. Chem. Soc. Chem. Commun.*, 1992, 1016.
- 40 J. Ezquerro, C. Pedregal, C. Lamas, J. Barluenga, M. Pérez, M. A. García-Martín and J. M. González, *J. Org. Chem.*, 1996, **61**, 5804.
- 41 G. Espuña, G. Arsequell, G. Valencia, J. Barluenga, M. Pérez and J. M. González, *Chem. Commun.*, 2000, 1307.
- 42 J. Barluenga, F. González-Bobes, M. C. Murguía, S. R. Ananthoju and J. M. González, *Chem. Eur. J.*, 2004, **10**, 4206.
- 43 J. S. Ward, G. Fiorini, A. Frontera and K. Rissanen, *Chem. Commun.*, 2020, **56**, 8428.
- 44 J. S. Ward, A. Frontera and K. Rissanen, *Dalton Trans.*, 2021, **50**, 8297.
- 45 E. Taipale, M. Siepmann, K.-N. Truong and K. Rissanen, *Chem. Eur. J.*, 2021, **27**, DOI:10.1002/chem.202103152.
- 46 J. S. Ward, A. Frontera and K. Rissanen, *Chem. Commun.*, 2021, **57**, 5094.
- 47 A. Vanderkooy, A. K. Gupta, T. Földes, S. Lindblad, A. Orthaber, I. Pápai and M. Erdélyi, *Angew. Chem. Int. Ed.*, 2019, **58**, 9012.
- 48 J. S. Ward, A. Frontera and K. Rissanen, *Inorg. Chem.*, 2021, **60**, 5383.
- 49 S. Yu, E. Kalenius, A. Frontera and K. Rissanen, *Chem. Commun.*, DOI:10.1039/d1cc05616f.
- 50 L. Turunen, U. Warzok, R. Puttreddy, N. K. Beyeh, C. A. Schalley and K. Rissanen, *Angew. Chem. Int. Ed.*, 2016, **55**, 14033.
- 51 U. Warzok, M. Marianski, W. Hoffmann, L. Turunen, K. Rissanen, K. Pagel and C. A. Schalley, *Chem. Sci.*, 2018, **9**, 8343.
- 52 L. Turunen, U. Warzok, C. A. Schalley and K. Rissanen, *Chem*, 2017, **3**, 861.
- 53 L. Turunen, A. Peuronen, S. Forsblom, E. Kalenius, M. Lahtinen and K. Rissanen, *Chem. Eur. J.*, 2017, **23**, 11714.
- 54 A.-C. C. Carlsson, J. Gräfenstein, J. L. Laurila, J. Bergquist and M. Erdélyi, *Chem. Commun.*, 2012, **48**, 1458.
- 55 Y. Yuan, Z.-L. Jiang, J.-M. Yan, G. Gao, A. S. C. Chan and R.-G. Xie, *Synth. Commun.*, 2000, **30**, 4555.
- 56 M. Bedin, A. Karim, M. Reitti, A.-C. C. Carlsson, F. Topic, M. Cetina, F. Pan, V. Havel, F. Al-Ameri, V. Sindelar, K. Rissanen, J. Gräfenstein and M. Erdélyi, *Chem. Sci.*, 2015, **6**, 3746.
- 57 W.-Y. Sun, J. Fan, J. Hu, K.-B. Yu and W.-X. Tang, *J. Chem. Crystallogr.*, 2000, **30**, 115.
- 58 S. N. L. Andree, A. S. Sinha and C. B. Aakeröy, *Molecules*, 2018, **23**, 163.
- 59 C. E. Willans, S. French, K. M. Anderson, L. J. Barbour, J.-A. Gertenbach, G. O. Lloyd, R. J. Dyer, P. C. Junk and J. W. Steed, *Dalton Trans.*, 2011, **40**, 573.
- 60 C. B. Aakeröy, M. Smith and J. Desper, *Can. J. Chem.*, 2015, **93**.
- 61 J. Fan, W.-Y. Sun, T. Okamura, J. Xie, W.-X. Tang and N. Ueyama, *New. J. Chem.*, 2002, **26**, 199.
- 62 J. Fan, H.-F. Zhu, T. Okamura, W.-Y. Sun, W.-X. Tang and N. Ueyama, *Chem. Eur. J.*, 2003, **9**, 4724.
- 63 A. L. Spek, *Acta Crystallogr. Sect. C*, 2015, **71**, 9.
- 64 A.-C. C. Carlsson, K. Mehmeti, M. Uhrbom, A. Karim, M. Bedin, R. Puttreddy, R. Kleinmaier, A. A. Neverov, B. Nekoueshahraki, J. Gräfenstein, K. Rissanen and M. Erdélyi, *J. Am. Chem. Soc.*, 2016, **138**, 9853.
- 65 A.-C. C. Carlsson, J. Gräfenstein, A. Budnjo, J. L. Laurila, J. Bergquist, A. Karim, R. Kleinmaier, U. Brath and M. Erdélyi, *J. Am. Chem. Soc.*, 2012, **134**, 5706.
- 66 M. A. Spackman and D. Jayatilaka, *CrystEngComm*, 2009, **11**, 19.
- 67 P. R. Spackman, M. J. Turner, J. J. McKinnon, S. K. Wolff, D. J. Grimwood, D. Jayatilaka and M. A. Spackman, *J. Appl. Cryst.*, 2021, **54**, 1006.
- 68 S. Mecozzi and J. Rebek Jr., *Chem. Eur. J.*, 1998, **4**, 1016.
- 69 K. Rissanen, *Chem. Soc. Rev.*, 2017, **46**, 2638.
- 70 E. Kalenius, M. Groessl and K. Rissanen, *Nat. Rev. Chem.*, 2019, **3**, 4.

DEPARTMENT OF CHEMISTRY, UNIVERSITY OF JYVÄSKYLÄ
RESEARCH REPORT SERIES

1. Vuolle, Mikko: Electron paramagnetic resonance and molecular orbital study of radical ions generated from (2.2)metacyclophane, pyrene and its hydrogenated compounds by alkali metal reduction and by thallium(III)trifluoroacetate oxidation. (99 pp.) 1976
2. Pasanen, Kaija: Electron paramagnetic resonance study of cation radical generated from various chlorinated biphenyls. (66 pp.) 1977
3. Carbon-13 Workshop, September 6-8, 1977. (91 pp.) 1977
4. Laihia, Katri: On the structure determination of norbornane polyols by NMR spectroscopy. (111 pp.) 1979
5. Nyrönen, Timo: On the EPR, ENDOR and visible absorption spectra of some nitrogen containing heterocyclic compounds in liquid ammonia. (76 pp.) 1978
6. Talvitie, Antti: Structure determination of some sesquiterpenoids by shift reagent NMR. (54 pp.) 1979
7. Häkli, Harri: Structure analysis and molecular dynamics of cyclic compounds by shift reagent NMR. (48 pp.) 1979
8. Pitkänen, Ilkka: Thermodynamics of complexation of 1,2,4-triazole with divalent manganese, cobalt, nickel, copper, zinc, cadmium and lead ions in aqueous sodium perchlorate solutions. (89 pp.) 1980
9. Asunta, Tuula: Preparation and characterization of new organometallic compounds synthesized by using metal vapours. (91 pp.) 1980
10. Sattar, Mohammad Abdus: Analyses of MCPA and its metabolites in soil. (57 pp.) 1980
11. Bibliography 1980. (31 pp.) 1981
12. Knuuttila, Pekka: X-Ray structural studies on some divalent 3d metal compounds of picolinic and isonicotinic acid N-oxides. (77 pp.) 1981
13. Bibliography 1981. (33 pp.) 1982
14. 6th National NMR Symposium, September 9-10, 1982, Abstracts. (49 pp.) 1982
15. Bibliography 1982. (38 pp.) 1983
16. Knuuttila, Hilka: X-Ray structural studies on some Cu(II), Co(II) and Ni(II) complexes with nicotinic and isonicotinic acid N-oxides. (54 pp.) 1983
17. Symposium on inorganic and analytical chemistry May 18, 1984, Program and Abstracts. (100 pp.) 1984
18. Knuutinen, Juha: On the synthesis, structure verification and gas chromatographic determination of chlorinated catechols and guaiacols occurring in spent bleach liquors of kraft pulp mill. (30 pp.) 1984
19. Bibliography 1983. (47 pp.) 1984
20. Pitkänen, Maija: Addition of BrCl, B₂ and Cl₂ to methyl esters of propenoic and 2-butenic acid derivatives and ¹³C NMR studies on methyl esters of saturated aliphatic mono- and dichlorocarboxylic acids. (56 pp.) 1985
21. Bibliography 1984. (39 pp.) 1985
22. Salo, Esa: EPR, ENDOR and TRIPLE spectroscopy of some nitrogen heteroaromatics in liquid ammonia. (111 pp.) 1985

DEPARTMENT OF CHEMISTRY, UNIVERSITY OF JYVÄSKYLÄ
RESEARCH REPORT SERIES

23. Humppi, Tarmo: Synthesis, identification and analysis of dimeric impurities of chlorophenols. (39 pp.) 1985
24. Aho, Martti: The ion exchange and adsorption properties of sphagnum peat under acid conditions. (90 pp.) 1985
25. Bibliography 1985 (61 pp.) 1986
26. Bibliography 1986. (23 pp.) 1987
27. Bibliography 1987. (26 pp.) 1988
28. Paasivirta, Jaakko (Ed.): Structures of organic environmental chemicals. (67 pp.) 1988
29. Paasivirta, Jaakko (Ed.): Chemistry and ecology of organo-element compounds. (93 pp.) 1989
30. Sinkkonen, Seija: Determination of crude oil alkylated dibenzothiophenes in environment. (35 pp.) 1989
31. Kolehmainen, Erkki (Ed.): XII National NMR Symposium Program and Abstracts. (75 pp.) 1989
32. Kuokkanen, Tauno: Chlorocymenes and Chlorocymenenes: Persistent chlorocompounds in spent bleach liquors of kraft pulp mills. (40 pp.) 1989
33. Mäkelä, Reijo: ESR, ENDOR and TRIPLE resonance study on substituted 9,10-anthraquinone radicals in solution. (35 pp.) 1990
34. Veijanen, Anja: An integrated sensory and analytical method for identification of off-flavour compounds. (70 pp.) 1990
35. Kasa, Seppo: EPR, ENDOR and TRIPLE resonance and molecular orbital studies on a substitution reaction of anthracene induced by thallium(III) in two fluorinated carboxylic acids. (114 pp.) 1990
36. Herve, Sirpa: Mussel incubation method for monitoring organochlorine compounds in freshwater recipients of pulp and paper industry. (145 pp.) 1991
37. Pohjola, Pekka: The electron paramagnetic resonance method for characterization of Finnish peat types and iron (III) complexes in the process of peat decomposition. (77 pp.) 1991
38. Paasivirta, Jaakko (Ed.): Organochlorines from pulp mills and other sources. Research methodology studies 1988-91. (120 pp.) 1992
39. Veijanen, Anja (Ed.): VI National Symposium on Mass Spectrometry, May 13-15, 1992, Abstracts. (55 pp.) 1992
40. Rissanen, Kari (Ed.): The 7. National Symposium on Inorganic and Analytical Chemistry, May 22, 1992, Abstracts and Program. (153 pp.) 1992
41. Paasivirta, Jaakko (Ed.): CEOEC'92, Second Finnish-Russian Seminar: Chemistry and Ecology of Organo-Element Compounds. (93 pp.) 1992
42. Koistinen, Jaana: Persistent polychloroaromatic compounds in the environment: structure-specific analyses. (50 pp.) 1993
43. Virkki, Liisa: Structural characterization of chlorolignins by spectroscopic and liquid chromatographic methods and a comparison with humic substances. (62 pp.) 1993
44. Helenius, Vesa: Electronic and vibrational excitations in some

DEPARTMENT OF CHEMISTRY, UNIVERSITY OF JYVÄSKYLÄ
RESEARCH REPORT SERIES

- biologically relevant molecules. (30 pp.) 1993
45. Leppä-aho, Jaakko: Thermal behaviour, infrared spectra and x-ray structures of some new rare earth chromates(VI). (64 pp.) 1994
46. Kotila, Sirpa: Synthesis, structure and thermal behavior of solid copper(II) complexes of 2-amino-2-hydroxymethyl-1,3-propanediol. (111 pp.) 1994
47. Mikkonen, Anneli: Retention of molybdenum(VI), vanadium(V) and tungsten(VI) by kaolin and three Finnish mineral soils. (90 pp.) 1995
48. Suontamo, Reijo: Molecular orbital studies of small molecules containing sulfur and selenium. (42 pp.) 1995
49. Hämäläinen, Jouni: Effect of fuel composition on the conversion of fuel-N to nitrogen oxides in the combustion of small single particles. (50 pp.) 1995
50. Nevalainen, Tapio: Polychlorinated diphenyl ethers: synthesis, NMR spectroscopy, structural properties, and estimated toxicity. (76 pp.) 1995
51. Aittola, Jussi-Pekka: Organochloro compounds in the stack emission. (35 pp.) 1995
52. Harju, Timo: Ultrafast polar molecular photophysics of (dibenzylmethine)borondifluoride and 4-aminophthalimide in solution. (61 pp.) 1995
53. Maatela, Paula: Determination of organically bound chlorine in industrial and environmental samples. (83 pp.) 1995
54. Paasivirta, Jaakko (Ed.): CEOEC'95, Third Finnish-Russian Seminar: Chemistry and Ecology of Organo-Element Compounds. (109 pp.) 1995
55. Huuskonen, Juhani: Synthesis and structural studies of some supramolecular compounds. (54 pp.) 1995
56. Palm, Helena: Fate of chlorophenols and their derivatives in sawmill soil and pulp mill recipient environments. (52 pp.) 1995
57. Rantio, Tiina: Chlorohydrocarbons in pulp mill effluents and their fate in the environment. (89 pp.) 1997
58. Ratilainen, Jari: Covalent and non-covalent interactions in molecular recognition. (37 pp.) 1997
59. Kolehmainen, Erkki (Ed.): XIX National NMR Symposium, June 4-6, 1997, Abstracts. (89 pp.) 1997
60. Matilainen, Rose: Development of methods for fertilizer analysis by inductively coupled plasma atomic emission spectrometry. (41 pp.) 1997
61. Koistinen, Jari (Ed.): Spring Meeting on the Division of Synthetic Chemistry, May 15-16, 1997, Program and Abstracts. (36 pp.) 1997
62. Lappalainen, Kari: Monomeric and cyclic bile acid derivatives: syntheses, NMR spectroscopy and molecular recognition properties. (50 pp.) 1997
63. Laitinen, Eira: Molecular dynamics of cyanine dyes and phthalimides in solution: picosecond laser studies. (62 pp.) 1997
64. Eloranta, Jussi: Experimental and theoretical studies on some

DEPARTMENT OF CHEMISTRY, UNIVERSITY OF JYVÄSKYLÄ
RESEARCH REPORT SERIES

- quinone and quinol radicals. (40 pp.) 1997
65. Oksanen, Jari: Spectroscopic characterization of some monomeric and aggregated chlorophylls. (43 pp.) 1998
66. Häkkänen, Heikki: Development of a method based on laser-induced plasma spectrometry for rapid spatial analysis of material distributions in paper coatings. (60 pp.) 1998
67. Virtapohja, Janne: Fate of chelating agents used in the pulp and paper industries. (58 pp.) 1998
68. Airola, Karri: X-ray structural studies of supramolecular and organic compounds. (39 pp.) 1998
69. Hyötyläinen, Juha: Transport of lignin-type compounds in the receiving waters of pulp mills. (40 pp.) 1999
70. Ristolainen, Matti: Analysis of the organic material dissolved during totally chlorine-free bleaching. (40 pp.) 1999
71. Eklin, Tero: Development of analytical procedures with industrial samples for atomic emission and atomic absorption spectrometry. (43 pp.) 1999
72. Välisaari, Jouni: Hygiene properties of resol-type phenolic resin laminates. (129 pp.) 1999
73. Hu, Jiwei: Persistent polyhalogenated diphenyl ethers: model compounds syntheses, characterization and molecular orbital studies. (59 pp.) 1999
74. Malkavaara, Petteri: Chemometric adaptations in wood processing chemistry. (56 pp.) 2000
75. Kujala Elena, Laihia Katri, Nieminen Kari (Eds.): NBC 2000, Symposium on Nuclear, Biological and Chemical Threats in the 21st Century. (299 pp.) 2000
76. Rantalainen, Anna-Lea: Semipermeable membrane devices in monitoring persistent organic pollutants in the environment. (58 pp.) 2000
77. Lahtinen, Manu: *In situ* X-ray powder diffraction studies of Pt/C, CuCl/C and Cu₂O/C catalysts at elevated temperatures in various reaction conditions. (92 pp.) 2000
78. Tamminen, Jari: Syntheses, empirical and theoretical characterization, and metal cation complexation of bile acid-based monomers and open/closed dimers. (54 pp.) 2000
79. Vatanen, Virpi: Experimental studies by EPR and theoretical studies by DFT calculations of α -amino-9,10-anthraquinone radical anions and cations in solution. (37 pp.) 2000
80. Kotilainen, Risto: Chemical changes in wood during heating at 150-260 °C. (57 pp.) 2000
81. Nissinen, Maija: X-ray structural studies on weak, non-covalent interactions in supramolecular compounds. (69 pp.) 2001
82. Wegelius, Elina: X-ray structural studies on self-assembled hydrogen-bonded networks and metallosupramolecular complexes. (84 pp.) 2001
83. Paasivirta, Jaakko (Ed.): CEOEC'2001, Fifth Finnish-Russian Seminar: Chemistry and Ecology of Organo-Element Compounds. (163 pp.) 2001
84. Kiljunen, Toni: Theoretical studies on spectroscopy and

DEPARTMENT OF CHEMISTRY, UNIVERSITY OF JYVÄSKYLÄ
RESEARCH REPORT SERIES

- atomic dynamics in rare gas solids. (56 pp.) 2001
85. Du, Jin: Derivatives of dextran: synthesis and applications in oncology. (48 pp.) 2001
86. Koivisto, Jari: Structural analysis of selected polychlorinated persistent organic pollutants (POPs) and related compounds. (88 pp.) 2001
87. Feng, Zhinan: Alkaline pulping of non-wood feedstocks and characterization of black liquors. (54 pp.) 2001
88. Halonen, Markku: Lahon havupuun käyttö sulfaattiprosessin raaka-aineena sekä havupuun lahontorjunta. (90 pp.) 2002
89. Falábu, Dezső: Synthesis, conformational analysis and complexation studies of resorcarene derivatives. (212 pp.) 2001
90. Lehtovuori, Pekka: EMR spectroscopic studies on radicals of ubiquinones Q-*n*, vitamin K₃ and vitamine E in liquid solution. (40 pp.) 2002
91. Perkkalainen, Paula: Polymorphism of sugar alcohols and effect of grinding on thermal behavior on binary sugar alcohol mixtures. (53 pp.) 2002
92. Ihalainen, Janne: Spectroscopic studies on light-harvesting complexes of green plants and purple bacteria. (42 pp.) 2002
93. Kunttu, Henrik, Kiljunen, Toni (Eds.): 4th International Conference on Low Temperature Chemistry. (159 pp.) 2002
94. Väisänen, Ari: Development of methods for toxic element analysis in samples with environmental concern by ICP-AES and ETAAS. (54 pp.) 2002
95. Luostarinen, Minna: Synthesis and characterisation of novel resorcarene derivatives. (200 pp.) 2002
96. Louhelainen, Jarmo: Changes in the chemical composition and physical properties of wood and nonwood black liquors during heating. (68 pp.) 2003
97. Lahtinen, Tanja: Concave hydrocarbon cyclophane π -prismans. (65 pp.) 2003
98. Laihia, Katri (Ed.): NBC 2003, Symposium on Nuclear, Biological and Chemical Threats – A Crisis Management Challenge. (245 pp.) 2003
99. Oasmaa, Anja: Fuel oil quality properties of wood-based pyrolysis liquids. (32 pp.) 2003
100. Virtanen, Elina: Syntheses, structural characterisation, and cation/anion recognition properties of nano-sized bile acid-based host molecules and their precursors. (123 pp.) 2003
101. Nättinen, Kalle: Synthesis and X-ray structural studies of organic and metallo-organic supramolecular systems. (79 pp.) 2003
102. Lampiselkä, Jarkko: Demonstraatio lukion kemian opetuksessa. (285 pp.) 2003
103. Kallioinen, Jani: Photoinduced dynamics of Ru(dcbpy)₂(NCS)₂ – in solution and on nanocrystalline titanium dioxide thin films. (47 pp.) 2004
104. Valkonen, Arto (Ed.): VII Synthetic Chemistry Meeting and XXVI Finnish NMR Symposium. (103 pp.) 2004

DEPARTMENT OF CHEMISTRY, UNIVERSITY OF JYVÄSKYLÄ
RESEARCH REPORT SERIES

105. Vaskonen, Kari: Spectroscopic studies on atoms and small molecules isolated in low temperature rare gas matrices. (65 pp.) 2004
106. Lehtovuori, Viivi: Ultrafast light induced dissociation of Ru(dcbpy)(CO)₂I₂ in solution. (49 pp.) 2004
107. Saarenketo, Pauli: Structural studies of metal complexing Schiff bases, Schiff base derived *N*-glycosides and cyclophane π -prismoids. (95 pp.) 2004
108. Paasivirta, Jaakko (Ed.): CEOEC'2004, Sixth Finnish-Russian Seminar: Chemistry and Ecology of Organo-Element Compounds. (147 pp.) 2004
109. Suontamo, Tuula: Development of a test method for evaluating the cleaning efficiency of hard-surface cleaning agents. (96 pp.) 2004
110. Güneş, Minna: Studies of thiocyanates of silver for nonlinear optics. (48 pp.) 2004
111. Ropponen, Jarmo: Aliphatic polyester dendrimers and dendrons. (81 pp.) 2004
112. Vu, Mân Thi Hong: Alkaline pulping and the subsequent elemental chlorine-free bleaching of bamboo (*Bambusa procera*). (69 pp.) 2004
113. Mansikkamäki, Heidi: Self-assembly of resorcinarenes. (77 pp.) 2006
114. Tuononen, Heikki M.: EPR spectroscopic and quantum chemical studies of some inorganic main group radicals. (79 pp.) 2005
115. Kaski, Saara: Development of methods and applications of laser-induced plasma spectroscopy in vacuum ultraviolet. (44 pp.) 2005
116. Mäkinen, Riika-Mari: Synthesis, crystal structure and thermal decomposition of certain metal thiocyanates and organic thiocyanates. (119 pp.) 2006
117. Ahokas, Jussi: Spectroscopic studies of atoms and small molecules isolated in rare gas solids: photodissociation and thermal reactions. (53 pp.) 2006
118. Busi, Sara: Synthesis, characterization and thermal properties of new quaternary ammonium compounds: new materials for electrolytes, ionic liquids and complexation studies. (102 pp.) 2006
119. Mäntykoski, Keijo: PCBs in processes, products and environment of paper mills using wastepaper as their raw material. (73 pp.) 2006
120. Laamanen, Pirkko-Leena: Simultaneous determination of industrially and environmentally relevant aminopolycarboxylic and hydroxycarboxylic acids by capillary zone electrophoresis. (54 pp.) 2007
121. Salmela, Maria: Description of oxygen-alkali delignification of kraft pulp using analysis of dissolved material. (71 pp.) 2007
122. Lehtovaara, Lauri: Theoretical studies of atomic scale impurities in superfluid ⁴He. (87 pp.) 2007
123. Rautiainen, J. Mikko: Quantum chemical calculations of structures, bonding, and spectroscopic properties of some sulphur and selenium iodine cations. (71 pp.) 2007
124. Nummelin, Sami: Synthesis, characterization, structural and

- retrostructural analysis of self-assembling pore forming dendrimers. (286 pp.) 2008
125. Sopo, Harri: Uranyl(VI) ion complexes of some organic aminobisphenolate ligands: syntheses, structures and extraction studies. (57 pp.) 2008
126. Valkonen, Arto: Structural characteristics and properties of substituted cholanoates and *N*-substituted cholanamides. (80 pp.) 2008
127. Lähde, Anna: Production and surface modification of pharmaceutical nano- and microparticles with the aerosol flow reactor. (43 pp.) 2008
128. Beyeh, Ngong Kodiah: Resorcinarenes and their derivatives: synthesis, characterization and complexation in gas phase and in solution. (75 pp.) 2008
129. Väliisaari, Jouni, Lundell, Jan (Eds.): Kemian opetuksen päivät 2008: uusia oppimisympäristöjä ja ongelmalähtöistä opetusta. (118 pp.) 2008
130. Myllyperkiö, Pasi: Ultrafast electron transfer from potential organic and metal containing solar cell sensitizers. (69 pp.) 2009
131. Käkölä, Jaana: Fast chromatographic methods for determining aliphatic carboxylic acids in black liquors. (82 pp.) 2009
132. Koivukorpi, Juha: Bile acid-arene conjugates: from photoswitchability to cancer cell detection. (67 pp.) 2009
133. Tuuttila, Tero: Functional dendritic polyester compounds: synthesis and characterization of small bifunctional dendrimers and dyes. (74 pp.) 2009
134. Salorinne, Kirsi: Tetramethoxy resorcinarene based cation and anion receptors: synthesis, characterization and binding properties. (79 pp.) 2009
135. Rautiainen, Riikka: The use of first-thinning Scots pine (*Pinus sylvestris*) as fiber raw material for the kraft pulp and paper industry. (73 pp.) 2010
136. Ilander, Laura: Uranyl salophens: synthesis and use as ditopic receptors. (199 pp.) 2010
137. Kiviniemi, Tiina: Vibrational dynamics of iodine molecule and its complexes in solid krypton - Towards coherent control of bimolecular reactions? (73 pp.) 2010
138. Ikonen, Satu: Synthesis, characterization and structural properties of various covalent and non-covalent bile acid derivatives of N/O-heterocycles and their precursors. (105 pp.) 2010
139. Siitonen, Anni: Spectroscopic studies of semiconducting single-walled carbon nanotubes. (56 pp.) 2010
140. Raatikainen, Kari: Synthesis and structural studies of piperazine cyclophanes – Supramolecular systems through Halogen and Hydrogen bonding and metal ion coordination. (69 pp.) 2010
141. Leivo, Kimmo: Gelation and gel properties of two- and three-component Pyrene based low molecular weight organogelators. (116 pp.) 2011
142. Martiskainen, Jari: Electronic energy transfer in light-harvesting complexes isolated from *Spinacia oleracea* and from three

- photosynthetic green bacteria *Chloroflexus aurantiacus*, *Chlorobium tepidum*, and *Prosthecochloris aestuarii*. (55 pp.) 2011
143. Wichmann, Oula: Syntheses, characterization and structural properties of [O,N,O,X'] aminobisphenolate metal complexes. (101 pp.) 2011
144. Ilander, Aki: Development of ultrasound-assisted digestion methods for the determination of toxic element concentrations in ash samples by ICP-OES. (58 pp.) 2011
145. The Combined XII Spring Meeting of the Division of Synthetic Chemistry and XXXIII Finnish NMR Symposium. Book of Abstracts. (90 pp.) 2011
146. Valto, Piia: Development of fast analysis methods for extractives in papermaking process waters. (73 pp.) 2011
147. Andersin, Jenni: Catalytic activity of palladium-based nanostructures in the conversion of simple olefinic hydro- and chlorohydrocarbons from first principles. (78 pp.) 2011
148. Aumanen, Jukka: Photophysical properties of dansylated poly(propylene amine) dendrimers. (55 pp.) 2011
149. Kärnä, Minna: Ether-functionalized quaternary ammonium ionic liquids – synthesis, characterization and physicochemical properties. (76 pp.) 2011
150. Jurček, Ondřej: Steroid conjugates for applications in pharmacology and biology. (57 pp.) 2011
151. Nauha, Elisa: Crystalline forms of selected Agrochemical actives: design and synthesis of cocrystals. (77 pp.) 2012
152. Ahkola, Heidi: Passive sampling in monitoring of nonylphenol ethoxylates and nonylphenol in aquatic environments. (92 pp.) 2012
153. Helttunen, Kaisa: Exploring the self-assembly of resorcinarenes: from molecular level interactions to mesoscopic structures. (78 pp.) 2012
154. Linnanto, Juha: Light excitation transfer in photosynthesis revealed by quantum chemical calculations and exciton theory. (179 pp.) 2012
155. Roiko-Jokela, Veikko: Digital imaging and infrared measurements of soil adhesion and cleanability of semihard and hard surfaces. (122 pp.) 2012
156. Noponen, Virpi: Amides of bile acids and biologically important small molecules: properties and applications. (85 pp.) 2012
157. Hulkko, Eero: Spectroscopic signatures as a probe of structure and dynamics in condensed-phase systems – studies of iodine and gold ranging from isolated molecules to nanoclusters. (69 pp.) 2012
158. Lappi, Hanna: Production of Hydrocarbon-rich biofuels from extractives-derived materials. (95 pp.) 2012
159. Nykänen, Lauri: Computational studies of Carbon chemistry on transition metal surfaces. (76 pp.) 2012
160. Ahonen, Kari: Solid state studies of pharmaceutically important molecules and their derivatives. (65 pp.) 2012

DEPARTMENT OF CHEMISTRY, UNIVERSITY OF JYVÄSKYLÄ
RESEARCH REPORT SERIES

161. Pakkanen, Hannu: Characterization of organic material dissolved during alkaline pulping of wood and non-wood feedstocks. (76 pp.) 2012
162. Moilanen, Jani: Theoretical and experimental studies of some main group compounds: from closed shell interactions to singlet diradicals and stable radicals. (80 pp.) 2012
163. Himanen, Jatta: Stereoselective synthesis of Oligosaccharides by *De Novo* Saccharide welding. (133 pp.) 2012
164. Bunzen, Hana: Steroidal derivatives of nitrogen containing compounds as potential gelators. (76 pp.) 2013
165. Seppälä, Petri: Structural diversity of copper(II) amino alcohol complexes. Syntheses, structural and magnetic properties of bidentate amino alcohol copper(II) complexes. (67 pp.) 2013
166. Lindgren, Johan: Computational investigations on rotational and vibrational spectroscopies of some diatomics in solid environment. (77 pp.) 2013
167. Giri, Chandan: Sub-component self-assembly of linear and non-linear diamines and diacylhydrazines, formylpyridine and transition metal cations. (145 pp.) 2013
168. Riisiö, Antti: Synthesis, Characterization and Properties of Cu(II)-, Mo(VI)- and U(VI) Complexes With Diaminotetraphenolate Ligands. (51 pp.) 2013
169. Kiljunen, Toni (Ed.): Chemistry and Physics at Low Temperatures. Book of Abstracts. (103 pp.) 2013
170. Hänninen, Mikko: Experimental and Computational Studies of Transition Metal Complexes with Polydentate Amino- and Aminophenolate Ligands: Synthesis, Structure, Reactivity and Magnetic Properties. (66 pp.) 2013
171. Antila, Liisa: Spectroscopic studies of electron transfer reactions at the photoactive electrode of dye-sensitized solar cells. (53 pp.) 2013
172. Kemppainen, Eeva: Mukaiyama-Michael reactions with α -substituted acroleins – a useful tool for the synthesis of the pectenotoxins and other natural product targets. (190 pp.) 2013
173. Virtanen, Suvi: Structural Studies of Dielectric Polymer Nanocomposites. (49 pp.) 2013
174. Yliniemelä-Sipari, Sanna: Understanding The Structural Requirements for Optimal Hydrogen Bond Catalyzed Enolization – A Biomimetic Approach. (160 pp.) 2013
175. Leskinen, Mikko V: Remote β -functionalization of β' -keto esters. (105 pp.) 2014
176. 12th European Conference on Research in Chemistry Education (ECRICE2014). Book of Abstracts. (166 pp.) 2014
177. Peuronen, Anssi: N-Monoalkylated DABCO-Based N-Donors as Versatile Building Blocks in Crystal Engineering and Supramolecular Chemistry. (54 pp.) 2014
178. Perämäki, Siiri: Method development for determination and recovery of rare earth elements from industrial fly ash. (88 pp.) 2014

DEPARTMENT OF CHEMISTRY, UNIVERSITY OF JYVÄSKYLÄ
RESEARCH REPORT SERIES

179. Chernyshev, Alexander, N.: Nitrogen-containing ligands and their platinum(IV) and gold(III) complexes: investigation and basicity and nucleophilicity, luminescence, and aurophilic interactions. (64 pp.) 2014
180. Lehto, Joni: Advanced Biorefinery Concepts Integrated to Chemical Pulping. (142 pp.) 2015
181. Tero, Tiia-Riikka: Tetramethoxy resorcinarenes as platforms for fluorescent and halogen bonding systems. (61 pp.) 2015
182. Löfman, Miika: Bile acid amides as components of microcrystalline organogels. (62 pp.) 2015
183. Selin, Jukka: Adsorption of softwood-derived organic material onto various fillers during papermaking. (169 pp.) 2015
184. Piisola, Antti: Challenges in the stereoselective synthesis of allylic alcohols. (210 pp.) 2015
185. Bonakdarzadeh, Pia: Supramolecular coordination polyhedra based on achiral and chiral pyridyl ligands: design, preparation, and characterization. (65 pp.) 2015
186. Vasko, Petra: Synthesis, characterization, and reactivity of heavier group 13 and 14 metallylenes and metalloid clusters: small molecule activation and more. (66 pp.) 2015
187. Topić, Filip: Structural Studies of Nano-sized Supramolecular Assemblies. (79 pp.) 2015
188. Mustalahti, Satu: Photodynamics Studies of Ligand-Protected Gold Nanoclusters by using Ultrafast Transient Infrared Spectroscopy. (58 pp.) 2015
189. Koivisto, Jaakko: Electronic and vibrational spectroscopic studies of gold-nanoclusters. (63 pp.) 2015
190. Suhonen, Aku: Solid state conformational behavior and interactions of series of aromatic oligoamide foldamers. (68 pp.) 2016
191. Soikkeli, Ville: Hydrometallurgical recovery and leaching studies for selected valuable metals from fly ash samples by ultrasound-assisted extraction followed by ICP-OES determination. (107 pp.) 2016
192. XXXVIII Finnish NMR Symposium. Book of Abstracts. (51 pp.) 2016
193. Mäkelä, Toni: Ion Pair Recognition by Ditopic Crown Ether Based bis-Urea and Uranyl Salophen Receptors. (75 pp.) 2016
194. Lindholm-Lehto, Petra: Occurrence of pharmaceuticals in municipal wastewater treatment plants and receiving surface waters in Central and Southern Finland. (98 pp.) 2016
195. Härkönen, Ville: Computational and Theoretical studies on Lattice Thermal conductivity and Thermal properties of Silicon Clathrates. (89 pp.) 2016
196. Tuokko, Sakari: Understanding selective reduction reactions with heterogeneous Pd and Pt: climbing out of the black box. (85 pp.) 2016
197. Nuora, Piia: Monitapaustutkimus LUMA-Toimintaan liittyvissä oppimisympäristöissä tapahtuvista kemian oppimiskokemuksista. (171 pp.) 2016

DEPARTMENT OF CHEMISTRY, UNIVERSITY OF JYVÄSKYLÄ
RESEARCH REPORT SERIES

198. Kumar, Hemanathan: Novel Concepts on The Recovery of By-Products from Alkaline Pulping. (61 pp.) 2016
199. Arnedo-Sánchez, Leticia: Lanthanide and Transition Metal Complexes as Building Blocks for Supramolecular Functional Materials. (227 pp.) 2016
200. Gell, Lars: Theoretical Investigations of Ligand Protected Silver Nanoclusters. (134 pp.) 2016
201. Vaskuri, Juhani: Oppiennätyksistä opetussuunnitelman perusteisiin - lukion kemian kansallisen opetussuunnitelman kehittyminen Suomessa vuosina 1918-2016. (314 pp.) 2017
202. Lundell Jan, Kiljunen Toni (Eds.): 22nd Horizons in Hydrogen Bond Research. Book of Abstracts. 2017
203. Turunen, Lotta: Design and construction of halogen-bonded capsules and cages. (61 pp.) 2017
204. Hurmalainen, Juha: Experimental and computational studies of unconventional main group compounds: stable radicals and reactive intermediates. (88 pp.) 2017
205. Koivistoinen Juha: Non-linear interactions of femtosecond laser pulses with graphene: photo-oxidation, imaging and photodynamics. (68 pp.) 2017
206. Chen, Chengcong: Combustion behavior of black liquors: droplet swelling and influence of liquor composition. (39 pp.) 2017
207. Mansikkamäki, Akseli: Theoretical and Computational Studies of Magnetic Anisotropy and Exchange Coupling in Molecular Systems. (190 p. + included articles) 2018.
208. Tatikonda, Rajendhrasrad: Multivalent N-donor ligands for the construction of coordination polymers and coordination polymer gels. (62 pp.) 2018
209. Budhathoki, Roshan: Beneficiation, desilication and selective precipitation techniques for phosphorus refining from biomass derived fly ash. (64 pp.) 2018
210. Siitonen, Juha: Synthetic Studies on 1-azabicyclo[5.3.0]decane Alkaloids. (140 pp.) 2018
211. Ullah, Saleem: Advanced Biorefinery Concepts Related to Non-wood Feedstocks. (57 pp.) 2018
212. Ghalibaf, Maryam: Analytical Pyrolysis of Wood and Non-Wood Materials from Integrated Biorefinery Concepts. (106 pp.) 2018

1. Bulatov, Evgeny: Synthetic and structural studies of covalent and non-covalent interactions of ligands and metal center in platinum(II) complexes containing 2,2'-dipyridylamine or oxime ligands. (58 pp.) 2019. JYU Dissertations 70.
2. Annala, Riia: Conformational Properties and Anion Complexes of Aromatic Oligoamide Foldamers. (80 pp.) 2019. JYU Dissertations 84.
3. Isoaho, Jukka Pekka: Dithionite Bleaching of Thermomechanical Pulp - Chemistry and Optimal Conditions. (73 pp.) 2019. JYU Dissertations 85.
4. Nygrén, Enni: Recovery of rubidium from power plant fly ash. (98 pp.) 2019. JYU Dissertations 136.
5. Kiesilä, Anniina: Supramolecular chemistry of anion-binding receptors based on concave macromolecules. (68 pp.) 2019. JYU Dissertations 137.
6. Sokolowska, Karolina: Study of water-soluble p-MBA-protected gold nanoclusters and their superstructures. (60 pp.) 2019. JYU Dissertations 167.
7. Lahtinen, Elmeri: Chemically Functional 3D Printing: Selective Laser Sintering of Customizable Metal Scavengers. (71 pp.) 2019. JYU Dissertations 175.
8. Larijani, Amir: Oxidative reactions of cellulose under alkaline conditions. (102 pp.) 2020. JYU Dissertations 217.
9. Kolari, Kalle: Metal-metal contacts in late transition metal polymers. (60 pp.) 2020. JYU Dissertations 220.
10. Kauppinen, Minttu: Multiscale computational investigation of catalytic properties of zirconia supported noble metals. (87 pp.) 2020. JYU Dissertations 231.
11. Ding, Xin: Halogen Bond in Crystal Engineering: Structural Studies on Crystals with Ruthenium Centered Complexes and 1-(4-Pyridyl)-4-thiopyridine Zwitterion as Halogen Bond Acceptors. (59 pp.) 2020. JYU Dissertations 323.
12. Neuvonen, Antti: Toward an Understanding of Hydrogen-Bonding Bifunctional Organocatalyst Conformations and Their Activity in Asymmetric Mannich Reactions. (77 pp.) 2020. JYU Dissertations 336.
13. Kortet, Sami: 2,5-Diarylpiperidines and Pyroglutamic-Acid-Derived 2-Diarylmethyl-5-Aryl-Piperidines: Their Synthesis and Use in Asymmetric Synthesis. (221 pp.) 2020. JYU Dissertations 337.
14. Saarnio, Ville: Fluorescent probes, noble metal nanoparticles and their nanocomposites: detection of nucleic acids and other biological targets. (80 pp.) 2021. JYU Dissertations 361.
15. Chernysheva, Maria: σ -hole interactions: the effect of the donors and acceptors nature in selenoureas, thioureas, halogenated species, substituted benzenes, and their adducts. (72 pp.) 2021. JYU Dissertations 370.
16. Bulatova, Margarita: Noncovalent interactions as a tool for supramolecular self-assembly of metallopolymers. (62 pp.) 2021. JYU Dissertations 377.

17. Romppanen, Sari: Laser-spectroscopic studies of rare earth element- and lithium-bearing minerals and rocks. (66 pp.) 2021. JYU Dissertations 393.
18. Kukkonen, Esa: Nonlinear optical materials through weak interactions and their application in 3D printing. (58 pp.) 2021. JYU Dissertations 441.
19. Kuosmanen, Riikka: The Effect of Structure on the Gel Formation Ability and the Properties of Bile Acid Based Supramolecular Organogels. (68 pp.) 2021. JYU Dissertations 465.
20. Reuna, Sini: Development of a Method for Phosphorus Recovery from Wastewaters. (67 pp.) 2022. JYU Dissertations 486.